OTTO VON GUERICKE UNIVERSITÄT MAGDEBURG

VST FAKULTÄT FÜR VERFAHRENS- UND SYSTEMTECHNIK

Direct conversion of ethene to propene on Ni-alumino-mesostructured catalysts: synthesis, characterization and catalytic testing

Dissertation

zur Erlangung des akademischen Grades

Doktoringenieur
(Dr.-Ing.)

von:

MSc. Leo Alvarado Perea

geb. am 13. September 1979 in Guadalupe Zacatecas Mexiko

genehmigt durch die Fakultät für Verfahrens- und Systemtechnik
der Otto-von-Guericke-Universität Magdeburg

Promotionskommission:

Prof. Dr. rer. nat. habil. Helmut Weiß	(Vorsitz)
Prof. Dr.-Ing. habil. Andreas Seidel-Morgenstern	(Gutachter)
Prof. Dr. rer. nat. Franziska Scheffler	(Gutachter)
Prof. Dr. Martin Hartmann	(Gutachter)

eingereicht am: 3. Januar 2014
Promotionskolloquium am: 28. März 2014

Abstract

In this work, synthesis and characterization of Ni/MCM-41 and Ni/AlMCM-41 catalysts with different Si/Al ratio (∞, 150, 60, 16 and 5) was carried out with respect to their application in the direct conversion of ethene to propene (ETP-reaction). All catalysts were characterized by powder XRD, N_2-physisorption, ^{29}Si and ^{27}Al MAS NMR, TEM, NH_3-TPD, pyridine-DRIFTS, H_2-TPR and TPO. Ni/MCM-41 showed relative low catalytic activity due to its low acidity. Ni/AlMCM-41 with a Si/Al ratio of 60 revealed the highest catalytic activity, reaching a conversion of ethene of 75% and a selectivity of propene close to 35%. Al could be incorporated into the MCM-41 framework up to a Si/Al ratio of 16. Two different Ni-composites were observed on the surface of the MCM-41 and AlMCM-41. These phases might correspond to a mixture of different nickel-aluminosilicates where Al is tetrahedral coordinated. Characterization after ETP experiments revealed a reduction of nickel and the presence of different types of carbon. The presence of these species deactivated the catalysts strongly.

The stability of the catalysts is an important issue for industrial application and was investigated by performing deactivation experiments at different temperature. Changes of the structure and acidity of the catalysts were monitored after these experiments. TPO and TEM characterization was also performed. These experiments revealed a strong deactivation of the catalysts at 450 °C. No significant deactivation was observed at 250 and 350 °C but not much propene was produced (selectivity of propene lower than 20%). The strong deactivation was due to the reduction of nickel during the experiments and the corresponding formation of so called monoatomic and filamentous carbon. Options for regenerating the catalysts were also studied. Successful reactivation of the catalysts could be performed after deactivation at 250 and 350 °C. However, irreversible deactivation of the catalysts took place after experiments at 450 °C.

The reaction mechanism was studied by performing isomerization and metathesis experiments. The results obtained are not in concordance with results reported in the literature. Instead of a metathesis reaction between ethene and *2*-butene, a conjunct polymerization of ethene is proposed to produce propene in the ETP-reaction. This conclusion is supported by performing *in-situ* DRIFTS experiments, where polymeric

chains could be identified during the ETP-reaction. This type of characterization also revealed that the Brønsted acidity is mainly responsible for the high catalytic activity of Ni/AlMCM-41.

Based on the catalytic results for *mono*-metallic Ni/AlMCM-41 and on the strong deactivation of the catalysts at 450 °C, where propene is one of the main reaction products, a strategy for optimizing these catalysts was proposed. This optimization consisted in the incorporation of a metathesis active site (molybdenum or rhenium) into the Ni/AlMCM-41 catalysts. Therefore, NiMo and NiRe based catalysts (*bi*-metallic catalysts) were synthesized, characterized and evaluated in the ETP-reaction. Very promising results were obtained on NiRe based catalysts where the selectivity of propene reached a value close to 70% at 225-250 °C. This result provides the possibility produce propene with high selectivity at significantly lower temperature than required for Ni/AlMCM-41. Moreover, at this reduced level of temperature irreversible deactivation might not take place. However, more and deeper characterization of the catalysts must be done to understand the nature of the active sites and their role in the ETP-reaction.

The results obtained in this PhD work represent an important contribution to the understanding of the ETP-reaction and open possibilities of producing propene from ethene at relative low temperatures.

Zusammenfassung

In dieser Arbeit wurde die Synthese, Charakterisierung und katalytische Untersuchung von Ni/MCM-41 und Ni/AlMCM-41 Katalysatoren mit verschiedenen Si/Al-Verhältnissen (∞, 150, 60, 16 und 5) in der direkten Umwandlung von Ethen zu Propen (ETP-Reaktion) durchgeführt. Die Katalysatoren wurden durch Pulver-XRD, N_2-Adsorption, ^{29}Si und ^{27}Al MAS NMR, TEM, NH_3-TPD, Pyridin-DRIFTS, H_2-TPR und TPO analysiert und bewertet. Ni/MCM-41 zeigte geringe katalytische Aktivität aufgrund seines geringen Anteils an Säuren Zentren. Ni/AlMCM-41 mit einem Si/Al Verhältnis von 60 zeigte die höchste katalytische Aktivität und erreichte einen Ethen-Umsatz von 75% und eine Propen-Selektivität von 35%. Al konnte in die MCM-41-Sturktur bis zu Si/Al-Verhältnis von 16 eingebracht werden. Die Die Anwesenheit von zwei verschiedenen Ni-Komponenten wurde auf den MCM-41- und AlMCM-41-Oberflächen festgestellt. Diese Komponenten können Mischungen aus verschiedenen Nickel-Aluminosilikaten entsprechen, wobei Al tetraedrick-koordiniert ist. Eine Charakterisierung nach Durchführung der ETP-Experimente zeigte eine Reduktion an Nickel und die Anwesenheit von verschiedenen Arten von Kohlenstoff. Diese Kohlenstoffspezies deaktivierten die Katalysatoren sehr stark.

Die Stabilität der Katalysatoren ist ein wichtiges Thema in Hinblick auf industrielle Anwendungen und wurde anhand von Experimenten bei verschiedenen Temperaturen untersucht. Veränderungen der Struktur und des Azidität der Katalysatoren wurden nach den Experimenten bewertet. TPO- und TEM-Charakterisierungen wurden auch durchgeführt. Diese Art von Experimenten zeigte eine starke Deaktivierung der Katalysatoren bei 450 °C. Keine signifikante Deaktivierung wurde bei 250° und 350 °C beobachtet, jedoch wurde nicht signifikantes Propen produziert (die Selektivität von Propen war niedriger als 20%). Die starke Deaktivierung erfolgte aufgrund der Reduktion des Nickels während des Experiments und der Ausbildung von sogenanntem monoatomarem und filamentöse Kohlenstoff. Die Möglichkeit der Regeneration der Katalysatoren wurde ebenfalls untersucht. Eine erfolgreiche Reaktivierung der Katalysatoren konnte nach einer Deaktivierung bei 250° und 350 °C erzielt werden.

Irreversible Deaktivierung der Katalysatoren wurde nach den Experimenten bei 450 °C beobachtet.

Der Reaktionmechanismus wurde durch Durchführung von Isomerisierung- und Metathese-Experimenten näher studiert. Die erhaltenen Ergebnisse widersprechen den Ergebnissen, die in der Literatur publiziert wurden. In dieser Arbeit wird im Gegensatz zur Metathese-Reaktion zwischen Ethen und *2*-Buten eine Konjunkt-Polymerisation von Ethen zu Propen vorgeschlagen. Dieses Ergebnis wird durch die Durchführung von *in-situ* DRIFTS-Experimenten unterstützt, in denen Polymerketten während der ETP-Reaktion nachgewiesen wurden. Diese Charakterisierung ergab auch, dass die Brønsted-Azidität für die hohe katalytische Aktivität von Ni/AlMCM-41 verantwortlich ist.

Auf der Grundlage der katalytischen Ergebnisse für *mono*-metall-Ni/AlMCM-41 und der starken Deaktivierung der Katalysatoren bei 450 °C, wo Propen eines der Hauptreaktionsprodukte ist, wurde eine Strategie zu der Optimierung dieser Katalysatoren vorgeschlagen. Die Optimierung bestand in der Einarbeitung eines aktiven Metathese-Zentrums (Molybdän oder Rhenium) in die Ni/AlMCM-41 Katalysatoren. Daher wurden NiMo- und NiRe-Katalysatoren (*Bi*-Metall-Katalysatoren) synthetisiert, charakterisiert und in der ETP-Reaktion bewertet. Sehr interessante Ergebnisse wurden auf NiRe-Katalysatoren erhalten. Die Selektivität an Propen betrug 70% bei 225 und 250 °C. Dieses Ergebnis bietet die Möglichkeit, eine hohe Selektivität an Propen bei signifikant niedrigen Temperaturen herbeizuführen mit Ni/AlMCM-41 erforderlichen. Ein weiterer Aspekt ist, dass auf dieser Stufe der Temperatur irreversible Deaktivierungen des Katalysators nicht stattfinden. Nichtsdestotrotz müssen mehr und detaillierte Charakterisierungen der Katalysatoren durchgeführt werden, um die Natur der katalytischen aktiven Zentren und ihre Rolle in der ETP-Reaktion besser zu verstehen.

Die Ergebnisse dieser Doktorarbeit stellen einen wichtigen Beitrag zum Verständnis der ETP-Reaktion und sie eröffnen die Möglichkeit, Propen bei relativ niedrigen Temperaturen direkt aus Ethen herzustellen.

Preface

This dissertation was written as a result of the research that I performed at the Max Planck Institute for Dynamics of Complex Technical Systems in Magdeburg Germany from January 2010 to December 2013. Herewith I would like to acknowledge to the people who contributed to this PhD project.

First and foremost, I would like to thank Prof. Dr.-Ing. Andreas Seidel-Morgenstern for giving me the opportunity to join his research group, for his guidance, teaching and support during my stay in Germany.

I would like to use this opportunity to thank Prof. Dr. rer. Nat. Franziska Scheffler and Prof. Dr. Martin Hartmann for reading this dissertation and being part of the jury for my PhD defense.

I would like to express my sincere gratitude to Dr.-Ing. Christof Hamel and Dr. Tanya Wolff for the fruitful discussions and for their important contributions to this work.

Thank you also to Mrs. Jutta Wilke for her support to perform the catalytic activity experiments. I am very grateful with Miss. Shiyan Chen and Mr. Tobias Fritsche for their important contributions to this work, especially with the metathesis catalysts. Many thanks to Mr. Markus Ikert for the facilities to perform the DRIFTS characterization.

Many thanks to Dr. Liane Hilfert, Dr. Peter Veit and Mrs. Marlies Kupfernagel from the Otto von Guericke University for their support with part of the characterization of the catalysts. Many thanks also to Mr. Tino Lehamnn for the fruitful discussions.

I would like to thank also to Dr.-Ing. Daniel Stoltenberg, Isaí González Martínez, Héctor Octavio Rubiera Landa, Miroslava Varnicic, Henning Haida and Volker Zahn for the very nice time together at work and outside of the Institute.

At this point I would like to thank all people of the PCG group for the very nice atmosphere at work and the very nice time together during these four years.

In this point I would like to thank to the Universidad Autónoma de Zacatecas and to the Programa para el Mejoramiento del Profesorado (PROMEP) from Mexico that together

with the Max Planck Institute supported me with the PhD scholarship. Many thanks also to Dr. Víctor Manuel García Saldivar for his support with the bureaucracy at the University in Zacatecas Mexico.

A great mention to express my gratitude to my family is mandatory; my parents Oralía Perea Gallegos and Leobardo Alvarado Dorado and my great brother Iván Alvarado Perea. Thank you very much for their love, patient and support in my professional and personal life. I would like to thank also to Miss. Nora Schmackert for her love, patient and invaluable support. Thank you very much.

Finally, a special mention has to be done to the "Banda B." (so called by Dr.-Ing. Jadwiga Mendrella before Nowak) constituted by Sammy, Jadwiga, Hector and Leo. Thank you very much!

Leo Alvarado Perea

To my family: Leobardo, Oralia and Iván
Muchas gracias por su amor

Table of Contents

Introduction

Ethene and propene are currently the two main building blocks of the chemical industry. This is due to the fact that they have versatile chemical properties to manufacture a wide spectrum of chemical products. Ethene has always reigned supreme and the industry evolved around the steam cracking technology has been designed to maximize the production of ethene. Propene and other building blocks, like butadiene and aromatics, are coming as *by*-products in the ethene production. However, currently the petrochemical industry is facing a major squeeze in propene availability as a result of the growth in propene derivatives. Hereby polypropene is the main driver for this increasing demand. For this reason, there is a concern that the supply of propene from its traditional sources will not be sufficient in the future to keep pace with demand. Consequently, to meet this demand, *on*-purpose technologies are of great interest and the market of propene will become dependent upon these processes.

The direct conversion of ethene to propene without addition of any other hydrocarbons (the so called ETP-reaction) was found to offer an attractive alternative for the propene production. For this reason, in this work a study of the direct transformation of ethene to propene on Ni alumino-mesostructured catalysts was carried out. In addition, an important contribution to the understanding of the catalytic properties and the nature of the actives sites of these catalysts was made.

The content of this PhD thesis is organized as follows. In chapter 1 are given the motivation and the context of the project as well as an overview of the production and market of ethene and propene. Chapter 2 describes the *on*-purpose technologies as an important option to face the increasing demand of propene. Chapter 3 summarizes the most important contributions to the field of the ETP-reaction. Besides, in this chapter the pioneering work of Iwamoto is discussed. He found that Ni loaded on MCM-41 shows good catalytic activity in the ETP-reaction and suggested a reaction mechanism for the

ETP-reaction on this catalyst. This reaction mechanism suggests that a molecule of ethene dimerizes on active Ni sites to *1*-butene, which then undergoes positional isomerization on acidic active sites to produce *2*-butene. In the final step, this *2*-butene reacts on Ni active sites with a third molecule of ethene trough a metathesis step to produce two molecules of propene. In this research, Ni on MCM-41 catalyst was modified with aluminum in order to change effectively the acidity of the catalysts influencing in particular the isomerization step. The main objective of modifying the acidity of the catalysts was to enhance the isomerization step in the ETP-reaction.

Chapter 4 describes the theoretical principles and the methods of the characterization techniques that were used to characterize the synthetized catalysts. Detailed conditions to perform this characterization are also described. Chapter 5 summarizes the experimental procedures applied to prepare the catalysts. Additionally, the experimental set up to carry out the catalytic testing of the catalysts is described. It is important to note that the synthesis of MCM-41 and AlMCM-41 materials was done by using two different procedures (Noreña-Franco et al. and Vinu et al. procedures). The same applies to the synthesis of the Ni catalysts, but here a total of three impregnation methods were used. Synthesis of Re and Mo on MCM-41 and AlMCM-41 catalysts was subsequently carried out using four impregnation methods. These catalysts were also tested in the ETP-reaction. In this step, only one procedure was used to synthesize MCM-41 and AlMCM-41. NiMo and NiRe *bi*-metallic catalysts were prepared in order to additionally optimize the catalytic performance of the Ni catalysts.

Chapter 6 summarizes the results obtained from all characterization techniques applied to study the catalysts synthesized. The first part of the chapter is devoted to describe the results of all characterization techniques used to study the catalysts prepared by Noreña-Franco et al. (2002). This characterization was performed for the catalysts before the experiments (fresh catalysts). Deeper characterization was done with respect to these catalysts because their catalytic behavior in the ETP-reaction. Corresponding catalytic activity results are shown for all catalysts. The second part of the chapter shows only the results of standard characterization of the catalysts prepared by the procedure reported by Vinu et al. (2004) because of their performance in the ETP-reaction. The effect of the reaction conditions (feed concentration and temperature effect) is shown in the third part of this chapter. Subsequently, a full study of the deactivation and regeneration of the catalyst with the best catalytic performance in the ETP-reaction was done.

Characterization of the catalyst was carried out after the ETP experiment and again after the deactivation experiments. These results are also shown and discussed in this part of the chapter. Systematic experiments were carried out to study the reaction mechanism of the ETP-reaction. Results of catalytic and kinetic experiments of the isomerization of *1*-butene, *iso*- and *trans*-butene and metathesis of *2*-butene and ethene and the *retro*-metathesis of propene are presented in the fourth part of the chapter. In this part, are also shown the results of *in-situ* diffuse-reflectance infra-red Fourier transform spectroscopy. The goal of using this characterization technique was to understand the form in which ethene and the ETP-reaction products adsorb on the surface of the catalysts. In another part of chapter 6, characterization and catalytic results of Re, Mo and *bi*-metallic based catalysts will be discussed. The goal of including Re and Mo into the Ni catalysts was to enhance the metathesis step that is reported to be part of the reaction mechanism for the ETP-reaction. Results in this part reveal that it is possible to obtain propene at temperature significantly lower temperature than required for the Ni based catalysts. With the goal of giving certainty to the experimental results, in the last part of the Chapter 6 an experimental error analysis in the ETP-reaction was performed.

Chapter 7 summarizes the most relevant conclusions obtained in this work.

CHAPTER I

Context and background of the work

Natural gas and petroleum are the main sources of seven chemical building blocks on which a vast organic chemical industry is based; ethene, propene, butenes and butadienes, benzene, toluene, xylenes (orto, meta, para) and methane [1]. Whether natural gas or petroleum is used for olefins varies throughout the world depending on the availability of natural gas and the demand for gasoline. In terms of quantity, ethene and propene are among the most important basic organic chemicals. Ethene and propene are the simplest olefins formed by two and three carbon atoms linked by a double bond.

The technology evolved around the stream cracking technology has been designed to maximize the production of ethene and propene only comes along as by-product. The demand of propene derivatives has grown rapidly over the years and is likely to continue doing so [2]. For this reason, the chemical industry is facing a dilemma, where the demand of propene is increasing considerably and its supply is relegated to a by-product in the ethene production. Thus, this raises the question of how the industry will address this imbalance and ensure adequate propene supplies into the future [2].

Propene is a versatile building block and is the feedstock for a wide range of important chemicals. This property comes from its chemical structure. Propene contains a double bond carbon-carbon and contains an allylic methyl group which is close to the double bond making it to a very important chemical to carry out chemical transformations. For

instance, these properties of the propene allow the formation of the following materials [2]:

a) Polypropene via Ziegler Natta polymerization.
b) Oxo alcohols via hydroformylation chemistry.
c) Propene oxide via chlorhydrin chemistry or peroxidation.
d) Cumene via benzene alkylation.
e) Methyl methacrylate via acetone cyanohydrin.
f) Isopropyl alcohol/acetone via hydration/dehydrogenation.

Other important propene derivatives are based on the reactivity of its allylic methyl group:

a) Acrylonitrile via ammoxidation chemistry.
b) Acrolein/acrylic acid via oxidation chemistry.
c) Allyl chloride/epichlorohydrin via high temperature chlorination/chlorohydrin chemistry.

As it can be observed, propene is a very important raw material to manufacture a wide spectrum of chemical products. Figure 1.1 illustrates the global demand breakdown for propene in 1970 and in 2004. It can be observed, polypropene consumed 64% of the propene production of the world and is the driver for propene demand [2].

Ethene is the feedstock for roughly 30% of all petrochemicals. Ethene was originally manufactured by partial hydrogenation of acetylene, dehydration of ethanol, or separation from coke-oven gas. These processes are insignificant for countries with a developed petrochemical industry. However, in developing countries, dehydration of ethanol produced by fermentation still provides an important supplement to ethylene derived from petroleum. On the other hand, propene only gained importance in the chemical industry after its manufacture from crude oil fractions or natural gas was possible to obtain [3]. Today, ethene and propene are obtained predominantly from thermal cracking of saturated hydrocarbons. Due to their high reactivity, ethene and propene must be manufactured in cleavage or cracking processes. Refinery technology employs essentially three different approaches in converting the range of products naturally occurring in crude oil to those meeting market requirements. These processes are; catalytic cracking, the hydrocatalytic cracking and thermal cracking process. In

catalytic cracking, higher boiling distillation fractions are converted into saturated branched paraffins, naphthenes and aromatics [3]. As the proportion of olefins is small, catalytic cracking is primarily used for producing motor fuels. The usual process conditions are 450-500 °C and a slight excess pressure. In hydrocracking (catalytic cracking in the presence of hydrogen), residues and higher boiling distillation fractions, can be converted into lower boiling products by various processes.

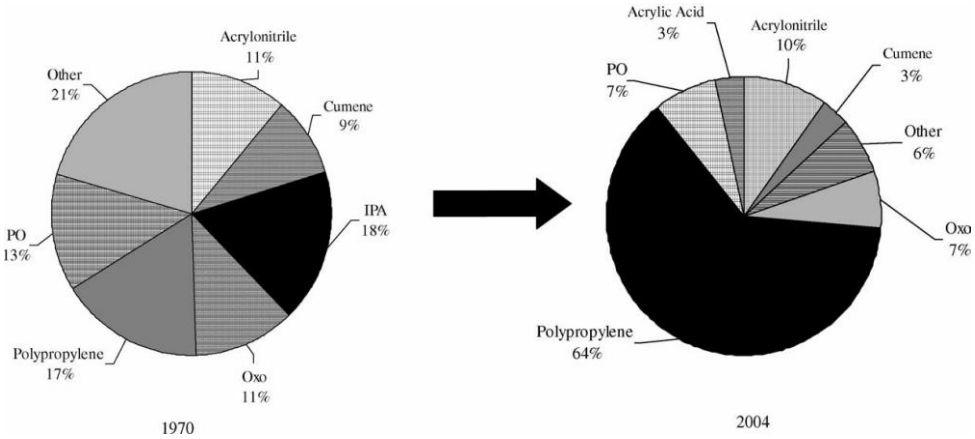

Figure 1.1. Global propene demand pattern [2]:

Alternative, bifunctional catalysts systems, consisting of metallic hydrogenation-dehydrogenation and acidic cracking components, are employed in the presence of hydrogen. Relatively high investment costs are required for the process which operates at 270-450 °C and 80-200 bar [3]. Additionally, hydrogen must be supplied, which is not manufactured in the refinery. Thermal cracking plays an important role in olefin manufacture. This process, which involves a radical cleavage of hydrocarbons takes place under pressure and starts at about 400-500 °C and the presence of a catalysts is not needed [3].

1.1 Production of ethene

As it has been mentioned in the previous section, natural gas and petroleum are the main sources of ethene. Its production involves the cracking refinery technologies of different hydrocarbons steams of petroleum. In 2010 the US production on ethene was around $2.95X10^{10}$ kg and the global production was around $7.26X10^{10}$ kg. About 80% of all

ethene produced is destined to end up as thermoplastic polymers. Ethene is a monomer for low, high and linear low-density polyethylene as well as for ethene oligomers. It is the raw material for other important monomers including vinyl chloride, vinyl acetate, styrene, and ethylene glycol. Ethene chemistry is the most mature in the petrochemical industry. The major chemistry of ethene can be divided into three categories; polymerization and oligomerization, four oxidation reactions that are practically unknown in textbook organic chemistry and two reactions called classical because they are typical of chemistry textbooks [1].

1.2 Market of ethene

The price of ethene in current and constant 2001 is illustrated in Figure 1.2. It can be observed that the price of ethene from 1970 to 1974 was almost constant. The OPEC embargo of 1974 increased the price to more than double amount. Inflation contributed to a steady increase with a precipitous rise in 1980 because of the Iranian crisis. Overcapacity, maturity, and weakening oil prices caused the price to decrease in 1985 and 1986. By 1988, price increased markedly due in part to increased demand but, more important, to industry restructuring, which eliminated marginal suppliers as well as effective producers who felt that capital redeployment would lead to greater profit [1].

1.3 Production of propene

After ethene, propene is the most important olefin. In 2001 about 49% of propene produced in US was prepared as a co-product of ethene production in the steam cracking of ethane, propane and higher alkanes [1]. The rest was produced as *by*-product of catalytic cracking and of other refinery processes. Catalytic cracking of higher petroleum fractions is a source of propene, although it is more dilute and thus more expensive to isolate than the propene from the stream cracking. The steam cracking of ethane, propane, butane, naphtha, or gas oil inevitably gives propene as one of the co-products, although the cracking of ethane yields so little it is usually not isolated. The amount depends on the feed and on severity of the cracking [1].

Owing to the strong global demand for polypropylene, there is concern that the supply of propene from its traditional sources will not be sufficient to keep pace with demand. Consequently, much effort has been expanded on improving propane dehydrogenation technology and in developing the new so-called *on*-purpose routes to propene [1].

Propene by using deep catalytic cracking

Deep catalytic cracking is a catalytic cracking process for producing light olefins from heavy feedstocks such as vacuum gas oil [1]. This process uses fluid catalytic cracking principles combined with a proprietary catalyst to produce up to 20% propene and other light olefins from vacuum gas oil and correspondingly less gasoline.

Propene from olefin metathesis

Phillips Petroleum Company discovered olefin metathesis in 1964. This technology, the interchange of olefins, while quite amazing from a theoretical point of view, has found only some niche applications [1]. In the mid-1980s, Lyondell was the first company to use metathesis chemistry to make one of the major building block chemicals, propene. Lyondell (purchasers of ARCO) achieved this by affecting the metathesis of ethylene and *2*-butene.

Recently, ABB Lummus bought the licensing rights to the Phillips metathesis technology. In 2002, BASF and Fina completed a new world scale steam cracker in Louisiana and are planning to incorporate ABB Lummus' olefin metathesis process for converting ethene and butenes to propene [1]. When run with the metathesis unit on, the new BASF/Fina cracker will have the capability of producing almost equal amounts of ethylene and propylene.

The ABB Lummus metathesis process uses tungsten oxide on silica as catalyst and operates at a temperature of 300–375 °C in a fixed-bed reactor [1]. Axens (formerly IFP) has developed a similar metathesis process. However, the Axens process uses a rhenium on alumina catalyst that operates at a much lower temperature of 25–50 °C in a moving bed reactor. Common to all metathesis processes is the need to remove from the feeds any polar impurities and dienes that poison the catalyst.

Propene from selective cracking of C_4/C_5

The chemistry involved in this process is based on cracking C_4 and C_5 olefins over specially formulated shape selective zeolite catalysts [1]. The feed stream can come from a steam cracker, raffinate, fluid catalytic cracking, C_4 streams, or C_5 streams from steam cracker pyrolysis gasoline. The only pretreatment needed is selective hydrogenation of all dienes. In addition to making relatively high amounts of propene, selective C_4/C_5

cracking gives small amounts of light gases, some ethene, C_5 and heavier components suitable for gasoline.

1.4 Market of propene

The price of propene has been consistently about 20% lower than the price of ethene as it is illustrated in Figure 1.2 [1]. The price relationship of propene to ethene was maintained until 1986 when the price of the two products became equal [1]. At that point, propene usage was growing faster than that of ethene. Also, there was a slight shortage of propene, particularly in Europe. The traditional price relationship resumed in the late 1980s and was maintained into the early 2000s when rapid propene growth again led to a shortage.

As it was mentioned above, due to the strong increasing demand of propene there is a concern that the supply of propene from its traditional sources will not be sufficient to keep pace with demand [4]. Consequently, to meet this demand, the *on*-purpose technologies will be of great interest and the market of propene will become dependent upon these processes for meeting the increasing demand. Several strategies have been proposed for propene production and they will be described in more detail in the next chapter.

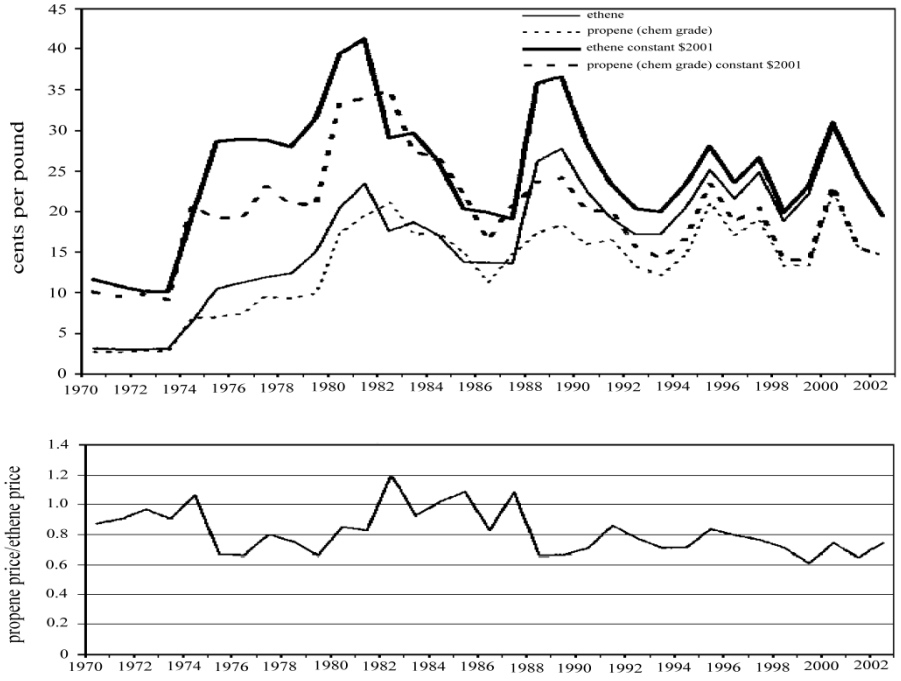

Figure 1.2. Average prices for ethene and propene and the ratio of their prices, United States 1970-2002 [1].

CHAPTER II

On-purpose technologies

In this section a short overview of the *on*-purpose technologies for the propene production will be described; dehydrogenation of propane, catalytic cracking of butenes, metathesis of ethene and *2*-butene and the direct conversion of ethene to propene, as it is shown in Chart 2.1.

On-purpose technologies

- *Dehydrogenation of propane:* This process evolves high temperatures and is expensive.
- *Catalytic cracking of butenes:* This process produces propene by catalytic cracking of intermediately formed oligomers of butene.
- *Metathesis of ethene and butene:* This process needs stoichiometric amounts of ethene and butene.
- *Direct transformation of ethene to propene:* Production of propene by feeding only ethene as reactant. Topic of this work.

Chart 2.1. *On*-purpose technologies for the production of propene.

In the next sections, features of each process will be described separately. Main characteristics will be mentioned and the reaction conditions for each process in which

each process takes place will be introduced. Specific advantages and disadvantages will be also mentioned.

2.1 Dehydrogenation of propane

Propane dehydrogenation processes have been available for several decades but have been of less interest because of the large amount of cheap propene produced by catalytic cracking [1]. The possibility of a propene shortage and improvements in catalysis have motivated their re-examination [5]. The chemistry is simple, involving catalytic abstraction of hydrogen from propane to give propene. The major competition reaction is cracking of propane to ethene and methane which, in turn leads, to hydrogenation of ethene to produce ethane [1]. Because of thermodynamic limitations, the process is operated above 600 °C in order to achieve acceptable conversions per pass, but above 700 °C cracking is the dominant reaction. The major process conditions are determined by thermodynamic limitations, reaction kinetics, and economics of the conversion-selectivity relationship.

Propane dehydrogenation process technology is offered by several licensors including UOP, ABB Lummus, Linde/BASF, Snamprogetti/Yarsintez, and Krupp Uhde. The processes vary among the licensors in terms of reactor design, pressure, temperature, heating method, catalysts, and catalysts regeneration techniques. The first propane dehydrogenation plant was built in Thailand. In the early 2000s, there were three propane dehydrogenation plants in Asia, one in Belgium, one in Mexico, and one under construction in Spain. Because of the increasing demand of propene much effort has been expended on improving propane dehydrogenation technology [5].

2.2 Catalytic cracking of butenes

In the process of hydrocarbon transformation, the catalytic performance and especially the product distribution depend strongly on the pore topology, the acidity of the catalyst and the reaction conditions. In recent years the catalytic cracking of butenes has opened a new alternative to produce ethene and propene. This reaction is a complicated process, besides the reaction that butene converts to propene and ethene, other reactions can also take place, such as hydrogen transfer, oligomerization, isomerization, aromatization and protolytic cracking. Therefore, a wide spectrum of reaction products is obtained during the catalytic cracking increasing significantly the effort of products purification [6].

Zeolites of the type ZSM-5, ZSM-23 and MCM-22 have presented a high conversion of butenes under classic catalytic cracking temperatures, 600-650 °C [7-12].

Different efforts have been made in order to improve the catalytic properties of these zeolites. The modification of the zeolite ZSM-5 with potassium showed a decrease of the conversion of *1*-butene [8] because of significant reduction of the acidity with the potassium incorporation. Also, the catalytic performance of this zeolite is strongly dependent on the pore structure and on the Si/Al ratio used (acidity) [10], the smaller the pore size of the zeolite, the higher selectivity of propene and ethene. With increasing the Si/Al ratio of the ZSM-5 zeolite, the selectivity of propene and ethene increased. The opposite behavior was observed for the ZSM-23 zeolite with different Si/Al ratio, where the lower Si/Al ratio, the higher the conversion and the selectivity of ethene and propene [7]. The modification of ZSM-5 zeolite with a trace of chromium enhanced its catalytic performance in the catalytic cracking of iso-butene [11]. MCM-22 zeolite also have shown attractive catalytic properties in the cracking of *1*-butene but this zeolite presented a rapid deactivation mainly provoked by fast coke formation reactions [9]. The mechanism of formation of propene via catalytic cracking of butenes involves the formation of butene oligomers with a subsequent cracking of the produced oligomers to produce propene and ethene.

As it has been stated, the catalytic cracking of butenes is an interesting process for the production of propene. Zeolites, ZSM-5, ZSM-23 and MCM-22 offer interesting catalytic properties. Therefore, with an adequate selection of the catalyst and of the reactions conditions, it is possible to obtain propene with a selectivity of around 45%. The main disadvantage of this process is that besides to the reactions involved in the propene formation other reactions take place. Therefore, it is difficult to reach high selectivity with respect to propene.

2.3 Metathesis of ethene and butene

Olefin metathesis is one of the very few fundamentally novel organic reactions discovered in the last 50 years. Among others, it opens up new industrial routes to important petrochemicals, polymers, oleochemicals and specialty chemicals. At Phillips Petroleum Co. this reaction was discovered by Banks and Bailey in 1964 [13], when they were seeking an effective heterogeneous catalysts to replace the HF acid catalyst for converting olefins into high-octane gasoline via olefin-isoparaffin alkylation. When they

used a supported molybdenum catalyst, they found that instead of alkylating the paraffin, the olefin molecules were split, and discovered that propene can be catalytically converted into ethene and butene. Since then, industrial applications of the olefin metathesis reaction have a great interest for the synthesis of different chemicals.

One of the industrial processes for the propene production is the Phillips triolefin process. It utilizes a heterogeneous catalyst system and was originally developed by Phillips Petroleum Co., USA, and operated from 1966 to 1972 for the conversion of propene into ethene and butene, due to less propene demand at that time. The Phillips process is now offered by ABB Lummus Global, Houston (USA), for license as olefins conversion technology for the production of propene [14]. The reaction takes place in a fixed bed reactor over a mixture of WO_3/SiO_2 and MgO at a temperature higher than 260 °C and 30-35 bar. The conversion of butene is above 60% per pass and the selectivity of propene is higher than 90%.

The Meta-4 process is a process developed by the Institut Francais de Petrole and the Chinese Petroleum Corporation. Also, in this process, ethene and *2*-butene react in the liquid phase in the presence of a Re_2O_7/Al_2O_3 catalyst at 35°C and 60 bar. The conversion is 63% per pass. The process involves the use of high cost catalyst and a high purity of the feed stream [14].

For the metathesis of ethene and butene a wide variety of transition metal compounds catalyze the alkene metathesis and the most successful are based on tungsten, molybdenum and rhenium. From these, rhenium based catalysts are more active and more selective even at room temperature [12]. However, the costs of rhenium compounds are high, and the catalyst with low rhenium loading exhibits only negligible activities. The supported tungsten catalysts are less active than rhenium and molybdenum. To achieve acceptable metathesis activity, high temperatures (250-500°C) have to be used for the tungsten catalysts. Zhu et al., reported a Mo/HBeta-Al_2O_3 catalyst which offers a *2*-butene conversion higher than 70% and the propene selectivity of around 90%. This catalyst consists of a Mo loading of 4-6 wt.% and a support composed by a mixture of HBeta-30%Al_2O_3 under the following reaction conditions 30-120°C and 0.4-1.0 MPa [12]. More recently WO_3/SiO_2 catalysts have showed catalytic activity in the metathesis of other alkenes, e. g. metathesis of decene [15].

2.4 Direct transformation of ethene to propene

One of the most attractive *on*-purpose processes for the propene production is the direct conversion of ethene to propene, the so-called ETP-reaction. This process involves the production of propene by feeding only ethene as reactant without mixing the feed with other hydrocarbons. This reaction was observed and studied at first in 1972 and again in 1980 but since 2000s it has become an important field of research. From then to now important contributions have been made.

Early catalysts were based on supported molybdenum hexacarbonyl and tungsten oxide. Lately, a number of heterogeneous catalysts have been developed. The samples allowed for sufficient conversion of ethene and selectivity of propene. These catalysts can be classified based on the supposed mechanism of propene formation. The first group of catalysts supports the ethene oligomerization and a subsequent cracking process, which produces propene as the main product. SAPO-34 and ZSM-5 belong to this group of catalysts. The second group is formed by transition metal compounds, i.e. nickel and tungsten based catalysts. On then, ethene is transformed by a sequence of single chemical reactions. In a first stage, ethene dimerizes to produce *1*-butene, which experiences positional isomerization to produce *2*-butene. This *2*-butene reacts with another molecule of ethene to produce propene trough a metathesis step (see chart 3.1). The state of the art in the ETP-reaction as well as the most important contributions on the understanding of this reaction will be described in the next chapter.

CHAPTER III

State of the art in the ETP-reaction

The direct conversion of ethene to propene (ETP-reaction) was observed, at first in 1972 and 1980 in a few early papers on olefin metathesis catalysts over supported molybdenum and tungsten catalyst [16, 17]. O´Neill et al. realized the metathesis of propene using a cobalt catalyst which caused a rapid disproportionation of propene to equal amounts of ethene and butene. A different distribution of the products was observed using a catalyst prepared with $Mo(CO)_6$ on Al_2O_3. This change of the products distribution could be satisfactory explained by proposing that ethene was reacting to form propene [16]. In 1980 Yamaguchi et al., studied the acidic properties of tungsten oxide on different supports. They studied the ethene reaction on WO_3-TiO_2 at 200 °C and they found that propene was present in the mixture of the reaction products [17].

From 2006 onwards, this field has been subject of intensive research by different groups worldwide. The main contributions can be classified in three different groups, based on the reaction mechanism that it is believed to take place to produce propene. First, there are catalysts which produce propene by ethene oligomerization and a subsequent catalytic cracking process to afford propene. These catalysts belong to the case of zeolite materials e. g. SAPO-34 and ZSM-5 [18, 19]. The second group is formed by transition metal based catalysts, which agree with the following reaction mechanism proposed by Iwamoto et al. [20, 21]. In the first step, a dimerization step of ethene to produce

1-butene is considered. In the second step, this *1*-butene undergoes positional dimerization to *2*-butene, and finally this molecule reacts with another molecule of ethene to produce two molecules of propene through a metathesis step, (Chart 3.1). Ni ion loaded on MCM-41 [20-28] and tungsten hydride on alumina belong to this group of catalysts [29]. Finally, the third group involves the more recent contributions to the field where bio-ethanol was used as raw material for propene production. In this type of catalysts the reaction mechanism is not fully elucidated and understood. In the next paragraphs a detailed description of each group of catalysts will be given. Ethene and/or ethanol conversion, selectivity of propene, catalyst used and reaction conditions will be described.

3.1 Propene from oligomerization and cracking of ethene

SAPO-34 and ZSM-5 zeolites have shown high catalytic performance in the ETP-reaction [18, 19, 30]. SAPO-34 presented a yield of 52.2% and a selectivity of propene of 73.3% at 400 °C. The high selectivity achieved can be attributed to a shape selectivity effect of the small pores and to the modest acid strength of the acid sites. Also, the catalytic results showed that SAPO-34 suffered a serious deactivation. Zeolite ZSM-5 presented a conversion of 58% with a selectivity of propene of 42% at 450 °C [30]. Here the Brønsted acidity played a crucial role in the ethene conversion. The reaction mechanism suggested in both contributions mentions that ethene undergoes oligomerization and in a second step these oligomers crack to produce propene because of the strong acidity of the catalysts.

3.2 Propene from the reaction mechanism proposed by Iwamoto et al.

The catalysts that support the reaction mechanism proposed by Iwamoto are based on Ni^{+2} ions loaded on mesoporous materials of the type MCM-41. This type of catalysts offer a regular pore size distribution in the interval of mesopores and a high specific surface, around 1000 m^2 g^{-1} [21]. Therefore, the shape selectivity that resulted very important for SAPO-34 and ZSM-5 catalysts is not present. With these interesting properties, nickel based mesoporous catalysts seem to be attractive to produce propene from ethene. The most important contributions to the field are shown in the following paragraphs.

In 2007 Iwamoto et al. found that Ni^{+2} ion loaded on MCM-41 is active for the direct transformation of ethene to propene. They suggested a reaction mechanism that explained the obtained results [20, 21]. Two important properties of the catalyst were found to be crucial for the high catalytic activity of the catalyst; the nickel active sites and the acidity of the MCM-41 (see Chart 3.1). The proposed reaction mechanism consists of a sequence of a three single chemical reactions. The first reaction that is taking place is the dimerization of ethene to *1*-butene. This step is taking place on nickel active sites. The second reaction of the reaction mechanism, is the positional isomerization of *1*-butene to *2*-butene on acid actives sites of the MCM-41. The last reaction that is taking place is a metathesis reaction between *2*-butene and another molecule of ethene to produce propene on nickel active sites [20, 21]. Chart 3.1 shows the detailed reaction mechanism.

$2C_2H_4 \rightarrow H_2C = CH - CH_2 - CH_3$ **Dimerization of ethene on Ni**
ethene *1*-butene

$H_2C = CH - CH_2 - CH_3 \rightarrow H_3C - HC = CH - CH_3$ **Isomerization of *1*-butene on acid sites**
1-butene *2*-butene

$H_2C - HC = CH - CH_3 + C_2H_4 \rightarrow \mathbf{2H_2C = CH - CH_3}$ **Metathesis of *2*-butene and ethene on Ni**
2-butene ethene propene

Chart 3.1. Reaction mechanism of the ETP-reaction according to Iwamoto et al [20].

Ni ion loaded MCM-41 catalysts have been prepared by template ion exchange (TIE method) [20-25, 27] and equilibrium adsorption method (EA) [21, 26]. A conversion of ethene of 68% and a selectivity of propene of 48% was observed on the catalyst prepared by TIE method. Conversion of ethene in the interval of 30-36% and the selectivity of propene in the interval of 12-45% was observed for the catalysts that were prepared by the EA method. These results have been obtained using a fixed bed reactor of continuous flow at 400 °C. It is has been shown that the acidity of the catalysts, the nickel state and the reaction conditions play an important role in the ETP-reaction. Also, the pore diameter of the catalysts has shown an important effect on the catalytic activity of the catalysts. This effect was explained because of the higher assemble of the silanol groups for the catalyst with the smallest pore diameter [24].

Deep characterization has been carried out to understand the nature of the active sites of the Ni^{+2} ion loaded on MCM-41 catalysts. Layered nickel-silicate like structure of the

type 2:1 phyllosilicate-like species seemed to be the active phase in the ETP reaction and in the dimerization of ethene [21, 24, 27]. This phase was formed independently of the pore diameter of the catalyst [24] and it is proposed that Ni^{+2} ion is the nickel state that is active in the dimerization of ethene. This phase will develop different types of acidity depending of the nickel content of the final catalysts, which it will be also responsible for the differences in catalytic activity in the catalysts with different nickel content [27].

All above results are obtained when TIE method was used to synthesize the Ni on MCM-41 catalyst. There is an intensive discussion about the nature of the TIE method because of the required conditions to form the active phase of the Ni on MCM-41 catalysts [24]. Lehmann et al. suggest that instead of a template ion exchange a template-protected deposition-precipitation is taking place, where a partial dissolution of the MCM-41 in the external surface is taking place [27]. Therefore, the nature of the formation of the nickel active sites on MCM-41 catalysts is under discussion [31, 32]. More recently, Frey et al. showed that the ETP-reaction can be carried out by using Ni on MCM-48 modified with aluminum [28]. Active catalysts were synthetized by using TIE method and incipient wetness impregnation. A conversion of ethene of around 40% and a selectivity of propene of 56% could be obtained with both methods at 350 °C. No deeper characterization was performed [28].

As conclusion, previous contributions have used a wide spectrum of characterization techniques to elucidate the nature of the active sites on Ni on MCM-41 catalysts. The results strongly support the reaction mechanism proposed by Iwamoto et al. (2007 and 2008). Because of the Ni based mesostructured catalysts have shown the most interesting catalytic activity in the ETP-reaction, the main contribution of this research is devoted on the same type of materials. Because of the acidity of the catalyst was found to be crucial in the catalytic behavior of these types of catalysts, a modification of the MCM-41 with aluminum was one aim of this study to effectively modify the acidity of the final catalysts.

3.3 Propene from *bio*-ethanol

Owing to the increasing concerns about global warming, the production of hydrocarbons from bio-ethanol obtained by fermentation of biomass has attracted considerable attention [33]. The conversion of ethanol to hydrocarbons such as ethene, gasoline and aromatics has been intensively studied over ZSM-5 zeolite [34]. Especially, the ethanol

to propene process has attracted the most increased interests from academic and industrial scientists because propene is one of the most important starting materials for the synthesis of different chemicals [33, 35, 36] as it was discussed in the previous chapter. The most important catalyst for the conversion of ethanol to hydrocarbons is the zeolite ZSM-5. Song et al (2013) studied the conversion of ethanol to propene on ZSM-5 co-modified with zirconium and phosphorous. The conversion of ethanol was 100% and the selectivity of propene was 29.2% at 550 °C [33]. The zirconium and phosphorous modified ZSM-5 exhibited a better catalytic performance than the H-ZSM-5 and the zirconium modified ZSM-5 catalyst. This behavior was due to an important reduction of the acidity of the H-ZSM-5. At the same time, the stability of the co-modified catalyst was improved because the suppression of the carbonaceous deposition and the dealumination of zeolite framework.

Recently it has been shown that Ni doped MCM-41 and Ni doped FSM-16, Y modified ceria, and scandium on In_2O_3, are attractive candidates for the direct conversion of *bio*-ethanol to propene reaching a maximum conversion of ethanol close to 100% [37-39]. Sugiyama et al. (2010) showed that the conversion of ethanol to ethene and propene proceeds more favorably on FSM-16 and Ni-FSM-16 than MCM-41 and Ni-MCM-41 [37]. The conversion of ethanol was around 100% on FSM-16 and the main reaction product was ethene with a selectivity of 95% at 400 °C in a fixed bed reactor. When nickel is included on FSM-16 and MCM-41 the conversion of ethene did not change significantly and the selectivity of propene was around 35% on Ni-FSM-16, which was higher that the correspondent Ni-MCM-41 (13%) [37]. Iwamoto et al (2013) and Hayashi et al. (2013) showed that the conversion of ethanol to ethene and propene can proceed on yttrium modified ceria and scandium on In_2O_3 catalysts [38, 39]. The scandium on In_2O3 catalyst showed a conversion of ethanol close to 100% with a yield of propene of 60% in the presence of water and hydrogen at 550 °C. The experiments were carried out in a fixed-bed reactor at atmospheric pressure. The main problem of this catalyst is its deactivation because of coke formation during the course of the reaction. Yttrium modified catalyst revealed a conversion of ethanol of 100% and a yield of propene of 25% at 420-430 °C [38]. The experiments were carried out by using a fixed-bed reactor at atmospheric pressure. The reaction mechanism has been not yet clarified on this type of catalyst. For both catalysts, the presence of water increased the

yield of propene and improved the long term activity of the catalyst because of the suppression of the coke formation.

An interesting Ni-Re/γ-Al_2O_3 dual function catalyst has been prepared by incipient wetness impregnation and tested in the ETP-reaction [40]. This catalyst opens the possibility of producing propene at significant lower temperatures than used for all the processes described above. A conversion of ethene of around 60% with a selectivity of propene of 48% was obtained at 60-100 °C [40]. Strong deactivation was observed because of the coke formation during the course of the reaction. Due to the lack of deep characterization and because the soft reaction conditions the deactivation of the catalysts due to coke formation, is questionable. These results also support the reaction mechanism suggested by Iwamoto et al. because it is believed that rhenium is enhancing the metathesis step combining *2*-butene with ethene to propene. In general, the production of propene from ethanol or ethene is a very attractive field where still more work is needed. This process is also a wide and open field from the catalytic design point of view [41].

3.4 Summary

A detailed description of the main contributions to the field of the ETP-reaction has been made. Independently of the reaction mechanism that is involved in the ETP-reaction, several common properties of the catalysts could be recognized. The acidity of the final catalyst and the reaction conditions that are used in the ETP-reaction, also including ethanol as reactant, play an important role in their catalytic performance. The transition metals which are active in the ETP-reaction are the following; W, Mo, Re, Ni, Y, Sc. The common materials that are used to prepare the catalysts are: MCM-41, ceria, In_2O_3, SAPO-34 and ZSM-5 which can be modified with Al, P and Zr. As it can be observed, the spectrum of possibilities to perform the ETP-reactions successfully is very broad. This fact makes the ETP-reaction to a very attractive process to face the increasing demand of propene worldwide.

This research focuses on the synthesis, characterization and application of Ni based aluminomesostructured catalysts for the ETP-reaction modified with aluminum. The basic materials are MCM-41 and Ni as metal active site. Aluminum was included to modify effectively the acidity of the catalysts. A deeper understanding of the catalytic active sites and of the reaction mechanism was acquired using a wide spectrum of

characterization techniques. Long time experiments were performed to study the stability of the catalyst with the highest selectivity of propene.

In the next chapter is provided a description of the characterization methods that were used during this project. The basic principles of each measurement technique and the information provided will be explained.

CHAPTER IV

Characterization, methods and techniques

The characterization of synthesized catalysts is important to obtain information about their structure, physicochemical properties and the nature of the active sites of the catalysts. Below is given a short description of the characterization techniques applied and the conditions used.

4.1 N_2-physisorption

Most catalysts of practical importance are highly porous and possess large specific surface areas. Although the catalytic activity may be only indirectly related to the total available surface, evaluation of the surface area and pore size distributions are generally considered an important requirement in catalyst characterization [42]. Physisorption is a general phenomenon that occurs whenever an adsorbable (the adsorptive) is brought into contact with the surface of a solid (the adsorbent). The molar amount, *n*, of gas adsorbed by unit mass of adsorbent is dependent on the equilibrium pressure *p*, the temperature T and the nature of the gas-solid system. It can be written [43]:

$$n = f(p, T, system)$$

If the particular gas is below its critical temperature and the adsorbent is maintained at a constant temperature, the general adsorption isotherm for a given gas-solid system is

$$n = f\left(\frac{p}{p^0}\right)_T$$

Where p^0 is the saturation pressure of the adsorptive at constant temperature T. The adsorption isotherm is thus the relationship between the amount adsorbed and the equilibrium pressure or relative pressure, at a fixed temperature. This relationship frequently is represented graphically.

The first step in the interpretation of a physisorption isotherm is the inspection of its shape. The classification of physisorption isotherms and associated hysteresis are shown in Figure 4.1 according to the IUPAC classification [44].

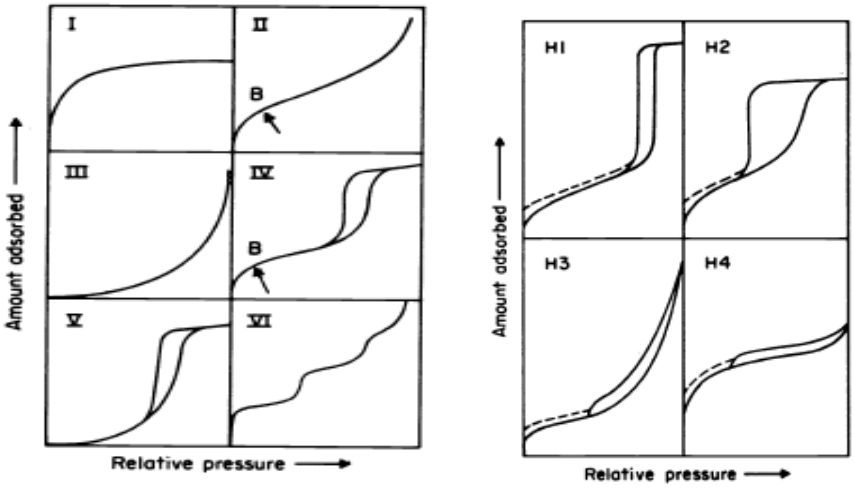

Figure 4.1. Types of physisorption isotherms, (a). Types of hysteresis loops, (b) [44].

Type I isotherm is given by microporous solids having relatively small external surfaces. Type II isotherm is the normal form of isotherm obtained with a non-porous or macroporous adsorbent. The Type II isotherm represents unrestricted monolayer-multilayer adsorption. Point B is often taken to indicate the stage at which monolayer coverage is complete and multilayer adsorption about to begin. Type III isotherm does not exhibit the Point B. Characteristic features of the Type IV isotherm are its hysteresis loop, which is associated with capillary condensation taking place in mesoporous, and the limiting uptake over the range of high relative pressure. The initial part of the Type IV isotherm is attributed to monolayer-multilayer adsorption since it follows the same path as the corresponding part of a Type II isotherm obtained with the given adsorptive on the same surface area of the adsorbent in a non-porous form. Type IV isotherms are given by many mesoporous adsorbents [44]. The Type V isotherm is uncommon, it is

related to the Type III isotherm in that the adsorbent-adsorbate interaction is weak, but is obtained with certain porous adsorbents. The Type VI isotherm represents stepwise multilayer adsorption on a uniform non-porous surface. Amongst the best examples of the Type VI isotherm are those obtained with argon or krypton on graphitized carbon blacks at liquid nitrogen temperature.

Hysteresis loops, which can be often observed in the multilayer range of physisorption isotherms is usually associated with capillary condensation in mesoporous structures. Such loops may exhibit a wide variety of shapes. Two extreme types are shown as H1 and H4 in Figure 4.1. Type H1 is often associated with porous materials that consist of agglomerates or compacts of approximately uniform spheres in fairly regular array. The H2 loop is difficult to make a deep interpretation of the structure of the pores of this type of materials. The H3 loop is observed with aggregates of plate-like particles giving rise to slit-shaped pores and the Type H4 loop is often associated with narrow slit-like pores.

The Brunauer-Emmet-Teller (BET) gas adsorption method has become the most widely used standard procedure for the determination of the surface area of finely-divided and porous materials, in spite of the oversimplification of the model on which the theory is based. It is customary to apply the BET equation in the linearized form [44]

$$\frac{p}{n^a * (p^0 - p)} = \frac{1}{n_m^a * C} + \frac{(C-1)}{n_m^a * C}\frac{p}{p^0}$$

Where n^a is the amount of gas that is adsorbed at the relative pressure $\frac{p}{p^0}$ and n_m^a is the monolayer capacity. The BET equation requires a linear relationship between $\frac{p}{n^a*(p^0-p)}$ and $\frac{p}{p^0}$ where the parameter that has to be known is the n_m^a that will be used to compute the specific BET-area by using the following equation;

$$a_s(BET) = n_m^a * L * a_m/m$$

Where L is the Avogadro constant and a_m is the adsorbent area of mass m. At present, nitrogen is considered to be the most suitable adsorptive for surface area determination.

Barret-Joyner-Halenda method (BJH-method) has been one on the most used methods to determine pore size distributions of the different porous solids. This method is based on

the Kelvin equation considering a cylindrical pore model and it is written as follows [43];

$$r_k = -\frac{2\gamma v}{RT} ln\left(\frac{p}{p^0}\right)$$

In which r_k is referred as the Kelvin radius, γ is the surface tension, v molar volume of the liquid, R the gas constant, T is the temperature and $\frac{p}{p^0}$ is the relative pressure.

This method is based on the notional emptying of the pores by a stepwise reduction of the relative pressure by taking into account the thinning of the multilayer in those pores already emptied of the condensate.

The non-local density functional theory (NLDFT) has been developed into powerful methods for the description of the physisorption and phase behavior of fluids confined in porous materials [43]. NLDFT describes the configuration of adsorbed molecules in pores on a molecular level and thus provides detailed information of about the local fluid structure near curved solids walls as compared with the bulk fluid. It is generally assumed that in an experimental system the adsorbate in a pore is in thermodynamic equilibrium with a bulk gas phase. The local density of the pore fluid is therefore determined by minimizing of the grand thermodynamic potential.

In the context of physisorption, it is expedient to classify pores according to their sizes; macropores, pores bigger than 50 nm; mesopores, between 2 and 50 nm; and micropores smaller than 2 nm [44].

In this project the nitrogen adsorption isotherms, BET specific surface areas, pore volumes and pore size distributions were determined as follows. Nitrogen physisorption analysis was performed at -196 °C using a Quantachrome Nova2200e analyzer. Prior to adsorption, the samples were degassed for 24 h at 110 °C in vacuum. Between 10 and 20 mg of sample were used for the measurements. Specific surface areas were calculated from the linear parts of BET plots while the total pore-volume was evaluated using the isotherm at a relative pressure of 0.995. BJH and NLDFT methods were used to perform the calculation of the pore size distribution.

4.2 Powder X-ray diffraction

Powder X-ray powder diffraction, (powder XRD) is nowadays used as the main characterization tool whenever ordered solid materials are synthesized. It is a fast method to provide first information about the synthesized materials such as the simple but important information on whether the wanted product has been formed [43]. X-ray diffraction is the elastic scattering of X-ray photons by atoms in a periodic lattice. The scattered monochromatic X-rays that are in phase produce constructive interference. Figure 4.2 illustrates how diffraction of X-rays by crystal planes allows one to derive lattice spacing by using the Bragg relationship:

$n\lambda = 2dsin\ \theta; n = 1, 2, 3,...$

Where λ is the wavelength of the X-rays; d is the distance between two lattice planes; θ is the angle between the incoming X-rays and the normal to the reflecting lattice plane; and n is the integer called the order of the reflection.

If one measures the angles, 2θ, under which constructively interfering X-rays leave the crystal, the Bragg relationship gives the corresponding lattice spacings, which are characteristic for a certain compound.

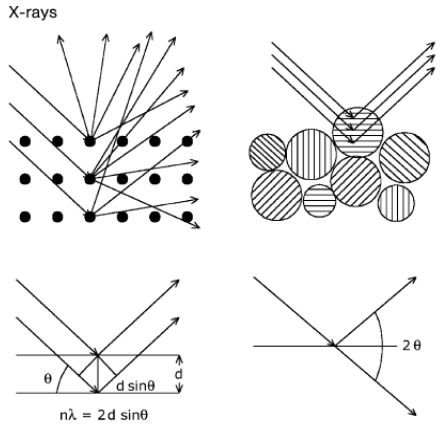

Figure 4.2. X-rays scattered by atoms in a ordered lattice interfere constructively in direction given by Bragg´s law [45].

The XRD pattern of a powdered sample is measured with a stationary X-ray source and a movable detector, which scans the intensity of the diffracted radiation as a function of the angle 2θ between the incoming and the diffracted beams. When working with powdered samples, an image of diffraction lines occurs because a small amount of the

powder particles will be orientated such that by chance a certain crystal plane is at correct angle θ with the incident beam for constructive interference. Rotation powders during measurement enhance the fraction of particles that contributes to diffraction pattern [45].

In this project, powder XRD patterns were collected on an X'Pert PRO diffractometer by PANalytik using Ni-filtered Cu Ka radiation. The generator was operated with a voltage of 40 kV and a current of 40 mA. A small amount of catalyst was placed on a silicon wafer and covered with a Vaseline layer. All samples were scanned in the region of (1° - 10°) 2θ with a step size of 0.016° using a scanning time of 10 s per step. Characteristic signals of the MCM-41 materials were observed.

4.3 Solid state ^{29}Silicon and ^{27}Aluminum Magic-Angle-Spinning Nuclear Magnetic Resonance

Nuclear Magnetic Resonance (NMR) spectroscopy is applicable to any nucleus that possesses a magnetic moment, a nuclear spin. NMR techniques are very useful for the investigation of framework atoms, extra-framework species and surface sites of solid catalysts and of adsorbate complexes and reaction intermediates formed on these materials [43]. Nuclear spin ensembles in liquids and gases cause narrow NMR signals since the influence of spatially anisotropic spin interactions on the linewidth is averaged to zero by isotropic motions. In contrast, solid materials such as catalysts and adsorbate complex give NMR spectra that are strongly affected by the anisotropic spin interactions. The analysis of solid-state signals occurring at characteristics resonance positions and having characteristic lineshapes is a source of structural information. On the other hand, to reach a separation of the NMR signals of nuclei in different local structures and different chemical surroundings, sophisticated experimental techniques allowing an averaging of the nuclear spin interactions must be applied [43]. The most important high-resolution solid-state NMR technique is fast sample rotation around an axis in the "magic" angle of 54.7° to the direction of the external magnetic field. This technique is known as magic-angle spinning (MAS). The Double Oriented Rotation (DOR) technique is a useful method to remove the second-order quadrupolar line broadening by using a simultaneous sample spinning around two axes. The Multiple-Quantum MAS (MQMAS) technique has been introduced as a new experimental approach for the study of the quadrupolar nuclei [43]. This technique enhances the resolution of the spectra

significantly. The Cross-Polarization (CP) experiment increases the sensitivity of the NRM spectroscopy. This technique is advantageously employed in the case of diluted spins in the neighborhood of dipolar coupled abundant spins [43]. This characterization was performed in collaboration with the Institute of Chemistry at the Otto von Guericke University.

Solid-State ^{29}Si NMR spectroscopy of solid catalysts

The basic structural units of zeolite catalysts are TO4 tetrahedra with silicon atoms at the central T-positions. In the second coordination sphere of these T-atoms various metal atoms, such aluminum, boron, gallium, iron and titanium, can be incorporated into the framework. Depending of the metal atoms that are incorporated the tetrahedrally coordinated silicon atoms (Q^4) are characterized by up to five different environments, denoted Si(nT) with n=0, 1, 2, 3 and 4. In the case of aluminum atoms incorporated at T-positions, each type of Si(nAl) species yields a ^{29}Si MAS NMR signal in a well-defined range of chemical shifts. Figure 4.3 summarizes the chemical shifts of these Si(nAl) species. The relative intensities of the ^{29}Si MAS NMR signals of the Si(nAl) species are a function of the framework composition.

In each catalyst, terminal hydroxyl groups bound to silicon atoms exist [Q^3, Si(3OSi,1OH); Q^2, Si(2OSi,2OH)]. These hydroxyl groups are located at the outer surface of zeolite particles or at internal framework defects. It is important to note that Si(1Al) species occur at the same resonance positions as Si(3Si,1OH).

The NMR spectra were recorded applying a Bruker Avance 300 NMR spectrometer at room temperature. The spectrometer was equipped with a 4 mm CP/MAS probehead BL4. The samples were introduced in 4 mm ZrO_2 rotors. The ^{29}Si CP-MAS spectra were recorded at 59.62 MHz. The proton 90° pulse was set to 2.7 μs, and the decoupling strength during acquisition was 69 kHz. The following conditions were applied: 15 kHz spinning rate, recycle delay of 8 s, contact time 5 ms. The ^{29}Si shifts was externally referenced to Q_8M_8.

Solid-State ^{27}Al NMR spectroscopy of solid catalysts

According to Löwenstein's rule, the formation of Al-O-Al bonds in aluminosilicates is forbidden and only Al(4Si) species can exist in the corresponding frameworks [43]. Therefore, ^{27}Al MAS NMR spectra of hydrated zeolite catalysts consist, in general, of

only one signal of framework aluminum atoms in a range of chemical shifts between ca. 35 and 60 ppm.

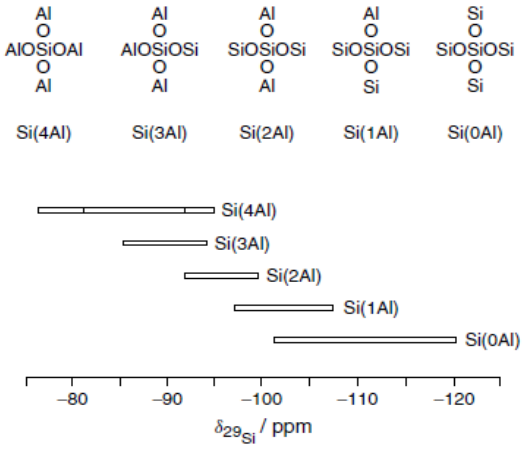

Figure 4.3. ^{29}Si NMR shift range of Si(nAl) species in the framework of zeolite catalysts. The shift values are referenced to tetramethylsilane [43].

Extra-framework aluminum species in hydrated zeolites are octahedrally coordinated AlO_6 species and cause ^{27}Al NMR signals at -15 and 0 ppm. In some cases, an additional broad signal occurs at 30-50 ppm, which is caused by aluminum atoms in a disturbed tetrahedral coordination or a pentacoordinated state.

The ^{27}Al MAS NMR spectra were recorded at 78.21 MHz at spinning rate of 8 kHz. The 90° pulse width 0.58 µs and 36000 scans were collected with a relaxation delay of 2 s. The ^{27}Al shifts scale was externally referenced to $[Al(H_2O)_6]^{3+}$. Spectra were acquired with a time domain of 8k data points and Fourier transformed using 16k data points.

4.4 Transmission Electron Microscopy

For studying supported catalysts, TEM is commonly applied form of electron microscopy. In general, the detection of supported particles is possible provided that there is sufficient contrast between the particles and the support. Contrast in the transmission mode is caused not only by the attenuation of electrons due to density and thickness variations over the sample, but also by diffraction and interference. One noteworthy of research is the application of TEM to investigate particle morphology in relation to metal support interaction [45]. This technique provides useful information about the topology and architecture of the solid catalyst. Also, it provides information about the pore diameter and about the structure of the pores in a porous material.

In transmission electron microscopy, which uses transmitted and diffracted electrons, the instrument is in a sense similar to an optical microscope, if one replaces optical lenses with electromagnetic lenses.

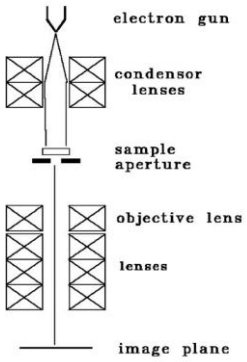

Figure 4.4. Schematic set-up of an electron microscope in TEM mode [45].

In TEM, a primary electron beam of high energy and high intensity passes through a condenser to produce parallel rays, which impinge on the sample. As the attenuation of the beam depends on the density and thickness, the transmitted electrons form a two-dimensional projection of the sample mass, which is subsequently magnified by the electron optics to produce the so-called bright-field image. The dark field image is obtained from the diffracted electron beams, which are slightly off-angle from the transmitted beam. Figure 4.4 shows a schematic representation of the electron microscope.

X-rays are among the *by*-products of electron microscopy. Today, it forms the basis for determining composition on a submicron scale and, with still increasing spatial resolution, in a technique referred to variously as electron microprobe analysis (EMA), electron probe microanalysis (EPMA) or energy-dispersive analysis of X-ray (EDX). The most convenient means of analyzing the emitted X-rays is with an energy dispersive X-ray detector located at a fixed position with respect to the sample. This detector is a liquid nitrogen-cooled solid-state device consisting of lithium-doped silicon [45].

TEM analyses were performed by using a Philips/FEI CM200 microscope. A sample of powdered catalyst was suspended in ethanol followed by ultrasonic dispersion. A drop of this suspension was placed on a carbon coated copper grid and it was allowed to dry. The apparatus was operated at an acceleration voltage of 200 kV and equipped with a CCD

camera for the imaging acquisition and ananalySISpro SIS/Olympus processing system. An EDAX DX-4 system was used for Energy Dispersive X-Ray analysis (EDX). This characterization was performed in collaboration with the Institute of Experimental Physics from the Otto von Guericke University.

4.5 Atomic absorption spectroscopy and optical emission spectroscopy

The determination and accurate control of bulk chemical composition is of paramount importance in monitoring and evaluating the properties and stability of catalysts. Bulk analysis is of crucial importance for quality assessment and for the assessment of the commercial value of typical materials before and after use in a catalytic processes [43]. Atoms in a flame absorb light. In atomic absorption spectroscopy (AAS), electronic transitions between the energy levels of atoms into excited states are generated by the absorption of photons in the visible frequency range. The change in intensity of the light beam is measured and correlated with the concentration relative to the absorbance of a calibration standard. The absorption lines are characteristic for each element. The comparatively low cost of the equipment, the high sample throughput, the wide concentration range, the low matrix and interference effects and the detection of element concentrations down to 0.1% explain the attraction of AAS.

In Inductively Coupled Plasma Optical Emission Spectroscopy (ICP-OES), a sample solution is transferred into the center of an inductively coupled argon plasma working at temperatures up to 8000 °C. The light emitted by the electronically excited elements passes through a diffraction grating and is resolved into a spectrum. After amplification and calibration against standards, quantitative analysis is possible. Simultaneous detection of many elements can be carried out down to about 0.5µg g^{-1}.

Elemental analysis based on Atomic Absorption Spectroscopy (AAS) was carried out using a Varian SpectrAA 800 system. The template-free samples were dissolved in nitric acid. With this technique bulk composition of nickel and aluminum was determined. This analysis was performed in collaboration with the Otto von Guericke University. The ICP analysis was performed in an external laboratory, LUS GmbH laboratory (Labor für Umweltschutz und chemische Analytik from Magdeburg Germany). This laboratory determined the bulk composition of molybdenum, wolfram, rhenium and nickel for the catalysts where these metals are involved.

4.6 NH_3-temperature programmed desorption

Temperature programmed desorption of NH_3, (NH_3-TPD) is a popular method for characterizing the acid strength of the sites from which the probe molecules were desorbed. Analogously, desorption of weak adsorbed probe molecules may be tested for characterizing the strength of basic sites. Desorption of the probe molecule may be monitored by gas chromatography (GC) or mass spectrometry (MS). In particular, when GC is employed one has a tool to measure simultaneously via the amount of the desorbed probes the density of sites. However, there are some pitfalls with the TPD technique. TPD is not selective, it is not possible to decide whether the probes are desorbing from Brønsted or Lewis acid sites when both are present. Therefore, in order to characterize the strength of the acid sites, it is advisable to combine TPD with an independent technique e.g. *in-situ* IR spectroscopy [43]. The TPD results may be corrupted by re-adsorption of the species desorbed from acid sites. In this case, the use of thin samples or sample layers may help [43].

TPD experiments are generally carried out in two experimental regimes: studies of materials having low surface areas at ultra-high vacuum conditions and studies of porous catalysts at ambient temperatures. In a typical experiment, the catalyst is contained in a reactor that can be heated at a linear rate. After pretreatment, the catalyst is saturated with a probe molecule under well-defined adsorption conditions. After the excess gas has been flushed out of the reactor, the sample is heated in a flowing inert gas stream. A thermocouple inserted in the catalyst measures the temperature and a detector downstream measures the effluent gas composition. The concentration of the desorbing gas in the effluent gas may be monitored by absorption/titration, thermal conductivity, flame ionization or mass spectrometry [43]. Alternatively, TPD experiments may be carried out using a microbalance to measure the changes in mass during heating.

By using NH_3-TPD, the total acidity of the catalysts was investigated. The samples were pretreated at 500 °C in helium for 2 h followed by cooling to 100 °C. Ammonia (1 vol.% NH_3 in He) was then adsorbed at the same temperature for 2 h. Physisorbed molecules were removed by switching back to a pure helium flow (also at 100 °C) for 1 h. Finally, the temperature was raised to 650 °C with 10 °C min^{-1}. Desorbed ammonia was detected with a thermal conductivity detector, TCD.

4.7 Diffuse reflectance infrared Fourier transform spectroscopy

The popularity of infrared spectrometry can in large part be attributed to its versatility, since samples may be readily studied as gases, liquids and solids [46]. The use of Diffuse Reflectance Infrared Fourier Transform Spectroscopy, (DRIFTS) helps to analyze samples under reactive atmosphere and without any previous preparation of the sample [47], which is considered its principal advantage. Any radiation focused on a surface can, depending on the characteristics of the surface and its environment, be absorbed, or diffused in all directions. The latter effect is of interest in diffuse reflection spectroscopy. As shown in Figure 4.5, infrared radiation may be directly reflected by the sample surface, giving rise to specular refraction. The radiation may undergo multiple reflections occurring at the surface on the particles and without penetrating the sample. The radiation that undergoes this type of diffuse specular reflection exits the surface at any angle relative to that of the incident beam. On the contrary, true diffuse reflection is the consequence of beam penetration into one or more particles and its diffusion in the sample. This component of the radiation also exits the sample at any angle but, since it has traveled through the particles, it contains data on the absorption properties of the material. However, diffuse reflection cannot be optically separated from specular reflection, but if the specular diffuse reflection component is weak compared with diffuse reflection it possible to obtain instructive information from a specific material.

As a rule, the specific properties of the material liable to influence the quality of the DRIFTS spectrum are as follows: (a) refractive index of the sample; (b) particle dimensions; (c) packing density; (d) homogeneity; (e) concentration; (f) absorption coefficients.

The DRIFTS technique offers the advantages of simpler sample preparation, the capacity to analyze nontransparent samples, irregular surfaces and coatings, exposure of the sample to simulated reaction conditions while analyzing the changes in the species at the material, recording of the spectrum of the powder at elevated temperature and/or under pressure.

The main drawback is the difficulty of performing quantitative measurements. The technique permits analysis of catalysts surfaces by using probe molecules. The acidity of MCM-41 materials can be determined [48]. Also, it is possible to study the nature of the

active sites for chemical reactions that are of industrial interest application, e. g. oligomerization of ethene on nickel containing molecular sieves [49].

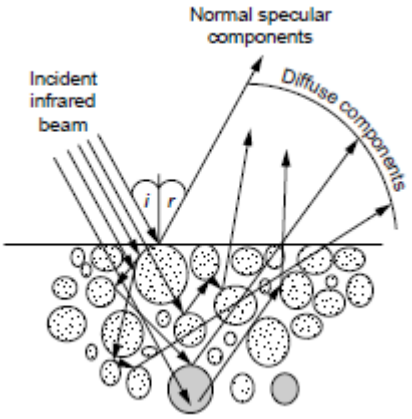

Figure 4.5. Mechanisms that generate the infrared spectrum of a powder [47].

The technique can be used under high pressure conditions, indicating that it is an attractive tool to study a catalytic system in similar conditions to those encountered during a catalytic reaction [47]. DRIFTS measurements were performed using a device available at the Max Planck Institute for Dynamics of Complex Technical Systems in the Process Systems Engineering group.

DRIFTS experiments to study the acidity of the catalysts

Pyridine-diffuse-reflectance FTIR spectra were collected using a smart collector and a high temperature environmental chamber equipped with ZnSe windows (Thermo Electron GmbH, Germany). The FTIR analyzer used in the experiments was a Nicolet 6700 equipped with a Ge/KBr beamsplitter and a DLaTGS detector (Thermo Electron GmbH, Germany). The stainless gas lines (He and He+pyridine) were connected to the collector. Initially, the powder catalyst was pre-treated at 400 °C for 60 min under a constant He flow, during the complete analysis, of 25 ml min^{-1}. The catalyst was cooled down at 50 °C and then the He was saturated with pyridine at room temperature and fed to the cell for 60 min. Finally, only He flow was passed through the cell during 30 min at 50 °C and the IR spectra was collected with a resolution of 4 cm^{-1} and 100 scans. The last procedure was repeated at 100 and 150 °C for all catalysts. The presented IR spectra were recorded against the background collected by using KBr dehydrated *in-situ* for 2 h at 400 °C under He flow.

In-situ ETP-DRIFTS experiments

In-situ ETP-DRIFTS experiments were performed to study the chemical species that are being formed during real reaction conditions in the ETP experiments. The apparatus is the same as used to study the acidity of the catalysts (see above). The conditions applied are described as follows: The stainless gas lines containing nitrogen and a mixture of 2.5 vol.% of ethene in nitrogen were connected to the cell. In the first step the catalyst was pretreated at 400 °C for 60 min under constant flow of nitrogen of 30 ml min^{-1} to clean the catalyst surface. The catalyst was cooling down to 50 °C and the spectrum (100 scans with a resolution of 4 cm^{-1}) was collected in presence of nitrogen against the background collected by using KBr dehydrated *in-situ* for 2 h at 400 °C under N_2 flow to analyze the surface of the catalyst. In this state the catalyst was used to collect the background to provide the reference when the mixture of ethene was present. In a second step, the mixture of ethene was fed to the collector with a flow rate of 11 ml min^{-1} and after 30 min the spectrum was collected. The following temperature was 100 °C and the spectrum was also collected after 30 min. In general, the temperature was changed in intervals of 50 °C, being 450 °C the highest. For all temperatures, the spectra were collected after 30 min at each temperature by using the background at 50 °C in the presence of nitrogen at 30 ml min^{-1}. At the end of experiments the catalyst was flushed with nitrogen during 15 minutes and the correspondent spectrum was recorded by using also the background at 50 °C only with nitrogen.

4.8 H_2-temperature programmed reduction and temperature programmed oxidation

In temperature programmed reduction (TPR) a reducible catalyst or catalyst precursor is exposed to a flow of a reducing gas mixture, typically nitrogen or argon containing hydrogen (H_2-TPR) while the temperature is increased linearly. The rate of reduction is continuously followed by measuring the composition of the reducing gas mixture at the outlet of the reactor. The experiment permits the determination of the total amount of hydrogen consumed, from which the degree of reduction of the solid material after reduction can be calculated. Since this simple and low-cost technique, it has become a very useful and important tool [43].

Figure 4.6 shows the scheme of a typical set-up for TPR experiments. It consists of a fixed-bed reactor in a furnace that can be temperature programmed and a thermal

conductivity detector for the determination of the gas composition. The gas flows are stabilized by mass flow controllers and the reducing feed gas mixture passes through a deoxygenation catalyst-molecular sieve unit before it enters the reference cell of the TCD.

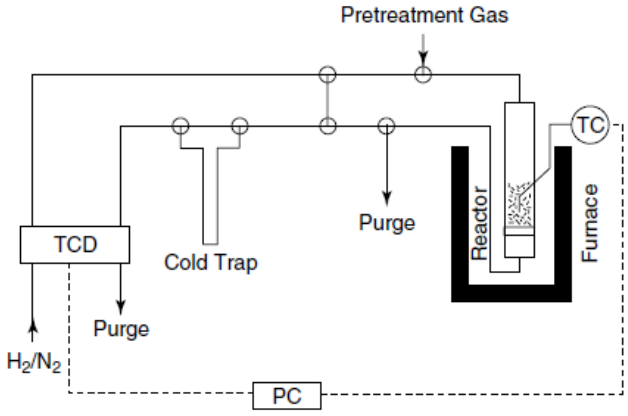

Figure 4.6. Scheme of a typical TPR setup; TCD, thermal conductivity detector; TC, thermocouple [43].

The gas mixture then flows through the catalyst bed in the reactor and through a cold trap before it enters the measuring cell of the TCD. The H_2 consumption is monitored and recorded simultaneously with the sample temperature on a computer. With some modifications and addition of a quadrupole mass spectrometer, systems of this type can also be used for CO-TPR, for TPD experiments and for TPO. TPR and TPO experiments are often carried out in a cyclic manner, particularly in investigations of redox properties of selective oxidation catalysts [43]. Information on structural changes and physical properties of solid catalyst cannot be obtained by using TPR or TPO experiments [43].

The reducibility of the catalyst was studied in a BEL-CAT Catalyst Analyzer (BEL Japan Inc.) using hydrogen. The samples were pretreated for 1 h at 600 °C in synthetic air (25 ml/min) followed by cooling to 100 ºC in a pure argon stream (25 ml/min). After switching to 10 vol % of H_2 in Ar (total flow rate: 25 ml/min), temperature was increased linearly with 10 °C min^{-1} from 100 to 1100 °C. TPO was carried out in the same device with a 5 vol.% of O_2 in He. The samples were pre-treated at 100 °C for 1 h under He flow followed by cooling to 50 °C. Then, the mixture of O_2 and He was passed through the sample and the temperature was raised to 1100 °C with a temperature ramp of 5 °C min^{-1}. Change in O_2 composition was detected with a TCD. All TPO and H_2-TPR data were normalized to the respective sample weight and expressed in arbitrary units.

4.9 Gas chromatography and mass spectrometry

Gas chromatography (GC) is probably the most versatile method for the analysis of complex mixtures [43]. Since many heterogeneously catalyzed reactions are gas-phase reactions where the products have sufficient volatility, they can be analyzed by GC on suitable columns using adapted temperatures programs. GC is not an inherently fast analytical method, especially if the separation method is not isothermal, the cooling times can increase the overall cycle time substantially. Two GC methods can be mentioned; the micro-GC systems where analysis times decrease substantially and the two-dimensional chromatographic methods allowing shortening the analysis times, since those sections of the chromatogram that are difficult to resolve and thus would need longer run times are injected into a second column, which allows efficient separation of these compounds [43]. Mass spectrometry is another generally applicable technology, which can be adapted to almost any high-throughput reactor. However, compared with gas chromatography, mass spectrometry is less easily quantified due to fragmentation and resulting overlap of signals [43].

The analysis of the reaction products was carried out by an online gas chromatograph (Agilent 6890 GC/TCD with a 5973 MSD) equipped with a 30 m length HP-Plot Q column (Agilent Technologies).

4.10 Summary

In this chapter a description of the characterization technique applied in this work has been given. The experimental procedures that were used to perform these characterization experiments were also provided. In the next chapter, details of the procedure and synthesis conditions of the metallic based mesostructured catalysts will be mentioned. Furthermore, a description of the experimental setup applied to perform the ETP experiments will be provided together with the reaction conditions under which the ETP-experiments were carried out.

CHAPTER V

Experimental methods

The first part of this chapter focuses on the synthesis of the MCM-41 and Al modified MCM-41. Their synthesis is based on two different synthesis procedures; namely Noreña-Franco et al., and Vinu et al., procedures. The second part is devoted to the procedures and the experimental conditions that were used to prepare the metallic based mesoporous catalysts. The last part provides a description of the experimental setup that was used to perform the ETP experiments with the synthesized catalysts. Additionally, it describes the reaction conditions under which the ETP experiments were carried out including deactivation experiments and deactivation-regeneration experiments. MCM-41 and AlMCM-41 were prepared in a wide interval of Si/Al ratios (∞-5), but it will be shown that the Si/Al ratios of ∞, 150, 60, 16 and 5 provided the catalysts where big changes in the ETP-reaction could be observed. For these reason, the discussion of the results obtained in this work will be focus only on these Si/Al ratios. A list of the equipment and chemicals used is detailed in the Appendix A and C.

5.1 Synthesis of MCM-41 and MCM-41 modified with aluminum, AlMCM-41

Synthesis of MCM-41 and MCM-41 modified with aluminum (AlMCM-41) according to Noreña-Franco et al (2002).

MCM-41 and AlMCM-41 were prepared by a modification of the method used by Noreña-Franco et al., [50]. Tetrabutylammonium silicate was prepared with a mixture of 5.4 g of a solution of tetrabutylammonium hydroxide 40 wt.% (Sigma-Aldrich, TBAOH)

and 0.6 g of silica fumed (Sigma-Aldrich). The latter component was mixed with another solution formed by 3.42 g of cetyltrimethylammonium bromide, CTABr (Merck, CTABr ≥ 97 %) and 9.1 g of deionized water. The resultant mixture was stirred by hand during 15 minutes and had a molar composition of 1 SiO_2: 0.35 CTABr: 0.31 TBAOH: 0.0-0.2 $NaAlO_2$: 25.5 H_2O. Sodium aluminate ($NaAlO_2$: Al_2O_3 50-56 % and Na_2O 40-45 %) was used as aluminum source and its amount was adjusted for having different Si/Al ratios (150, 60, 16 and 5). After that, the mixture was transferred into a Nalgene bottle and aged 48 hours at 100 °C. The white solid was recovered by vacuum filtration and washed with deionized water. The final powder was dried at 80 °C for 6 hours (as-synthesized AlMCM-41). A sample was calcinated in air at 225 °C for 3 hours and at 540 °C for 6 hours at a heating rate of 1 °C min^{-1} in order to carry out the corresponding characterization. Siliceous MCM-41 was synthesized in the same manner but without any use of $NaAlO_2$. A mixture composition of 1 SiO_2: 0.35 CTABr: 0.31 TBAOH: 0.0-0.2 $NaAlO_2$: 55.0 H_2O provide a better structured MCM-41 and AlMCM-41 but the catalytic behavior was not improved (see chapter VI).

Synthesis of MCM-41 and MCM-41 modified with aluminum (AlMCM-41) according to Vinu et al (2004).

MCM-41 and AlMCM-41 were also prepared alternatively using a different method reported in the literature by Vinu et al in 2004 [51]. A solution of 16 g of tetradecyltrimethylammonium bromide (Sigma Aldrich, TDTABr) together with 55 g of deionized water was prepared and stirred during 30 min. Thereafter, 18.7 g of sodium silicate solution (Sigma Aldrich) was added drop wise to the surfactant solution during 30 min under vigorous stirring. The resultant mixture was vigorous stirred for other 30 min. In this step $NaAlO_2$ (Al_2O_3 50-56 % and Na_2O 40-45 %) in 5 g of deionized water was added to the components mixture and stirred 15 min. The amount of $NaAlO_2$ was adjusted for having the following Si/Al ratios, ∞, 400, 60, 16 and 5. An amount of 1.2 g of H_2SO_4 in 5.0 g of H_2O was used to adjust the pH value of around 11.5. The mixture of all components was stirred for 30 min additionally. After that, the mixture was transferred into a Nalgene bottle and aged 24 hours at 100 °C. The composition of the resultant mixture is the following; 1 SiO_2: 0.58 TDTABr: 0.39 Na_2O: 0.0-0.2 $NaAlO_2$: 0.15 H_2SO_4: 51.8 H_2O. The white solid was recovered by vacuum filtration and washed with deionized water. The final powder was dried at 80 °C for 6 hours (as-synthesized AlMCM-41). A sample was calcinated in air at 225 °C for 3 hours and at 540 °C for 6

hours at a heating rate of 1 °C min^{-1} in order to carry out the corresponding characterization. Siliceous MCM-41 was synthesized in the same manner but without any use of $NaAlO_2$.

The synthesis of the catalysts was carried out as follows.

5.2 Synthesis of Ni, Re and Mo on MCM-41 and AlMCM-41 catalysts

Nickel on MCM-41 and Ni on AlMCM-41 catalysts were prepared by using the template ion exchange method (TIE), incipient wetness impregnation (IWI), and equilibrium adsorption method (EA). Mo and Re on MCM-41 and on AlMCM-41 catalysts were prepared by TIE, IWI, thermal spreading, (TS) and wet impregnation, (WI). The *bi*-metallic catalysts nickel-rhenium and nickel-molybdenum were synthesized by using the TIE method unless another method is stated. A full description of synthesis conditions that were used for each method is provided as follows:

a) Template ion exchange method, TIE

This method was reported in 1997 by Yonemitsu et al. [52]. In this method the template ions of as-synthesized (uncalcinated) MCM-41 and AlMCM-41 can be exchanged for metallic ions in an aqueous solution. In a typical procedure 3.0 g of as-synthesized MCM-41 or AlMCM-41 was mixed with 30 ml of deionized water. The latter mixture was contacted with 30 ml of a 0.03 molar nickel solution under dropwise dosing and vigorous stirring. Nickel nitrate (Merck, $Ni(NO_3)_2 \bullet 6H_2O \geq 99.0$ %) was used as Ni precursor. The resulting mixture was transferred into a Nalgene bottle and treated at 80 °C for 20 h without stirring. The light-green solid was recovered by vacuum filtration, washed with 300 ml of deionized water and dried at 80 °C for 24 h. The final product was calcinated at 600 °C for 6 h in air. The rate of heating was 5 °C min^{-1}.

b) Incipient wetness impregnation, IWI

This method is described as follows; the previously dried and calcinated support (in this case, MCM-41 and AlMCM-41) with a volume of solution containing the selected precursor that contains the metal of interest. This volume of solution is equivalent to the pore volume of the corresponding MCM-41 and AlMCM-41 [43]. In a classical procedure 1.2 g of MCM-41 or AlMCM-41 was put in contact with a solution of 1.45 mg

of nickel precursor dissolved in 1.65 ml of deionized water. The precursor of nickel was nickel nitrate (Merck, $Ni_2(NO_3)_2 \bullet 6H_2O \geq 99.0$ %). After this, the resultant material was dried at room temperature for 24 h and calcinated at 600 °C for 6 h with a heating rate of 5 °C min^{-1}. The precursors for Mo and Re based catalysts are the following; ammonium heptamolybdate tetrahydrate (Merck, 99.3%) and ammonium perrhenate (Sigma Aldrich, 99%), respectively.

c) Equilibrium adsorption, EA

Surface layered silicate is widely reported to be produced by loading of nickel ion as amine-complex onto silica in a basic aqueous solution and heating at 350-800 °C [21]. For this reason, this method was also used to prepare Ni on MCM-41 and Ni on AlMCM-41. In a typical procedure, 1.3 g of calcinated MCM-41 or AlMCM-41 was put in contact with 26 ml of a solution containing 10.2 ml of ammonia solution (32% ammonia) and nickel. After the mixture of these components, the total concentration of nickel was 0.015 molar. The suspension was vigorous stirred during 60 min. The resulting mixture was transferred into a Teflon bottle and treated at 80 °C for 20 h without stirring. The solid was recovered by vacuum filtration, washed with 300 ml of deionized water and dried at 80 °C for 24 h. The final product was calcinated at 600 °C for 6 h in air. The rate of heating was 1 °C min^{-1}.

d) Thermal spreading, TS

Recently results in the literature have shown that molybdenum trioxide can be transported in the gas phase and spread at the surface of another solid if an appropriate thermal treatment is applied. This treatment can be successfully applied for the synthesis of metathesis catalysts [53]. A normal synthesis procedure can be described as follows: 1.2 g of calcinated MCM-41 or AlMCM-41 was put in contact with a fixed amount of metal precursor. The amount could be manipulated for adjusting the desired metal loading. These components were mechanically mixed by using an agata mortar during 15 min. The mixture was then placed in a muffle furnace and heated to 500 °C for 8 h under static air. The heating rate was of 1 °C min^{-1}. This method was used to prepare only the Mo and Re based catalysts. The Mo and Re precursors were molybdenum oxide (Merck) and ammonium perrhenate (Sigma Aldrich, 99%), respectively.

e) Wet impregnation, WI

In this method, an excess of solution containing the metal precursor is put in contact with the calcinated support, MCM-41 or AlMCM-41. In a normal procedure, 1.2 g of MCM-41 or AlMCM-41 was put in contact with 60 g of a solution of precursor containing the metal of interest. The amount of precursor depends on the desired metal loading in each catalyst. This solution was stirred vigorously for 2 h. Water was then evaporated under reduced pressure in a rotavapor at 40 °C. The recovered solid was dried at 110 °C for 24 h and calcinated at 500 °C for 2 h in a muffle furnace in air. The heating rate was 1 °C min^{-1}. This method was used to prepare only the Mo and Re based catalysts.

5.3 Testing of the catalysts in the ETP-reaction

Catalytic activity measurements in the ETP-reaction were carried out using a fixed-bed reactor operated automatically. A scheme is given in Figure 5.1. This reactor consists of a quartz tube with an inner diameter of 0.6 cm and it is operated at atmospheric pressure. A standard ETP experiment was carried out with 0.5 g of catalyst and at a constant GHSV of 1.4 l $h^{-1}g_{cat}^{-1}$ (Gas Hourly Space Velocity, GHSV = feed flow g_{cat}^{-1}). The feed was a mixture of 10% ethene (99.95 %) in nitrogen (99.999 %). The length of the catalytic bed was around 10 cm. The temperature was modified in the interval from 50 to 475 °C by increments of 25 °C. A list with all gases and hydrocarbons that were used in this project can be found in Appendix A and B.

The configuration of the reactor allowed performing different type of experiments by changing the reactor feed. This was used to perform isomerization of butene isomers and metathesis of ethene and *2*-butene and the *retro*-metathesis of propene. Additionally, the experimental setup allowed studying the effect of the reaction conditions on the ETP-reaction. The experimental setup is capable to operate during long periods. Therefore, deactivation and regeneration experiments could be performed.

The previous aspects were studied based on the conditions used in the standard ETP experiment (described previously) and changing a parameter that have an important effect in the ETP-reaction. The experimental setup contained a total oxidation reactor to burn the hydrocarbons to CO_2 and H_2O.

Additionally to the standard ETP experiment described previously, the following experiments were performed;

1. Effect of the reaction conditions; ETP experiments with changes in feed composition, and feed flow rate were carried out. The reactions conditions were the same used in the standard ETP experiment.

2. Temperature effect; heating up and cooling down cycles were carried out by using the same reaction conditions that were used in the standard experiment. These experiments were performed to study the stability of the catalysts by a repetition of the standard experiment.

3. Deactivation experiments –Time on stream--; experiments at 250, 350 and 450 °C were carried out under different reaction times; 1, 5, 15, 30, 60 and 107 h. The reaction conditions were the same used in the standard ETP experiment.

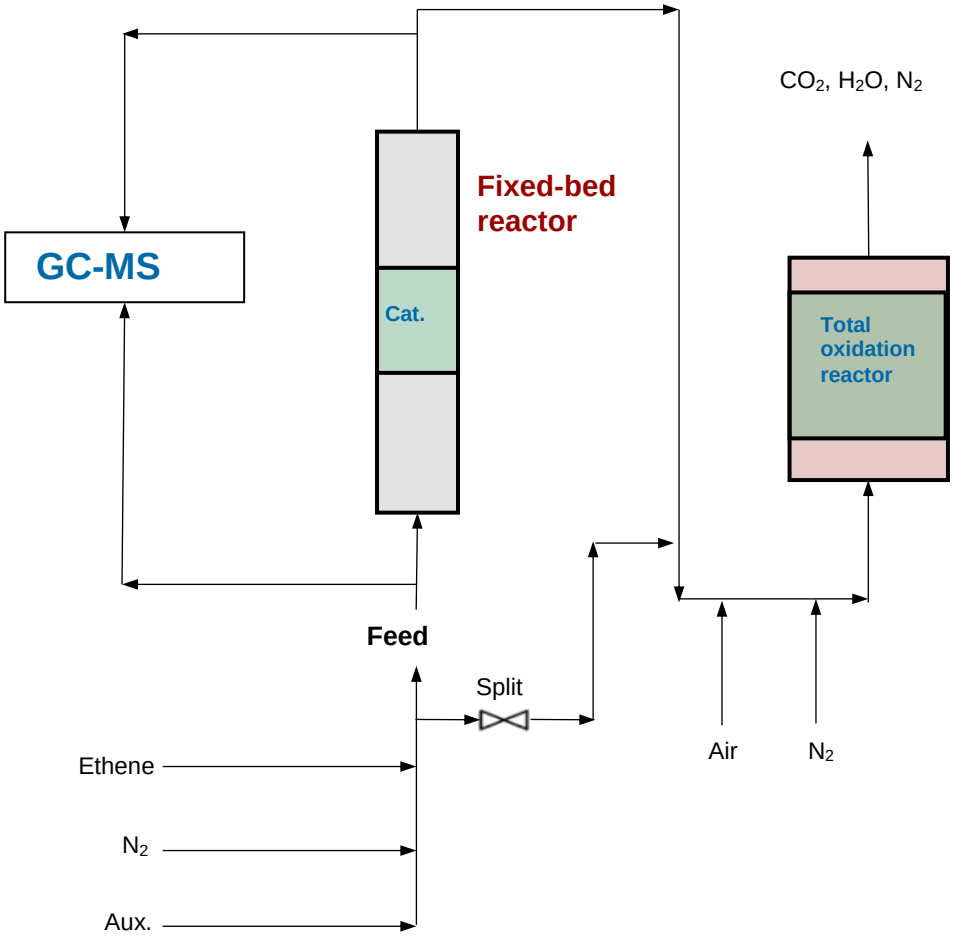

Figure 5.1. Experimental setup used for studying the ETP-reaction; fixed bed reactor and total oxidation reactor.

4. Deactivation-regeneration experiments; A deactivation-regeneration cycle consists of a step of deactivation of the catalysts for 30 h in the first part and its regeneration by using a mixture of oxygen of 5 vol.% in nitrogen for 1 h in a second part. The reaction conditions were the same as the ones for a standard ETP experiment but with a GHSV of 2.8 $l\ h^{-1}g_{cat}^{-1}$ in the regeneration step. Deactivation of the catalyst was carried out at 250 °C for 30 h where the temperature of the first regeneration cycle was 450 °C. The reactivation temperature for the second and the third cycles was 500 and 550 °C, respectively. The same type of experiments was carried out at 350 and 450 °C in the deactivation step.

5. Isomerization of 1-butene, cis-butene, trans-butene; to study the reaction mechanism in the ETP-reaction, the isomerization of butene isomers were carried out. The reaction conditions were the same as used in the standard ETP experiment but the feed consists of 2 vol.% of *1*- or *cis*- or *trans*-butene with a GHSV of 200 $l\ h^{-1}g_{cat}^{-1}$.

6. Metathesis of ethene and 2-butene (trans- or cis-butene); metathesis of ethene and *trans*- or *cis*-butene was carried out. The reactions conditions were the same used in the standard ETP experiment but the feed consists of a mixture of ethene and *trans*- or *cis*-butene with a feed concentration of 2.5 vol.% for each. Total hydrocarbon composition was 5 vol.%.

7. Metathesis of propene to 2-butene and ethene; metathesis of propene was carried out by feeding a mixture of propene in nitrogen at 5 vol.% of feed composition. The reaction conditions were the same used in the standard ETP experiments.

The identification and quantification of the reactants and reaction products can be made by gas chromatography coupled to mass spectrometry (GC/MS). For this reason, the experimental setup is connected to an Agilent 6890 GC/TCD with a 5973 MSD chromatograph/mass spectrometer equipped with two 30 m length HP-Plot Q columns (Agilent Technologies). One column was used to perform the gas chromatography analysis and the second one to perform the mass spectrometry analysis. In the next chapter the results obtained in this work will be presented.

The criteria to define the behavior of the experiments involved in the study of the ETP-reaction is defined in function of three kinetic parameters; conversion of the

reactants and the selectivity and yield of the reaction products. These parameters are defined as follows:

$$reactant\ conversion = \frac{reactant\ consumed}{reactant\ fed} * 100$$

$$products\ selectivity = \frac{product\ generated}{reactant\ consumed} * \frac{\gamma_{react.}}{\gamma_{prod.}} * 100$$

where $\gamma_{react.}$ is the reactant stoichiometric coefficient and $\gamma_{prod.}$ is the corresponding product stoichiometric coefficient. The yield can be obtained by multiplying conversion with the respective selectivity.

The selectivity for the metathesis of ethene and *2*-butene (*cis*- or *trans*-butene) was defined as:

$$products\ selectivity = \frac{product\ generated}{total\ products\ formed} * 100$$

CHAPTER VI

Results and discussion

This main chapter of the thesis is structured as follows: the first part is devoted to the results obtained with the catalysts synthetized according to Norena-Franco et al. (2002) [50]. The second part shows the results obtained according to Vinu et al. (2004) [51]. The results devoted to the effect of the reaction conditions and to the deactivation, deactivation-regeneration experiments are discussed in the third part. The fourth part of this chapter is devoted to study the reaction mechanism in the ETP-reaction. In the fifth part, results of the metathesis experiments using Mo, and Re based catalysts are shown. The results of the *bi*-metallic formulation of the catalysts are given in sixth part of chapter VI. Finally, in the last part of this chapter an error analysis will be provided to estimate the uncertainty of the results in the ETP-reaction experiments

As it was stated in chapter V, MCM-41 was prepared at different Si/Al ratios; ∞, 150, 60, 16 and 5 according to Noreña-Franco et al., (2002) and ∞, 400, 60 16 and 5 according to Vinu et al., (2004). For this reason, the final catalysts were selected to these Si/Al ratios independently of the method used to prepare them. All the results and discussion are based on these Si/Al ratios.

It has been reported in the literature that template ion exchange is the best method to prepare Ni ion loaded MCM-41 catalysts with high catalytic activity [20-24, 27, 37]. Therefore, the results obtained from the catalysts prepared by template ion exchange are shown in the first part of the chapter. A brief catalytic comparison with the catalysts prepared by equilibrium and incipient wetness impregnation methods is shown. This is to

confirm the effectiveness of the template ion exchange method to prepare Ni ion loaded MCM-41/AlMCM-41 catalysts.

The results of the first part of this chapter have been already published in the Journal of Catalysis (J. Catal. 305(2013)154). For this reason, the results shown in this part are very similar to the results already published.

In the next sections, all the results obtained from the different characterization and catalytic tests will be analyzed and discussed.

6.1 Ni/MCM-41 and Ni/AlMCM-41 based on Noreña-Franco et al.

6.1.1 N_2-adsorption, powder XRD and AAS

Figure 6.1.1.1 reveals the structural characterization of the prepared Ni/MCM-41 and Ni/AlMCM-41 catalysts. The crystalline Ni/MCM-41 and Ni/AlMCM-41 are characterized by a broad band at low angles in a XRD diffraction pattern and by a Type IV N_2-adsorption isotherm [54, 55]. In Figure 6.1.1.1(a) the diffraction patterns and in Figure 6.1.1.1(b) the N_2-adsorption isotherms of the synthesized catalysts are given. From the spectra 6.1.1.1(a), it is possible to observe that the catalyst without Al has a highly hexagonal ordered structure with the classic diffractions (100), (110), (200) and (210) [54]. For Ni/AlMCM-41 catalysts the intensity of all last diffractions is diminished, which means that the hexagonal phase in these catalysts is less ordered compared to the catalyst without Al. Therefore, it is concluded that the hexagonal ordering degree of the MCM-41 is very sensitive to the presence of Al during the synthesis, even at high Si/Al ratios.

Table 6.1.1.1
N_2-adsorption data and Ni-composition of Ni/MCM-41 and Ni/AlMCM-41.

Catalyst Si/Al ratio	BET specific surface area, $m^2\ g^{-1}$	PV[1] $cm^3\ g^{-1}$	BJH-PD[2], nm	NLDFT-PD[3], nm	Ni-content[4], wt.%
∞	1 087	1.0	3.0	4.1	4.0
150	1 385	1.0	3.0	3.9	4.4
60	919	1.0	3.0	4.1	4.6
16	928	0.9	3.0	4.1	3.7
5	533	0.5	3.0	3.5	2.8

[1]Pore Volume. [2]Pore diameter determined by Barret-Joyner-Halenda method (BJH) and [3]nonlocal density functional theory (NLDFT) from the desorption branch. [4]determined by atomic absorption spectroscopy (AAS).

The N_2-adsorption measurements for these catalysts are characterized by a type-IV isotherm and H1 hysteresis according to IUPAC classification [44]. Such behavior corresponds to the MCM-41 materials and they present capillary condensation at relative

pressure between 0.30-0.35 [54]. The N_2-adsorption data and Ni-content of the Ni/MCM-41 and Ni/AlMCM-41 are summarized in Table 6.1.1.1. Two different methods were used to determine the pore size distribution, Barret-Joyner-Halenda method (BJH-method) and the nonlocal density functional theory (NLDFT) from the desorption branch. From these results it is observed that BJH-pore diameter is the same for all catalysts, which is an indication that this method underestimate the pore diameter size and the NLDFT is more accurate to determine the pore diameter of the MCM-41 materials [56, 57].

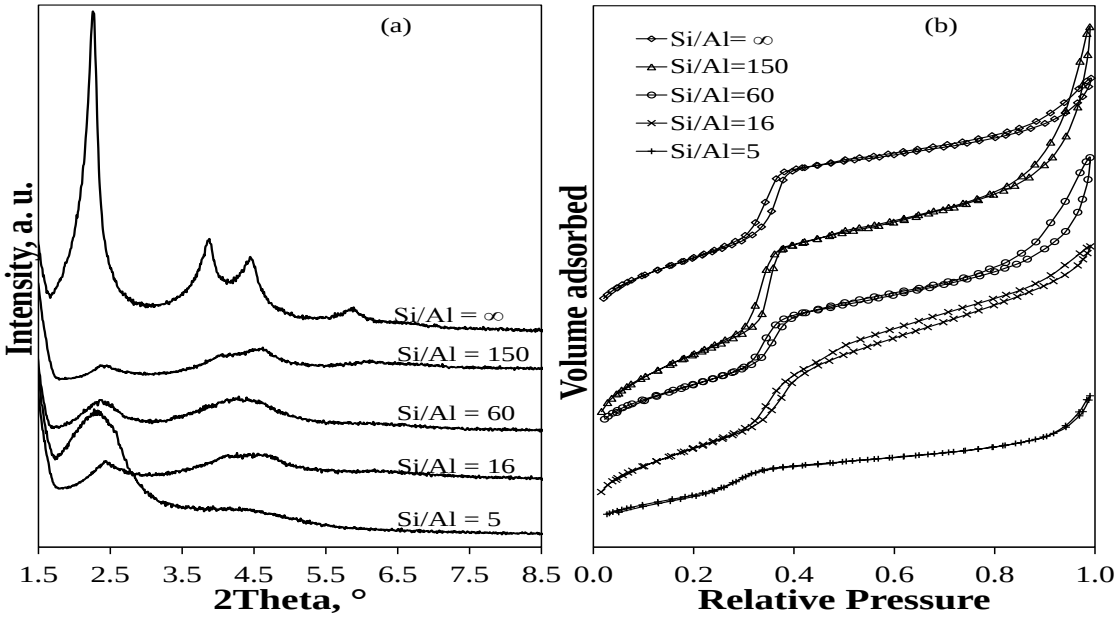

Figure 6.1.1.1. Powder XRD patterns (a) and N_2-physisorption isotherms (b) of Ni/MCM-41 and Ni/AlMCM-41 at different Si/Al ratios.

The N_2-adsorption data depend on the Si/Al ratio. The BET specific surface was around 1000 m^2 g^{-1} for almost all catalysts, which is typical for MCM-41 materials [54]. More detailed data are given in Table 6.1.1.1. The catalyst with a Si/Al ratio of 5 showed the lowest BET specific surface, pore volume and pore size. Therefore, from the XRD and N_2-physisorption results it is concluded that the Ni/MCM-41 and Ni/AlMCM-41 with a Si/Al ratio of 150, 60 and 16 presented the classic structure of the MCM-41 materials.

The Ni content depends also on the Si/Al ratio and the catalyst with a Si/Al ratio of 60 revealed the highest Ni content, 4.6 wt.%. For lower Si/Al ratios than 60, the Ni content decreased reaching 2.8 wt.% for the catalyst with a Si/Al ratio of 5. This fact must have

an impact on the catalytic behavior and might be also responsible of the differences in catalytic activity. The catalytic results are shown in the next section.

6.1.2 Testing of the catalysts in the ETP-reaction

Figure 6.1.2.1 and 6.1.2.2 illustrate the conversion of ethene and the selectivity of the major reaction products (propene and butenes) in the ETP-reaction as a function of temperature for the catalysts with different Si/Al ratios. The Ni/MCM-41 catalyst revealed a low conversion of ethene and low propene selectivity. Thus, the results are not comparable to the observations of Iwamoto et al., and Lehmann et al., but they used a different synthesis procedure and different conditions during the synthesis, as well as different source of silica [20, 21, 26]. The addition of small amounts of Al during the synthesis of the support has a strong impact on the catalytic behavior of the Ni/MCM-41 catalysts.

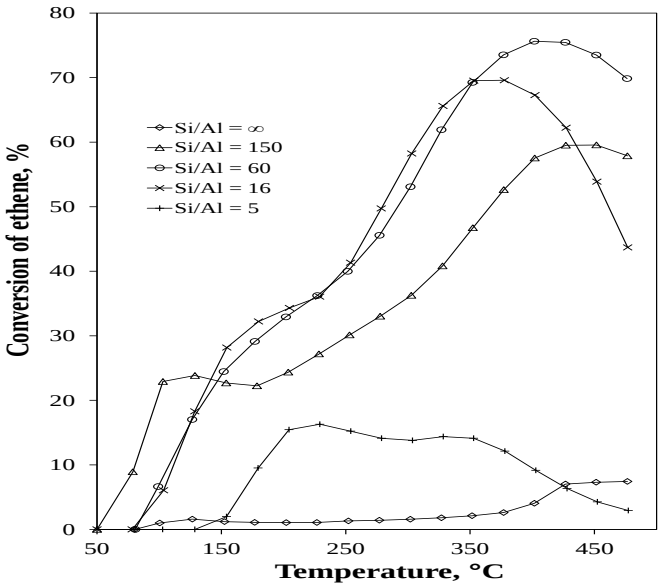

Figure 6.1.2.1. Conversion of ethene on Ni/MCM-41 and Ni/AlMCM-41 at different Si/Al ratios as a function of temperature. Ethene conversion = (ethene consumed / ethene fed)*100.

It can be seen in Figure 6.1.2.1 that the conversion of ethene increased with an increasing amount of Al (lower Si/Al ratios). The same behavior is observed for the selectivity of propene, depicted in Figure 6.1.2.2(a), which reached a maximum at a Si/Al ratio of 16. This behavior is in a good agreement with the results obtained by Lin et al., in the ETP-reaction on H-ZSM-5 [30]. They conclude that the Al incorporation increases the Brønsted acidity of the H-ZSM-5 and they are the active sites for the ETP-reaction.

Therefore this fact may also explain the differences between the results obtained in this work and the results obtained by Iwamoto et al., and Lehmann et al., for Ni/MCM-41.

For Si/Al ratios lower than 16 both, the conversion and selectivity of propene diminished. This reduction in the catalytic activity might be influenced by the reduction of the specific surface and the reduction of the Ni content. The selectivity of butenes is also given in Figure 6.1.2.2. From this Figure it is possible to observe that the selectivity of the two different butenes isomers is also directly influenced by the Si/Al ratio. The selectivity of *2*-butene is the sum of the selectivities of *cis*-butene and *trans*-butene. These selectivities can be grouped in three different intervals, low temperatures (50-150 °C), intermediate temperatures (150-300 °C) and high temperatures (300-475 °C).
The Ni/MCM-41 catalyst showed a high selectivity of *1*-butene at the low temperature region, indicating a dimerization reaction of ethene.

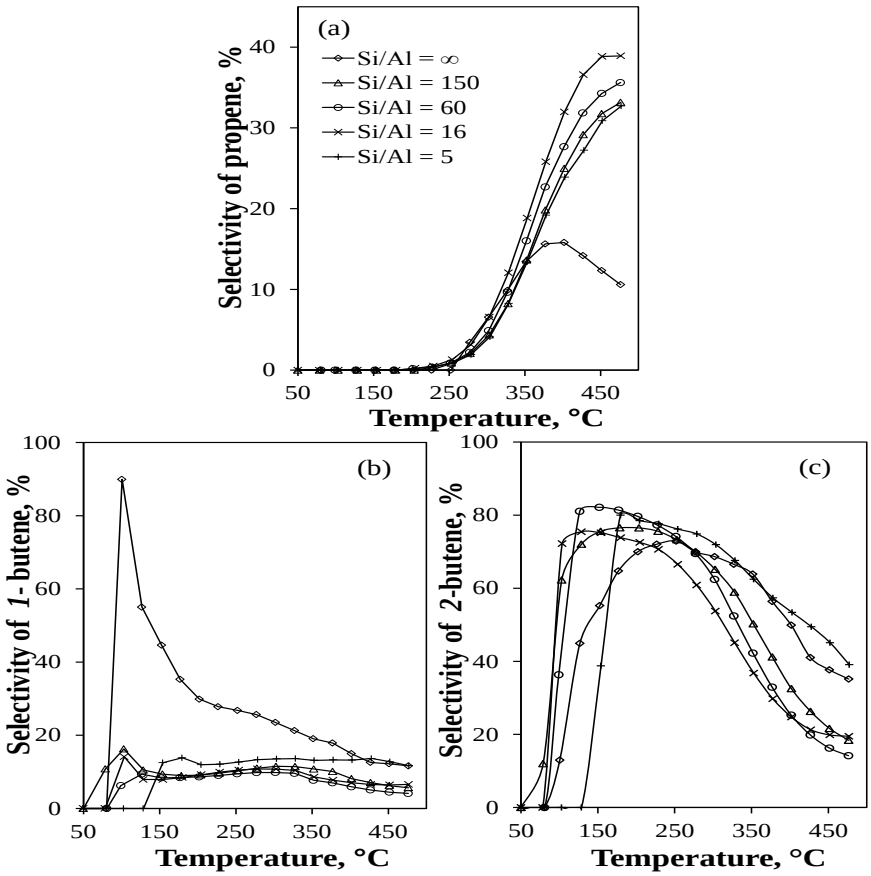

Figure 6.1.2.2. Selectivity of the major reaction products as a function of temperature and the Si/Al ratio: (a) propene, (b) *1*-butene and (c) *2*-butene. Propene selectivity = (propene generated / ethene consumed) (3/2)*100. Butene selectivity = (butene generated / ethene consumed) (4/2)*100.

With increasing temperature, the selectivity of *1*-butene is decreased (Figure 6.1.2.2(b)) and the selectivity of *2*-butene increases (Figure 6.1.2.2(c)) reaching a maximum in the

interval of intermediate temperatures. This is an indication that the *1*-butene is being isomerized to *2*-butene. No formation of *iso*-butene was observed indicating a low acidity of the catalysts. According to Hulea et al., [58] Ni-exchanged AlMCM-41 is an efficient bifunctional catalyst for the ethylene oligomerization [58].

Therefore this type of reactions may also take place for the reaction conditions investigated in this work. In the interval of high temperature it is observed that the selectivity of *2*-butene is diminishing and the selectivity of propene is increased, reaching a maximum at around 375 °C, (Figure 6.1.3(a)). This result suggests that on Ni/MCM-41 a metathesis reaction between *2*-butene and another molecule of ethene is taking place, as reported by Iwamoto [20]. The maximum in Figure 6.1.2.2(a) indicates that propene is consumed at higher temperatures to form probably long-chain hydrocarbons according to Hulea et al. [58].

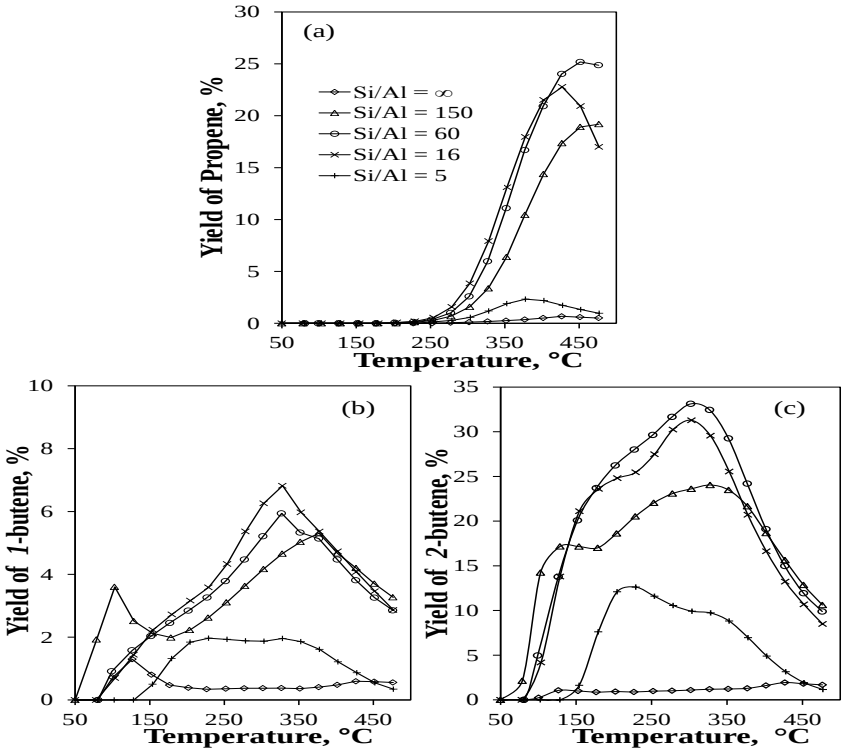

Figure 6.1.2.3. Yield of the major reaction products as a function of temperature and the Si/Al ratio: (a) propene, (b) *1*-butene and (c) *2*-butene. Propene yield = (propene generated / ethene fed) (3/2)*100. Butene yield = (butene generated / ethene fed) (4/2)*100.

The selectivity of *1*-butene was lower than 20 % for all Ni/AlMCM-41 catalysts at all temperatures investigated. This behavior indicates that the isomerization step is fast in comparison with the dimerization and metathesis steps, which is in concordance with the results reported in the literature regarding the isomerization of *1*-butene [59, 60]. The selectivity of *2*-butene (*cis*- and *trans*-butene) strongly depends on the Si/Al ratio. A

higher selectivity is obtained for lower Si/Al ratios reaching a maximum at Si/Al = 60. In the region of low temperatures, the selectivity of *2*-butene is high and showed a light decrement in the interval of intermediate temperatures. This behavior was observed for all Ni/AlMCM-41 catalysts. For the region of high temperatures this decrement is more pronounced, indicating probably that *2*-butene is consumed for the production of propene through a metathesis step. Figure 6.1.2.3 shows the yield of propene, *1*-butene and *2*-butene as a function of temperature at different Si/Al ratios. From this Figure it is possible to observe that the Ni/AlMCM-41 catalyst with a Si/Al ratio of 60 provides the highest yield of propene in the region of high temperatures, Figure 6.1.2.3(a). These results show that the Si/Al ratio, i. e. the number of active sites of the catalysts and their relative acidity, has a strong influence on the product distribution in the ETP-reaction.

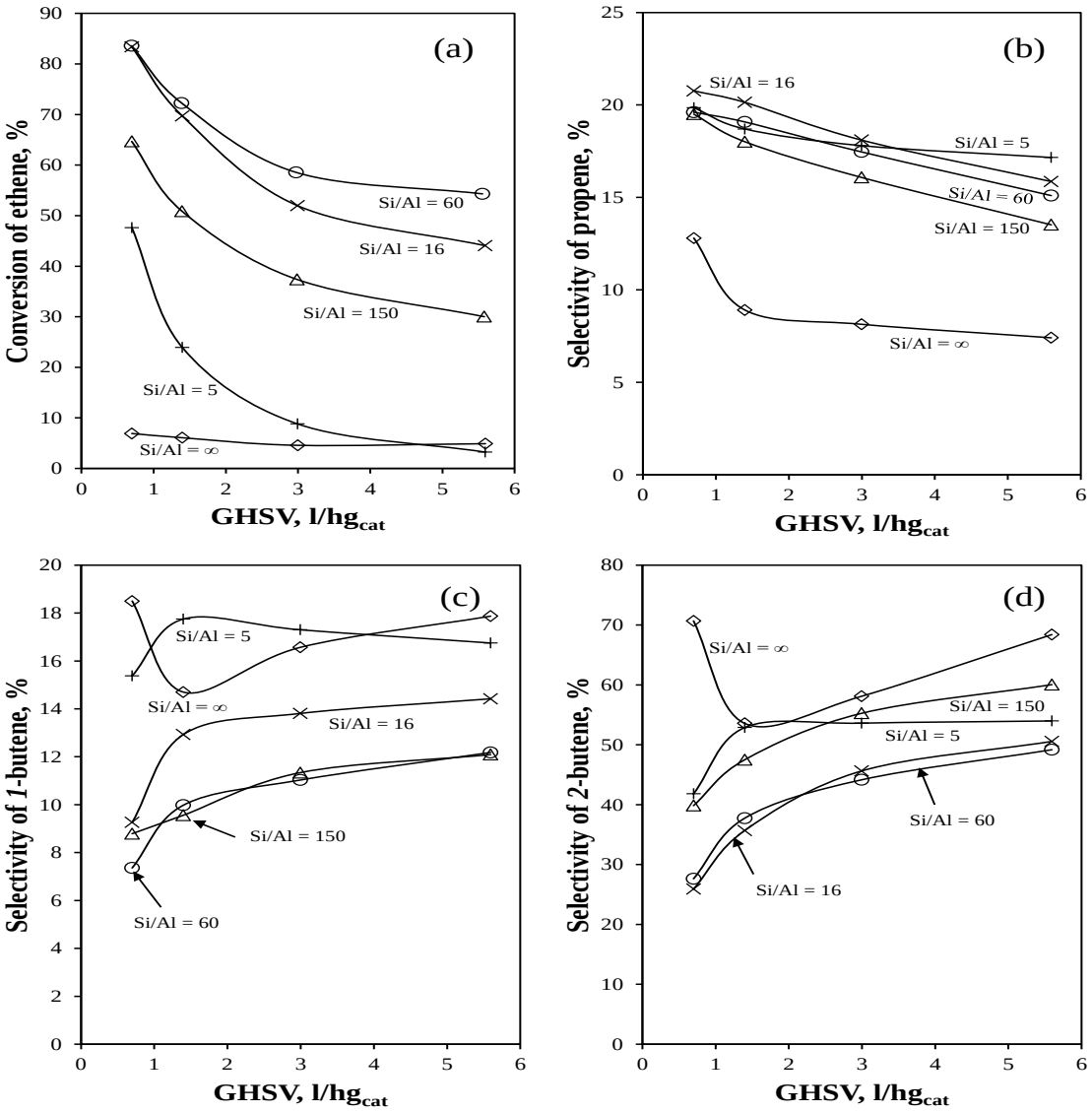

Figure 6.1.2.4. Change in ethene conversion and product distribution with GHSV at different Si/Al ratios. T = 350 °C and 10% of ethene in N_2.

Figure 6.1.2.4 shows the change in product distribution as a function of the GHSV, i. e., the contact time dependence on the ETP-reaction. Clearly, high GHSV (shorter contact time) corresponds to a lower conversion of ethene and a lower selectivity of propene. The selectivity of butenes increases at higher GHSV. The catalyst with a Si/Al ratio of 60 and without Al revealed the highest and the lowest conversion of ethene, respectively. The highest selectivity of propene was observed with the rich Al catalyst (Si/Al ratios of 16 and 5) but there is no significant difference. At a constant ethene conversion of around 48 % it is possible to observe the effect of the Si/Al ratio on the selectivity of the major reaction products for the catalysts with Si/Al ratios of 150, 16 and 5. From this comparison it is possible to observe that the selectivity of *1*-butene increases with the Al content indicating that the dimerization step is being favored with increasing the Al content. The selectivity of propene increases also but at less extent. On the contrary the selectivity of *2*-butene diminished slightly. This result indicates that the Si/Al ratio modifies mainly the dimerization step and other types of reaction are taking place to produce propene.

At the reaction conditions used in this work the major reaction products were *1*-butene, *2*-butene and propene and their behavior during the ETP-experiment supports the reaction mechanism for the propene production suggested by Iwamoto [21]. The conversion of ethene and the yield of propene reached close to 75% and 27% respectively. This results is comparable with the results reported by Iwamoto et al. [20, 21] but is considerable higher than the yield of propene reported by Lehmann et al. (around 16%) [26]. It is important to emphasize that the catalysts were prepared by TIE and EA respectively. In the next section the catalysts characterization results will be used in order to understand the observed catalytic activity results.

Based on the standard characterization, powder XRD and N_2-physisorption results showed that the ordering degree of the hexagonal structure does not have a significant influence on the catalytic behavior of the Ni/MCM-41 and Ni/AlMCM-41 on the ETP-reaction. The Al containing catalysts have the highest activity in the ETP-reaction even when their hexagonal ordering is low. Low Si/Al ratios have a negative influence on the ETP-reaction due to the reduction of the BET specific area and the difficulty to incorporate high amounts of Ni and Al into the MCM-41 framework [61]. Additional characterization was performed in order to understand the obtained catalytic results and they are shown in the next sections.

6.1.3 ^{29}Si and ^{27}Al MAS NMR

Figure 6.1.3.1 illustrates the ^{29}Si CP-MAS NMR 6.1.3.1(a) and ^{27}Al MAS NMR in direct detection 6.1.3.1 (b) of the Ni/MCM-41 and Ni/AlMCM-41 catalysts. The ^{29}Si CP-MAS NMR of Ni/MCM-41 showed a broad peak in the interval of chemical shift of -84 ppm and -118 ppm. This peak is centered at chemical shift of -100 ppm which is assigned to $Si(OSi)_3OH$ units (Q^3 units) corresponding to a layer condensation of the SiO_4 tetrahedral units. Around a chemical shift of -94 ppm a shoulder of lower intensity is found. This shoulder can be assigned to the $Si(OSi)_2(OH)_2$ units (Q^2 units). At high-field shifts there is a small contribution of $Si(OSi)_4$ units (Q^4 units) at a chemical shift less than -118 ppm [62].

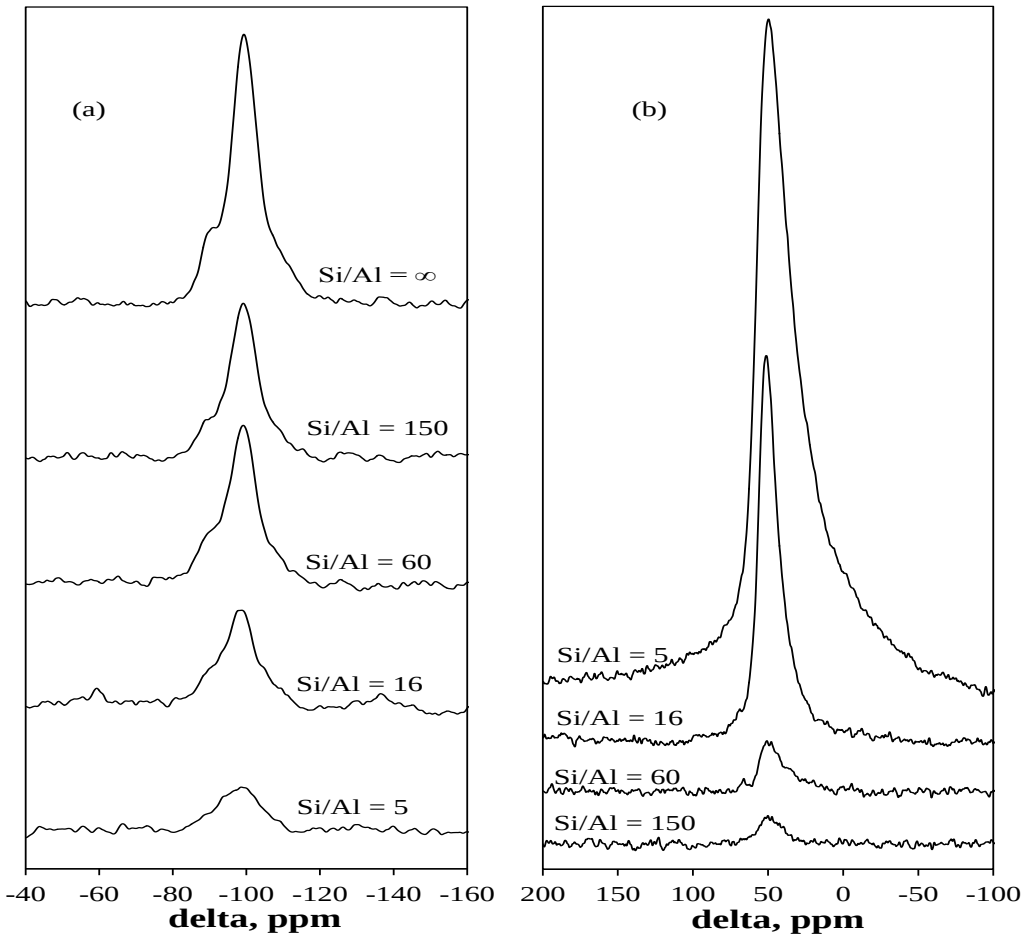

Figure 6.1.3.1. ^{29}Si CP-MAS NMR spectra (a) and ^{27}Al MAS NMR spectra in direct detection (b) of Ni/MCM-41 and Ni/AlMCM-41 at different Si/Al ratios.

The ^{29}Si CP-MAS NMR spectra for Ni/AlMCM-41 are observed in Figure 6.1.3.1 (a) at different Si/Al ratios. From these results, a broad peak centered at chemical shift of -100

ppm is recognized. This peak is assigned to $Si(OSi)_3(OAl)$ structural units in three-dimensionally connected aluminosilicate-like thermal treated structures where Al is tetrahedral coordinated. These aluminosilicates have been already described in [63]. A shoulder of lower intensity with a chemical shift of around -91 ppm has been observed. This shoulder is assigned to $Si(OSi)_3OH$ units [63] and a very small contribution on this peak around -87 ppm attributed to $Si(OSi)_2(OAl)OH$ units could be observed [63]. The intensity of these peaks is diminishing for lower Si/Al ratios, which is an indication that the difficulty to incorporate Al into the MCM-41 framework was increased. Therefore, from these results it is concluded that the Al incorporation is quite successful and the acidity of the Al containing catalysts has to be increased.

The results presented above clearly show that the Al is being incorporated into the MCM-41 framework up to a Si/Al ratio of 16. This fact is probed with the ^{27}Al MAS NMR results, which are presented in Figure 6.1.3.1(b). The Al framework (tetrahedral coordinated) gives a peak at a chemical shift between 47 and 52 ppm and extra-framework Al (octahedral coordinated) at a chemical shift of 3 ppm [64, 65]. From this Figure it can be clearly observed that there is no peak at 3 ppm for the catalysts with a Si/Al ratio of 150, 60 and 16, which means that all Al is being incorporated into the MCM-41 framework. For all last samples the peaks are centered at around 50 ppm and they are width peaks, therefore this result is associated with Al tetrahedral coordinated (framework Al) in a highly distorted environment [63]. For the catalyst with a Si/Al ratio of 5 a very broad peak of high intensity centered at 48.8 ppm is observed. This peak contains an important contribution of octahedral Al and pentahedral Al species (ca. 33 ppm) according to the results of Kosslick et al., [66, 67]. The high intensity peak centered at 50 ppm might be due to tetrahedral Al coordinated as extra-framework and forming a condensate phase that has been observed by Kloetstra et al., for AlMCM-41 with low Si/Al ratios [61]. This condensate phase causes an important reduction of the BET specific surface because it is blocking the pores of the MCM-41 as extra-framework Al tetrahedrally coordinated.

6.1.4 Transmission electron microscopy, TEM

In Figure 6.1.4.1 TEM micrographs of Ni/MCM-41 (6.1.4.1 (a)) and Ni/AlMCM-41 with Si/Al ratio of 16 (6.1.4.1 (b)) are depicted. This Figure reveals the hexagonal structure of the Ni/MCM-41 and the low hexagonal ordering degree of the catalyst with a Si/Al ratio

of 16. Ni-particles could not be observed. The condense phase observed by Kloetstra and co-workers [61] could not be recognized for the catalyst with a Si/Al ratio of 16. Thus, it is concluded, that at this Si/Al ratio only tetra-coordinated Al belonging to the MCM-41 framework.

Figure 6.1.4.1 also illustrates the EDX spectra of the catalysts without Al and with a Si/Al ratio of 16. It can be observed that the intensity of the bands that correspond to nickel was lower in the catalysts with a Si/Al ratio of 16. The band corresponding to Al can be recognized on the catalyst with a Si/Al of 16, indicating a successful incorporation of Al into the framework of the MCM-41. The EDX analysis revealed a local Si/Ni composition of 2/1 for Ni/MCM-41 catalyst and a local Al/Si/Ni composition of 4.2/28.8/2.3 for the Ni/AlMCM-41 catalyst with a Si/Al ratio of 16. These values are close to the experimental values determined by Atomic Absorption Spectroscopy (AAS), Table 6.1.1.1.

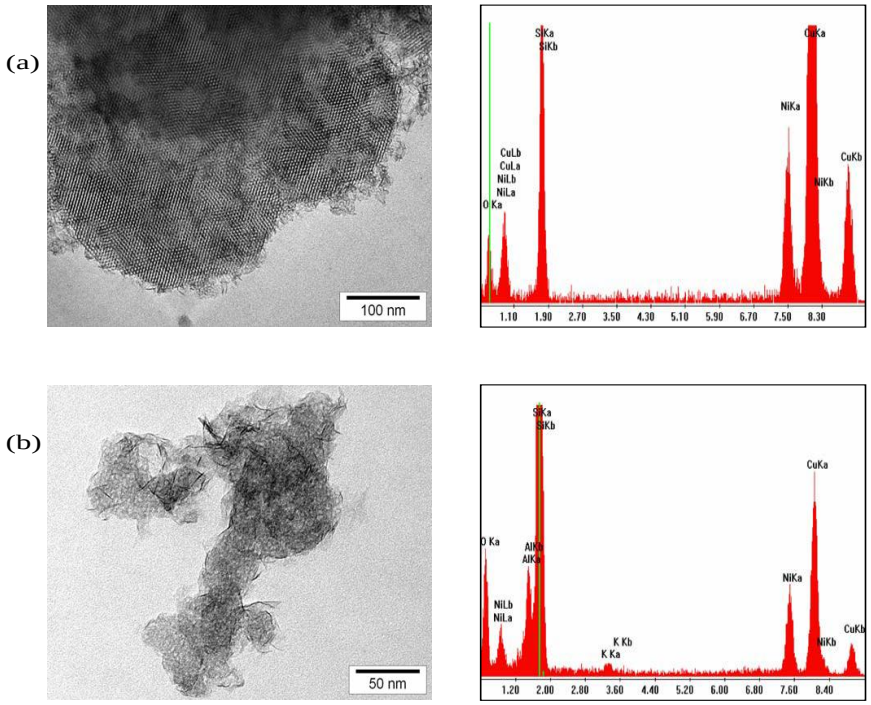

Figure 6.1.4.1. TEM micrographs and EDX spectra of Ni/MCM-41 (a) and Ni/AlMCM-41 with a Si/Al ratio of 16 (b).

6.1.5 NH_3-temperature programmed desorption, NH_3-TPD

As it has been widely stated in the literature that MCM-41 is slightly acidic and the Al incorporation can modify its acidity [59, 64, 66, 67], NH_3-TPD of Ni/MCM-41 and Ni/AlMCM-41 was carried out and the results are depicted in Figure 6.1.5.1. These

results show the total acidity of the catalysts (Brønsted and Lewis acid sites) and it is observed that their surface density and strength depend on the Si/Al ratio, which simultaneously have a strong influence on the ETP-reaction (Figures 6.1.2.1-6.1.2.4).

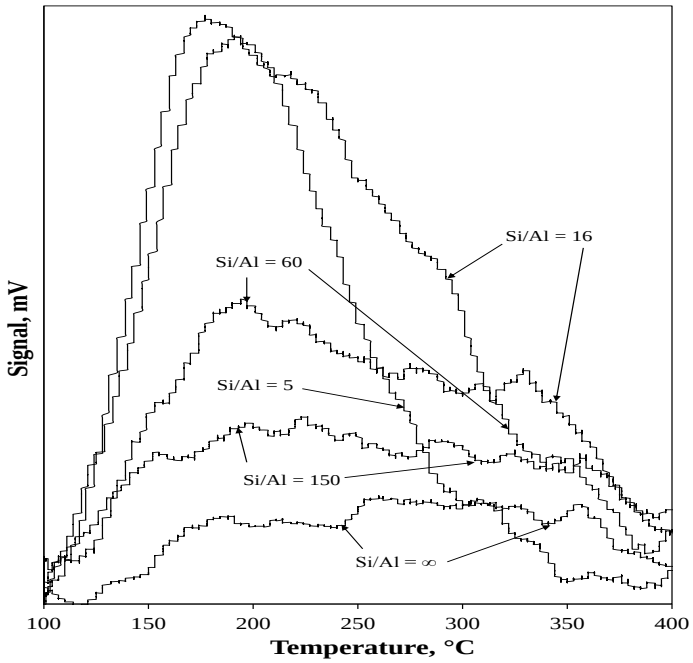

Figure 6.1.5.1. NH_3-TPD of Ni/MCM-41 and Ni/AlMCM-41 as a function of the Si/Al ratio.

In the NH_3-TPD spectra two peaks, viz. at ca. 150-250 °C and at 270-370 °C are recognized. In the interval of low temperature the amount of desorbed NH_3 increased with the Al content. This NH_3 desorption is associated with weak Brønsted and Lewis acid sites. The high temperature interval corresponds to Brønsted and Lewis acid sites of medium strength [66, 67]. This type of acidity seems to have a strong effect in the ETP-reaction. The catalyst with a Si/Al ratio of 60 showed the highest acidity in the interval of high temperature and revealed the highest catalytic activity in the ETP-reaction. For the catalyst Ni/MCM-41 the surface density of the acid sites is low, therefore the catalytic activity should be also low. From these results it can be concluded that the ETP-reaction requires a catalyst providing an intermediate acidity.

6.1.6 Pyridine-diffuse reflectance infrared Fourier transform spectroscopy, pyridine-DRIFTS

It is well know that the Al incorporation into the MCM-41 framework produces Brønsted acid sites [66, 67] and they can catalyze the ethene dimerization and oligomerization

reactions in zeolite materials [68-70]. Therefore it is important to distinguish between Brønsted and Lewis acid sites on the surface of the catalysts. Pyridine-diffuse-reflectance FTIR of Ni/MCM-41 and Ni/AlMCM-41 was carried out and the results are depicted in Figure 6.1.6.1.

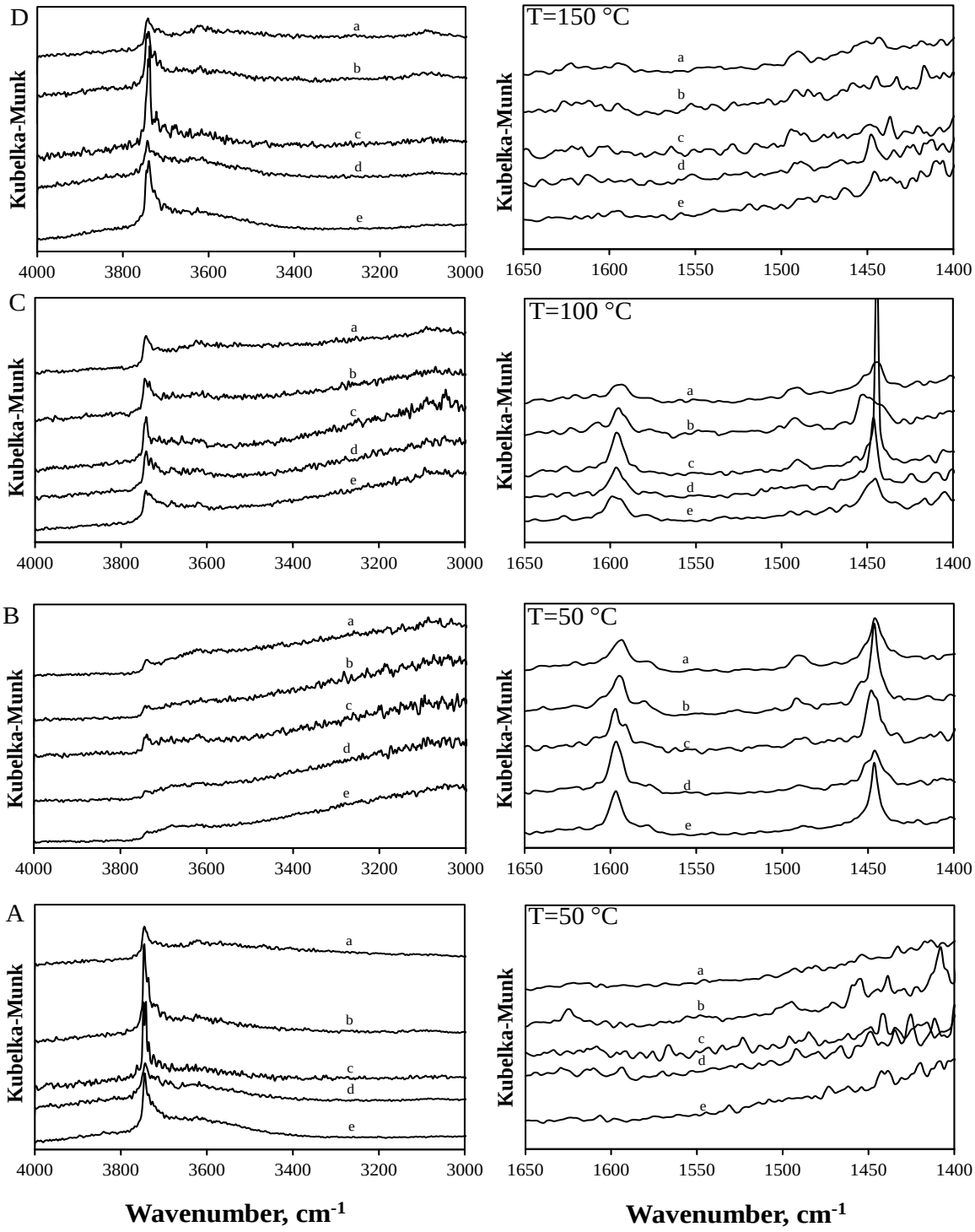

Figure 6.1.6.1. Pyridine-diffuse-reflectance FTIR spectra of the Ni/MCM-41 and Ni/AlMCM-41 with different Si/Al ratio; a = 5, b = 16, c = 60, d = 150, e = ∞ , before (A) and after pyridine adsorption at 50 °C (B), 100 °C (C) and 150 °C (D).

The Figure illustrates the spectra of the catalyst powder before and after saturation with pyridine at 50, 100 and 150 °C as a function of the Si/Al ratio. All catalysts exhibit two characteristic bands at 3745 cm^{-1} corresponding to Si-OH groups and at 3550 – 3700 cm^{-1} corresponding to Al-OH and Si-OH-Al groups [71]. Before the pyridine adsorption, the intensity of these bands increases for lower Si/Al ratio but for the catalyst with a Si/Al ratio of 5 their intensity was found to be the lowest. The catalyst with a Si/Al ratio of 60 offered the highest intensity of both bands.

New bands in the interval of 1400 and 1650 cm^{-1} were observed after the pyridine treatment while the bands in the interval 3800 and 3550 cm^{-1} almost disappeared. All catalysts presented absorption bands at 1596 cm^{-1}, 1580 cm^{-1}, 1489 cm^{-1}, 1460 cm^{-1} and 1448 cm^{-1} of different intensity. The peak at 1448 cm^{-1} is related to binding to Lewis acid sites and the peak at 1596 cm^{-1} is significant due to the adsorption to hydroxyl groups with a weak acidic character [54, 72]. The band at 1460 cm^{-1} may be indicative of pyridine chemisorption at Lewis sites of higher acid strength [66, 67]. The band at 1489 cm^{-1} is due to an adduct formation with both Lewis and Brønsted acid sites [73]. Finally, the band at 1580 cm^{-1} is consistent with the presence of a liquid layer of pyridine, which also contributes to the band around 1448 cm^{-1} [74]. At 50 °C all the bands associated with Lewis acid sites showed high intensity because the sample was saturated with pyridine at this temperature. The band associated with the Brønsted acid sites, 1489 cm^{-1}, increased for lower Si/Al ratio because of the Al incorporation into the MCM-41 framework which is in agreement with the ^{27}Al NMR results.

At 100 °C the intensity of the band at 1596 cm^{-1} diminished for lower Si/Al ratio indicating that the acidity of the catalyst was weak for the catalysts with high Al content. At 150 °C almost all bands disappeared indicating the weak acidity of all catalysts. At this temperature the band at 1489 cm^{-1} (associated with the Brønsted acid sites) became more intense. According to the catalytic activity results, this type of acidity has the most important effect on the ETP-reaction.

6.1.7 H_2-Temperature programmed reduction, H_2-TPR

To study the reducibility of Ni on Ni/MCM-41 and Ni/AlMCM-41, H_2-TPR was carried out. On the basis of manifold H_2-TPR results made for Ni on MCM-41, AlMCM-41 and silica [75-78], the TPR peak regions of nickel on silica can be summarized as follows;

Ni-oxide could be reduced between 327 and 527 °C, the cationic form of Ni on the silica surface could be reduced between 527 and 627 °C and the Ni ion forming some composite compounds might be reduced between 627 and 727 °C.

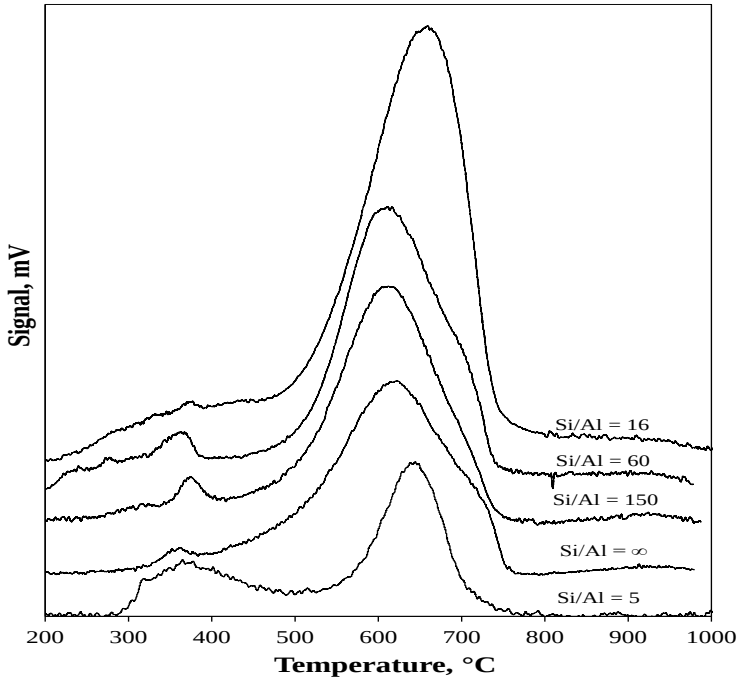

Figure 6.1.7.1. H_2-TPR of Ni/MCM-41 and Ni/AlMCM-41 as a function of the Si/Al ratio.

Figure 6.1.7.1 illustrates the H_2-TPR results of Ni/MCM-41 and Ni/AlMCM-41 as a function of the Si/Al ratio. A small peak in the temperature interval between 300 and 500 °C has been observed for all catalyst. This peak is assigned to Ni-oxide which is more pronounced to the catalyst with a Si/Al ratio of 5. For all catalyst a broad peak of high intensity is observed in the interval of 500 and 750 °C, which might be due to the formation of bulk mixed nickel-silicates and nickel-aluminosilicates. This designation is in concordance with the ^{29}Si CP-MAS NMR. For the siliceous catalyst (Si/Al = ∞) the peak presented a maximum reduction temperature of 625 °C with a shoulder at higher temperature (700 °C). These results can be interpreted in a manner that Ni is present as a mixture of its cationic form and it is forming Ni composite compounds. For the catalyst with a Si/Al ratio of 150 and 60 this shoulder is less pronounced which is an indication that Ni is present mostly in its cationic form and it is more homogeneously distributed in the AlMCM-41. For the catalysts with a lower Si/Al ratio (16 and 5) the maximum is shifted to higher temperature, 650 and 675 °C. Thus, Ni is forming composite

compounds in the AlMCM-41. From these results it is concluded that Al plays an important role in the Ni state in the MCM-41 and at Si/Al ratio of 60 the Ni state that is more active in the ETP-reaction is formed.

6.1.8 Characterization after the ETP experiment

A second characterization of the catalysts was carried out after the ETP-experiment. Table 6.1.8.1 summarizes the physical features of all catalysts after the ETP experiment. An important reduction of the BET specific surface area was observed for the catalysts with a Si/Al ratio of ∞ and 150 (see Table 6.1.1.1, BET specific surface are before the ETP experiment). This change was less pronounced for the other catalysts. The pore volume increased and the pore diameter did not suffer important modifications. Modification of the N_2-physisorption data might be mainly due to the blocking of the pores with long-chain hydrocarbons [58].

Table 6.1.8.1
N_2-adsorption data of the Ni/MCM-41 and Ni/AlMCM-41 catalysts after the ETP-experiment.

Catalyst Si/Al ratio	BET specific surface area, $m^2\ g^{-1}$	PV[1] $cm^3\ g^{-1}$	BJH-PD[2], nm	NLDFT-PD[3], nm
∞	876	0.9	3.0	4.1
150	852	0.9	3.0	3.9
60	858	0.9	3.0	4.1
16	772	0.9	3.0	4.1
5	435	0.5	3.2	3.7

[1]Pore Volume. [2]Pore diameter determined by Barret-Joyner-Halenda method (BJH) and [3]nonlocal density functional theory (NLDFT) from the desorption branch.

XRD results showed that the structure and ordering degree of the catalysts was retained after each experiment (spectra not depicted). The same conclusion follows for the deactivation experiments (results shown in the next sections). Ni or carbonaceous particles were not detected by conventional XRD because of the small content of Ni and carbon in the catalysts. Considering that Ni-oxide was observed by H_2-TPR and its reduction starts at temperatures higher than 175 °C [79-81], after the ETP-experiments, Ni^0 particles might be observed on MCM-41 and AlMCM-41. This fact is illustrated in Figure 6.1.8.1(a) where Ni-particles could be observed for the catalyst with a Si/Al ratio of 60. Carbonaceous species could be also observed and Buchireddy at al., [82] suggested that these species result from the growth of Ni particles during tar reduction. Therefore, Ni particles might promote the carbonaceous species formation on Ni/AlMCM-41 catalysts.

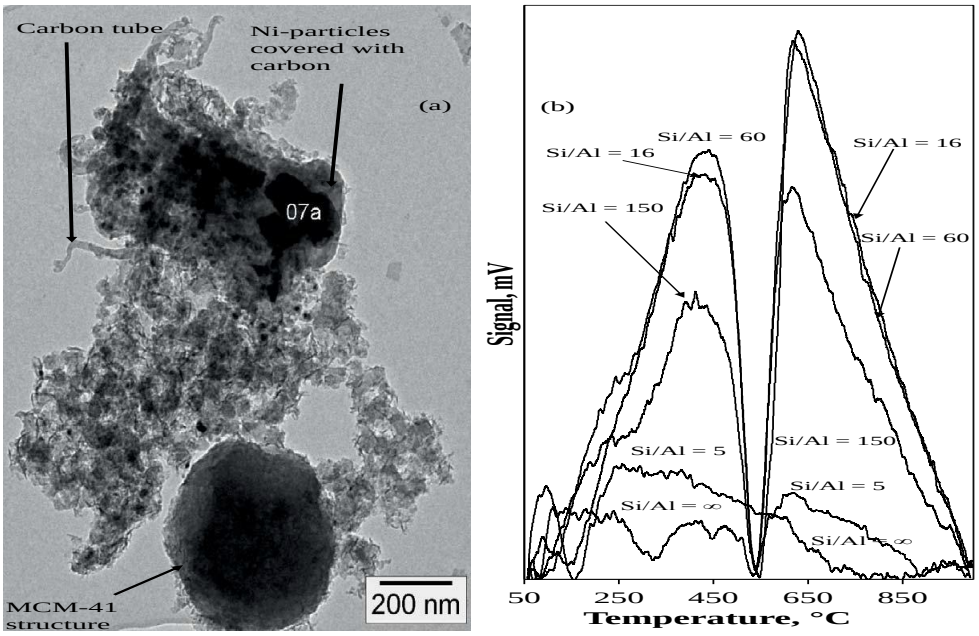

Figure 6.1.8.1. TEM micrograph of Ni/AlMCM-41 catalyst with a Si/Al ratio of 60 (a) and TPO of the Ni/MCM-41 and Ni/AlMCM-41 catalysts after the ETP experiment.

The Figure 6.1.8.1(b) also illustrates the TPO results after the ETP-experiment for the catalysts with different Si/Al ratio. Two very broad peaks with a maximum centered in the interval of 400-500 °C and 600-700 °C were observed. The contribution at temperatures lower than 300 °C can be associated with the oxidation of Ni^0 [83]. The interval of 300-500 °C might correspond to the oxidation of monoatomic carbon with a low rate of oxidation [84]. The oxidation peak at higher temperature could be assigned to the oxidation of filamentous carbon [80]. The catalysts with a Si/Al ratio of 60 and 16 presented the highest formation of carbonaceous species. From these results it is concluded that carbon formation reactions are taking place besides to the formation of propene and butenes and they might deactivate the catalysts. Therefore, deeper deactivation studies should be done in order to explain the nature of the carbonaceous species formation during the ETP-reaction.

6.1.9 Effectiveness of the template ion exchange method

Figure 6.1.10.1 shows the conversion of ethene and the selectivity of the major reaction products on Ni/AlMCM-41 with a Si/Al ratio of 60 prepared by template ion exchange, (TIE), equilibrium adsorption, (EA) and incipient wetness impregnation, (IWI).

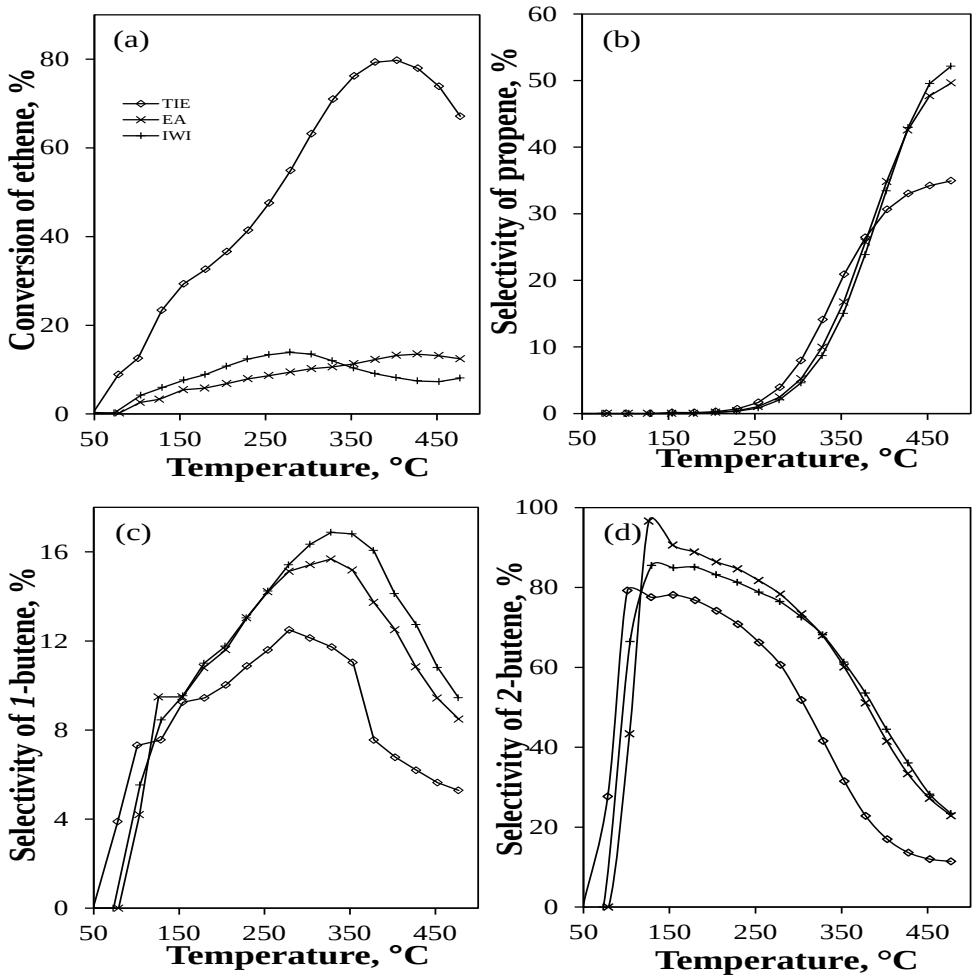

Figure 6.1.10.1. Conversion of 66thane (a), selectivity of; propene (b), *1*-butene (c), and *2*-butene (d) on Ni/AlMCM-41 with a Si/Al ratio of 60 prepared by template ion exchange, TIE; equilibrium adsorption, EA; and incipient wetness impregnation, IWI. GHSV = 1.4 $h^{-1}g_{cat}^{-1}$ and 10% of ethene in N_2.

This Figure clearly shows that the TIE method provides the catalyst with the best catalytic behavior in the ETP-reaction. The catalysts prepared by IWI and EA methods produced higher selectivity of propene but the conversion level was very low, in comparison to the TIE method. The selectivity of the different butene isomers is always higher for the catalysts prepared by IWI and EA than the selectivity for the corresponding catalysts prepared by TIE method.

Figure 6.1.10.2 shows the yield of the major reaction products. Once again, it can be observed that the TIE method provided the catalyst with the highest yield of all reaction products. This fact confirms that the TIE method is the most effective method to prepare catalysts with high catalytic activity in the ETP-reaction. For this reason, no deeper characterization was performed on the catalysts synthesized by EA and IWI.

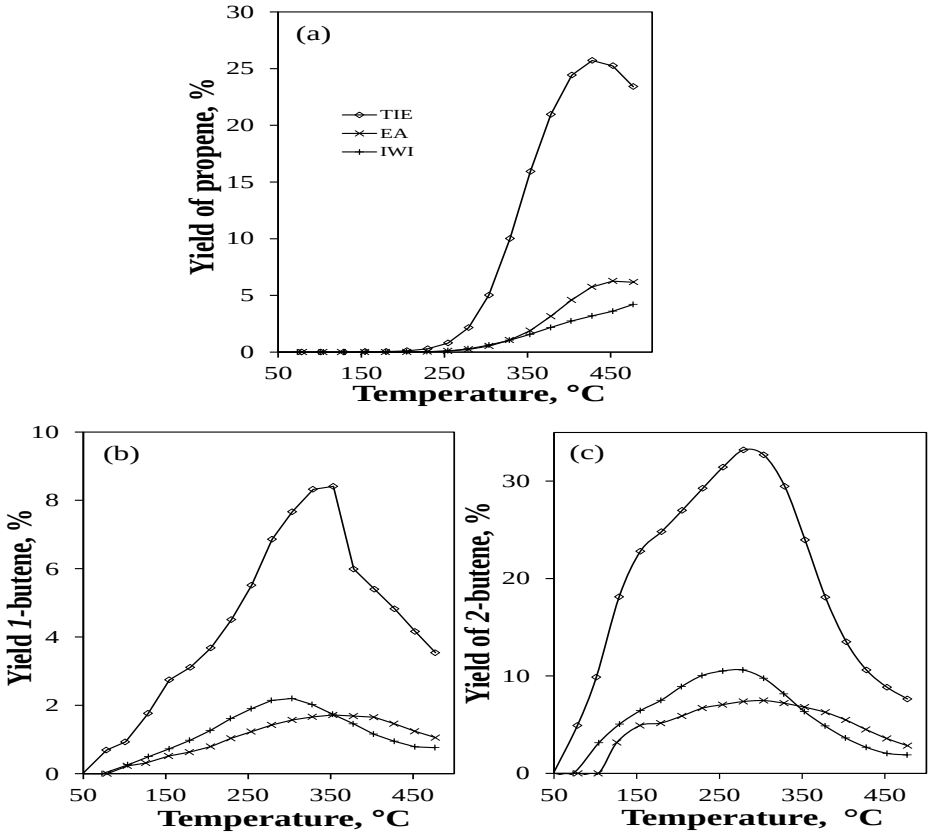

Figure 6.1.10.2. Yield of; propene (a), *1*-butene (b), and *2*-butene (c) on Ni/AlMCM-41 with a Si/Al ratio of 60 prepared by template ion exchange, TIE; equilibrium adsorption, EA; and incipient wetness impregnation, IWI. GHSV = 1.4 $h^{-1}g_{cat}^{-1}$ and 10% of ethene in N_2.

6.1.10 Discussion and analysis of the catalytic and characterization results

The standard characterization techniques for alumino-mesostructured materials with low Si/Al ratios are XRD, N_2-Physisorption, ^{29}Si CP-MAS NMR and ^{27}Al MAS NMR and TEM [61]. NH_3-TPD, pyridine-diffuse-reflectance FTIR and H_2-TPR analysis were done to study the surface composition of the catalysts. In Figures 6.1.2.1 to 6.1.2.4 can be observed that the catalyst with a Si/Al ratio of 60 leads to the highest conversion of ethene and the highest yield of propene. Preliminarily, XRD and N_2-physisorption results revealed that this catalyst is characterized by low hexagonal ordering but it has an N_2 isotherm type IV and high specific surface, which are characteristics of the MCM-41 materials [54, 55]. Therefore, it is concluded that the hexagonal ordering of the MCM-41 has not an important effect on the catalytic behavior of the Ni/AlMCM-41. As it has been already observed in Figure 6.1.4.1, Ni/MCM-41 revealed a highly ordered hexagonal structure but its behavior on the ETP-reaction is poor. This fact supports the previous explanation.

The presence of Al in the catalysts has a strong impact on the ETP-reaction when it belongs to the MCM-41 framework. This incorporation is modifying its surface acidity as it has been shown by NH_3-TPD and pyridine-diffuse reflectance FTIR. The results of ^{29}Si CP-MAS NMR showed that the Q^3 is the main unit in the Ni/MCM-41 which corresponds to surface $(SiO)_3Si$-OH (phyllosilicate phase) [62] and it has a low density and weak surface acidity, as it is reported in Figures 6.1.6.1 and 6.1.7.1. This phase also has been observed by Lehmann et al., and Tanaka et al., on Ni/MCM-41 [27, 85]. Thus, the low acidity of this catalyst might be the responsible for the low catalytic activity of the Ni/MCM-41.

The results of ^{27}Al MAS NMR analysis indicate that Al is incorporated to the MCM-41 framework. The presence of Al in the catalysts generates an important modification of the Ni state (according to the H_2-TPR results) and a modification of their acidity. Therefore, these differences might be responsible to explain the differences in catalytic activity between the Al containing catalysts. The Ni-oxides reduce at temperatures lower than 400 °C to form Ni^0 particles that have been observed by TEM, therefore the differences in catalytic activity might be also influenced by the formation of Ni^0, which is not active in the ETP-reaction. Hartmann et al., reported that Ni^{+1} is the active state of nickel for the dimerization of ethene on Ni/AlMCM-41 and the Al tetrahedral coordinated in the MCM-41 framework improves its stability [59]. Thus, Ni^{+1} could be the active state of nickel in the ETP-reaction for the catalyst with a Si/Al ratio of 60. For Ni/AlMCM-41 catalysts it is concluded that the isomerization of *1*-butene is fast for all Si/Al ratios and for all temperatures investigated. At these reaction conditions the *1*-butene isomerization is in equilibrium [60].

The results in this investigation showed that Ni could have indeed activity on this reaction stage of the ETP-reaction. These results are in accordance with the results obtained in [21, 26]. Deeper characterization has to be done in order to investigate the Ni state of the Ni/AlMCM-41 catalysts e. g. *in-situ* EPR, diffuse reflectance infrared Fourier transform spectroscopy of adsorbed CO, and its role in the metathesis step during the ETP-reaction. The maximum in the selectivity and yield of propene, 38 % and 25 % respectively, on Ni/AlMCM-41 is a clear indication that propene is reacting to form other products, probably larger-chain hydrocarbons (oligomers). Therefore, not only the reactions involved in the reaction mechanism proposed by Iwamoto are taking place [21]. Carbonaceous species could be observed after the ETP experiment. This fact also

proofs that coke formation reactions are taking place during the ETP experiment. Therefore, a deeper study of the reaction mechanism is required in order to understand and to optimize the behavior of the Ni/AlMCM-41 catalyst in the ETP-reaction.

The results obtained in this part of the project are in a good agreement with the results reported in the literature where Ikeda et al., [23] and Lehmann et al., [26] obtained similar results. The effectiveness of the TIE was also confirmed in this section. The reason of the low catalytic activity for the catalysts prepared by IWI method might be influenced by the formation of NiO particles [23] while the EA method has shown only prominent properties for the ETP-reaction [23, 26].

6.2 Ni/MCM-41 and Ni/AlMCM-41 based on Vinu et al.

Results of standard characterization and catalytic activity of the second set of catalysts prepared using the Vinu et al., (2004) procedure to synthesize the MCM-41 and AlMCM-41 [51] are described in this section. Only standard characterization was performed to these catalysts because their catalytic behavior in the ETP-reaction was lower than the ones prepared by using the Noreña-Franco et al. (2002) procedure (results shown in the previous section). In the first part, powder XRD and N_2-adsorption results are shown. In the second part, the catalytic results are discussed.

6.2.1 N_2-adsorption and powder-XRD

Figure 6.2.1.1 reveals the structural characterization of the Ni/MCM-41 and Ni/AlMCM-41 catalysts. The crystalline Ni/MCM-41 and Ni/AlMCM-41 are characterized by a broad band at low angles in a XRD diffraction pattern and by a Type IV N_2-adsorption isotherm [54, 55]. In Figure 6.2.1.1(a) the diffraction patterns and in Figure 6.2.1.1(b) the N_2-adsorption isotherms of the synthesized catalysts are given. From the spectra 6.2.1.1(a), it is possible to observe that the catalysts with a Si/Al ratio of ∞, 400, 60 and 16 have a highly hexagonal ordered structure with the classic diffractions (100), (110), (200) and (210) [54]. For Ni/AlMCM-41 catalysts with a Si/Al ratios of 5 no diffractions were found, which means that the hexagonal ordering in this catalyst is totally lost. Therefore, it is concluded that the Vinu et al. procedure produces catalysts with higher hexagonal ordering than the catalysts prepared by Noreña-Franco et al. The hexagonal ordering degree is totally lost for the rich Al content catalyst. It is important to note, that the Al content shifts the diffraction peaks to higher values.

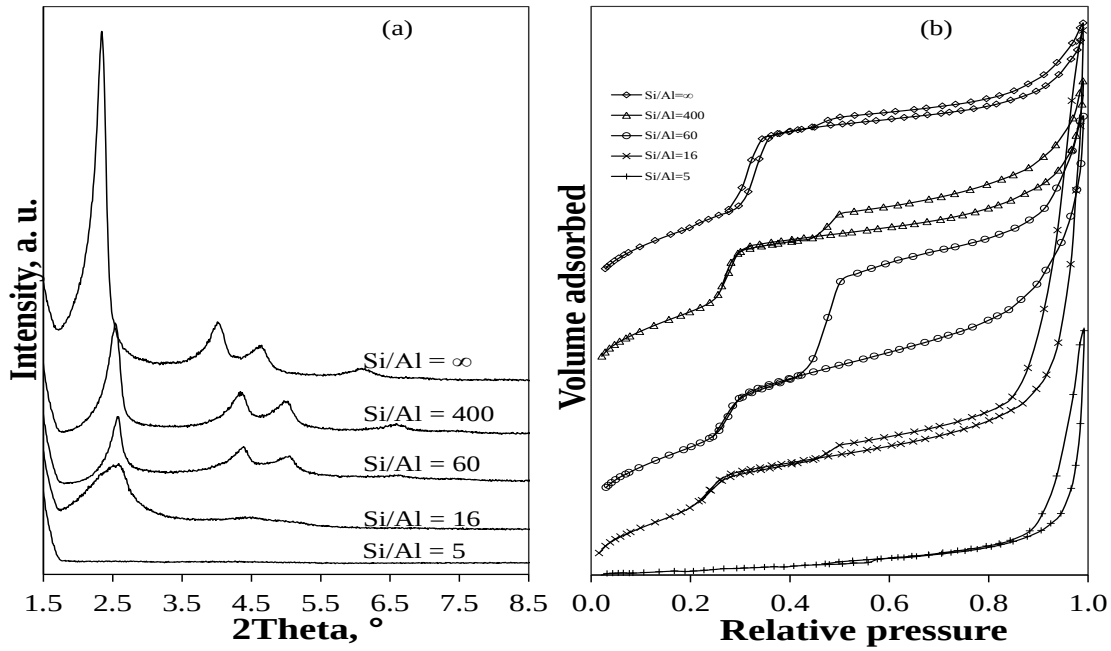

Figure 6.2.1.1. Powder XRD patterns (a) and N_2-physisorption isotherms (b) of Ni/MCM-41 and Ni/AlMCM-41 at different Si/Al ratios.

This shifting might be explained by the increase in the wall thickness of the MCM-41 materials and on the bases of replacement of shorter Si-O bonds (0.160 nm) by longer Al-O bonds (0.175 nm) in the MCM-41 structure [86].

The N_2-adsorption measurements for these catalysts are characterized by a type-IV isotherm according to IUPAC classification [44]. Such behavior corresponds to the MCM-41 materials and they present capillary condensation at relative pressure between 0.30-0.35 [54]. The catalyst with a Si/Al ratio of 5 clearly does not correspond to the MCM-41 materials. The catalysts presented a hysteresis of type H3 and the catalyst with a Si/Al of 60 revealed a hysteresis of type H2 and H3. The H2 hysteresis loop corresponds to systems where the pore size and shape is not well-defined [44]. The H3 hysteresis loop is observed with aggregates of plate-like particles giving rise to slit-shaped pores [44]. In general, it is concluded that the Vinu et al. procedure provides catalysts with more complex pore size and shape than the catalysts prepared by using the Noreña-Franco et al. procedure. The N_2-adsorption data of the Ni/MCM-41 and Ni/AlMCM-41 are summarized in Table 6.2.1.1. Also for these catalysts, two different methods were used to determine the pore size distribution, the BJH-method and the NLDF theory from the desorption branch.

Table 6.2.1.1

N_2-adsorption data of Ni/MCM-41 and Ni/AlMCM-41.

Catalyst Si/Al ratio	BET specific surface area, $m^2\ g^{-1}$	PV[1], $cm^3\ g^{-1}$	BJH-PD[2], nm	NLDFT-PD[3], nm
∞	1 021	0.9	3.7	3.8
400	928	0.9	3.9	3.5
60	932	1.0	3.7	5.1
16	795	0.8	3.9	3.4
5	141	0.2	3.7	5.5

[1]Pore Volume. [2]Pore diameter determined by Barret-Joyner-Halenda method (BJH) and [3]nonlocal density functional theory (NLDFT) from the desorption branch.

The N_2-adsorption data strongly depend on the Si/Al ratio. The BET specific surface was around 1 000 $m^2\ g^{-1}$ for almost all catalysts, which is typical for MCM-41 materials [54]. The catalyst with a Si/Al ratio of 16 showed a BET surface of around 800 $m^2\ g^{-1}$, with a pore volume of 2.1 $cm^3\ g^{-1}$. The catalyst with a Si/Al ratio of 5 lost totally the hexagonal structure and its corresponding nitrogen adsorption isotherm does not correspond to the MCM-41 materials according to IUPAC classification. Besides, it has a very low specific BET specific surface and pore volume. It is important to note that, independently of the method used to compute the pore size distribution, the pore diameter is smaller than the catalysts prepared by using the Noreña-Franco et al. procedure. According to the results obtained from powder XRD and N_2-physisorption analysis, it is concluded that Ni/MCM-41 and Ni/AlMCM-41 with a Si/Al ratio of 400, 60 and 16 presented the classic structure of the MCM-41 materials.

6.2.2 Testing of the catalysts in the ETP-reaction

Figure 6.2.2.1 shows the conversion of ethene and the selectivity of the major reaction products in the ETP-reaction at different Si/Al ratios. It can be observed that the catalysts without Al revealed a conversion close to 40% at 400 °C with a selectivity of propene of 25%. These results are in a good concordance with the results of Iwamoto et al [20, 21] and Lehmann et al [26] but they do not agree with the results obtained in the section 6.1. It is important to note, that in the Vinu et al., procedure, a different synthesis procedure and different silica source were used. These aspects might be considered to explain the differences in the catalytic properties observed for the catalysts with different Si/Al ratio.

These results, together with the results of the section 6.1 show that the ETP-reaction is strongly affected by the synthesis procedure and the silica source during the synthesis of MCM-41 and AlMCM-41. The correct synthesis procedure of MCM-41 and AlMCM-41 is a crucial step in the catalytic behavior of the final catalysts.

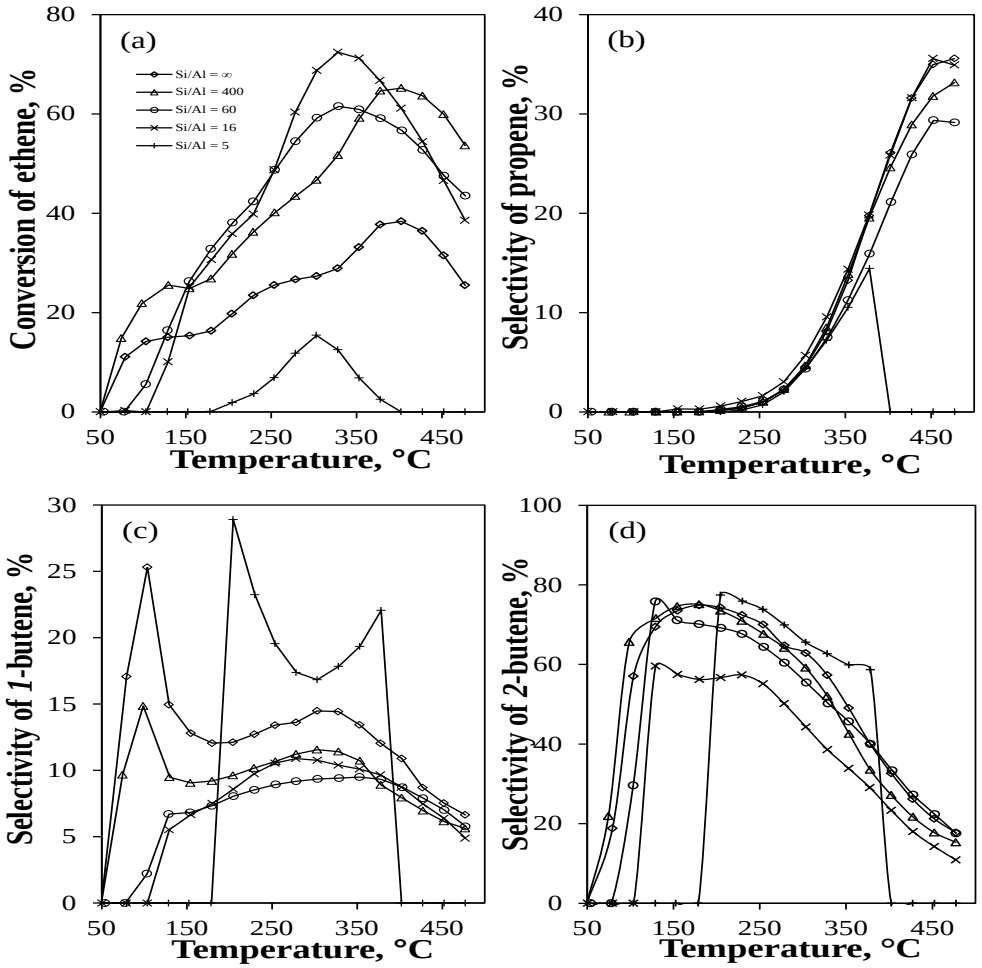

Figure 6.2.2.1. Conversion of ethene (a), selectivity of propene (b), *1*-butene (c) and *2*-butene (d) on Ni/MCM-41 and Ni/AlMCM-41 at different Si/Al ratios as a function of temperature. GHSV = 1.4 $h^{-1}g_{cat}^{-1}$ and 10% of ethene in N_2.

The conversion of ethene increased with the Al content but decreased strongly for the catalyst with the highest Al content. The highest conversion was observed on the catalysts with a Si/Al ratio of 16 at 325 °C. The highest selectivity of propene was obtained with the catalysts with a Si/Al ratio of 60 and 16 at 450 °C. The behavior of the selectivity of propene, *1*-butene, and *2*-butene suggests that also on these type of catalysts, propene is formed through the reaction mechanism suggested by Iwamoto et al [20, 21].

On Figure 6.2.2.2 the yield of the major reaction products can be observed. It can be recognized that the highest yield of propene was around 18%. Therefore, the Vinu et al., procedure produced catalysts with lower selectivity and yield than the Noreña-Franco et

al., procedure. Therefore, the Vinu et al. procedure showed only interesting catalytic results in the ETP-reaction.

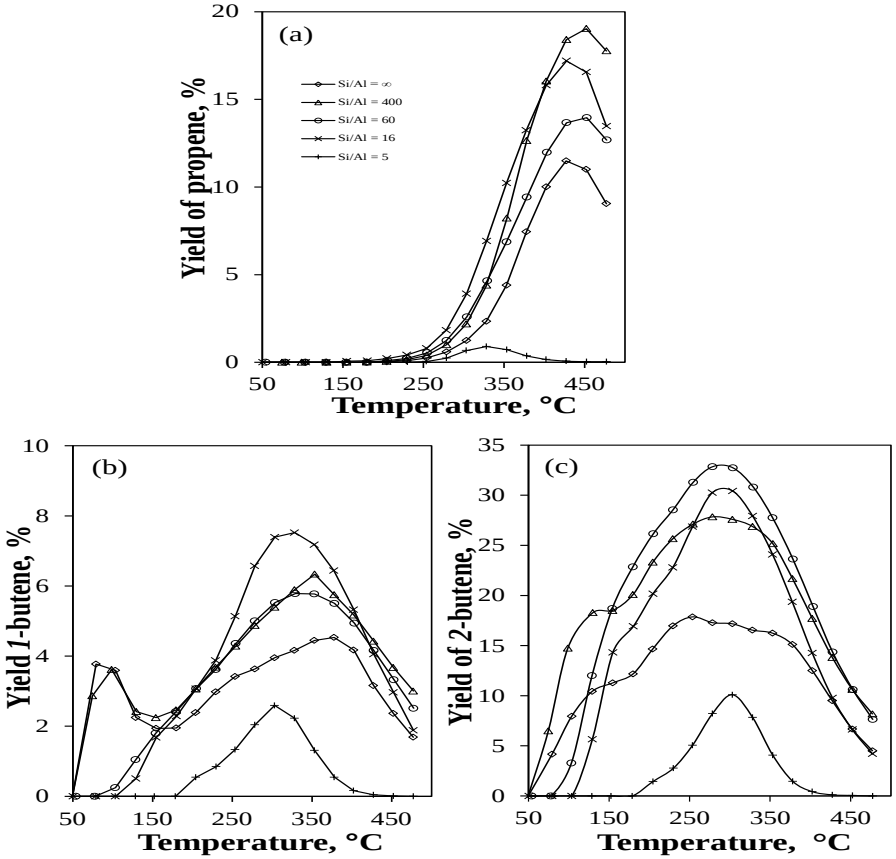

Figure 6.2.2.2. Yield of propene (a), *1*-butene (b) and *2*-butene (c) on Ni/MCM-41 and Ni/AlMCM-41 at different Si/Al ratios as a function of temperature. Butene yield = (ethene generated / ethene fed) (4/2)*100. GHSV = 1.4 $h^{-1}g_{cat}^{-1}$ and 10% of ethene in N_2.

The catalysts prepared by this procedure, produced higher amounts of by-products. This might be the reason to explain the lower selectivity and yield of the reaction products. For these reasons, the characterization and the full study of the ETP-reaction was focused only on the catalysts prepared by the Noreña-Franco et al. procedure.

6.2.3 Discussion and analysis of the catalytic and characterization results

Highly structured Ni/AlMCM-41 catalysts could be synthesized using the Vinu et al. procedure. The catalysts revealed a high BET specific surface area up to a Si/Al ratio of 16. The conversion of ethene and the selectivity of propene were similar to the catalysts prepared using the Noreña-Franco et al. procedure. The yield of propene was lower on this type of catalysts than the catalysts prepared using the Noreña-Franco et al procedure.

For this reason the study of this work was focused on the catalysts prepared by this method.

In the next section results of the effect of the reaction conditions and deactivation and regeneration will be shown on the catalysts prepared by Noreña-Franco et al. procedure.

6.3 Effect of the reaction conditions, deactivation and deactivation-regeneration of Ni/AlMCM-41 in the ETP-reaction

In section 6.1 has been shown that Ni/AlMCM-41 catalysts are active in the ETP-reaction. Nickel active sites and the acidity of the catalyst play an important role in this behavior. The reaction conditions that are used to perform the ETP-reaction play also an important role in its catalytic performance [19, 21, 26, 30]. Therefore, a study of the reaction conditions and its effect on the ETP-reaction was carried out and the results are shown in this section. The catalyst that revealed the highest catalytic activity was the Ni/AlMCM-41 catalyst with a Si/Al ratio of 60. For this reason, this catalyst was selected to perform this study.

Effect of the feed concentration on the ETP-reaction is shown in the first part of this section. Heating up and cooling down experiments were carried out to study the stability of the catalyst under changes in temperature. Deactivation and deactivation-regeneration experiments were also performed. Characterization after the catalytic experiments was carried out. This characterization includes N_2-physisorption, powder XRD, NH_3-TPD, TEM and TPO.

6.3.1 Effect of the feed concentration

Figure 6.3.1.1 illustrates the conversion of ethene and the selectivity of the major reaction products at different ethene feed concentration. The conversion of ethene was increased enhancing the ethene feed concentration and reached a maximum at 7.5 vol.% ethene.

This difference could be observed only in the intervals of intermediate and high temperature, 150-300 °C and 300-475 °C, respectively. In the interval of low temperature, the main reaction products were *1*-butene and *2*-butene. In the interval of intermediate temperature propene started to appear. Propene reached a maximum selectivity of around 35% at 400 °C with a feed ethene concentration of 2.5%. Once

again, this maximum is a clear indication that propene is participating in other type of reaction, e. g. oligomerization and coke formation reactions. Additionally, the C-balance was close to 100% in the interval of low and intermediate temperature for low ethene feed concentration indicating a low formation of by-products. In the interval of high temperature, the C-balance at 10% ethene feed was higher than for lower ethene feed concentration. This result shows that at this concentration the production of by-products is lower than at lower ethene feed concentration.

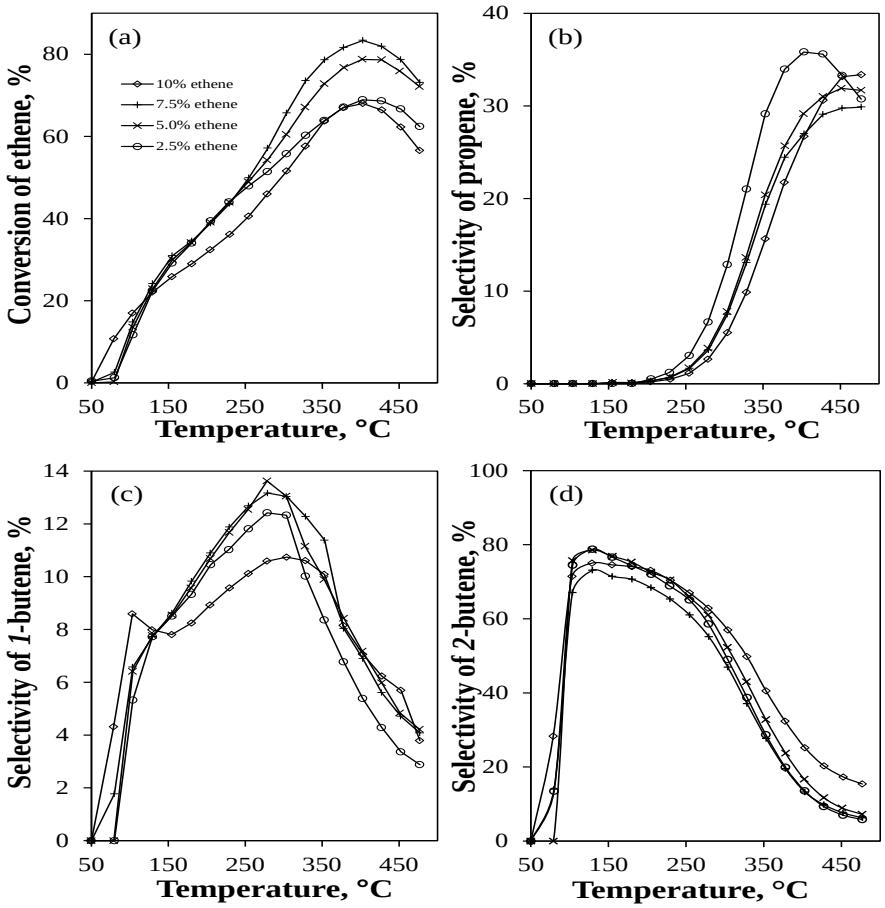

Figure 6.3.1.1. Conversion of ethene (a), selectivity of propene (b), *1*-butene (c) and *2*-butene (d) on Ni/AlMCM-41 (Si/Al=60) at different ethene fed concentration. GHSV = 1.4 $h^{-1}g_{cat}^{-1}$ and 10% of ethene in N_2.

No important differences were observed for the selectivity of *1*-butene at all temperatures. This selectivity reached a maximum in the interval of intermediate temperature, reaching a maximum of around 13%. Selectivity of *2*-butene was always higher at 10 vol.% of ethene concentration than for the other concentration values in the interval of high temperature. According to the reaction mechanism proposed by Iwamoto et al., an increasing ethene feed concentration had to produce an increase in the

selectivity of *1*-butene and *2*-butene [21]. This behavior was not observed in this type of experiments, where no important changes of selectivity of butenes were observed. This fact might be due probably to the side reactions that are taking place. The results are also not in concordance with the results reported by Lehmann et al [26]. The differences might be due also to occurrence of side reactions.

6.3.2 Effect of the temperature

The stability of the catalyst was tested by performing experiments at different temperature. Heating up and cooling down experiments were carried out. In the first step, the temperature was modified from 50 to 475 °C (number 1 in the Figures). Without interruption of the experiment, the temperature was changed in the opposite direction until 50 °C (number 2 in the Figures). This procedure was repeated five times. At the end, the final temperature was 475 °C and it is represented by number 7 in the Figures. Figure 6.3.2.1 illustrates the conversion of ethene for these experiments.

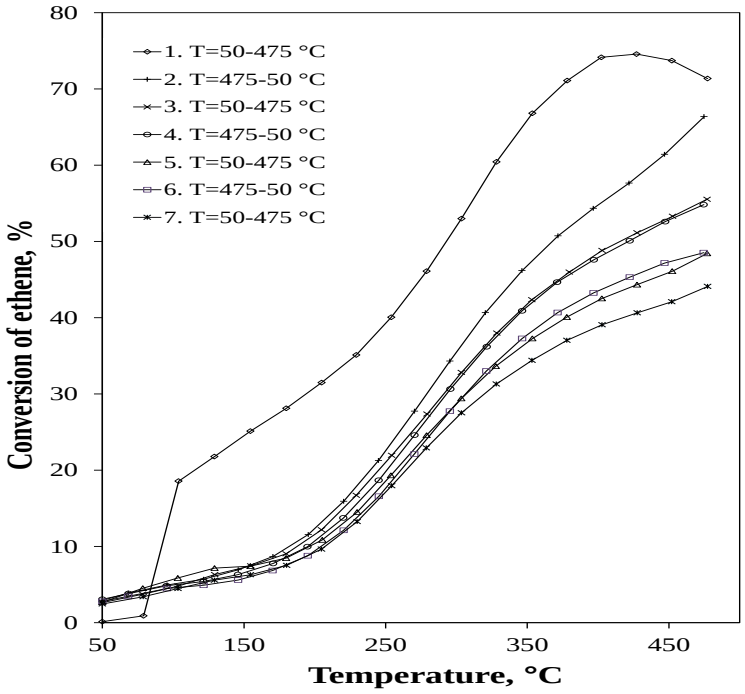

Figure 6.3.2.1. Conversion of ethene for the heating up and cooling down experiments on Ni/AlMCM-41 (Si/Al=60).

A strong decreasing in the conversion of ethene was observed in the experiment number 2. The conversion decreased gradually for the rest of experiments. An important characteristic of the experiments from 2 to 7 is that at 50 °C the conversion of ethene was not zero. This result suggests that the adsorbed species after the experiment number 1

presented active sites for the dimerization of ethene. The selectivity of propene did not change significantly and reached a maximum of around 35% (see Figure 6.3.2.2). These results suggest that the reaction that yields propene is not being affected by the adsorbed species produced in each experiment. Important changes in the selectivity of butenes were observed in the interval of low temperature.

The selectivity of *1*-butene was less than 10% at all temperatures for the experiment number 1. The selectivity of *2*-butene was lower in the experiment number 1 than in the other experiments. In the interval of low temperature the selectivity of *1*-butene changed considerably. The highest selectivity was obtained in the experiment number 3, with a value of around 45% for the experiment number 3. These results can be observed in the Figure 6.3.2.2(b).

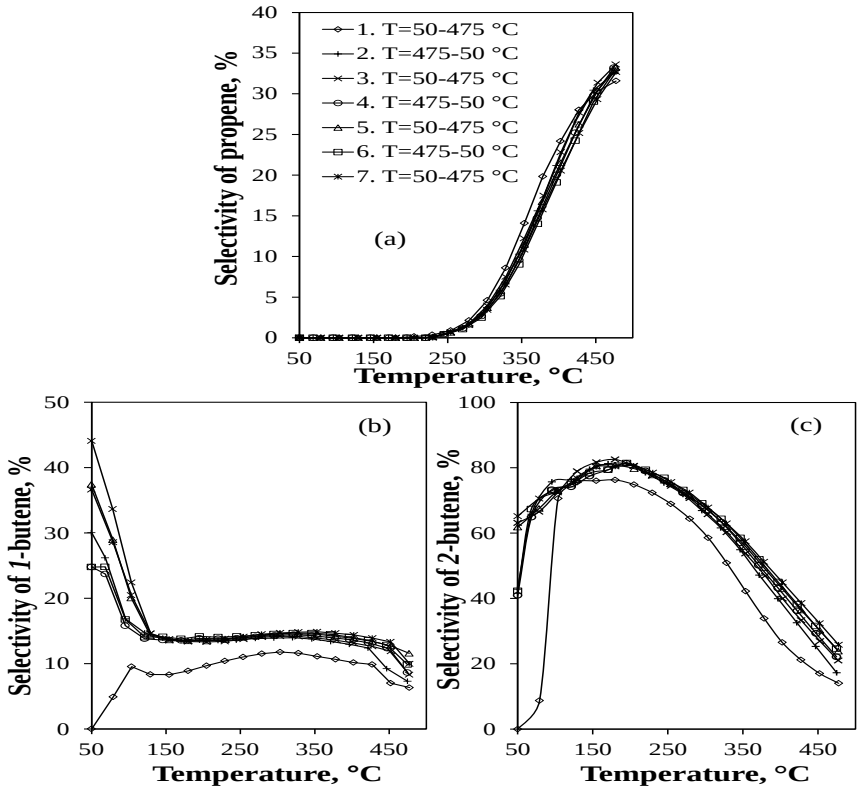

Figure 6.3.2.2. Selectivity of (a) propene, (b) *1*-butene and (c) *2*-butene for the heating up and cooling down experiments on Ni/AlMCM-41 (Si/Al=60).

From the Figure 6.3.2.2, it can be observed that for odd experiments the selectivity of *1*-butene was always higher than for the even experiments. The loss in the catalytic activity of the Ni/AlMCM-41 (Si/Al=60) might be influenced by the formation of nickel particles and by coke reactions formation. This fact was probed by TEM in the section

6.1.8. It is important to note that under these reaction conditions, the positional isomerization of *1*-butene is being strongly influenced. This is an indication that the acidity of the catalysts is being significantly modified.

Characterization after each experiment was performed to determine changes in the structure and surface properties of the catalyst. This characterization includes powder XRD, N_2-physisorption, NH_3-TPD and TPO. Figure 6.3.2.3 illustrates the powder XRD and N_2-physisorption results.

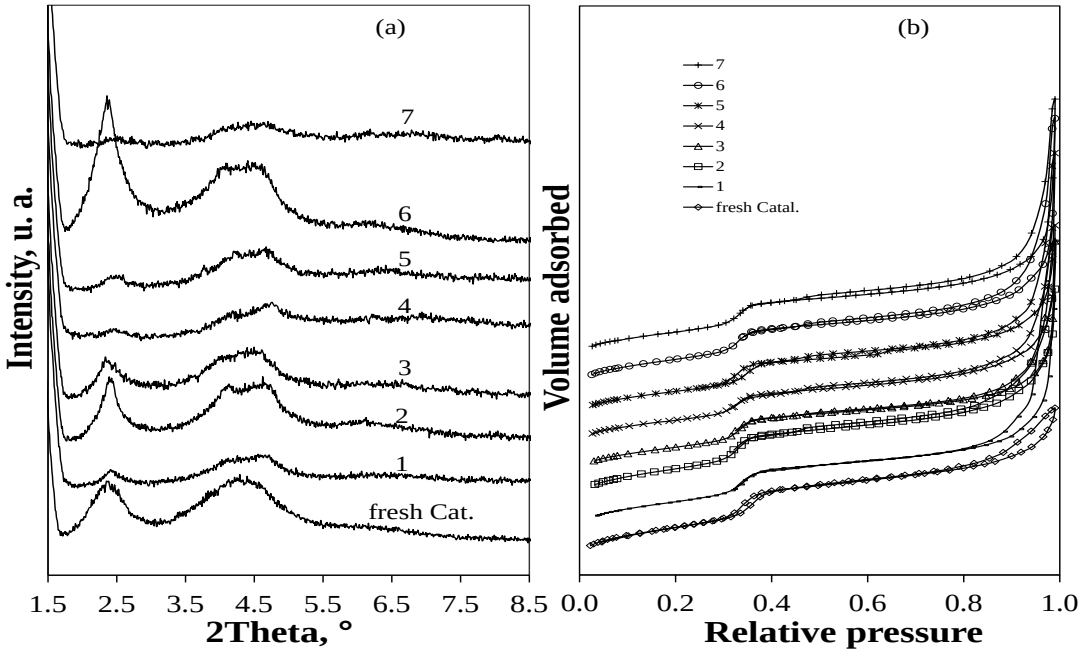

Figure 6.3.2.3. Powder XRD patterns (a) and N_2-physisorption isotherms (b) for the heating up and cooling down experiments on Ni/AlMCM-41 (Si/Al=60).

From this Figure, it is possible to observe that the catalysts did not change considerably its structure and the original structure was retained after all experiments (see Figure 6.1.1.1, powder XRD patterns of the fresh catalysts). The classical diffractions (100), (110) and (200) where retained after the heating up and cooling down experiments. This diffraction patterns correspond to the MCM-41 materials [54]. Therefore, the deactivation of the catalyst was not provoked by changes in the structure of the catalyst. Nickel or carbonaceous particles could be not detected by conventional powder XRD. N_2-adsorption isotherms did not change after the heating up and cooling down experiments. The isotherms correspond to the type IV isotherms with an H1 hysteresis according to the IUPAC classification [44].

Table 6.3.2.1.
N_2-adsorption data after heating and cooling experiments of Ni/AlMCM-41 (Si/Al=60).

Experiment	BET specific surface area, m^2 g^{-1}	PV[1] cm^3 g^{-1}	BJH-PD[2], nm	NLDFT-PD[3], nm
Fresh catal.	919	1.0	3.0	4.1
1	858	0.9	3.0	4.1
2	941	1.0	3.7	3.8
3	810	0.8	3.0	3.8
4	780	0.8	3.7	3.8
5	790	0.8	3.7	3.9
6	860	0.9	3.0	3.8
7	832	0.9	3.7	3.8

[1]Pore Volume. [2]Pore diameter determined by Barret-Joyner-Halenda method (BJH) and [3]nonlocal density functional theory (NLDFT) from the desorption branch.

N_2-adsorption data are shown in the Table 6.3.2.1. It can be observed that there is no tendency in the decreasing of the BET specific surface. The same behavior was observed for the pore volume. The experiment number 4 revealed the highest decrement in the BET specific surface with around 140 m^2 g^{-1}. The pore diameter decreased 0.3 nm and was constant for the experiments 2-7.

The reduction of BET specific surface and pore diameter can be attributed to the coke formation (see Figure 6.3.2.5). Also, this reduction might be influenced by the formation of oligomers that do not leave the pores of the catalyst. The formation of oligomers is favorable on this type of catalysts according to Hulea et al. [58].

As it has been shown in the results of the section number 6.1, the catalytic activity of the Ni/MCM-41 is strongly influenced by the Si/Al ratio. This parameter modifies the acidity of the catalysts. Therefore, the acidity of the catalysts is crucial for having a catalyst with high catalytic activity. According to the obtained results, it is important to study how the acidity of the catalyst is changing in the heating up and cooling down experiments. The Figure 6.3.2.4 shows the NH_3-TPD spectra for these experiments.

The acidity associated with weak Brønsted and Lewis acid sites decreased considerably after the experiment number 1. This type of acidity reached a minimum for the experiment number 7. After the experiment number 1 the medium strength acidity increased considerably but decreased also considerable after the experiment number 2. According to the selectivity of *1*-butene, especially in the interval of low temperature, this acidity presents a strong influence on the isomerization step in the ETP-reaction. The acidity of medium strength decreased gradually. The lowest acidity of the catalyst was

observed for the experiment number 7. This decrease might be associated to the covering of the surface of the catalyst with carbonaceous species, as it has been stated in section 6.1.8 and is shown in Figure 6.3.2.5.

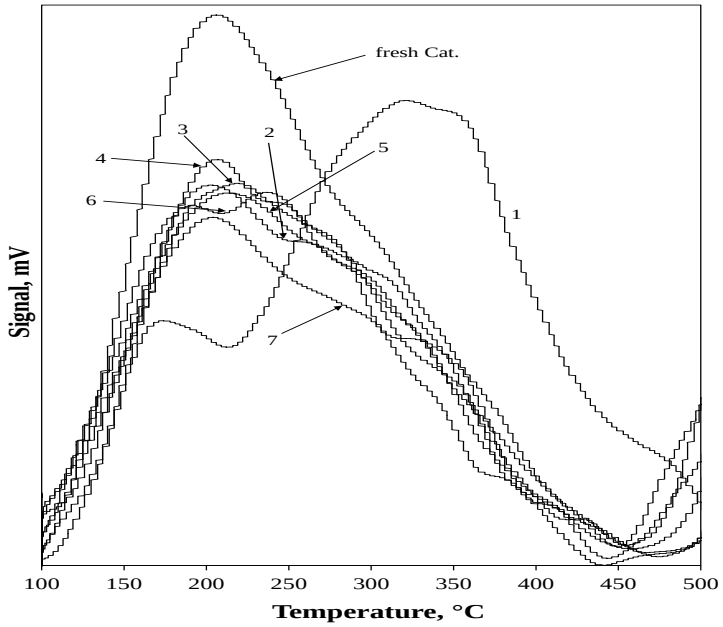

Figure 6.3.2.4. NH_3-TPD of the heating up and cooling down experiments on Ni/AlMCM-41 (Si/Al=60).

The medium strength acidity of the catalyst decreased gradually for the heating up and cooling down experiments. At the same time, the conversion of ethene decreased gradually. This result suggests that the medium strength acidity of the catalyst could be the acidity that is involved in the dimerization and metathesis step in the ETP-reaction. The conversion of ethene at 50 °C for the experiments 2-7 suggests that the adsorbed species after experiment 1 act as active sites for the dimerization of ethene and isomerization of *1*-butene.

Considering that after the ETP experiment nickel particles and carbonaceous species could be observed, this type of species might be present after the heating up and cooling down experiments. On the other hand, it is known that nickel particles promote the formation of carbonaceous species [82]. Therefore, this phenomenon can also take place during heating up and cooling down experiments.

Figure 6.3.2.5 illustrates the TPO results after the heating up and cooling down experiments. As well as the TPO results after the ETP experiment, two very broad peaks with a maximum centered in the intervals of 400-500 °C and 600-700 °C were observed.

The oxidation of nickel particles took place at temperatures lower than 300 °C [83]. The oxidation of monoatomic carbon took place at temperatures between 300 and 500 °C [84]. The oxidation peak at high temperature is associated to the oxidation of filamentous carbon [80]. The production of carbonaceous species was important for the experiment number 1 and this production increased for the rest of the experiments. These species are adsorbed on the surface of the catalysts and produce an important reduction of the acidity of the catalyst. At the same time, this reduction of acidity produces a reduction of the catalytic activity of the Ni/AlMCM-41 (Si/Al=60).

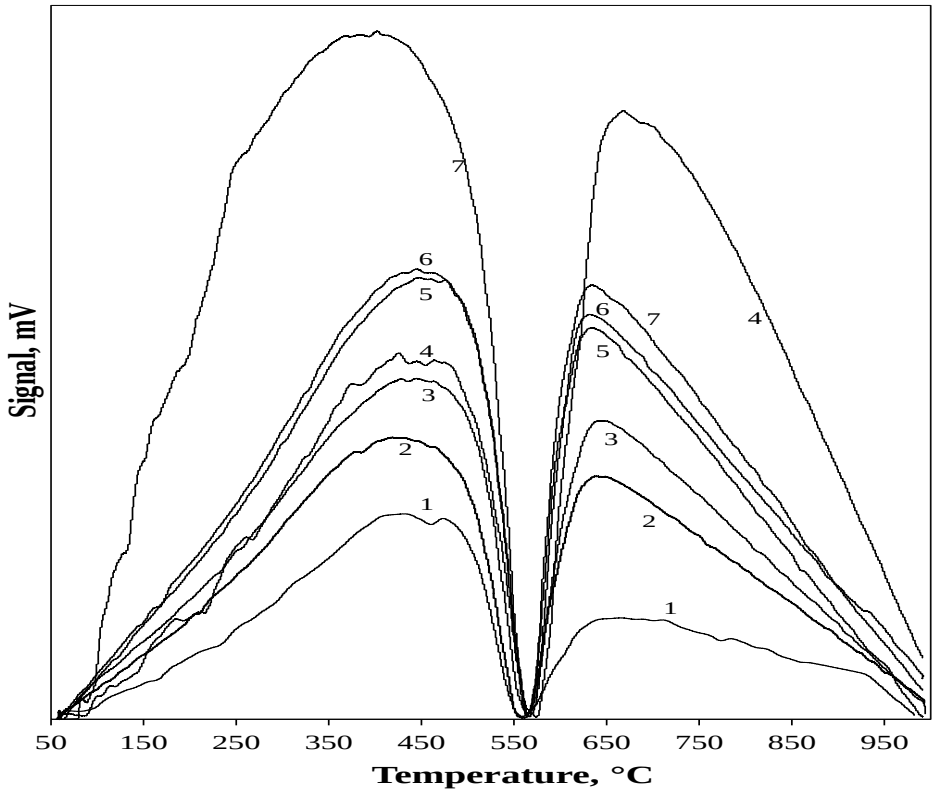

Figure 6.3.2.5. TPO of the heating up and cooling down experiments on Ni/AlMCM-41 (Si/Al=60).

According to the previous results, the following conclusions can be formulated; the catalytic activity of the Ni/AlMCM-41 (Si/Al = 60) catalyst decreased during the heating up and cooling down experiments. The temperature did not change the structural properties of the catalyst considerably. The selectivity of butenes was modified considerably in the interval of low temperatures. This modification was strongly influenced by changes in the acidity of the catalyst. TPO measurements confirmed the production of carbonaceous species and this production increased considerable for the experiment number 7.

Additionally to these experiments, it is crucial to study the stability of the catalyst under long term conditions. Therefore, a study of the stability of the catalyst under long time reaction conditions is presented in the next section.

6.3.3 Deactivation of Ni/AlMCM-41 --time on stream--

Catalyst deactivation is highly relevant in the study, development and operation of the catalytic processes and presents many scientific and technological challenges [87-102]. This deactivation occurs simultaneously with the main reaction and can be both of a chemical nature, such as poisoning, and of a physical nature, such as fouling and thermal degradation [43]. Therefore, in this section a study of the deactivation of the Ni/AlMCM-41 (Si/Al=60) under long term conditions was carried out. Powder XRD, N_2-physisorption, NH_3-TPD and TPO characterization was performed after the deactivation experiments. Deactivation experiments were carried out during 107 hours on stream. Characterization was performed after 1, 5, 15, 30, 60 and 107 hours on stream.

Figure 6.3.3.1 shows changes of the conversion of ethene and the selectivity of the major reaction products in the ETP after 107 h on stream at 250, 350 and 450 °C. At 250 °C the conversion of ethene decreased from 48% to 28% after 107 h on stream. At this temperature, the main reaction products were *2*-butene and *1*-butene. The selectivity of butenes was around 80% and 10% for *2*-butene and *1*-butene respectively. At 350 °C the conversion of ethene decreased from 70% to 58% after 107 h on stream. The main reaction products at this temperature were propene, *2*-butene and *1*-butene. The selectivity of *2*-butene increased with the time on stream and the selectivity of *1*-butene and propene did not change significantly and was around 18%. No important deactivation was observed at 250 and 350 °C. At 450 °C serious deactivation was observed, the conversion of ethene decreased from 80% to 20% after 107 h on stream. At this temperature, propene was the major reaction product, reaching a maximum selectivity close to 50% after 10 h of reaction. After this time, a slight decrement could be observed. The selectivity of propene was higher at 450 °C than at 350 and 250 °C.

The major modifications in selectivity were observed in the first 10 h of experiment at 450 °C. The selectivity of propene increased from 34 to 47% which decreased gradually after this time. In this period of time the selectivity of butenes was low (less than 20%),

which is an indication that other reactions are taking place. At 450 °C the selectivities of *1*-butene and *2*-butene were lower than at 250 and 350 °C. This behavior suggests that *1*-butene was isomerized to *2*-butene and propene was probably formed through a metathesis step between *2*-butene and ethene. This last step was favored at high temperature, 450-475 ºC (see Figures 6.1.2.2 and 6.1.2.3).

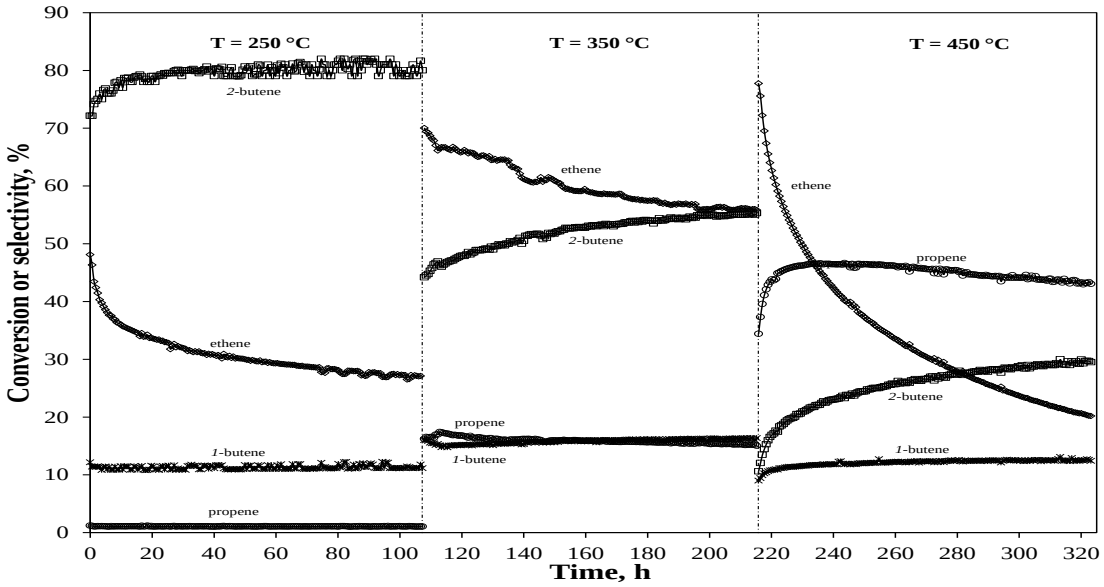

Figure 6.3.3.1. Conversion of ethene and selectivity of the major reaction products as a function of the time on stream on Ni/AlMCM-41 (Si/Al=60). T = 250, 350 and 450 °C during 107 h for each temperature.

To observe in more detail the changes in the catalytic activity in the early steps, Figure 6.3.3.2 shows the conversion of ethene and the selectivity of the major reaction products for 30 h on stream. In this Figure it can be observed that at 450 °C important changes in the selectivity of the products are taking place. In the early stages, the selectivity of propene changed from 34 to 45% and the selectivity of butenes was low. The reason of these big changes in the early stages, suggest that other reactions are taking place e. g. coke formation and oligomerization. These type or reactions might be the responsible also of the strong deactivation of the catalysts at 450 °C.

V. Hulea et al., have shown that the Ni/AlMCM-41 with different Si/Al ratios are active for the ethene oligomerization and the presence of a uniform pore-size distribution in the ordered mesoporous materials is very favorable for the oligomerization process [58]. For high temperature, these reactions might be highly favored to produce longer chain-hydrocarbons in the first 10 h on stream. These oligomers do not leave the pore and the conversion of ethene might decrease.

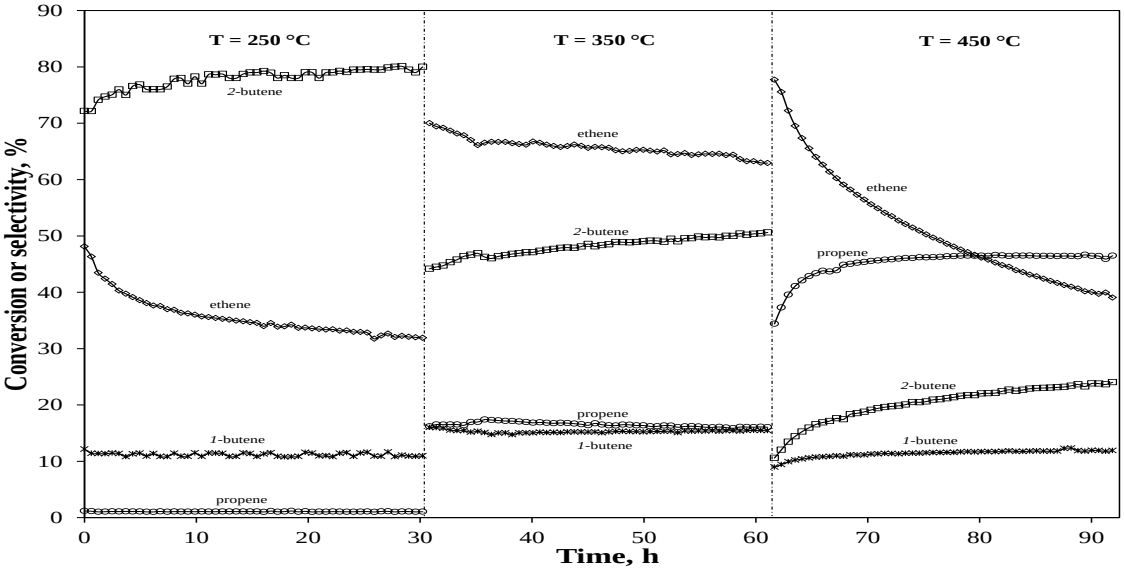

Figure 6.3.3.2. Conversion of ethene and selectivity of the major reaction products as a function of the time on stream on Ni/AlMCM-41 (Si/Al=60). T = 250, 350 and 450 °C during 30 h for each temperature.

Characterization after the deactivation experiments were carried out. Changes in the catalyst structure, pore structure, acidity and carbonaceous species production were monitored after 1, 5, 15, 30, 60 and 107 h on stream. Figure 6.3.3.3 shows the powder diffraction patterns after the deactivation experiments at 250, 350 and 450 °C.

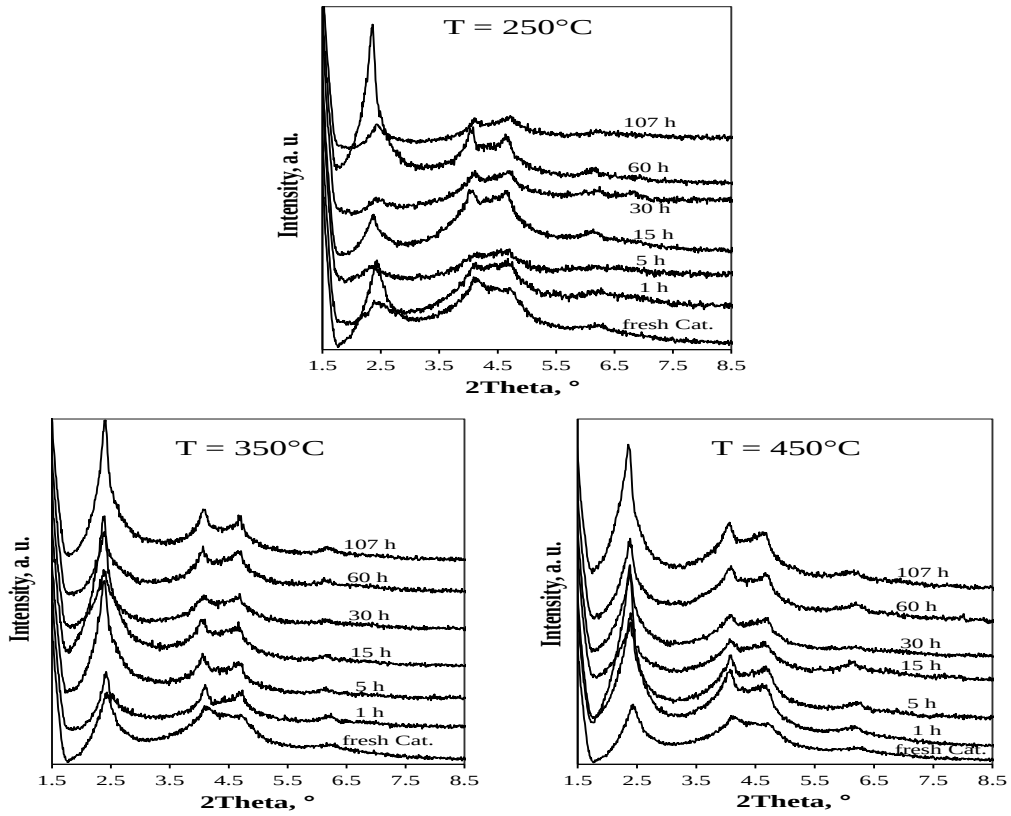

Figure 6.3.3.3. Powder XRD patterns after the deactivation experiments on Ni/AlMCM-41 (Si/Al=60).

The classical diffractions corresponding to the MCM-41 materials were preserved after the deactivation experiments at all temperatures. This result shows that the structure of the catalyst was preserved after the deactivation experiments and the deactivation of the catalyst is not related to structural changes of the catalyst.

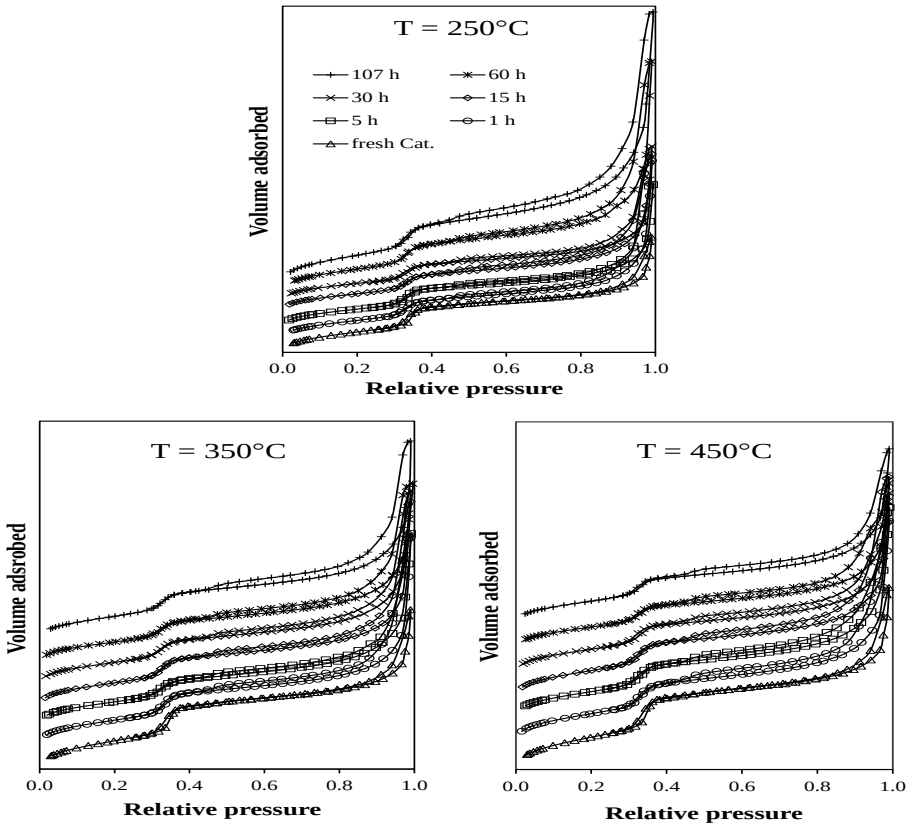

Figure 6.3.3.4. N_2-physisorption isotherms after the deactivation experiments on Ni/AlMCM-41 (Si/Al=60).

N_2-physisorption isotherms are depicted in Figure 6.3.3.4. The shape of the isotherm did not change significantly after the deactivation experiments. This result suggests small changes in the pore structure of the catalyst after the deactivation experiments. The N_2-adsorption isotherms correspond to the Type IV isotherms according to the IUPAC classification [44]. This isotherm type is classic for MCM-41 materials [54].

The fresh catalyst revealed a hysteresis of the type H1. After the deactivation experiments the N_2-adsorption isotherms showed H3 hysteresis. This type of hysteresis increased with time and with temperature. The H1 hysteresis is often associated with porous materials known to consist of agglomerates or compacts of approximately uniform spheres in fairly regular array, and hence to have narrow distributions of pore size [44]. On the other hand, the type H3 loop, is observed with aggregates of plate-like

particles giving rise to slit-shaped pores [44]. This change of the pores shape might be associated to the adsorption of oligomers or carbonaceous species during the course of the ETP-reaction [58, 80, 84].

Table 6.3.3.1.
N_2-adsorption data after the deactivation experiments of Ni/AlMCM-41 (Si/Al=60).

Temperature, °C	Time, h	BET specific surface area, m^2 g^{-1}	PV[1], cm^3 g^{-1}	BJH-PD[2], nm	NLDFT-PD[3], nm
	fresh catal.	919	1.0	3.0	4.1
250	1	1000	1.1	3.7	3.8
	5	952	1.0	3.7	3.9
	15	941	1.1	3.0	4.1
	30	940	1.0	3.7	3.8
	60	1252	1.5	3.7	4.1
	107	1025	1.8	3.7	3.8
350	1	934	1.0	3.7	4.1
	5	850	0.9	3.7	3.8
	15	890	1.0	3.7	3.8
	30	861	1.0	3.7	3.8
	60	772	0.9	3.7	3.8
	107	921	1.0	3.7	3.8
450	1	933	1.0	3.7	3.8
	5	876	1.0	3.7	3.8
	15	903	0.9	3.7	3.8
	30	823	0.9	3.7	3.8
	60	769	0.8	3.7	3.8
	107	791	0.8	3.7	3.8

[1]Pore Volume. [2]Pore diameter determined by Barret-Joyner-Halenda method (BJH) and [3]nonlocal density functional theory (NLDFT) from the desorption branch.

N_2-pyhsisorption data are shown in Table 6.3.3.1. No big changes in the BET specific surface were observed at 250 °C. The biggest change was observed at 450 °C where the specific surface decreased from 918.8 to 791.3 m^2 g^{-1}. This reduction might be due to the adsorption of oligomers and carbonaceous species. The pore volume increased and the pore diameter decreased according to the NLDF theory. This behavior is in comparison with the fresh catalyst.

The carbonaceous species might be adsorbed on the surface of the catalyst and might be the responsible of the deactivation of the catalyst, especially at 450 °C. This adsorption might also modify the acidity of the catalyst. Therefore, NH_3-TPD analysis was performed to observe changes in the acidity of the catalyst after the deactivation experiments. Figure 6.3.3.5 shows the NH_3-TPD after the deactivation experiments at 250, 350 and 450 °C. The scale of the Figures is the same, consequently a direct comparison of the intensities of the peaks can be done. Big changes of the acidity of the

catalyst were observed after the deactivation experiments. These changes were more important at 450 °C, where the intensity of the peaks decreased significantly. The acidity of the catalyst did not decrease sequentially with the time on stream. For some cases, at first the acidity decreased after one hour but after five hours on stream the acidity of the catalyst increased. This behavior suggests that the adsorbed species act as an acidic active site and they are active for the ETP-reaction. This affirmation was also stated in the section 6.4.2.

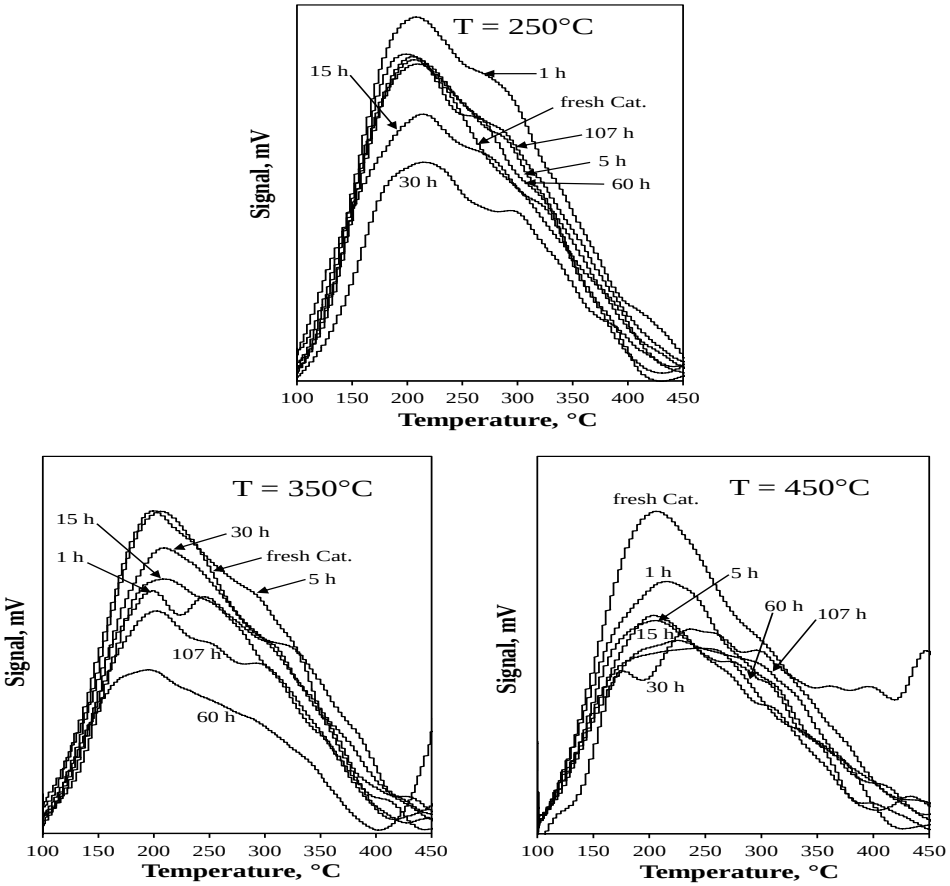

Figure 6.3.3.5. NH_3-TPD spectra after the deactivation experiments on Ni/AlMCM-41 (Si/Al=60).

A higher reduction of the medium strength acidity was observed at 450 °C than at 250 and 350 °C. According to the catalytic results, this reduction of the acidity might be the responsible of the strong deactivation of the catalyst at 450 °C.

As it has been stated oligomerization and carbon reactions formation might be the responsible of the strong deactivation of the Ni/AlMCM-41 (Si/Al = 60). This statement has been proved by performing TPO measurements. These results are depicted in the Figure 6.3.3.6.

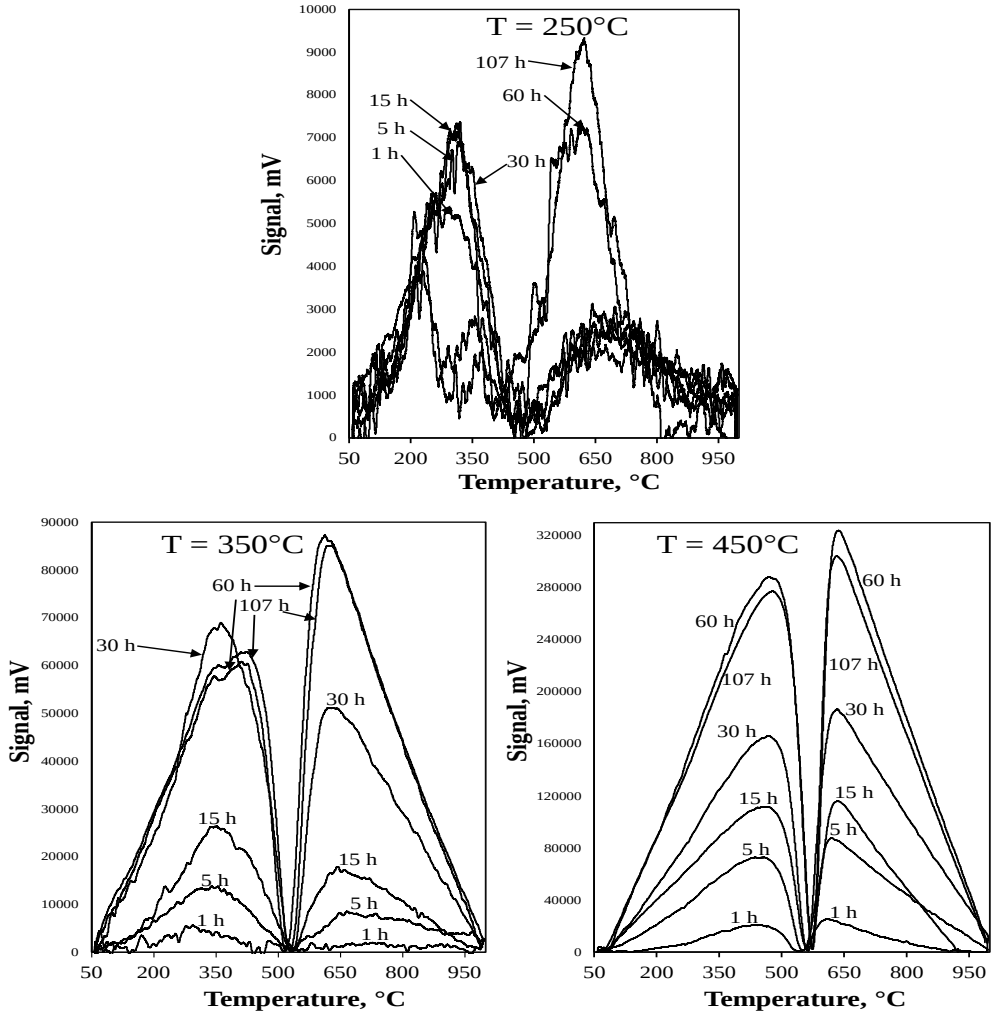

Figure 6.3.3.6. TPO profiles after the deactivation experiments on Ni/AlMCM-41 (Si/Al=60).

At 250 °C the amount of carbonaceous species was very low. At 350 °C the amount of carbonaceous increased and at 450 °C a high production of these species was observed. At all temperatures, this amount increased with the time on stream. As it has been stated in the previous section, two types of carbonaceous species are being formed during the course of the ETP-reaction; monoatomic carbon and filamentous carbon [80, 84], interesting results can be observed at 250 °C. In the early steps in the ETP-reaction, only monoatomic carbon is being formed. After 60 h on stream the formation of filamentous carbon is being favored. The same behavior was observed at 350 °C but the amount of both carbon species was higher. The opposite results were observed at 450 °C. At this temperature, the formation of filamentous carbon was higher that the formation of monoatomic carbon after five hours on stream. Therefore, filamentous carbon could be the responsible of the deactivation of the catalyst.

As well as the case of the ETP experiments, for the deactivation experiments carbon tubes and Ni particles could be observed by TEM. Figure 6.3.3.7 shows two micrographs where carbon particles and nickel particles covered by carbon can be observed after 60 h on stream. The structure of the MCM-41 was retained after the deactivation experiments. It is important to emphasize that the color of the catalyst changed after the deactivation experiments. The color changed from light-green (fresh catalyst) to light-gray and black depending on the temperature and time on stream.

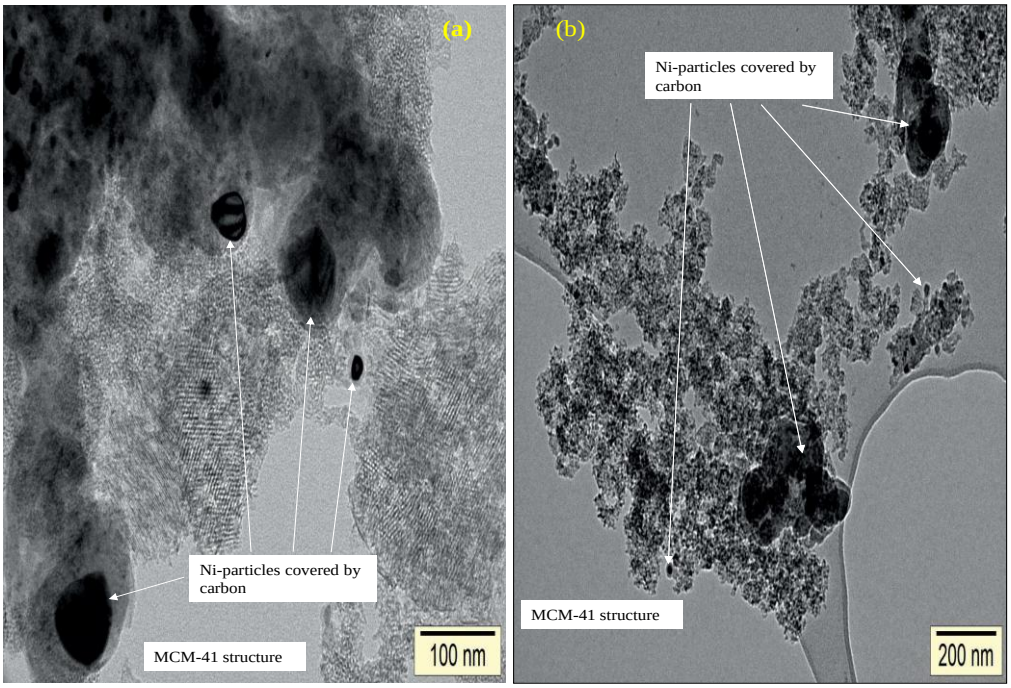

Figure 6.3.3.7. TEM micrographs of Ni/AlMCM-41 (Si/Al=60) after 60 h on stream.

From these results, the following conclusions can be formulated; strong deactivation of the catalyst was observed at 450 °C where the main reaction product is propene; the catalyst did not change its structure after 107 h on stream; BET-specific surface decreased at 450 °C and the shape of the pores was modified after the deactivation experiments. This modification was provoked by the adsorption of carbonaceous species on the surface of the catalyst; important changes in the acidity of the catalyst were observed; the acidity of medium strength might be the acidity that is active in the ETP-reaction. At 450 °C this type of acidity decreased significantly and could be the responsible of the strong deactivation of the catalyst.

Ni-particles and two different species of carbon could be observed; filamentous carbon seems to be the responsible of the deactivation of the catalyst and its production was

maximal at 450 °C after 107 h on stream. Additionally, NH_3-TPD results suggest that the adsorbed species have acidic properties that are active in the ETP reaction.

Due to the strong deactivation of the catalyst at 450 °C, where the highest production propene is taking place, a study of the capacity of regeneration of the catalyst was made. The results are shown in the next section.

6.3.4 Deactivation-regeneration of Ni/AlMCM-41

Experiments of deactivation-regeneration were carried out at the reaction conditions described in section 5.3. Figure 6.3.4.1 shows the conversion of ethene and the selectivity of the major reaction products. The major reaction products were *1*-butene and *2*-butene. The deactivation of the catalyst was carried out at 250 °C. The catalytic activity could be totally reestablished after 30 h of ETP experiment.

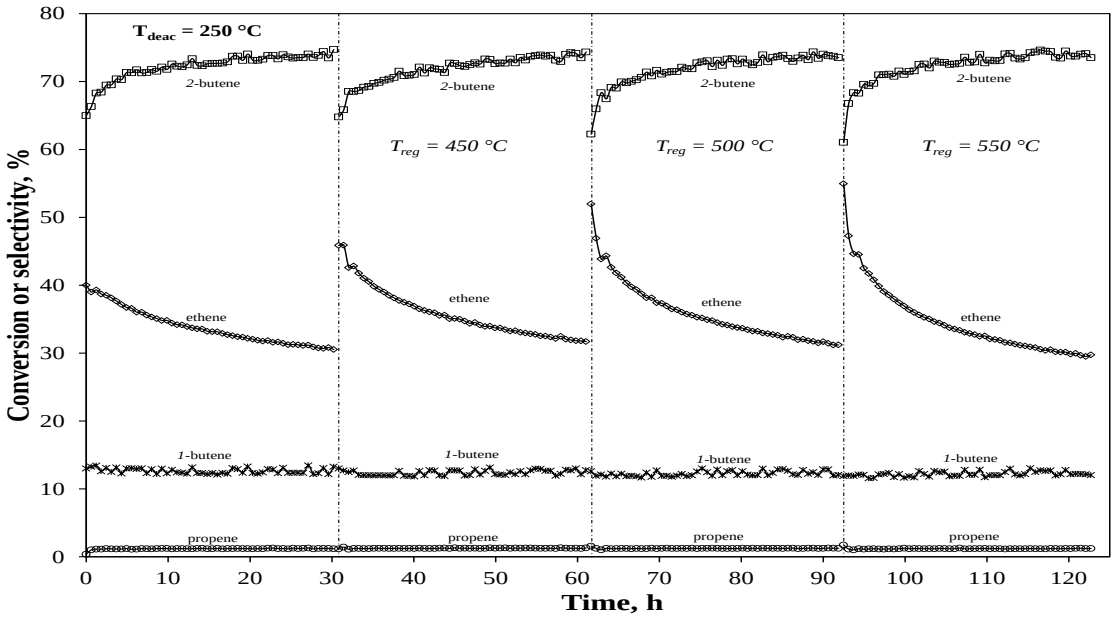

Figure 6.3.4.1. Conversion of ethene and selectivity of the major reaction products in the deactivation-regeneration experiments on Ni/AlMCM-41 (Si/Al=60). Deactivation time = 30 h. Reactivation with a mixture of 5 vol.% O_2 in N_2 for 1 h.

The initial conversion of ethene increased with the regeneration temperature from 40% to 55% at 550 °C as regeneration temperature. The conversion of ethene after the regeneration treatment dropped faster at higher regeneration temperatures. The initial selectivity of *2*-butene also decreased for higher regeneration temperatures. The selectivity of *1*-butene did not changed after 30 h of deactivation and it was not

influenced by the regeneration temperature. The regeneration temperature did not reveal any effect on the selectivity of propene, which at this temperature was very low.

The higher the conversion of ethene the lower the selectivity of *2*-butene and the selectivity of the rest of the reaction products did not change. This result suggests that the regeneration temperature is promoting the formation of side products e. g. carbonaceous species as it has been stated in the previous section.

The same type of experiments was carried out at 350 °C, as deactivation temperature. The initial conversion of ethene increased slightly from 70 to 76% with the regeneration temperature. The selectivity of propene did not change with the regeneration temperature and reached a constant value close to 20%. The selectivity of *1*-butene also did not suffer any modification after the deactivation and regeneration steps. Important changes in the selectivity of *2*-butene were observed in the early steps of the deactivation steps. This selectivity changed from 33% and reached a value of 45% after 30 h on stream. This selectivity was not affected by the regeneration temperature. The changes in the selectivity of *2*-butene suggest that side reactions are taking place. As it has been stated in the previous section, these reactions evolve reactions of carbon generation. The original catalytic activity of the catalyst was fully reestablished after the regeneration step after the deactivation experiments at 350 °C.

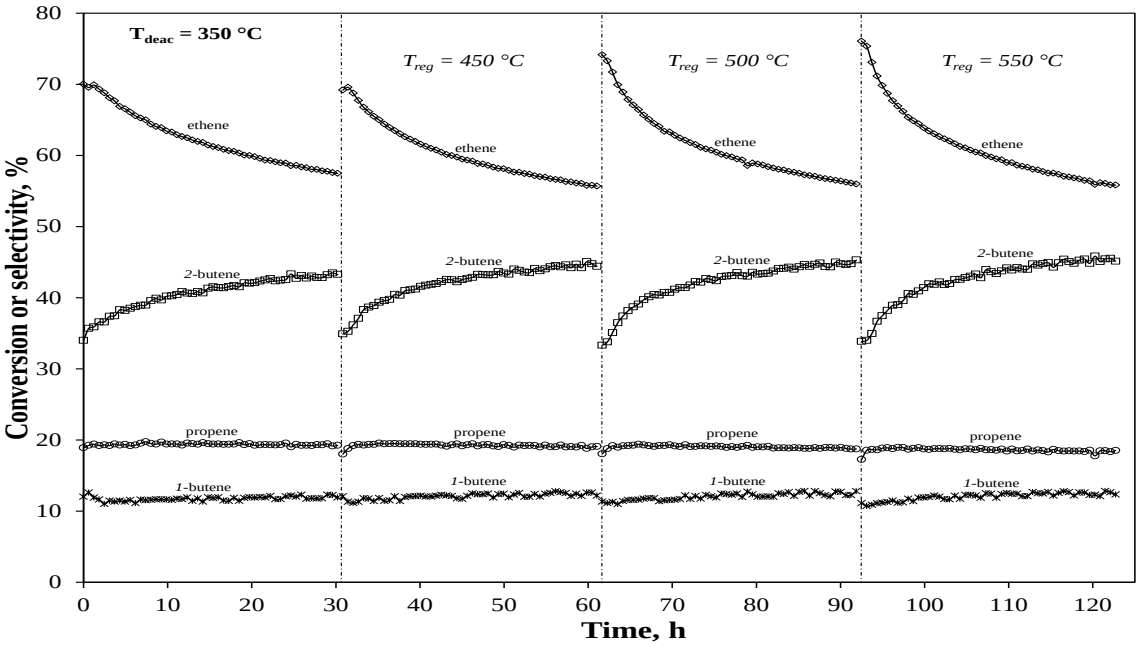

Figure 6.3.4.2. Conversion of ethene and selectivity of the major reaction products in the deactivation-regeneration experiments on Ni/AlMCM-41 (Si/Al=60). Deactivation time = 30 h. Reactivation with a mixture of 5 vol.% O_2 in N_2 for 1 h.

Finally, deactivation experiments were carried out at 450 °C. Different regeneration temperature was used, 450, 500 and 550 °C. As it has been discussed in the previous section, important deactivation of the catalyst was observed after 30 h on stream.

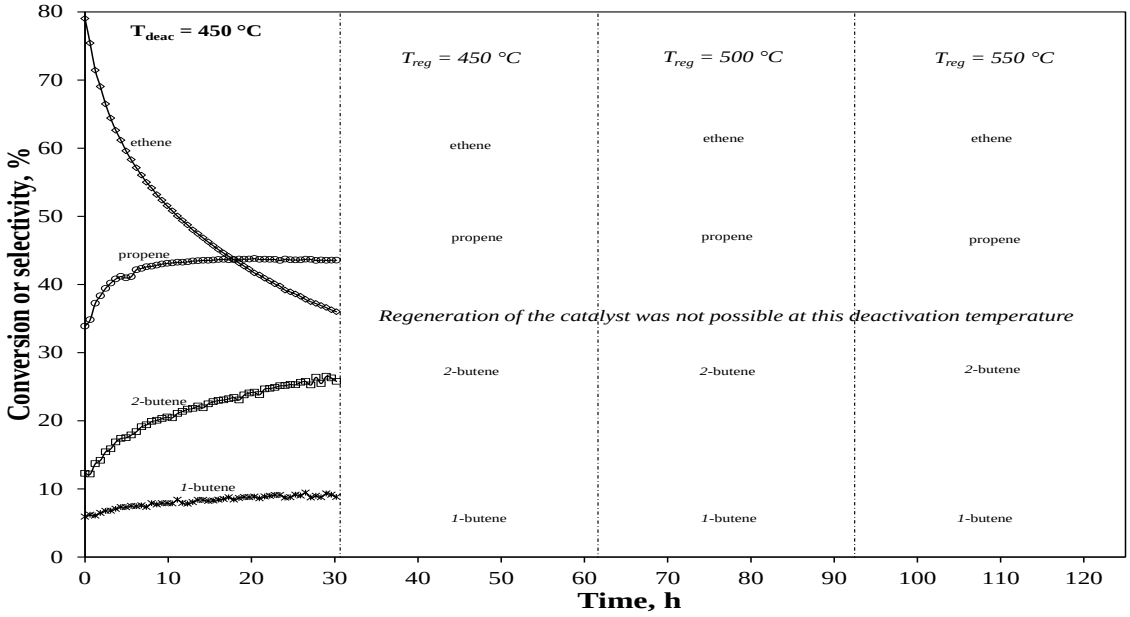

Figure 6.3.4.3. Conversion of ethene and selectivity of the major reaction products in the deactivation-regeneration experiments on Ni/AlMCM-41 (Si/Al=60). Deactivation time = 30 h. Reactivation with a mixture of 5 vol.% O_2 in N_2 for 1 h.

At this temperature, the main reaction product was propene. Important changes of selectivity were observed in the first 10 h on stream. Surprisingly, the reactivation of the catalyst was not possible at any regeneration temperature. This result revealed an irreversible adsorption of the carbonaceous species on the surface of the catalyst.

In the previous section was shown that the deactivation of the catalyst is due to the formation on different types of carbonaceous species during the course of the ETP-reaction. This deactivation is influenced also by the formation of nickel particles. At 450 °C was shown that a high production of filamentous carbon was taking place. According to the results obtained in the deactivation-regeneration, this type of carbon is highly stable and provokes a strong deactivation of the catalyst at 450 °C. Therefore, this deactivation is due to the irreversible adsorption and high stability of this type of carbon.

6.3.5 Summary

At this point, it has been shown that the acidity and the nickel state of the catalyst are the responsible of the high catalytic activity of Ni/AlMCM-41 catalyst. The TIE method

provides catalysts with high catalytic activity in the ETP-reaction. At 450 °C strong deactivation of the catalyst was observed. The strong deactivation of the catalyst is highly influenced by the production of stable carbonaceous species that are adsorbed strongly on the surface of the catalyst. The catalytic results shown in section 6.1 could be satisfactory explained according to the reaction mechanism suggested by Iwamoto et al. but in this section it has been shown that side reactions are taking place.

Additionally, this type of reactions provokes a strong deactivation of the catalyst at the temperature in which the highest production of propene was observed. For this reason, a more detailed study of the reaction mechanism in the ETP-reaction has to be done. The results concerning to this study are shown in the next section.

6.4 Study of the reaction mechanism

As it was been stated in the section 6.1, the catalytic behavior of the Ni/MCM-41 and Ni/AlMCM-41 could be satisfactory explained by the reaction mechanism proposed by Iwamoto et al., [20, 21] and at the same time, there is evidence that other type of reactions are taking place. On the other hand, the results in the previous section revealed that at 450 °C carbonaceous species are being formed and they deactivate strongly the catalyst. Therefore, these results are the confirmation that other types of reactions are taking place. In general, for hydrocarbon transformations, coke formation at temperatures lower than 200 °C means that condensation and rearrangement reactions occur [90]. At temperatures higher than 350 °C hydrogen transfer and dehydrogenation reactions, in addition to condensation and rearrangement reactions, explain the formation of coke on silica-alumina catalysts [90].

Recent results have shown that nickel-exchanged AlMCM-41 is active in the dimerization of ethene and it is an efficient bifunctional catalyst for the ethene oligomerization [58, 59]. The presence of uniform pore-size distribution is very favorable for the oligomerization process where the formation of only hydrocarbons with even carbon number took place [58]. Whereby, hydrogen transfer reactions are not occurring in a significant level during the oligomerization of ethene.

An improvement of the chemical analysis of reaction products was performed and a more complete spectrum of reaction products is depicted in Figure 6.4.1 for the catalyst with a Si/Al ratio of 60. The butene isomers and the C-balance are depicted separately.

Pentenes and hexenes are also included. In the interval of low temperature (50-150 °C) can be observed that at low conversion of ethene, the main reaction products are *trans*- and *cis*-butene. The presence of these two isomers proves that the Ni/AlMCM-41 catalysts are active for the dimerization of ethene and isomerization of *1*-butene and the results are in a good agreement with the results reported in the literature [21, 59]. Hexenes also could be observed with a selectivity of around 10%. This product is consequence of the trimerization of ethene [58]. Therefore, oligomerization reactions are taking place on Ni/AlMCM-41.

In the interval of intermediate temperature (150-300 °C) a gradual reduction of the selectivity of butenes could be observed. The selectivity of *trans*-butene decreased more significantly than the selectivity of *cis*-butene. The selectivity of *1*-butene and hexenes was kept at around 10% but two hydrocarbons with an odd number of carbons could be observed; propene and pentenes.

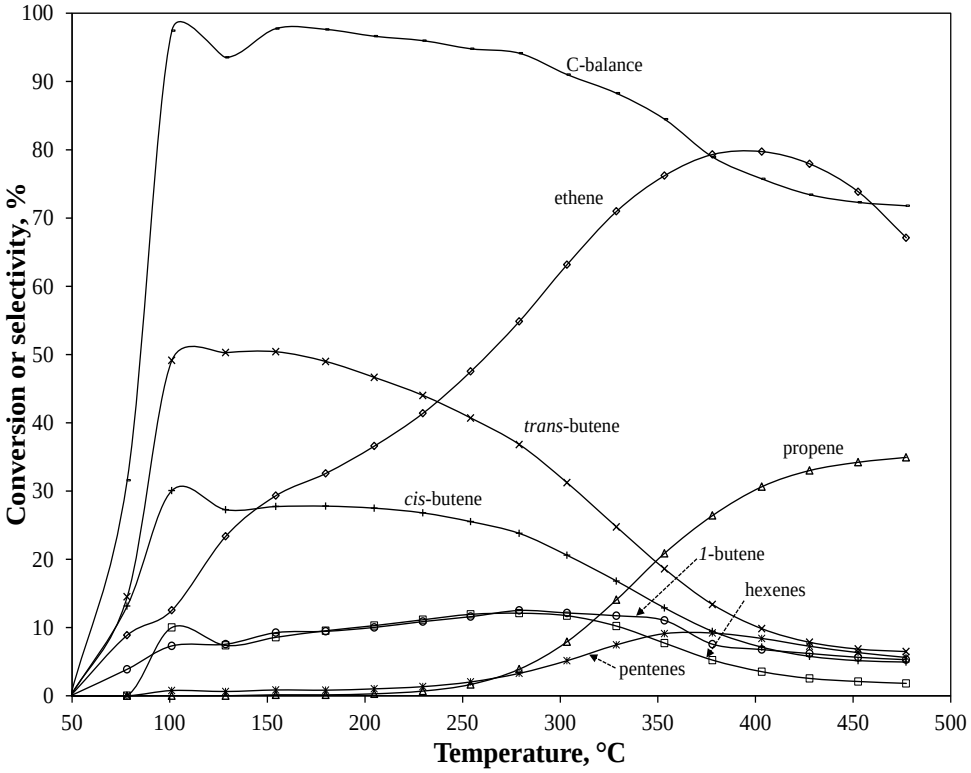

Figure 6.4.1. Product distribution and C-balance for the ETP experiment on Ni/AlMCM-41 (Si/Al=60).

The selectivity of propene reached a value ca. of 35% and the selectivity of pentenes was lower than 10% in the interval of high temperature, 300-475 °C. In this interval of temperature, the selectivity of butenes decreased and reached a lower value than 10%.

The selectivity of hexenes was close to zero at this temperature interval. At the interval of high temperature, the main reaction product was propene and reached a maximum at 450 °C.

The C-balance is also shown in Figure 6.4.1. At temperatures lower than 300 °C the mass balance was around 90%, indicating a low production of *by*-products. For this reason, a low deactivation of the catalyst was observed at 250 °C. The C-balance showed an important lack in the interval of high temperature. This lack indicates that around of 30% of the consumed ethene is wasted in side reactions, which are responsible of the coke formation at 450 °C.

The catalytic results obtained in the ETP-reaction on Ni/AlMCM-41 catalysts can be satisfactorily explained by the reaction mechanism suggested by Iwamoto [21] but definitely other type of reactions are simultaneously taking place. These reactions are oligomerization and hydrogen transfer reactions. This assessment is in concordance with the results reported in the literature [58].

To study in more detail the reaction mechanism in the ETP-reaction, the isomerization of the isomers of butene, the metathesis of propene and the metathesis of *2*-butene and ethene were carried out. *In-situ* DRIFTS characterization was used to gain deeper understanding in the reaction mechanism in the ETP-reaction. The obtained results are shown in the following sections.

6.4.1 Dimerization and oligomerization of ethene

The dimerization and oligomerization of ethene has been subject of intensive research since more than 50 years ago [59, 68, 69, 103-114]. Zeolite H-ZSM-5 have shown high catalytic activity for the ethene oligomerization where the high Brønsted acidity of the zeolite is responsible of the catalytic activity [68, 69, 103, 104]. Nickel-based catalyst systems constitute one of the important catalysts for olefin dimerization because it is the only metal which can control the mode of linking of olefins [108]. The specific activity of the nickel is high, and it is one of the less expensive of the transition elements. Because of these advantages much research has gone into the study of nickel catalyzed dimerization [59, 107-114]. In the case of heterogeneous catalysts, Hartmann et al. (1996) showed that the dimerization of ethene and isomerization of *1*-butene can proceed on Ni/MCM-41 and on Ni/AlMCM-41 [59]. The catalytic activity was higher on

Ni/AlMCM-41 than on Ni/MCM-41. In 2004, Hulea et al. performed the oligomerization of ethene on Ni/AlMCM-41 and they found that these catalysts have high catalytic activity in this reaction [58]. In general, the acidity of the catalysts and the nickel state are stated to be the active sites in the ethene dimerization and ethene oligomerization. The nickel state in the final catalysts it is believed to be Ni^{+1}[59] or Ni^{+2} [24, 27, 58].

Concerning to the ETP-reaction, Figure 6.4.1 illustrates that in the intervals of low and intermediate temperature, the main reaction products were *1*-butene, *cis*- and *trans*-butene. This is a confirmation that Ni/AlMCM-41 catalysts are active in the dimerization of ethene and in the isomerization of *1*-butene. Hexenes have been also formed during the course of reaction. This product is the product of the trimerization of ethene. These results are in a good agreement with the ones reported by Hartmann et al. and Hulea et al. [58, 59]. Additionally, electron paramagnetic resonance analysis (EPR) of the catalysts was carried out, but no signal was observed. This result suggests that nickel is present in the catalysts as Ni^{+2} and it is active in the di- and trimerization of ethene on Ni/AlMCM-41. AlMCM-41 did not show any catalytic activity, which indicates that nickel plays an indispensable role in these type of reactions. Isomerization of *1*-butene, *cis*- and *trans*-butene was carried out in order to have a better understanding of the reaction mechanism in the ETP-reaction and the results are shown in the next section.

6.4.2 Isomerization of 1-, cis- and trans-butene

Double bond migration, *cis-trans* isomerization, and skeletal isomerization are the characteristic isomerization transformations of alkenes in the presence of acidic catalysts [115]. Double-bond migration and *cis-trans* isomerization are facile transformations than can take place under mild conditions and they have been subject of intensive research to investigate the acidity of different catalysts [60, 115-129]. Since the thermodynamic stability of alkenes increases with increasing substitution on the sp^2carbon atoms, terminal alkenes exhibit the highest reactivity in double-bond migration [130]. Migration of the double bond of terminal alkenes to internal position is favored by the equilibrium. Thus, *1*-butene in the presence of activated clay, silica gel, alumina, or phosphoric acid on pumice may yield equilibrium product mixtures comprised of about 20% of *1*-butene and 80% of *2*-butene [131]. In contrast to expectations, the isomerization of *1*-butene over a silica-alumina catalyst leads to a reaction mixture rich in the thermodynamically unfavored *cis*-butene, particularly at low conversions [129]. This was explained by

evoking a bridged carbocation that cannot adopt the conformation necessary to the formation of the *trans* isomer and gives exclusively *cis*-butene. Usually, if the *cis*-/*trans*- ratio is about 1, isomerization is considered to proceed on Brønsted acid sites. If the ratio is more than 1, it proceeds on Lewis acid sites [120].

In this work, the isomerization of the butene isomers was carried out on Ni/MCM-41 and on Ni/AlMCM-41 catalysts. The reaction conditions were described in section 5.3. It should be mentioned that only under these reaction conditions, differences between the catalytic activities of the catalysts could be observed. In Figure 6.4.2.1 the conversion of *1*-butene and the selectivity of *cis*- and *trans*-butene can be observed. The conversion of *1*-butene increased for lower Si/Al ratio reaching a maximum for the catalyst with a Si/Al ratio of 16. The catalyst without Al had only activity in the interval of high temperature (300-475 °C). The main reaction product was *trans*-butene with selectivity higher than 50%. Additionally, this result reveals that the catalyst without Al presented a weak acidity.

Ni/AlMCM-41 catalysts offered a high conversion of *1*-butene at low temperature. The main reaction product was *cis*-butene at this temperature (low conversion of *1*-butene). These results agree with the results reported in the literature [120]. At temperatures higher than 425 °C the catalytic activity did not change for the catalysts with a Si/Al ratio of 150, 60 and 16 being *trans*-butene favored. The carbon balance for the *1*-butene isomerization was around 90%. Figure 6.4.2 shows the isomerization of *cis*-butene on Ni/MCM-41 and Ni/AlMCM-41 catalyst. The conversion of *cis*-butene is lower than the conversion of *1*-butene, indicating that *1*-butene is more reactive than *cis*-butene. The conversion of *cis*-butene started at higher temperature. The catalytic activity did not change significantly for the catalysts with a Si/Al ratio of 150, 60 and 16 at this temperature. The selectivity of the products is much stronger affected by the Si/Al ratio than for the case if the isomerization of *1*-butene. Independently of the Si/Al ratio, *1*-butene is the main reaction product at low temperature and *trans*-butene is the main reaction product in the interval of high temperature. The catalytic activity of the catalysts with a Si/Al ratio of 150, 60 and 16 did not change at temperatures higher than 450 °C. The carbon balance for the isomerization of *cis*-butene was very close to 100%, indicating that no by-products were formed.

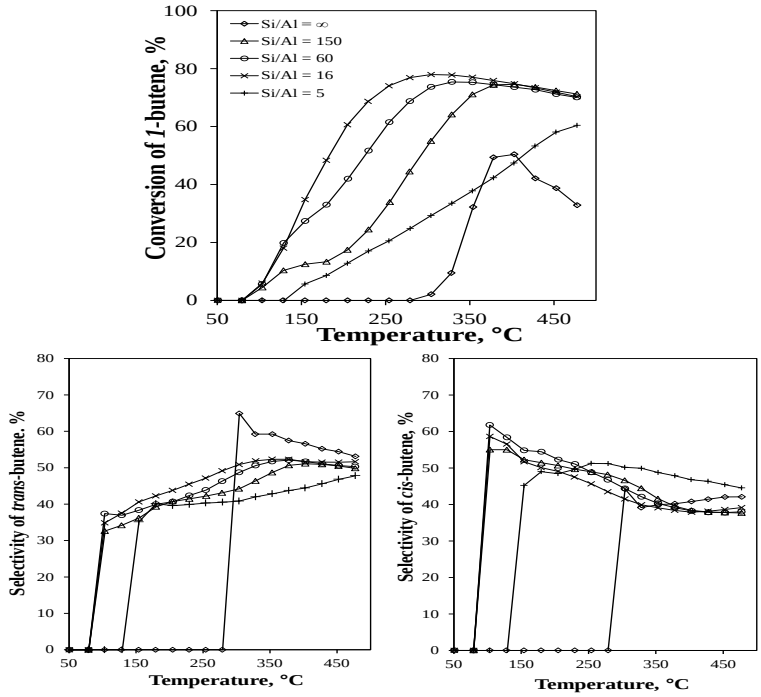

Figure 6.4.2.1. Isomerization of *1*-butene on Ni/MCM-41 and Ni/AlMCM-41 at different Si/Al ratio. *1*-butene conversion = (*1*-butene consumed / *1*-butene fed)*100. Butene selectivity = (*cis*- or *trans*-butene generated / *1*-butene consumed)*100.

Results of the isomerization of *trans*-butene are depicted in Figure 6.4.2.3. The conversion of *trans*-butene is lower than the conversion of *cis*-butene and the conversion of *1*-butene. These results agree with the results reported in the literature [129].

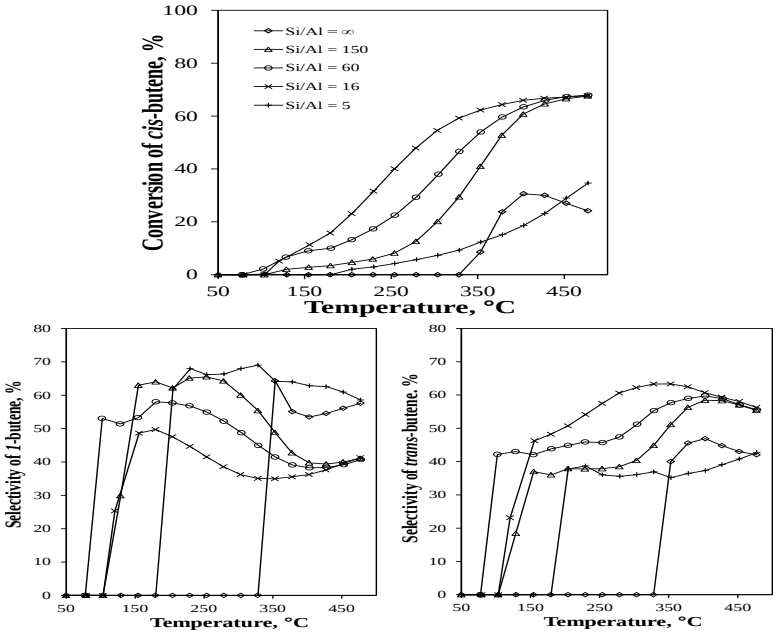

Figure 6.4.2.2. Isomerization of *cis*-butene on Ni/MCM-41 and Ni/AlMCM-41 at different Si/Al ratio. *cis*-butene conversion = (*cis*-butene consumed / *cis*-butene fed)*100. Butene selectivity = (*1*- or *trans*-butene generated / *cis*-butene consumed)*100.

The highest conversion of *trans*-butene took place at temperatures higher than 400°C and was the same for the catalysts with a Si/Al ratio of 150, 60 and 16.

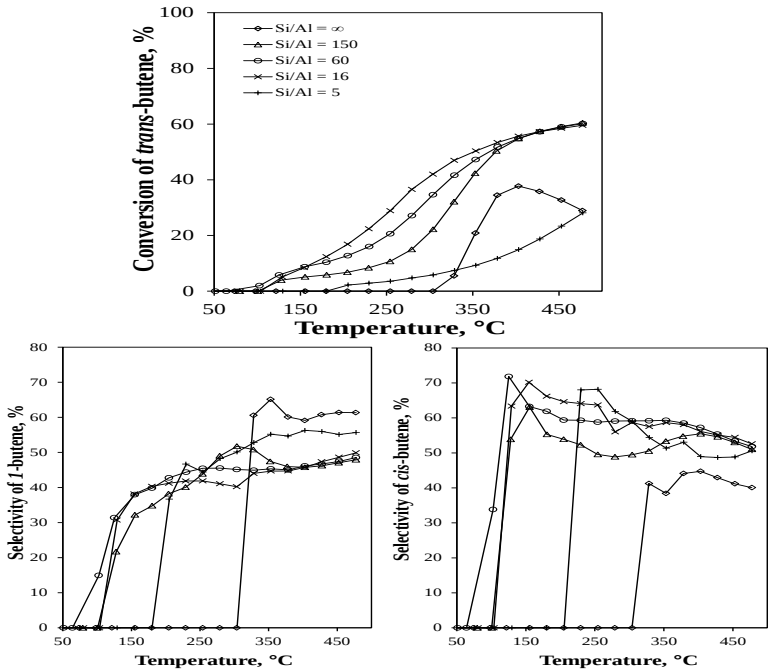

Figure 6.4.2.3. Isomerization of *trans*-butene on Ni/MCM-41 and Ni/AlMCM-41 at different Si/Al ratio. *Trans*-butene conversion = (*trans*-butene consumed / *trans*-butene fed)*100. Butene selectivity = (*1*- or *cis*-butene generated / *trans*-butene consumed)*100.

At low level of conversion, the main reaction product was *cis*-butene and its selectivity decreased slightly at higher level of conversion (high temperature). The carbon balance in the isomerization of *trans*-butene was also very close to 100%.

Bilhou et al. [132] have described that in homogeneous catalytic systems *trans*-pentene alone cannot initiate metathesis, and after initiation it has a metathesis rate which is lower than that obtained with *cis*-pentene. The opposite behavior was observed for heterogeneous systems where *trans*-butene was observed to be more reactive than *cis*-butene in the cross metathesis with *1*-butene [122, 133]. Therefore, the *trans*-butene formation might be beneficial for the ETP-reaction.

From the butenes isomerization experiments, the following conclusion can be formulated; the Al content has a strong impact on the butenes isomerization and the acidity of the catalysts reached a maximum for a Si/Al ratio of 16; the C-balance was close to 100% for the isomerization of *cis*- and *trans*-butene, indicating that no side reactions took place during the course of the reaction; the contrary was observed for the isomerization of *1*-butene where the C-balance was around 90% indicating that side-

reactions took place; no catalytic cracking of butene was observed because of the modest acidity of the catalyst. Under typical conditions like for the ETP experiment, the isomerization of butenes isomers took place very fast and no differences could be observed.

Ni/AlMCM-41 catalysts have shown catalytic activity in the dimerization of ethene and in the isomerization of butenes, but no catalytic activity in the metathesis of *2*-butene and ethene has been reported in the literature. However, Iwamoto et al. suggested that nickel on MCM-41 is active in this reaction. Therefore, to verify this affirmation the metathesis of *2*-butene and ethene was carried out and the results are shown in the next section.

6.4.3 Metathesis experiments

In section 2.3 a description of the main characteristics of the metathesis of ethene and *2*-butene were described. The classic and widely studied metathesis reaction take place on tungsten, molybdenum and rhenium based catalyst [12]. However, in this work the unusual metathesis of ethene and *2*-butene on Ni/MCM-41 and Ni/AlMCM-41 with a Si/Al ratio of 60 was carried out. The metathesis experiments were performed by feeding to the reactor a mixture of ethene and *cis*- or *trans*-butene. Figure 6.4.3.1 shows the results of the metathesis of *cis*-butene and ethene on Ni/AlMCM-41 with a Si/Al ratio of 60 (a) and on Ni/MCM-41 (b). The feed molar ratio was 1:1 with a GHSV 1.4 l $h^{-1}g_{cat}^{-1}$.

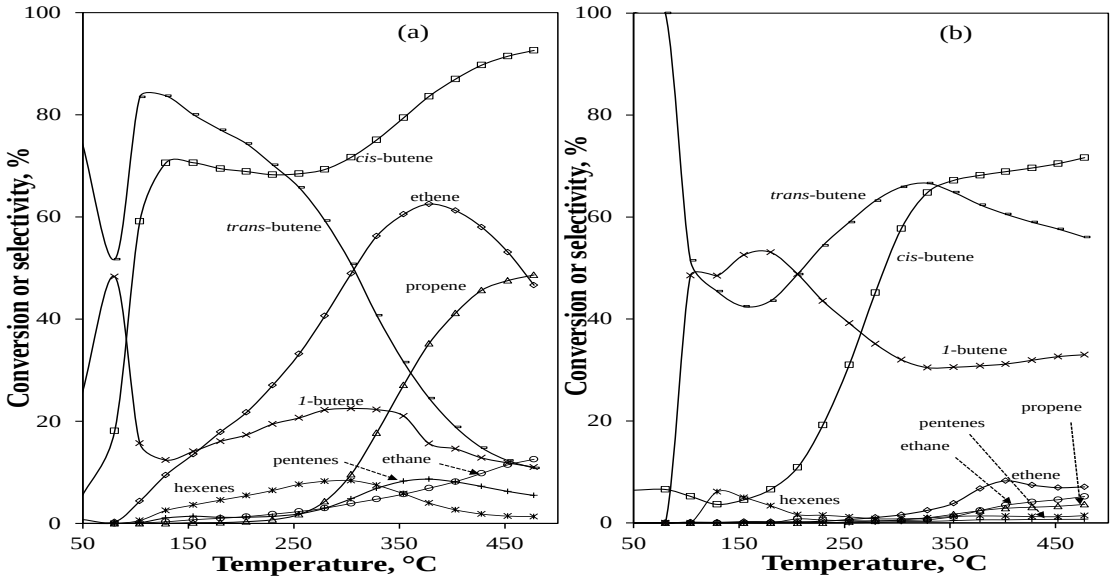

Figure 6.4.3.1. Metathesis of *cis*-butene and ethene on Ni/AlMCM-41, Si/Al=60 (a) and on Ni/MCM-41 (b). Feed molar ratio 1:1. Ethene or *cis*-butene conversion = (ethene or *cis*-butene consumed / ethene or *cis*-butene fed)*100. Products selectivity = (product generated / total products formed)*100.

In the interval of low temperature (50-150 °C) the conversion of *cis*-butene increased from 5% to around 70% and the conversion of ethene reached ca. 12%. The main reaction products in this interval were butene isomers, *1*-butene and *trans*-butene. In the interval of 150 and 300 °C, also the major reaction products were the butene isomers, but the conversion of ethene was close to 50%. In this interval, propene started to be formed and the selectivity of products like ethane, pentenes and hexenes reached a value lower that 10%.

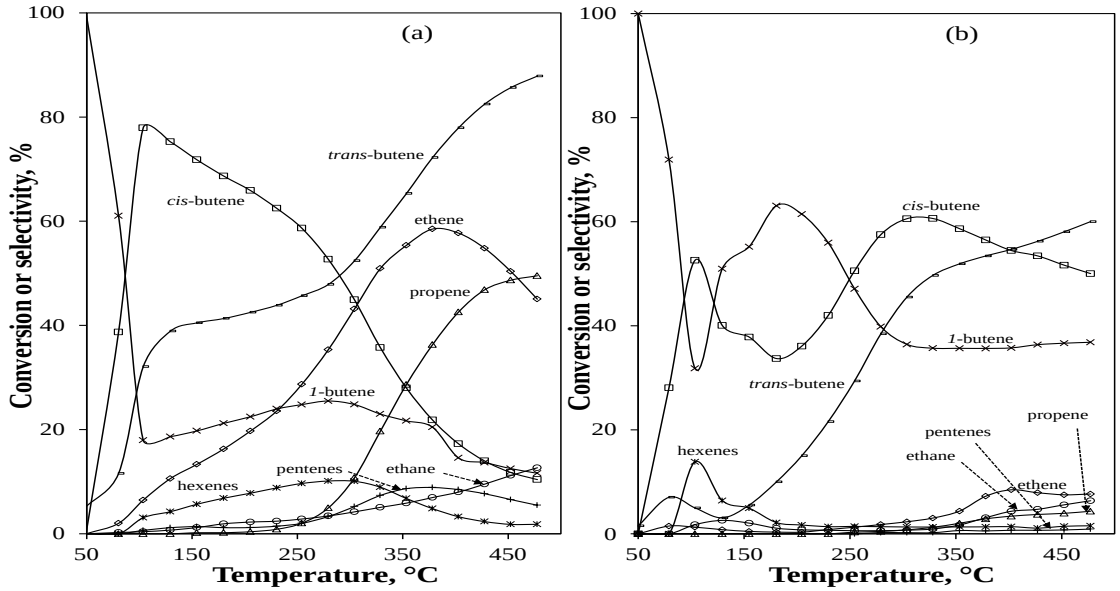

Figure 6.4.3.2. Metathesis of *trans*-butene and ethene on Ni/AlMCM-41, Si/Al=60 (a) and on Ni/MCM-41 (b). Feed molar ratio 1:1. Ethene or *trans*-butene conversion = (ethene or *trans*-butene consumed / ethene or *trans*-butene fed)*100. Products selectivity = (product generated / total products formed)*100.

In the interval of high temperature, the conversion of *cis*-butene was higher than 90% and the conversion of ethene reached a maximum of around 60% at 375°C. At this temperature, the major reaction products were butene isomers and propene. The selectivity of ethane, pentenes and hexenes was lower than 10%. Similar results were observed for the catalyst with a Si/Al ratio of 150 and 16 (see Appendix C). According to the results reported in the literature, the metathesis of *2*-butene and ethene can take place even at room temperature [134]. However, these results were not observed on Ni/AlMCM-41 catalysts. Figure 6.4.3.1 illustrates also the metathesis results for the catalyst Ni/MCM-41. It can be observed that the main reaction products were butene isomers at all temperatures. The selectivity of ethene, ethane, propene, pentenes and hexes were lower than 10% in the interval of high temperature. Similar results were observed on the catalyst with a Si/Al ratio of 5 (see Appendix C).

Metathesis experiments, between *trans*-butene and ethene were also carried out and the results are depicted in Figure 6.4.3.2. Similar results were observed like the metathesis of *cis*-butene and ethene (the catalytic activity for the catalysts with a Si/Al ratio of 150, 16 and 5 are depicted in Appendix C). Independently, of *cis*- or *trans*-butene, the main reaction product was propene in the interval of high temperature for the Al containing catalysts (this conclusion is not valid for the catalyst with a Si/Al ratio of 5 where the main reaction products were butene isomers). Therefore, these results suggest that at high temperature the metathesis of *2*-butene (*cis*- or *trans*-) and ethene is taking place. To test this hypothesis, the retro-metathesis of propene was also carried out. Theoretically, an equimolar mixture of ethene and *2*-butene should be obtained when the metathesis reaction is taking place. However, different results were obtained during the retro-metathesis of propene at the same reaction conditions like the ETP experiment. The feed composition was 5 vol.% of propene in nitrogen. This reaction was carried out on Ni/AlMCM-41 with a Si/Al ratio of 60 and on Ni/MCM-41. The results are depicted in figure 6.4.3.3. On Ni/AlMCM-41 (Si/Al=60), the main reaction products in the interval of low and intermediate temperature were hexenes isomers. Thus, instead a retro-metathesis reaction of propene, the dimerization of propene is the dominant reaction. From these results, it can be concluded that in these intervals of temperature, retro-metathesis reaction of propene is not taking place.

At the interval of high temperature the conversion of propene increased and the main reaction product was ethene with a selectivity of around 20%. The selectivity of butenes, pentenes and hexenes was lower than 10%. Therefore, these results strongly suggest that no retro-metathesis of propene was taking place. The C-balance value was around 60% at high temperature. Ni/MCM-41 presented almost no catalytic activity in this experiment, Figure 6.4.3.3(b). The lack in the C-balance suggests that other reaction took place in these experiments. Similar results were observed on the catalysts with a Si/Al ratio of 150 and 16 (Figure shown in Appendix E). The conversion of propene decreased dramatically (lower than 10%) for the catalyst with a Si/Al ratio of 5 and the selectivity of hexenes was higher than 90% in the interval of low temperature (Figure shown in Appendix E). The selectivity of ethene was around 20% in the interval of high temperature and the selectivity of the other reaction products was lower than 10% at all temperatures.

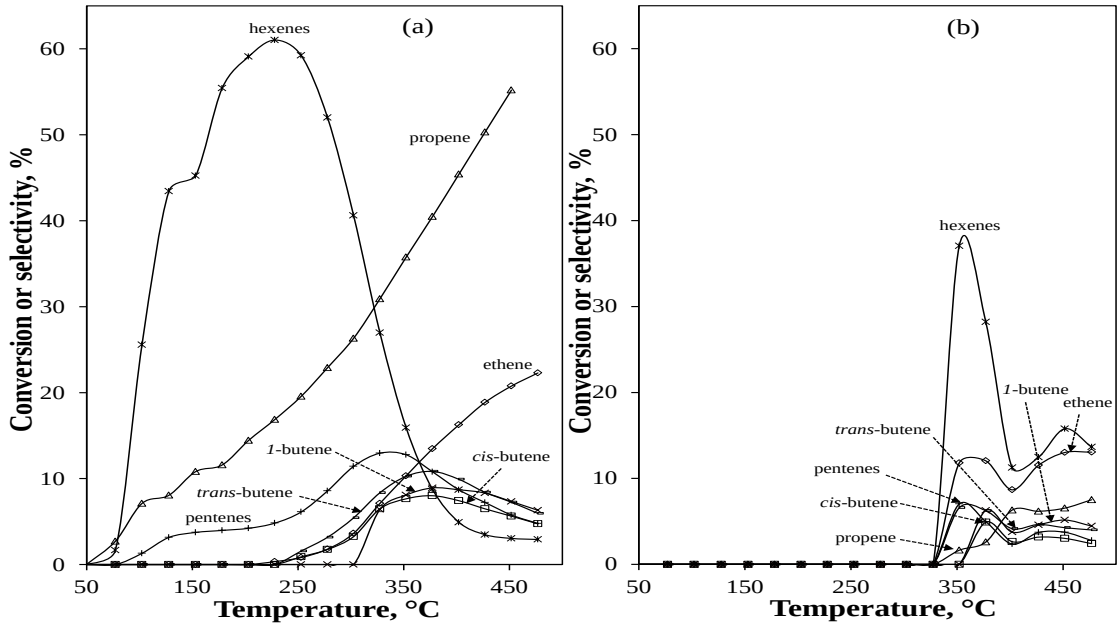

Figure 6.4.3.3. Retro-metathesis of propene on Ni/AlMCM-41, Si/Al=60 (a), and on Ni/MCM-41 (b).

Lewis acid sites and Brønsted acids, may effect oligomerization of alkenes [130]. Two types of transformation may occur; true oligomerization and conjunct polymerization. In the true oligomerization the products are alkenes having molecular weights that are integral multiples of the molecular weight of the monomer alkene. Conjunct polymerization, also called hydropolymerization, in contrast, yields a product that is a complex mixture of saturated (alkanes and cycloalkanes) and unsaturated (alkenes, alkapolyenes, cycloalkenes, and cycloalkapolyenes) hydrocarbons, and occasionally even aromatic compounds [130]. The obtained results strongly suggest that a conjunct polymerization instead of a metathesis or retro-metathesis reaction is taking place. The lack in the C-balance also supports this conclusion.

To support this affirmation, *in-situ* DRIFTS experiments were carried out during the ETP experiments. The results obtained from this characterization are presented in the next section.

6.4.4 In-situ DRIFTS characterization in the ETP experiment

The reaction conditions and the experimental procedure to perform the *in-situ* DRIFTS experiments were described in section 4.7. The DRIFTS spectra of pure Ni/MCM-41 and Ni/AlMCM-41 catalyst (pre-treated at 400 °C for 60 min under a constant nitrogen flow of 30 ml min^{-1}) were shown in Figure 6.1.6.1.

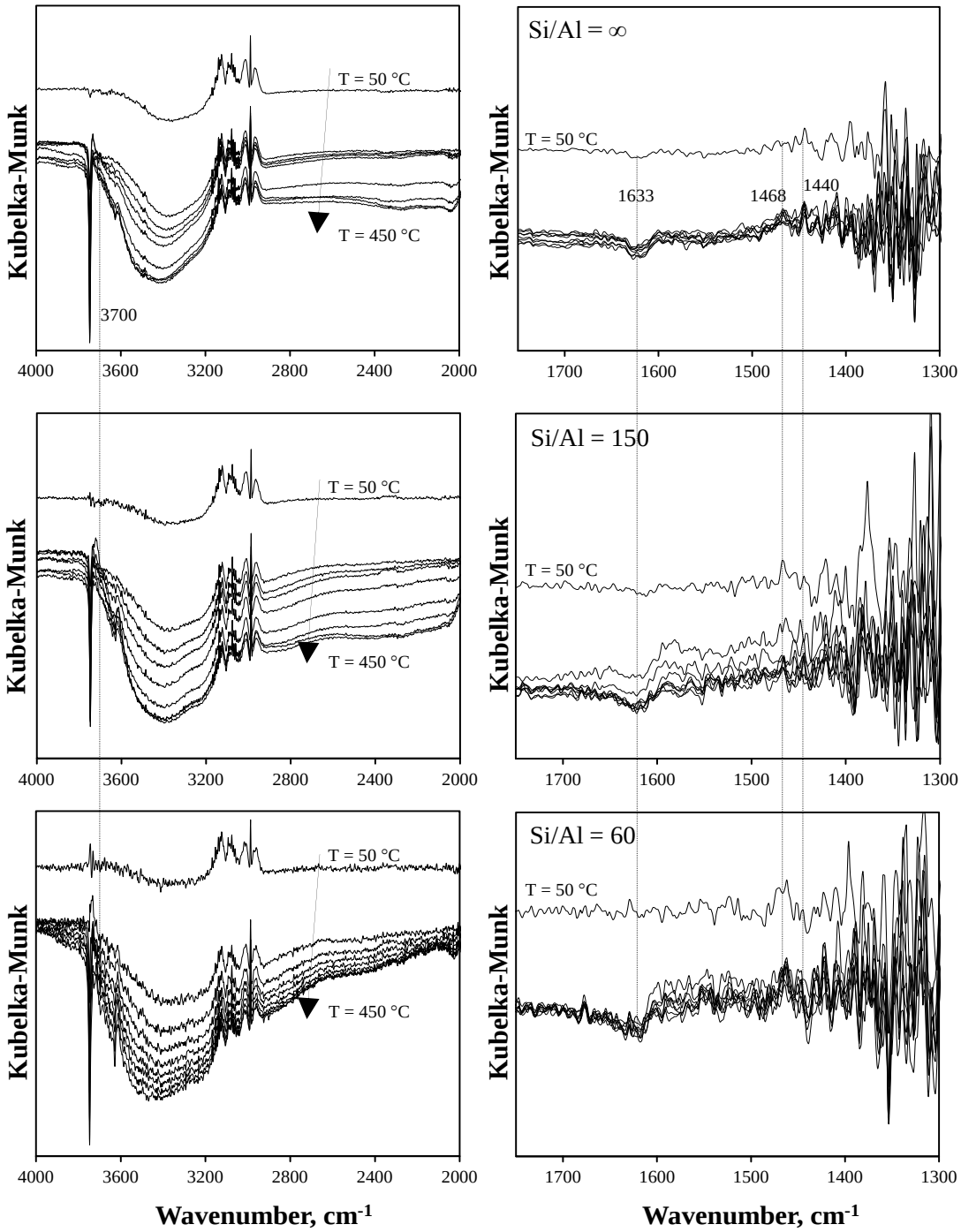

Figure 6.4.4.1. *In-situ* diffuse-reflectance FTIR spectra during the ETP experiment for the catalyst with different Si/Al ratio. Feed = 2.5 vol.% ethene in N_2. 0.7 l h^{-1}.

All catalysts exhibited two characteristic bands at 3745 cm^{-1} corresponding to Si-OH groups and at 3550 – 3700 cm^{-1} corresponding to Al-OH and Si-OH-Al groups [71]. Before the ETP experiment, the intensity of these bands increases for lower Si/Al ratio but for the catalyst with a Si/Al ratio of 5 their intensity was found to be the lowest. The catalyst with a Si/Al ratio of 60 offered the highest intensity of both bands.

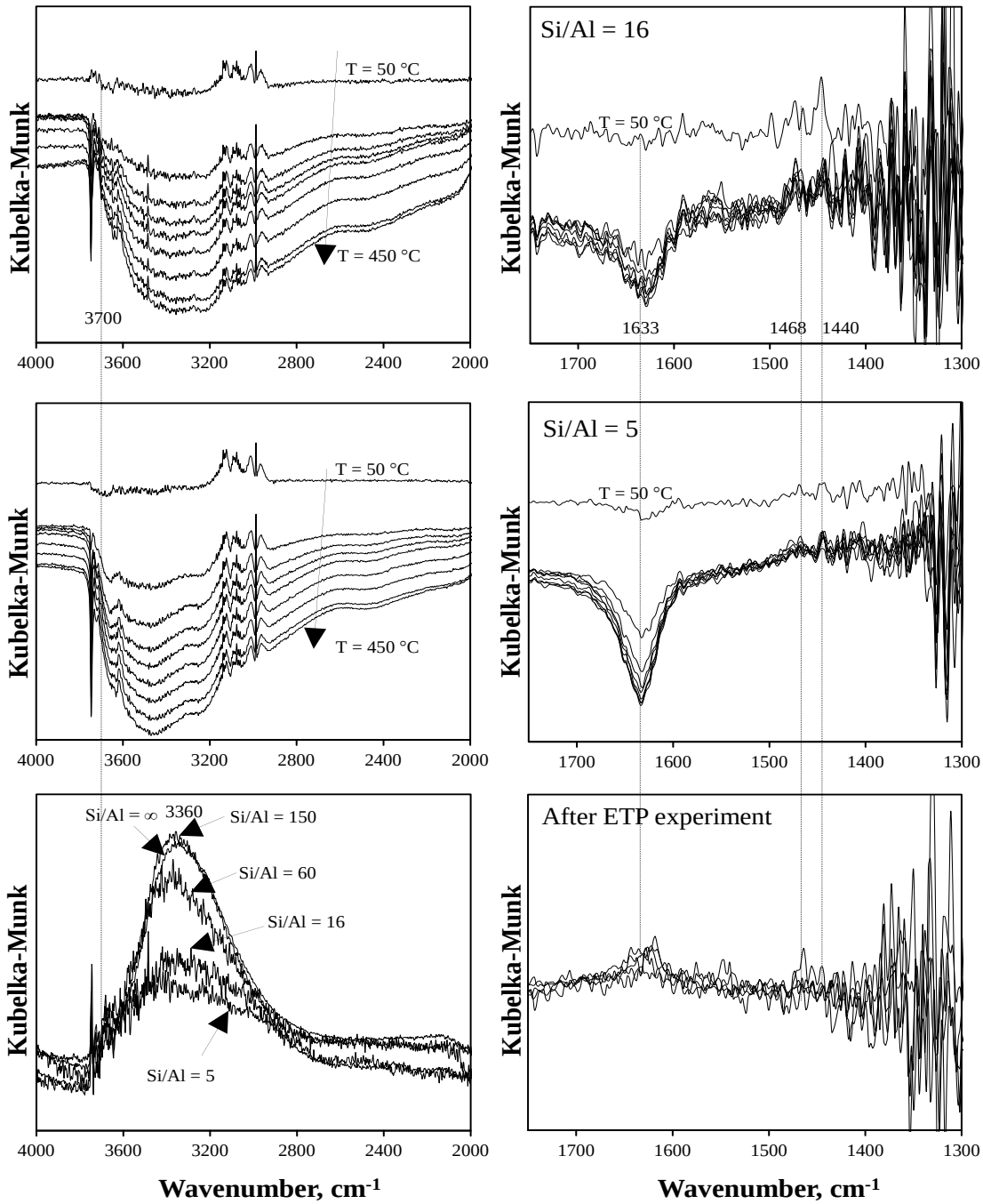

Figure 6.4.4.2. *In-situ* diffuse-reflectance FTIR spectra during the ETP experiment for the catalyst with different Si/Al ratio and after the ETP experiment. Feed = 2.5 vol.% ethene in N_2. 0.7 l h^{-1}.

Figure 6.4.4.1 shows the *in-situ* DRIFTS spectra during the ETP experiment for the catalysts with a Si/Al ratio of ∞, 150 and 60 at different temperature. The temperature was changed from 50 °C to 450 °C in steps of 50 °C. At each temperature the DRIFTS spectrum was recorded without interruption of the ethene feed. According to the catalytic results in the section 6.1.2, at 50 °C no chemical reaction is taking place. Therefore, at

this temperature only adsorption of ethene occurred. Only the difference spectra, obtained by using the spectrum of the pure catalyst as background, are reported. In this representation the bands appearing as negative peaks belong to species which are consumed, while those that are appearing as positive peaks belong to species that are formed during the ETP experiment.

Independently of the Si/Al ratio but at 50 °C only adsorption of ethene was observed. Because of this adsorption, a slight decrement in the OH stretching region was observed at this temperature. With the increase of temperature, the interaction of ethene with the OH groups became stronger. This interaction could be observed for the apparition of a peak at 3745 cm^{-1} for all catalysts, also Figure 6.4.4.2. This fact means that ethene is interacting with Si-OH groups but, according to the catalytic results showed in the section 6.1.2, this interaction is not activating the ethene molecule. Thus, the Si-OH groups are not active centers for the ETP-reaction. This conclusion was observed for the Ni/MCM-41 catalyst which revealed a very low catalytic activity.

The interaction of ethene with the OH groups on the catalysts revealed the apparition of a very good resolved peak at 3627 cm^{-1}. This peak is associated with Si-OH-Al groups (Brønsted acidity) [71, 86] where nickel is also involved. This interaction reached a maximum for the catalyst with a Si/Al ratio of 60. According to the catalytic results discussed in section 6.1.2, this catalyst revealed the highest catalytic performance in the ETP-reaction. Therefore, this result strongly suggests that Si-OH-Al groups are the active centers in the ETP reaction. This interaction became stronger at higher temperature. The positive bands in the interval of 3200 and 2900 cm^{-1} correspond to ethene in gas phase [30] and their intensity decreased because of the interaction of ethene with silanols groups.

Important changes were observed in the interval of 1750 and 1300 cm^{-1} for all catalysts, Figures 6.5.4.1 and 2. A broad and complex band in the interval of 1680 and 1600 cm^{-1} with a minimum at 1613 cm^{-1} could be observed. This band is assigned to the formation of hydrogen-bonded complexes formed by the interaction of ethene with acidic Brønsted sites [135]. These adsorbed complex can suffer easily isomerization, oligomerization and cracking reactions even at room temperature [135]. This complex band can be also assigned to the presence and reaction of butene isomers according to the results reported by Wu et al. [136]. A very weak band at 3700 cm^{-1} could be also recognized. This band

can be associated to the gradual interaction of the silanols groups with the polymeric chain that progressively is covering the surface of the catalysts [137]. This band was observed during the adsorption and reaction of ethene on a Cr^{2+}/SiO_2 Phillips catalyst [137]. Two weak bands could be distinguished at 1468 and 1440 cm^{-1}. These bands can be associated to protonation and growing of the polymeric chain [137, 138]. The interval of 1400 and 1300 cm^{-1} was characterized of high absorbance of the adsorbed species and clear bands could not be observed.

The band centered at 1633 cm^{-1} was strongly affected by the Si/Al ratio. For the Ni/MCM-41 the reactivity of the ethene-complexes was very low. This result might be explained by the absence of Si-OH-Al groups which are the active sites in the ETP-reaction. This band reached a minimum for the catalyst with a Si/Al ratio of 5. Thus, the presence of aluminum in the catalyst is increasing the reactivity of the adsorbed ethene-complexes. It can be recognized that, the higher the reaction temperature the higher the reactivity of adsorbed ethene-complexes for the catalyst with a Si/Al ratio of 5. The stronger decrease of this band can be explained by the low conversion of ethene and the high selectivity of propene (results shown in section 6.1.2), where most probably the adsorbed ethene-complexes are being consumed to produce mainly propene. This lack of the adsorbed ethene-complexes could not be observed for the catalysts with a Si/Al ratio of 150, 60 and 16 because of the stronger interaction of ethene with the Brønsted acid sites. For this reason no significant changes in the intensity of the band at 1633 cm^{-1} were observed at different temperatures. The intensity of the bands 1468 and 1440 cm^{-1} was not strongly affected by the aluminum content and by the temperature. This result means that the protonation and the growing of the polymeric chain are fast reactions. It is important to emphasize that according to the DRIFTS experiments, the most plausible route to produce propene might be trough hydropolymerization reactions. This process involves the formation and cracking of oligomers to produce a complex mixture of hydrocarbons, where in this project it has been shown, one of the main reaction products is propene. On the other hand, according to the DRIFTS analysis, the oligomerization observed on Ni/MCM-41 and Ni/AlMCM-41 catalysts take place in a very different manner in contrast to zeolitic materials, clays and some metal based catalysts [135-138]. On these materials high intensity bands were observed in the interval of 3000 and 2800 cm^{-1}. These bands are assigned to polymeric compounds and they were not recognized on Ni/MCM-41 and

Ni/AlMCM-41 catalysts. Therefore, the oligomerization reaction mechanism on the catalyst used in this work might be different to the reaction mechanism observed for zeolites and other metal based catalysts.

Figure 6.4.4.2 also illustrates the DRIFTS spectra for the catalyst after the ETP experiment. The spectra were collected after flushing the catalysts with a nitrogen flow of 30 ml min^{-1} during 30 min at 450 °C. The spectra were collected at 30 °C. The spectra revealed a very broad peak in the interval of 3800 and 2800 cm^{-1} and centered at around 3360 cm^{-1}. This complex band is due to OH groups that interact with polymeric chains [135]. After the ETP experiment a band at 3745 cm^{-1} showed up. This band corresponds to Si-OH groups and became less intense for the catalyst with a Si/Al ratio of 60. This observation confirms that the Si-OH-Al groups are the active centers in the ETP-reaction. The positive band observed at 1633 cm^{-1} shows the presence of ethene-complex strongly adsorbed after the ETP-experiment.

6.4.5 Discussion and analysis of the obtained results

The study of the reaction mechanism performed in this section, provides experimental evidence that during the ETP-reaction a complex set of chemical reactions are taking place. The dimerization of ethene was confirmed specially at temperatures lower than 250 °C, where a mixture of butene isomers could be observed. This isomerization of butene isomers is taking place because of the acidity of the catalysts prepared in this work. Therefore, the join properties of nickel and the acidity make the Ni/AlMCM-41 catalyst very attractive for the dimerization of ethene.

The suggested metathesis reaction of ethene and *2*-butene reported by Iwamoto et al. on Ni/MCM-41 could not be confirmed on Ni/AlMCM-41 catalysts. The same result was observed for the *retro*-metathesis of propene. The Ni/MCM-41 catalyst revealed a very low catalytic activity. Instead of this unusual *retro*-metathesis reaction a conjunct polymerization, also called hydropolymerization, reactions is taking place. This conclusion is supported by DRIFTS experiments that revealed the presence of polymeric species on the surface of the catalyst while the ETP-reaction proceeds. These polymeric species are the coke precursors observed in the deactivation experiments at high temperature as discussed in section 6.3.3. On this temperature range, propene is one of

the main reaction products and its formation is via the cracking of the formed oligomers on the surface of the catalyst that interact with Si-OH-Al groups (Brønsted acid sites).

At this point of this project, all results have shown that Ni/AlMCM-41 catalysts are active in the ETP-reaction. The presence of nickel and acidic acid sites are crucial to have an active catalyst in this reaction. The main drawback of these catalysts is their serious deactivation exactly at the temperature where propene is the main reaction product. For this reason, a careful strategy has to be developed in order to improve the performance of these catalysts in the ETP-reaction. In this sense, the synthesis of *bi*-metallic catalysts based on nickel-molybdenum or nickel-rhenium can represent an attractive alternative to improve the catalytic activity of Ni/AlMCM-41 catalysts. This suggestion is based on three different aspects; the first one is that the ETP-reaction was observed at first on metathesis catalysts; the second one is that at temperatures lower than 250 °C the main reaction product in the ETP-reaction is *2*-butene and the introduction of a metathesis active site might promote this reaction at temperatures lower than 250 °C; and finally, molybdenum and rhenium are classic metathesis catalysts.

In order to have a better understanding of the results of the nickel-molybdenum and nickel-rhenium based catalysts (*bi*-metallic), at first, the synthesis, characterization and catalytic testing of molybdenum and rhenium based catalyst (*mono*-metallic) is required. The next section will present the results regarding the *mono*-metallic catalysts.

6.5 Metathesis molybdenum and rhenium based catalysts

In this section, results of the molybdenum and rhenium based catalysts (*mono*-metallic catalysts) are presented. The synthesis conditions were described in section 5.2. These catalysts were prepared by template ion exchange (TIE), incipient wetness impregnation (IWI), wet impregnation (WI) and thermal spreading (TS). TIE method was used to allow an objective comparison with nickel based catalysts studied in the previous sections. IWI and WI are classic impregnation methods for metathesis catalysts [12, 53]. Finally, TS method was used as novel and simple method to synthesize metathesis molybdenum based catalysts [53]. In this section, results of molybdenum based catalysts are shown in the first part and rhenium based catalysts are shown in the second part.

6.5.1 Molybdenum based catalysts

Figure 6.5.1.1 reveals the structural characterization of the molybdenum (Mo) based catalysts prepared by different synthesis procedures.

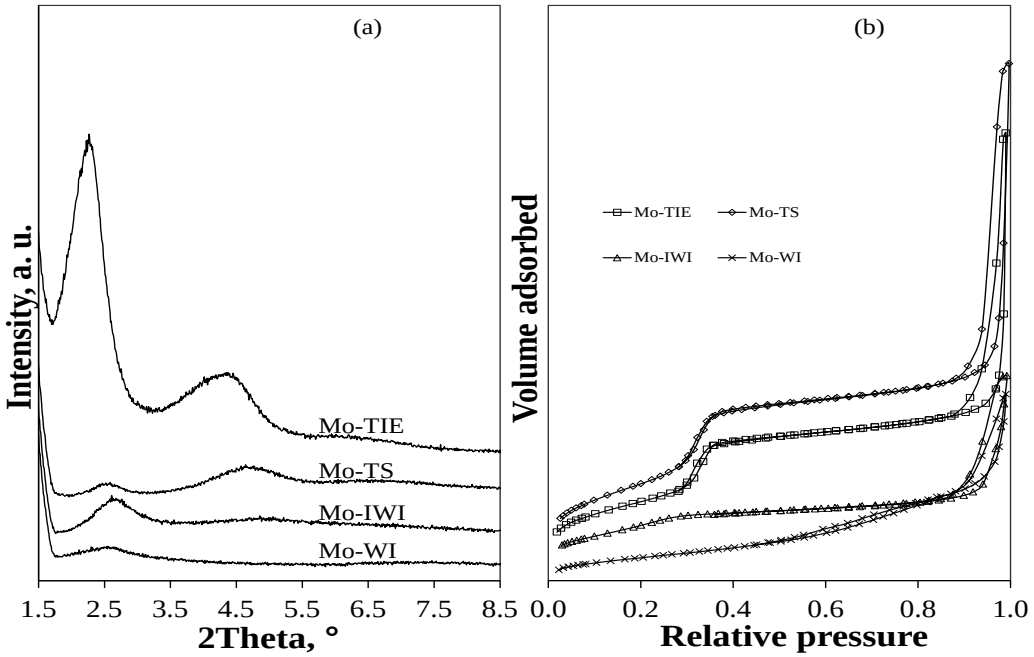

Figure 6.5.1.1. Powder XRD patterns (a) and N_2-physisorption isotherms (b) of Mo/AlMCM-41(Si/Al=60) synthesized by different procedures.

The Si/Al ratio of the final catalysts was 60. Powder XRD patterns are depicted in Figure 6.5.1.1(a) and the N_2-physisorption isotherms are presented in Figure 6.5.1.1(b). Classic diffraction peaks of different intensity corresponding to MCM-41 materials can be recognized. These materials are characterized by the (100), (110) and (200) diffractions peaks [54]. TIE method provides the catalyst with peaks of high intensity corresponding to (100) and (110) diffractions. These diffraction peaks correspond to catalysts with high hexagonal ordering degree, which is typical of the MCM-41 materials [54]. The intensity of these peaks decreased for the catalysts prepared by TS, IWI and WI. Therefore, the hexagonal ordering degree was lower for the catalysts synthesized by these methods.

Only the catalysts prepared by TIE and TS revealed N_2-physisorption isotherms of the type IV according to the IUPAC classification [44]. These type of isotherms correspond to MCM-41 materials [54]. On the other hand, catalysts prepared by IWI and WI did not show the classic type IV isotherm corresponding to MCM-41 materials. Therefore, the

modification of the hexagonal structure was favored after the IWI and WI treatments. This conclusion is supported by the data summarized in table 6.5.1.1, where also the Mo content can be observed. An important reduction of the BET specific surface area can be observed for the catalysts synthesized by IWI and WI. This reduction was more important for the catalyst prepared by WI. This catalyst revealed the largest pore volume, independently of the method used to compute it, indicating an important modification of the catalyst structure after the WI treatment.

Table 6.5.1.1
N_2-adsorption data and Mo content of molybdenum based catalysts prepared by different procedures.

Catalyst	BET specific surface area, $m^2\ g^{-1}$	PV[1] $cm^3\ g^{-1}$	BJH-PD[2], nm	NLDFT-PD[3], nm	Mo content[4], wt.%	Mo nominal content, wt.%
AlMCM-41	1213	1.0	3.0	3.1	----	---
Mo-IWI	632	0.5	3.3	3.2	5.9	7
Mo-TIE	943	0.9	3.0	3.8	1.4	0.015*
Mo-WI	452	0.6	4.9	6.1	6.0	7
Mo-TS	1150	1.1	3.0	3.8	4.2	7

[1]Pore Volume. [2]Pore diameter determined by Barret-Joyner-Halenda method (BJH), [3]nonlocal density functional theory (NLDFT) from the desorption branch and [4]determined by ICP. *molar concentration.

TIE and TS methods provided catalysts with high BET specific surface and pore diameters in the mesoporous interval. Therefore, these methods are suitable to prepare Mo mesostructured catalysts. On the other hand, IWI and WI methods are suitable to incorporate high amount of Mo to the AlMCM-41 materials ca. 6 wt.% for both methods, which is close to the nominal value of 7%. This incorporation might be the responsible of the strong modification of the hexagonal structure of the final catalyst. The concentration of Mo was very low for the catalysts prepared by TIE indicating that this method is not suitable to synthesize catalysts with high Mo loadings.

All catalysts were catalytically tested in the ETP-reaction at the same conditions as described in section 5.3 for the ETP experiment. These results are illustrated in the Figure 6.5.1.2. This Figure shows the conversion of ethene and the selectivity of the major reaction products; propene, *1*-butene and *2*-butene. The conversion of ethene was lower than 16% for all catalysts in the interval of high temperature, 300-475 °C. The catalyst prepared by IWI revealed the highest conversion, around 15%, in the interval of high temperature but revealed the lowest selectivity of propene. The catalysts synthesized by WI, TS and TIE offered a very low conversion of ethene in the interval of high temperature. The highest selectivity of propene was observed for the catalyst prepared by TIE. On the other hand, the selectivity of *1*-butene and *2*-butene (*cis*- and

trans-butene) was very low. Catalysts prepared by IWI and WI revealed the highest conversion of ethene and the lowest BET specific surface. Therefore, the relative high conversion cannot be associated to the BET specific surface, but it can be associated to the fact that more active Mo sites are produced by IWI and WI methods. Thus, the catalytic activity of Mo/AlMCM-41(Si/Al=60) synthesized by TIE, TS, IWI and WI revealed low catalytic activity in the ETP-reaction which is in concordance with the results reported in the literature [16].

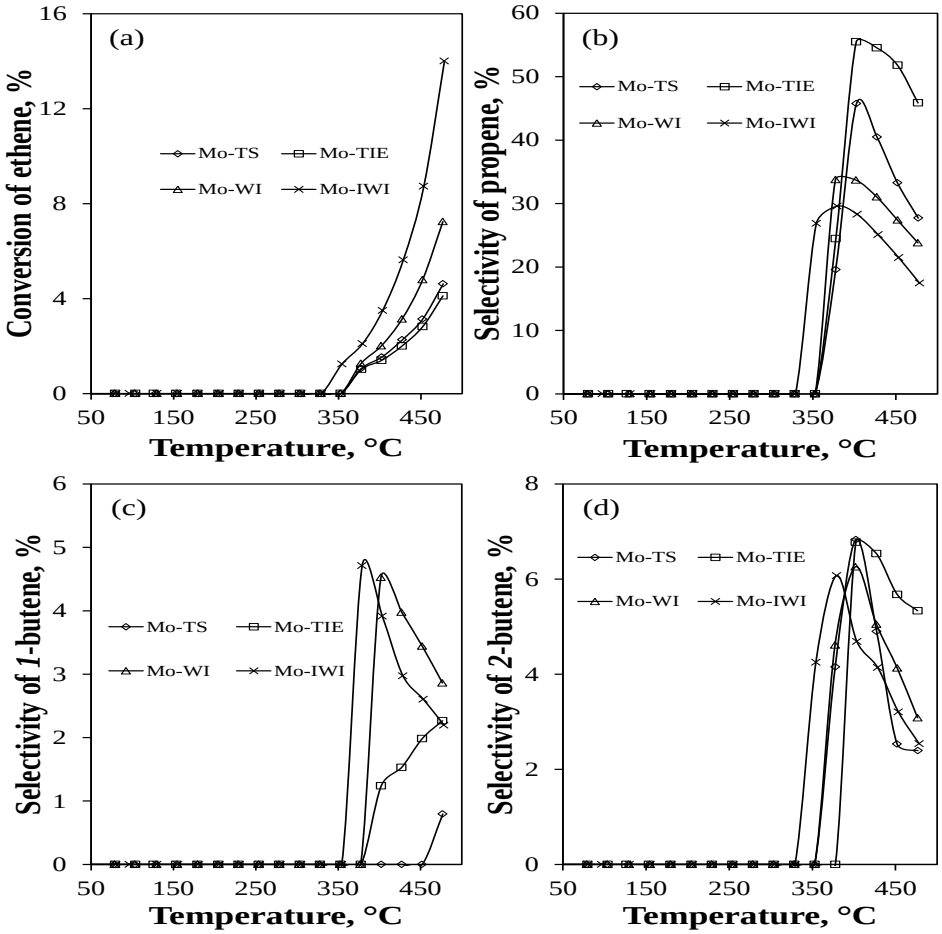

Figure 6.5.1.2. Conversion of ethene (a), selectivity of; propene (b), *1*-butene (c) and *2*-butene (d) on Mo/AlMCM-41 (Si/Al=60) prepared by, TS, TIE, IWI and WI. GHSV = 1.4 $h^{-1}g_{cat}^{-1}$ and 10% of ethene in N_2.

In the previous sections, it has been shown that the ETP reaction is strongly influenced by the acidity of the catalyst. Therefore, synthesis of Mo/AlMCM-41 catalysts with different Si/Al ratio was carried out by IWI method. This method was chosen because the catalyst prepared by this method revealed the highest ethene conversion in the ETP-reaction. The results of the standard characterization and catalytic activity in the ETP-reaction are given below.

Figure 6.5.1.3 shows the structural characterization of the Mo based catalyst at different Si/Al ratios. Figure 6.5.1.3(a) illustrates the powder XRD patterns and the Figure 6.5.1.3(b) shows the N_2-physisorption isotherms. All catalysts were prepared with a nominal Mo loading of 7%. The catalysts with a Si/Al ratio of 16 and 60 revealed the classic diffraction peaks that correspond to MCM-41 materials [54]. On the contrary, the catalysts with a Si/Al ratio of 150, 5 and without Al only straight lines could be obtained.

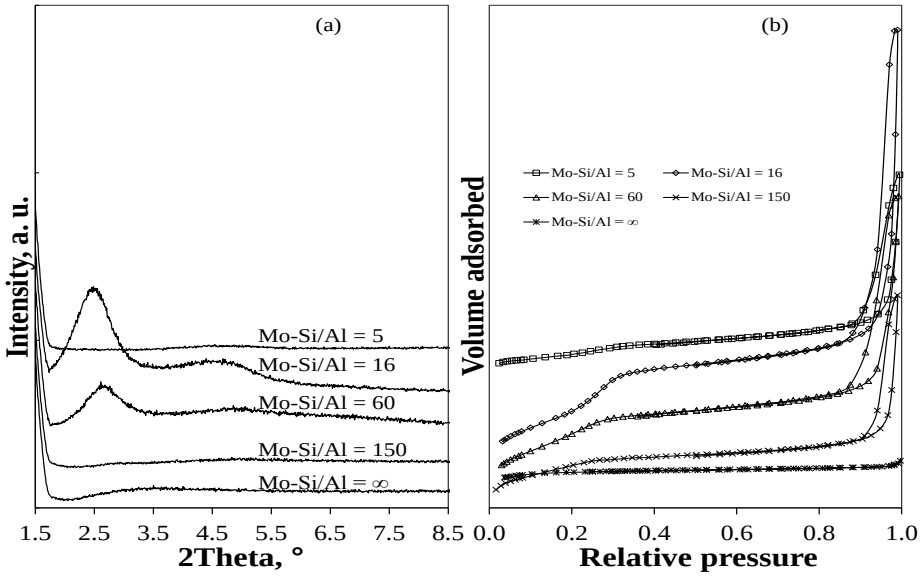

Figure 6.5.1.3. Powder XRD patterns (a) and N_2-physisorption isotherms (b) of Mo/MCM-41 and Mo/AlMCM-41 at different Si/Al ratio.

This result indicates that the hexagonal ordering degree was totally lost in these catalysts. Therefore, the presence of an optimal amount of Al is necessary to obtain a structure that corresponds to the MCM-41 materials. Figure 6.5.1.3 shows also the N_2-physisorption isotherms and can be recognized that only the catalysts with a Si/Al ratio of 16 and 60 revealed the type IV isotherm that corresponds to the MCM-41 materials.

Table 6.5.1.2

N_2-adsorption data and Mo content of molybdenum based catalysts at different Si/Al ratio.

Support, Si/Al ratio	BET specific surface area, $m^2\ g^{-1}$	PV[1], $cm^3\ g^{-1}$	BJH-PD[2], nm	NLDFT-PD[3], nm	Mo content[4], wt.%	Mo nominal content, wt.%
∞	930	0.9	3.0	3.7	----	----
150	1158	1.0	3.0	3.8	----	----
60	1213	1.0	3.0	3.7	----	----
16	951	0.9	3.0	3.8	----	----
5	554	0.5	3.0	3.7	----	----
Catalyst						
Mo-Si/Al = ∞	297	1.4	3.2	1.9	6.6	7
Mo-Si/Al = 150	486	0.3	3.2	3.2	6.1	7
Mo-Si/Al = 60	632	0.5	3.3	3.2	6.0	7
Mo-Si/Al = 16	638	0.6	3.0	3.5	6.5	7
Mo-Si/Al = 5	183	0.2	3.0	3.7	6.4	7

[1]Pore Volume. [2]Pore diameter determined by Barret-Joyner-Halenda method (BJH), [3]nonlocal density functional theory (NLDFT) from the desorption branch and [4]determined by ICP.

Therefore, only these catalysts retained their hexagonal structure after the IWI treatment. In table 6.5.1.2 the N_2-physisorption data and the Mo composition of the catalysts after the IWI treatment are summarized. The N_2-physisorption data of the (Al)MCM-41 materials before the IWI treatment are also shown.

A very important reduction of the BET specific surface was observed for all catalysts. The catalysts with a Si/Al ratio of 16 and 60 revealed the highest BET specific surface. The rest of the catalysts is characterized by a very low specific surface. The actual Mo composition was close to the nominal Mo loading for all catalysts. Based on the results from the powder XRD and N_2-physisorption, it can be concluded that the Si/Al ratio modify strongly the structural properties of the Mo based catalyst prepared by IWI. Finally, all catalysts were tested in the ETP-reaction at the same reaction conditions described in section 5.3 for the ETP activity tests. The results are shown in Figure 6.5.1.4.

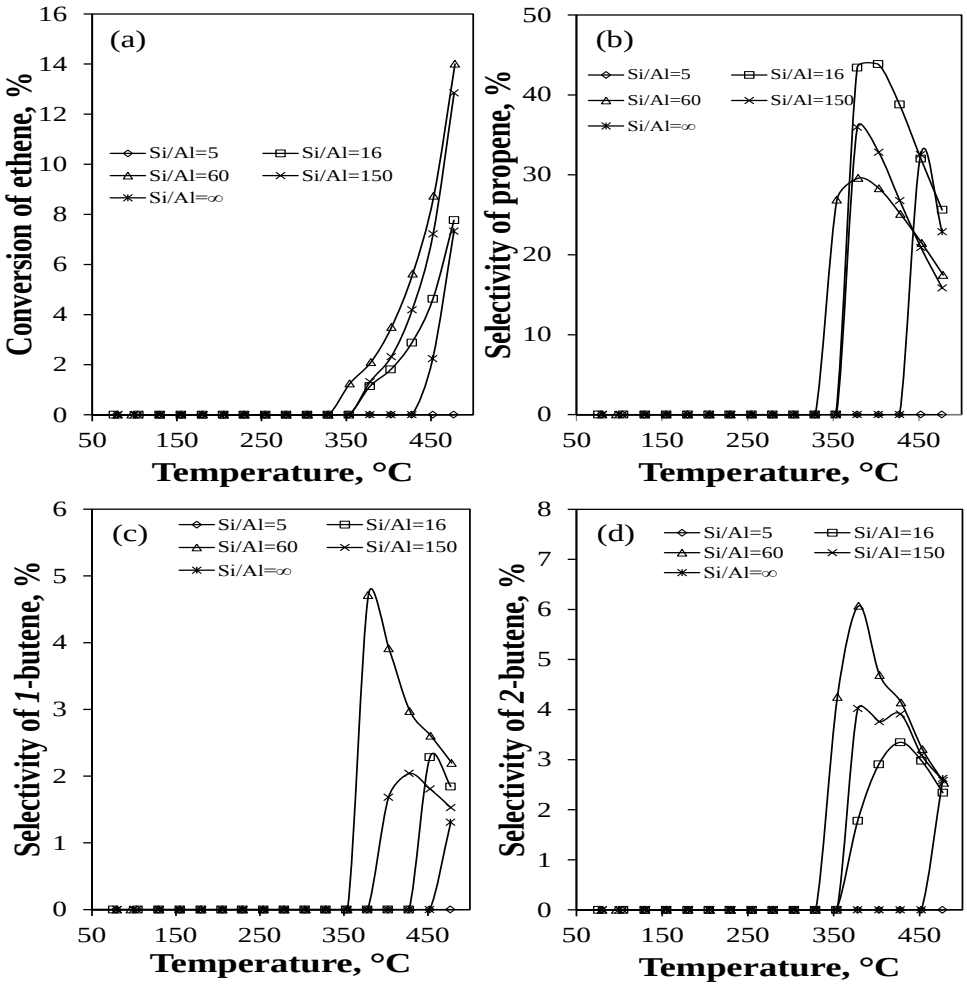

Figure 6.5.1.4. Conversion of ethene (a), selectivity of; propene (b), *1*-butene (c) and *2*-butene (d) on Mo/MCM-41 and Mo/AlMCM-41 with different Si/Al ratio. GHSV = 1.4 $h^{-1}g_{cat}^{-1}$ and 10% of ethene in N_2.

The conversion of ethene for the catalysts with different Si/Al ratio can be observed in Figure 6.5.1.4(a). It is possible to recognize that the highest conversion of propene was observed on the catalysts with a Si/Al ratio of 60 in the interval of high temperature, 300-475 °C. The catalyst without Al revealed almost the same conversion of ethene, reaching a value close to 14%. The selectivity of the major reaction products can be observed also in Figure 6.5.1.4. The highest selectivity of propene was found regarding the catalysts with a Si/Al ratio of 16 in the interval of high temperature. The selectivity of butene isomers was low at all temperatures. From these results it can be concluded that the Si/Al ratio did not improve the catalytic activity of the Mo based catalysts. Therefore, Mo/MCM-41 and Mo/AlMCM-41 prepared by different methods revealed low catalytic activity in the ETP-reaction.

The reducibility of the different Mo species present in the catalysts was investigated by H_2-TPR. The H_2-TPR profiles for the catalysts prepared by different methods and for the catalysts with different Si/Al ratios are depicted in Figure 6.5.1.5.

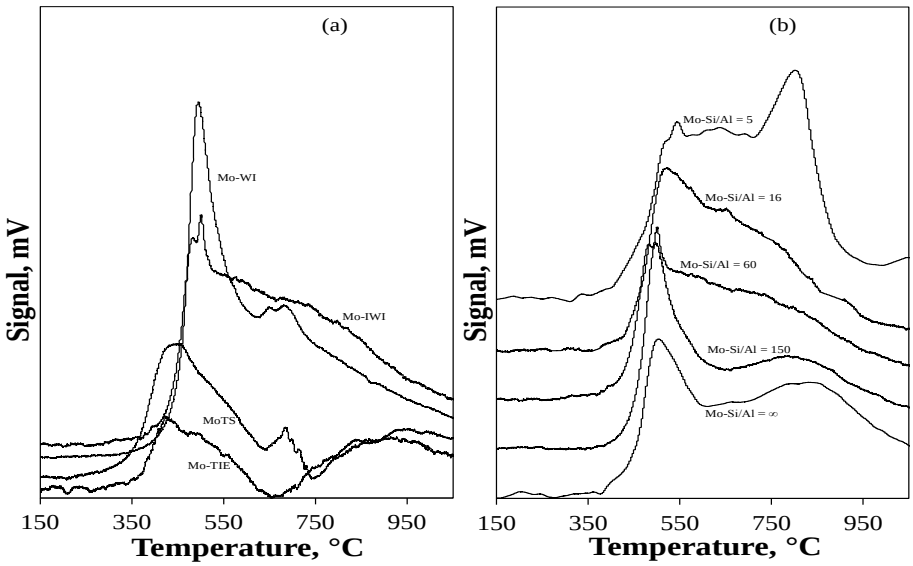

Figure 6.5.1.5. H_2-TPR of (a) Mo/AlMCM-41(Si/Al=60) prepared by TIE, IWI, TS and WI and (b) Mo/MCM-41 and Mo/AlMCM-41 with different Si/Al ratio prepared by IWI.

The H_2-TPR profiles reveal three reduction intervals of temperatures; temperatures lower than 570 °C, between 570-750 °C and higher than 750 °C. These intervals of reduction temperatures can be assigned as follows; the interval of low temperature is associated to the partial reduction of amorphous, highly defective, multi-layered Mo oxides or heteropolymolybdates (octahedral Mo species) [139, 140]; the interval of intermediate

temperature might be due to the intermediate-reducible crystal phases of orthorhombic MoO_3 and $Al_2(MoO_4)_3$ [139, 140], and the interval of high temperature can be assigned to the deep reduction of all Mo species, including highly dispersed Mo species [139, 140]. The H_2-TPR intensity of the catalysts prepared by TIE and TS methods is low because of the low composition of Mo in the final catalyst. These catalysts revealed the presence of mainly Mo species assigned in the interval of low reduction temperatures. These species have no strong interaction with the support and are not active in the ETP-reaction. IWI and WI methods provided catalysts where the interaction of Mo with the AlMCM-41 is stronger, where the species assigned in the intervals on intermediate and high temperatures could be recognized, but the species assigned to the low temperature of reduction were the dominant species. The presence of the orthorhombic MoO_3 and $Al_2(MoO_4)_3$ suggests high dispersion and strong interaction of Mo with AlMCM-41. This dispersion might be the responsible of the relative high catalytic activity of the catalysts.

Important changes in the reduction properties of the Mo species were observed for the catalysts with different Si/Al ratio, Figure 6.5.1.5(b). A very complex distribution of the Mo species could be found, where the main species correspond to the species assigned in the interval of low and high temperatures. The intensity of the peak observed in the interval of high temperature became more intense for low Si/Al ratios but this catalyst revealed no catalytic activity in the ETP-reaction (see Figure 6.5.1.4). Therefore, the species observed in the interval of intermediate temperature could act as active center in the ETP-reactions. However, more and deeper characterization is mandatory to identify the Mo phases that are active in the ETP-reaction. The ETP-reaction was carried out also on rhenium based catalysts. Characterization and catalytic results are described below.

6.5.2 Rhenium based catalysts

Figure 6.5.2.1 shows the powder XRD patterns (a) and the N_2-physisorption isotherms (b) of rhenium (Re) based catalysts synthesized by different procedures. Classic diffraction peaks corresponding to MCM-41 materials can be recognized for all catalysts [54]. Also, all catalysts revealed type IV N_2-adsorption isotherms, according to the IUPAC classification [44] that correspond to MCM-41 [54]. According to these results, catalysts with classic hexagonal structure corresponding to MCM-41 materials were successfully synthesized by TIE, TS, IWI and WI.

Table 6.5.2.1

N_2-adsorption data and Re content of rhenium based catalysts prepared by different procedures.

Catalyst	BET specific surface area, $m^2\ g^{-1}$	PV[1] $cm^3\ g^{-1}$	BJH-PD[2], nm	NLDFT-PD[3], nm	Re content[4], wt.%	Re nominal content, wt.%
AlMCM-41	1213	1.0	3.0	3.7	----	----
Re-IWI	939	0.8	3.0	3.7	4.1	7
Re-TIE	1009	0.9	3.0	3.8	5.8	0.015*
Re-WI	978	0.9	3.0	3.7	6.0	7
Re-TS	1037	1.0	3.0	3.8	5.1	7

[1]Pore Volume. [2]Pore diameter determined by Barret-Joyner-Halenda method (BJH), [3]nonlocal density functional theory (NLDFT) from the desorption branch and [4]determined by ICP. * molar concentration.

In table 6.5.2.1 N_2-physisorption data and Re composition of the catalysts after the impregnation procedures are summarized. All catalysts revealed a BET specific surface around 1000 $m^2\ g^{-1}$ and a pore diameter of 3.7 and 3.8 nm. This table also shows the Re composition of the catalysts after the impregnation treatment. It can be recognized that the IWI, TIE and TS methods leads to a low Re content due to the low solubility of the Re precursor in water.

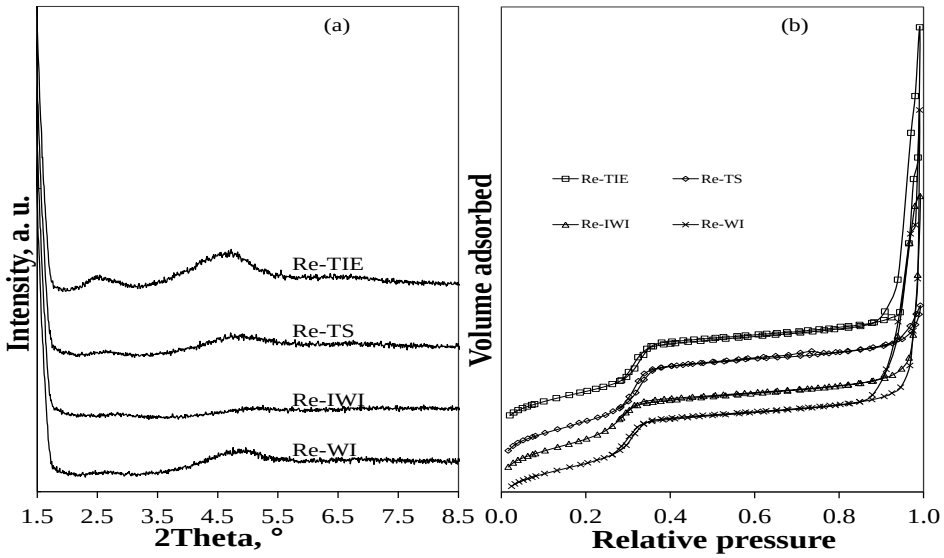

Figure 6.5.2.1. Powder XRD patterns (a) and N_2-physisorption isotherms (b) of Re/AlMCM-41(Si/Al=60) synthesized by different procedures.

This problem could not be detected for the catalysts prepared by WI because of the excess of precursor solution during the WI treatment. Difference with respect to Re content in the final catalysts can explain the differences in the catalytic activity in the ETP-reaction. All catalysts were tested in the ETP-reaction at the same reaction conditions used in the ETP experiments. Figure 6.5.2.2 shows the conversion of ethene and the selectivity of the major reaction products; propene, *1*-butene and *2*-butene (*cis*- and *trans*-butene). In general, all catalysts are characterized by a very low conversion of ethene at all temperatures. The highest conversion was observed on the catalysts

prepared by WI which reached a value of around 6%. At this level of conversion and on all catalysts, propene was produced at lower temperature than the corresponding Ni and Mo based catalysts. The selectivity of butene isomers was low for all catalysts at all temperatures considered.

In the previous sections was found that, the acidity of the catalyst is a crucial parameter in the ETP-reaction. Therefore, Re based catalysts prepared by IWI at different Si/Al ratios and with a nominal Re loading of 11 wt.% were synthesized. Results of structural characterization are depicted in Figure 6.5.2.3.

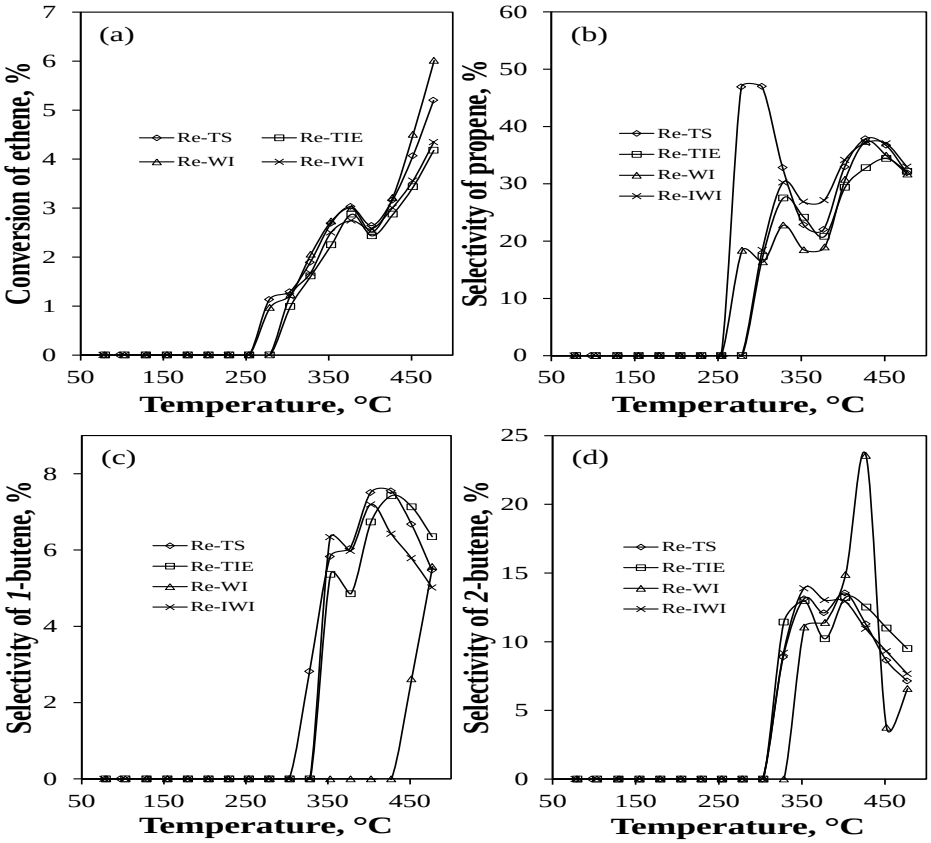

Figure 6.5.2.2. Conversion of ethene (a), selectivity of; propene (b), *1*-butene (c) and *2*-butene (d) on Re/AlMCM-41 (Si/Al=60) prepared by, TS, TIE, IWI and WI. GHSV = 1.4 $h^{-1}g_{cat}^{-1}$ and 10% of ethene in N_2.

Figure 6.5.2.3(a) illustrates the powder diffraction patterns and the N_2-physisorption isotherms of the Re based catalysts at different Si/Al ratios. The diffraction patterns are strongly affected by the Si/Al ratio. The classic diffraction peaks corresponding to MCM-41 materials can be recognized for the catalysts with a Si/Al ratio of 150, 60 and 16. The intensity of these bands almost disappeared for the other catalysts.

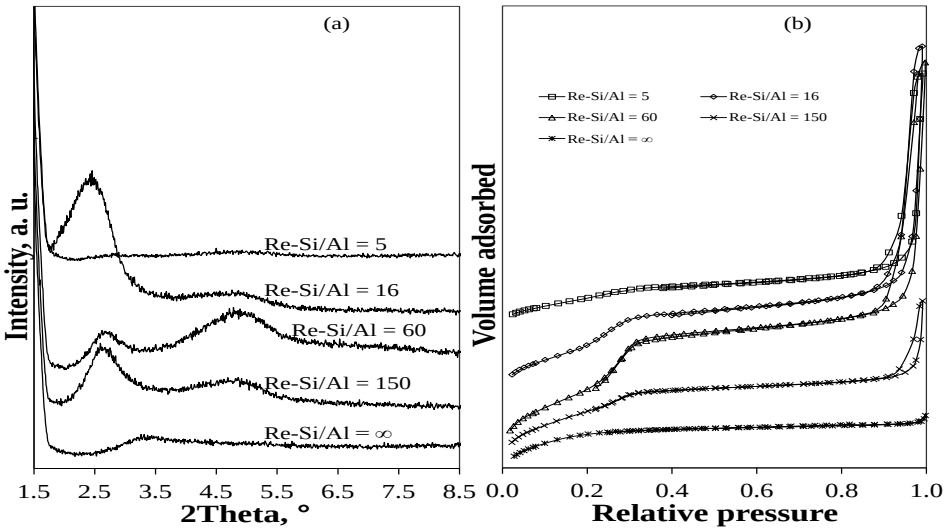

Figure 6.5.2.3. Powder XRD patterns (a) and N_2-physisorption isotherms (b) of Re/MCM-41 and Re/AlMCM-41 at different Si/Al ratio.

Figure 6.5.2.3(b) shows the N_2-physisorption isotherms of the catalysts. It can be recognized that only the catalysts with a Si/Al ratio of 150, 60 and 16 reveal the type IV isotherm according to IUPAC classification [44]. This type of isotherms are classic of the MCM-41 materials [54]. Therefore, the catalysts with these Si/Al ratios correspond to classical structure of the MCM-41 materials.

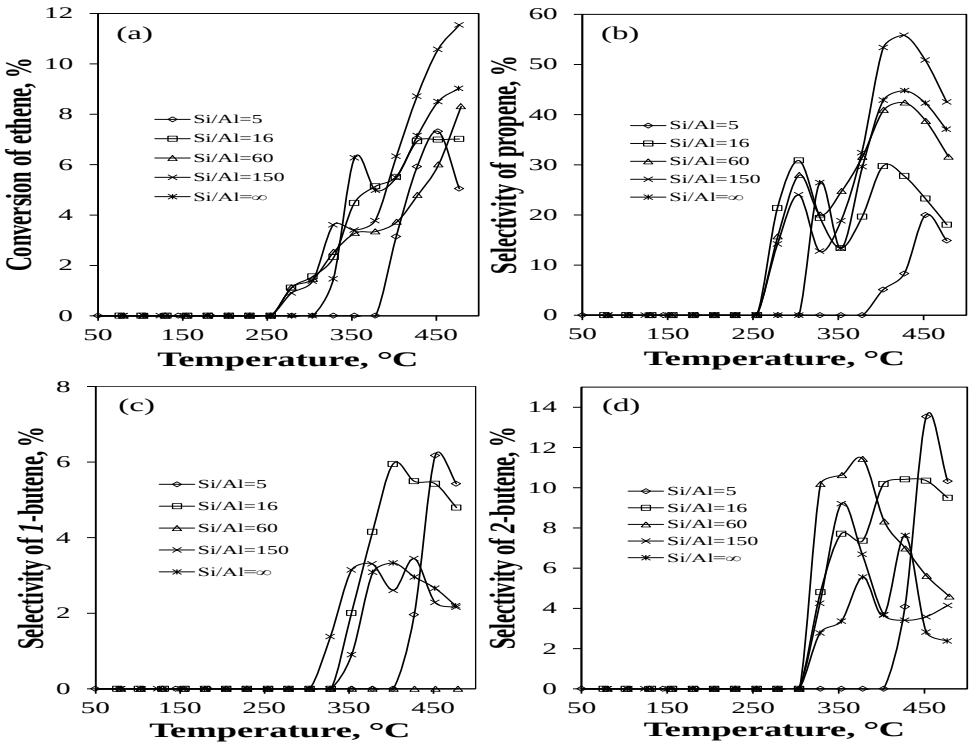

Figure 6.5.2.4. Conversion of ethene (a), selectivity of; propene (b), *1*-butene (c) and *2*-butene (d) on Re/MCM-41 and Re/AlMCM-41 with different Si/Al ratio. GHSV = 1.4 $h^{-1}g_{cat}^{-1}$ and 10% of ethene in N_2.

Table 6.5.2.2 gives the N_2-physisorption data and the Re composition of the final catalysts with different Si/Al ratio. The catalyst with a Si/Al ratio of 60 had the highest BET specific surface and pore volume. The Re content was lower than the nominal value of 11%. This is due to the low solubility of the Re precursor in distilled water [141].

Table 6.5.2.2
N_2-adsorption data and Re content of rhenium based catalysts at different Si/Al ratio.

Catalyst	BET specific surface area, $m^2\ g^{-1}$	PV[1] $cm^3\ g^{-1}$	BJH-PD[2], nm	NLDFT-PD[3], nm	Re content[4], wt.%
Re-Si/Al = ∞	670	0.3	3.1	2.6	7.2
Re-Si/Al = 150	738	0.5	3.0	3.5	7.3
Re-Si/Al = 60	842	0.8	3.0	3.5	5.9
Re-Si/Al = 16	615	0.5	3.2	3.4	9.4
Re-Si/Al = 5	367	0.3	3.2	3.5	9.1

[1]Pore Volume. [2]Pore diameter determined by Barret-Joyner-Halenda method (BJH), [3]nonlocal density functional theory (NLDFT) from the desorption branch and [4]determined by ICP.

Figure 6.5.2.4 illustrates the conversion of ethene and the selectivity of the major reaction products, propene, *1*-butene and *2*-butene (*cis*- and *trans*-butene). The conversion of ethene reached a value of around 11% on the catalyst with a Si/Al ratio of 150 in the interval of high temperature. Very interesting results were observed for the selectivity of propene. This selectivity was close to 30% and 55% in the interval of intermediate and of high temperature, respectively. The selectivity of butene isomers was lower than 14% at all temperatures. These results suggest that propene can be obtained at significant lower temperature in contrast to Mo and Ni based catalysts. Therefore, Re based catalysts showed attractive catalytic properties in the ETP-reaction.

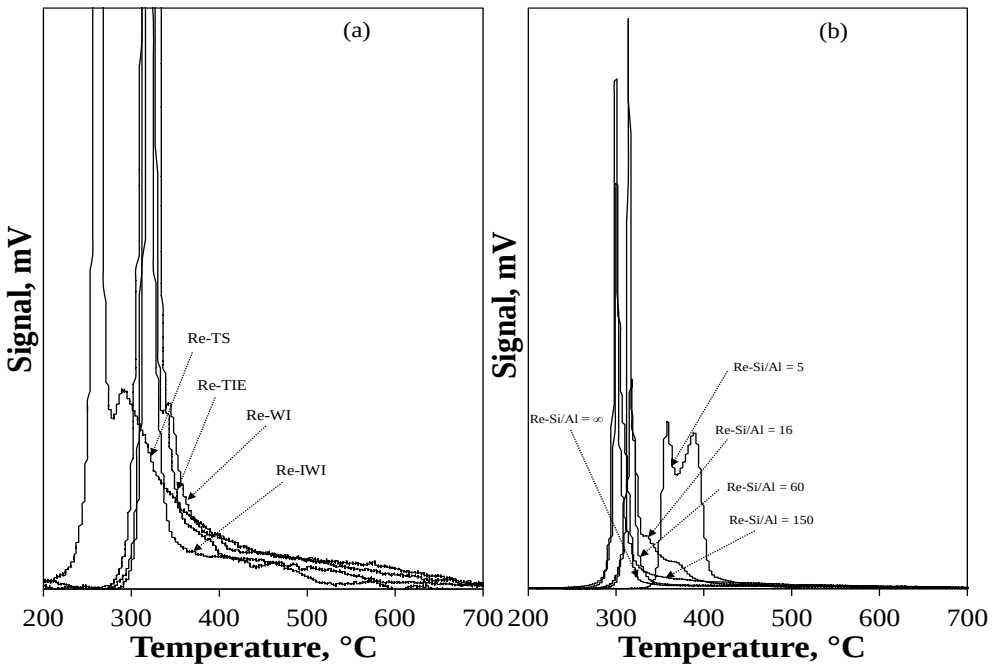

Figure 6.5.2.5. H_2-TPR of (a) Re/AlMCM-41(Si/Al=60) prepared by TIE, IWI, TS and WI and (b) Re/MCM-41 and Re/AlMCM-41 with different Si/Al ratio prepared by IWI.

Reducibility of the different Re species that are present in the catalyst was studied by H_2-TPR. Figure 6.5.2.5 illustrates the H_2-TPR profiles of the catalysts prepared by different impregnation procedures (a) and at different Si/Al ratios (b). The reduction of the different species of Re supported on alumina or silica take place in a small interval of temperature. Therefore, the profiles shown in Figure 6.5.2.5 are very similar to the observed on Re on alumina or silica [141].

The reduction of Re species supported on alumina and silica take place as follows; the peak at lower temperature of reduction than 290 °C corresponds to the reduction of NH_4ReO_4 crystallites that do not interact strongly with the support [141]; All other peaks observed at reduction temperatures higher than 240 °C are assigned to reduction of Re^{+7} surface ions which interact stronger with the support [141]. According to this assignation, the interpretation of the Figure 6.5.2.5 can be done as follows. The TS method revealed a sharp reduction peak at 270°C and a very broad peak in the interval of 280 and 650 °C with a maximum at 300 °C. This low reduction peaks correspond to the species described previously and the interaction of Re with the support is weak because of the mechanical mixture performed during the TS treatment (see section 5.2). The reduction temperature of the catalysts prepared by TIE, WI and IWI was shifted to higher temperature indicating a stronger interaction with the support. This reduction might correspond to the reduction of Re^{+7} surface ions.

The reduction of the different Re species present in the catalysts with different Si/Al ratio is depicted in Figure 6.5.2.5(b). All H_2-TPR profiles fall at temperatures higher than 300 °C indicating that only the reduction of Re^{+7} is taking place. This peak is shifted to higher temperature for lower Si/Al ratio. Thus, a stronger interaction of Re with the support for the catalysts with high Al content can be concluded. The same behavior was observed by Arnoldy et al. (1985). Re interacted much stronger with the support in the catalyst with a Si/Al ratio of 5. This strong interaction did not build Re active sites in the ETP-reaction, Figure 6.5.2.4(a).

According to the results obtained in this section, Mo and Re based catalysts showed low catalytic activity in the ETP-reaction. Important changes of the structure of the catalysts were observed on Mo based catalysts. On the other hand, Re based catalysts revealed very interesting properties, especially in the selectivity of propene, where propene was

produced at significantly lower temperature than the temperature used on Mo and Ni based catalysts.

The catalytic properties of Mo and Re based catalysts have been incorporated to the Ni based catalysts to generate synergetic effects and the results are shown in the next section. This incorporation builds the so called, *bi*-metallic catalysts for the direct conversion of ethene to propene.

6.5.3 Summary

In this section characterization and catalytic results of Mo and Re based catalysts were shown (*mono*-metallic catalysts). For both type of catalysts the catalytic activity was lower than the corresponding Ni based catalysts. The characterization of these catalysts was only focus to observe changes on the structure of the catalysts and in the interaction between the corresponding metal active and the AlMCM-41 support. The purpose of synthesizing this type of catalysts was to evaluate their catalytic behavior in the ETP-reaction as a previous step of the preparation of NiMo and NiRe based catalysts (*bi*-metallic catalysts).

6.6 *Bi*-metallic formulation: NiMo and NiRe/AlMCM-41 catalysts

In this section, characterization and catalytic results of NiMo and NiRe based catalysts are shown. All catalysts were prepared by TIE method, where the metal precursors were dissolved simultaneously in deionized water. In the first part of this section, catalysts with different Ni/Mo and Si/Al ratios were synthesized. The concentration of Ni in solution was kept constant and the Mo concentration in the solution was varied. The amount of Mo precursor used to prepare the solution was adjusted to have the desired Ni/Mo ratio. The same procedure was applied for the *bi*-metallic NiRe based catalysts but the results are shown in the second part of the section. Structural characterization based on powder XRD and N_2-physisorption, as well as H_2-TPR was carried out for all catalysts. These results are shown below.

6.6.1 Nickel-molybdenum based catalysts

Figure 6.6.1.1 illustrates the structural characterization of the NiMo catalysts with different Ni/Mo ratios. Figure 6.6.1.1 (a) shows the powder XRD patterns and Figure 6.6.1.1(b) shows the N_2-physisorption isotherms. Powder XRD patterns show classical

diffraction peaks corresponding to MCM-41 materials [54] and N_2-physisorption analysis revealed isotherms of the type IV according to the IUPAC classification [44] corresponding to MCM-41 materials [54].

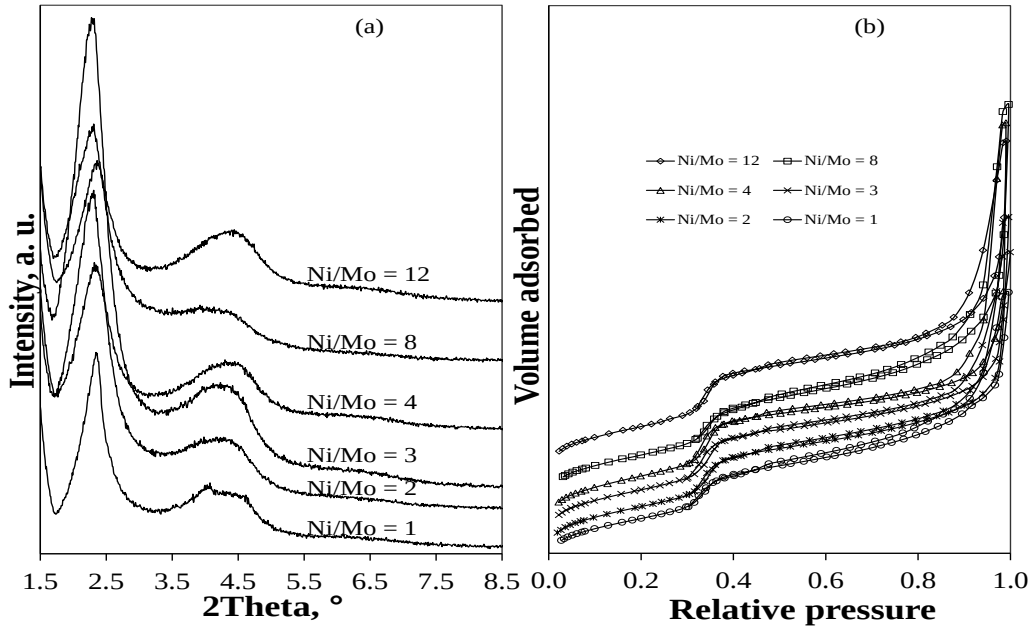

Figure 6.6.1.1. Powder XRD patterns (a) and N_2-physisorption isotherms (b) of NiMo/AlMCM-41(Si/Al=60) at different Ni/Mo ratios.

The structure of the catalysts was not affected by the Ni/Mo ratio, even for the catalysts with the highest Mo content (lowest Si/Al ratio). Table 6.6.1.1 shows the N_2-physisorption data for the catalysts with different Ni/Mo ratios. It can be observed that the BET specific surface area was close to 1000 m^2 g^{-1} for all catalysts. Pore diameter that corresponds to mesoporous materials can be observed (3.7-4.1 nm). The metal content was not determined by all catalysts. However, Mo is more easily incorporated to the catalyst when there is the presence of Ni than when it is alone during the TIE treatment (see Table 6.5.1.1).

According to the powder XRD and N_2-physisorption, it can be concluded that NiMo based catalysts are mesoporous materials with a highly hexagonal structure corresponding to MCM-41 materials.

All catalysts were catalytically tested in the ETP-reaction under the same reaction conditions corresponding to the ETP experiment (section 5.3). Figure 6.6.1.2 illustrates the conversion of ethene and the major reaction products, *1*-butene and *2*-butene (*cis*- and *trans*-butene). The catalyst with a Ni/Mo ratio of 12 showed a similar catalytic

activity of the Ni based catalyst with a Si/Al ratio of 60 because of the low amount of Mo in the catalyst.

Table 6.6.1.1
N_2-adsorption data and metal content of the *bi*-metallic catalysts.

Catalyst	BET specific surface area, $m^2\ g^{-1}$	PV[1] $cm^3\ g^{-1}$	BJH-PD[2], nm	NLDFT-PD[3], nm	Ni-Re/Mo content[4], wt.%	Experimental Ni/Mo-Re ratio
Ni/Mo=1	917	1.0	3.7	4.1	3.5-2.9	1.97
Ni/Mo=2	951	1.0	3.0	4.1	------	------
Ni/Mo=3	959	1.0	3.0	4.1	3.7-1.2	5.04
Ni/Mo=4	997	1.0	3.0	4.1	------	------
Ni/Mo=8	944	1.1	3.0	4.1	------	------
Ni/Mo=12	978	1.1	3.0	4.1	3.7-0.3	20.15
NiMo-Si/Al=∞	847	0.9	3.7	3.8	------	------
NiMo-Si/Al=150	851	1.1	3.7	3.8	------	------
NiMo-Si/Al=60	917	1.0	3.7	4.1	------	------
NiMo-Si/Al=16	833	0.9	3.0	3.8	------	------
NiMo-Si/Al=5	425	0.4	3.0	3.7	------	------
Ni/Re=1	883	1.1	3.0	4.1	2.8-4.5	1.97
Ni/Re=1.5	894	1.1	3.0	4.1	------	------
Ni/Re=2	905	1.0	3.0	4.1	3.5-2.5	4.49
Ni/Re=3	991	1.1	3.0	4.1	3.7-1.8	6.52
Ni/Re=4	1027	1.1	3.0	3.8	2.5-1.2	6.61
Ni/Re=12	1037	1.1	3.0	3.8	2.9-0.5	18.39
NiRe-Si/Al=∞	1032	1.0	3.9	3.8	------	------
NiRe-Si/Al=150	932	1.1	3.7	3.8	------	------
NiRe-Si/Al=60	894	1.0	3.0	4.1	------	------
NiRe-Si/Al=16	865	0.9	3.0	3.8	------	------
NiRe-Si/Al=5	457	0.5	3.0	3.7	------	------

[1]Pore Volume. [2]Pore diameter determined by Barret-Joyner-Halenda method (BJH), [3]nonlocal density functional theory (NLDFT) from the desorption branch and [4]determined by ICP.

The conversion of ethene decreased for lower Ni/Mo ratio and was close to 40% at 400 °C on the catalyst with a Ni/Mo = 1. The selectivity of propene decreased also at lower Ni/Mo ratios and reached a maximum of 20% at 375 °C on the catalyst with a Ni/Mo ratio of 1. This selectivity decreased at higher temperatures. On the other hand, the selectivity of butene isomers did not change significantly with the NiMo ratio studied. The selectivity of *1*-butene reached a maximum of around 16% for the catalyst with a Ni/Mo ratio of 1 in the interval of intermediate temperature. In this interval, propene begins to appear and the selectivity of *2*-butene started to decrease. Therefore, the reactions evolved in the conjunct polymerization, where propene is one the reaction products, are promoted by the presence of Mo. This type of reactions is strongly enhanced for the catalysts with a Ni/Mo ratio of 1, 2 and 3, where no propene and butene isomers were observed at temperatures higher than 425 °C.

According to these results, the presence of Mo is not enhancing the metathesis of ethene and *2*-butenes in the interval of low temperature under the conditions considered in this work. Contrary, the results suggest that Mo is promoting the reactions that are taking place during the conjunct polymerization. Therefore, Mo is not acting as a metathesis

active site in the ETP-reaction and no improvement of the Ni based catalysts was obtained.

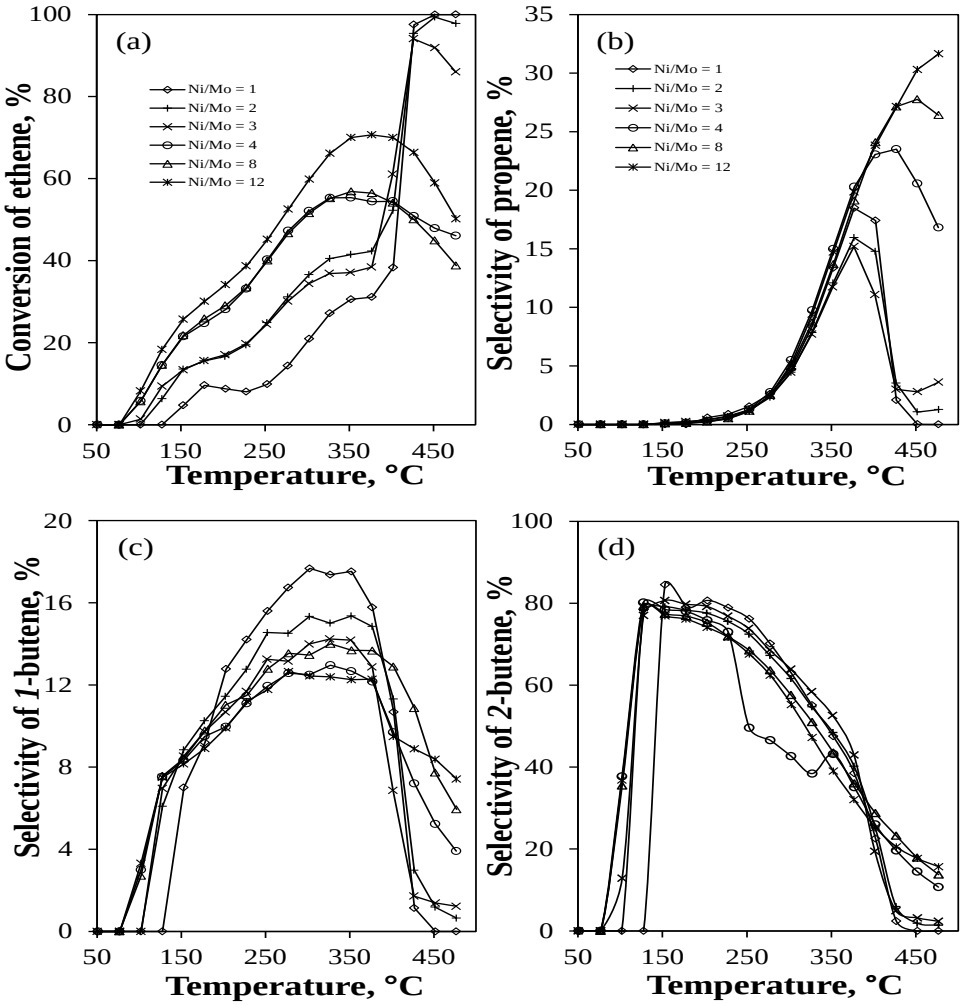

Figure 6.6.1.2. Conversion of ethene (a), selectivity of; propene (b), *1*-butene (c) and *2*-butene (d) on NiMo/AlMCM-41(Si/Al=60) with different NiMo ratios. GHSV = 1.4 $h^{-1}g_{cat}^{-1}$ and 10% of ethene in N_2.

In the previous sections, it has been shown that the ETP reaction is strongly influenced by the acidity of the catalyst. Therefore, synthesis of NiMo/AlMCM-41 catalysts with different Si/Al ratio was carried out by TIE method. The results of the standard characterization and catalytic activity in the ETP-reaction are discussed below.

Powder XRD and N_2-physisorption isotherms of the NiMo based catalysts with different Si/Al ratios are depicted in Figure 6.6.1.3(a) and (b) respectively. The Ni/Mo ratio of all catalysts was 1. Classic diffraction peaks that correspond to MCM-41 materials can be recognized for almost all catalysts [54]. The only catalyst that showed a very weak diffraction peaks was the catalysts with a Si/Al ratio of 5. N_2-physisorption isotherms of

the type IV according to IUPAC classification [44], can be also recognized. The catalysts with a Si/Al ratio of ∞, 150 and 60 revealed a H3 hysteresis loop. This hysteresis loop is observed with aggregates of plate-like particles giving rise to slit-shaped pores. Therefore, the incorporation of Al into the final catalysts is modifying the pore structure of the final catalysts.

N_2-physisorption data are shown in table 6.6.1.1. The BET specific surface area increased with the Si/Al ratio reaching a maximum for the catalyst with a Si/Al ratio of 60. This area reached a minimum value of 425. 3 m^2 g^{-1} for the high Al content catalyst, Si/Al = 5.

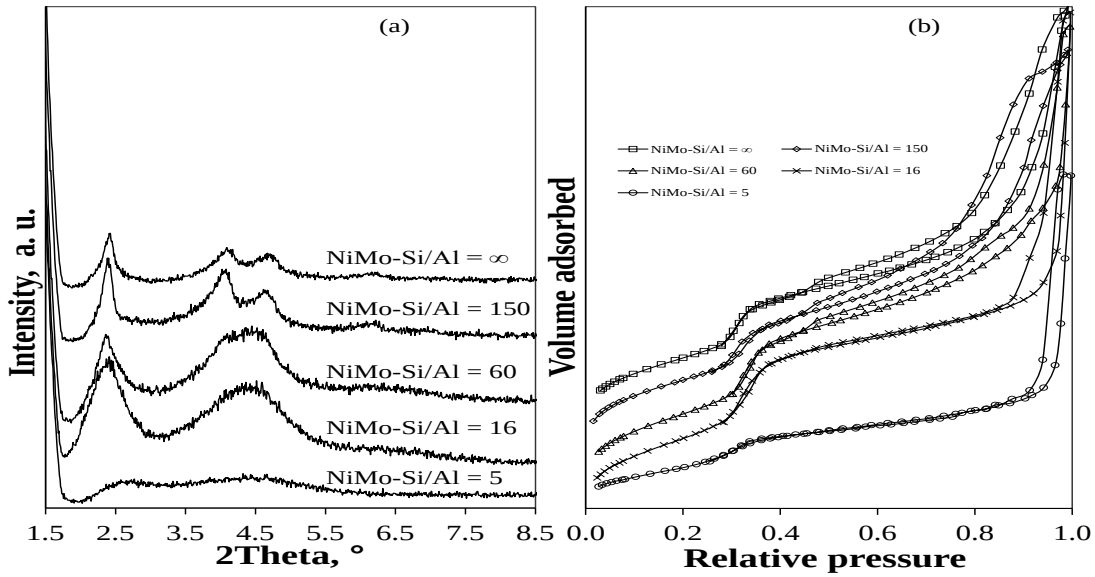

Figure 6.6.1.3. Powder XRD patterns (a) and N_2-physisorption isotherms (b) of NiMo/MCM-41 and NiMo/AlMCM-41 at different Si/Al ratio. Ni/Mo=1.

The pore diameter varied from 3.7 to 4.1 nm, which correspond to pores in the interval of mesoporous range. Therefore, from the powder XRD and N_2-physisorption, NiMo catalysts with different Si/Al ratio correspond to mesostructured catalysts with high hexagonal ordering.

Figure 6.6.1.4 illustrates the conversion of ethene and the selectivity of the major reaction products; propene, *1*-butene and *2*-butene (*cis*- and *trans*-butene). The conversion of ethene reached a value of around 40% on the catalysts with a Si/Al ratio of 16 in the interval of intermediate temperature, 150 to 300 °C. The catalysts without Al and with highest Al content did not revealed catalytic activity at temperatures lower than

375 °C. In the interval of high temperature, the conversion of propene reached around 100% but no products could be detected. The main reaction product was ethane (Figure not shown). The selectivity of propene reached a maximum of 18% at 375 °C almost for all catalysts. The selectivity of *1*-butene reached a maximum in the interval of intermediate temperature reaching a value of around 16%. The selectivity of *2*-butene was close to 90% for the catalyst with a Si/Al ratio of 150. These results show that NiMo based catalysts are efficient catalysts for the selective dimerization of ethene to *2*-butene in the interval of intermediate temperature.

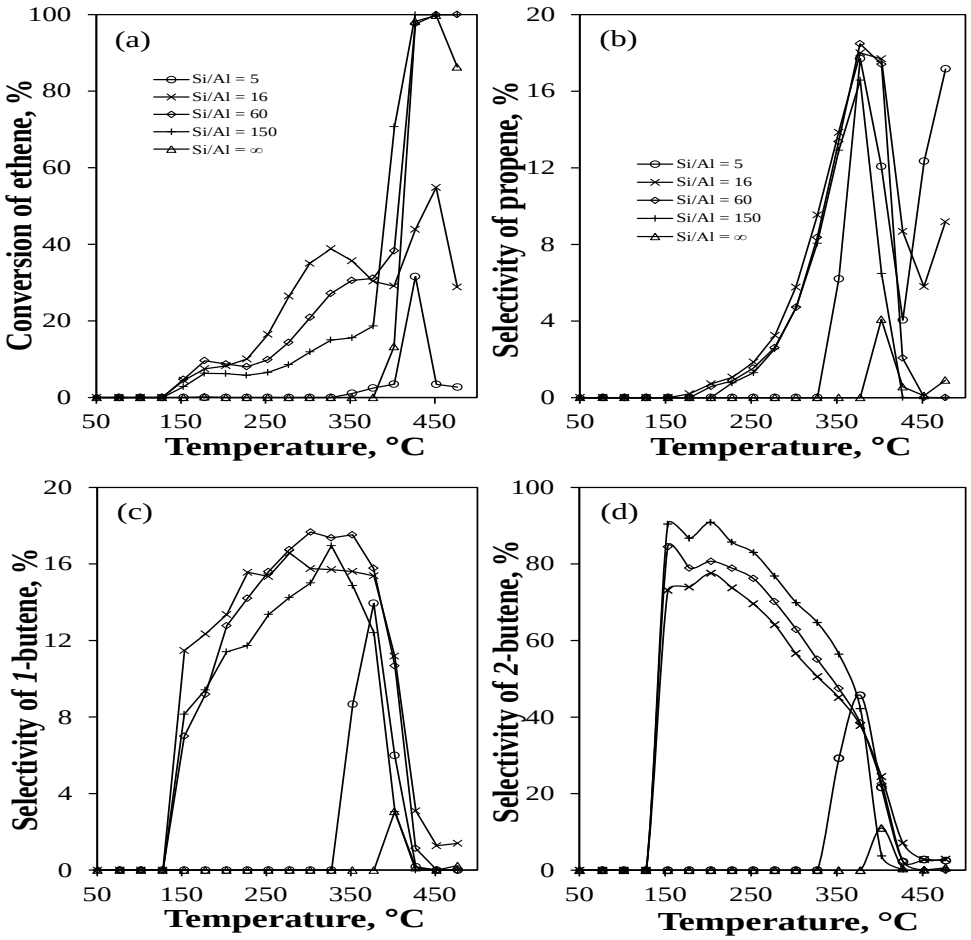

Figure 6.6.1.4. Conversion of ethene (a), selectivity of; propene (b), *1*-butene (c) and *2*-butene (d) on NiMo/MCM-41 and NiMo/AlMCM-41 with different Si/Al ratio. GHSV = 1.4 $h^{-1}g_{cat}^{-1}$ and 10% of ethene in N_2.

From the catalytic testing can be concluded that the NiMo catalysts did not show any improvement in the selectivity of propene. Therefore, Mo is not acting as metathesis site in the ETP-reaction and deeper characterization hast to be done in order to understand the role of Mo in this type of catalysts.

H_2-TPR of NiMo based catalysts with different Ni/Mo ratio and with different Si/Al ratio was carried out and the results are depicted on the Figure 6.6.1.5. The catalysts with a Ni/Mo of 12, which contains the lowest amount of Mo, revealed two very broad peaks between 300 and 800 °C. The peak at low temperatures might correspond to the reduction of amorphous highly defective multi-layered Mo oxides or heptamolybdates (octahedral Mo species) that do not interact strongly with Ni [140]. The peak centered at around 660 °C might correspond to the Ni species that were discussed in section 6.1.7, bulk mixed nickel-aluminosilicates. The shape of this peaks suggest that even at low Mo loadings, Mo interacts strongly with Ni. The increasing amount of Mo content, lower Ni/Mo ratio shifts the peaks to lower reduction temperatures and the maximum temperature of the peaks decreased.

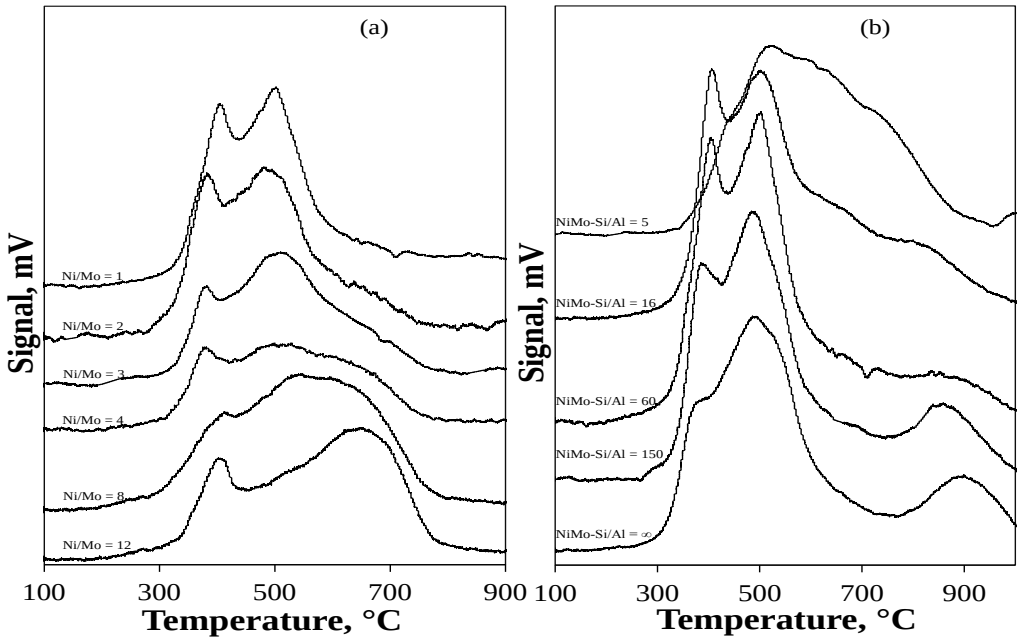

Figure 6.6.1.5. H_2-TPR of (a) NiMo/AlMCM-41(Si/Al=60) at different Ni/Mo ratios, and (b) NiMo/MCM-41 and NiMo/AlMCM-41 with different Si/Al ratio prepared by TIE. Ni/Mo=1.

This result suggests a stronger interaction between Ni and Mo than between Ni or Mo with the support. This interaction might correspond to the formation of bulk mixed molybdenum-nickel-aluminosilicates. At the lowest Ni/Mo ratios the Mo species became dominant and the maximum of the peaks might correspond to the reduction of the Mo species of the catalysts. According to the catalytic results, the Mo presence is forming active sites for the cracking of the reaction products during the ETP-reaction instead of acting as a metathesis active site.

Figure 6.6.1.5 shows also the H_2-TPR profiles of the NiMo based catalysts with different Si/Al ratio and with a Ni/Mo ratio of 1. From this Figure, it can be observed that the Mo species are the dominants and Ni is stronger interacting with Mo at lower Si/Al ratios. This conclusion can be formulated because the intensity of the peak at high reduction temperature decreased.

According to the catalytic results, no metathesis active sites are formed by modifying the Si/Al ratio. Therefore, under the synthesis conditions used in this work, the optimization of the Ni based catalysts was not successful with the incorporation of Mo into the Ni based catalysts. Deeper characterization of the catalysts is mandatory to understand the phenomena that are taking place during the synthesis of the catalysts. This understanding will allow improving and optimizing the Ni based catalysts. In the next section, results of the synthesis, characterization and catalytic testing of NiRe based catalysts are described.

6.6.2 Nickel-rhenium based catalysts

Figure 6.6.2.1 depicts the structural characterization of the NiRe based catalysts at different Ni/Re ratios. Figure 6.6.2.1(a) shows the powder XRD patterns and Figure 6.6.2.1(b) the N_2-physisorption adsorption isotherms. Classic diffraction peaks belonging to MCM-41 materials could be recognized at all Ni/Re ratios [54].

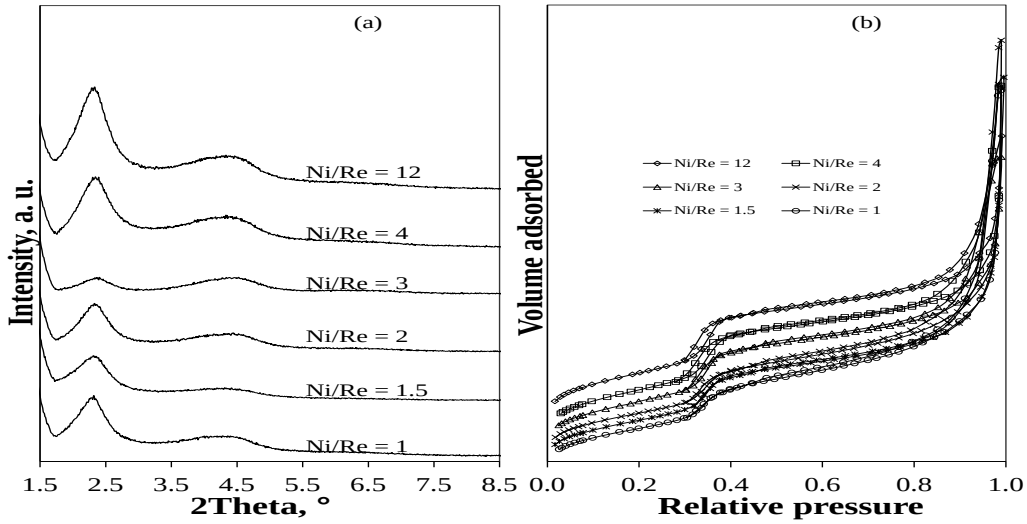

Figure 6.6.2.1. Powder XRD patterns (a) and N_2-physisorption isotherms (b) of NiRe/AlMCM-41(Si/Al=60) with different Ni/Re ratios.

N_2-physisorption isotherms of the type IV, according to IUPAC classification [44] can be observed. This type of isotherms correspond to MCM-41 materials [54]. Therefore, these

catalysts revealed a structure that corresponds to hexagonal arrangement that is observed in the MCM-41 materials. This structure did not suffer important modification even for the catalysts with the highest content of Re.

N_2-physisorption data are summarized in table 6.6.1.1. A gradual reduction of the BET specific surface area could be observed with the increasing of the Re content in the catalyst but all catalysts revealed high specific surface, close to 1000 m^2 g^{-1}. Pore diameter that corresponds to mesoporous materials can be observed. The Ni and Re content was not determined for all catalysts, but for the samples where their Ni and Re content was determined, the experimental Ni/Re ratio was close to the nominal value.

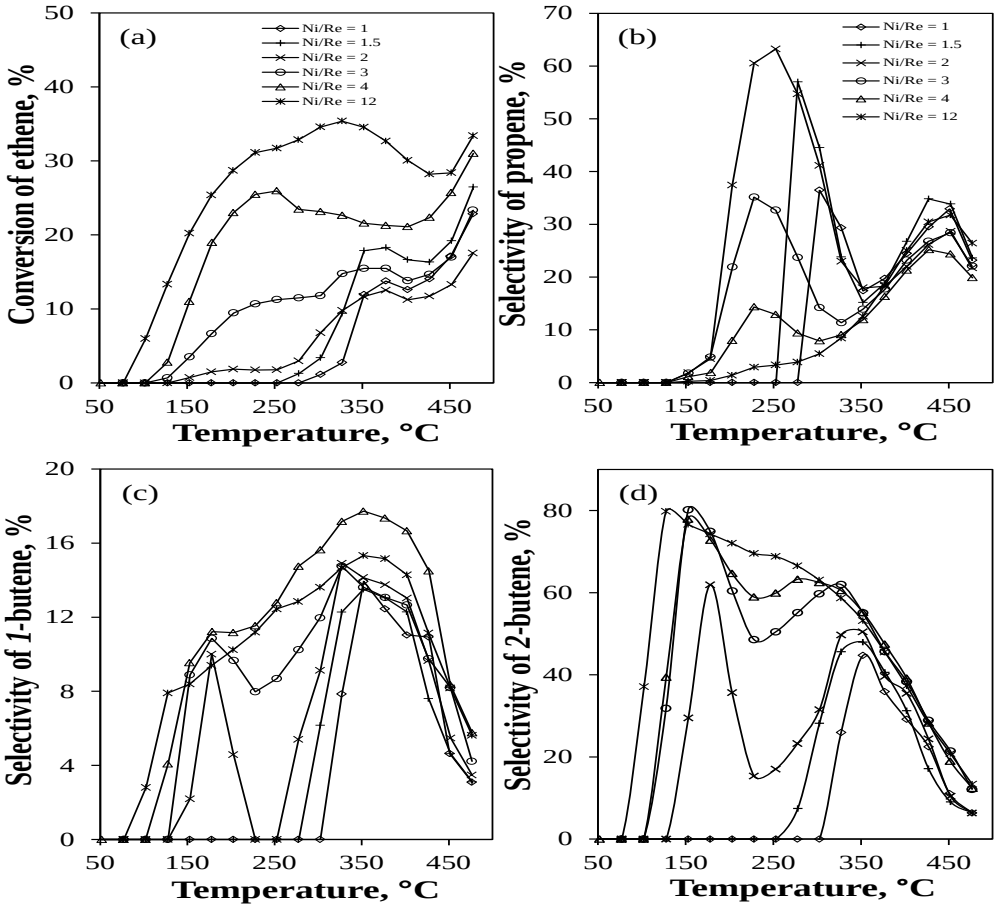

Figure 6.6.2.2. Conversion of ethene (a), selectivity of; propene (b), *1*-butene (c) and *2*-butene (d) on NiRe/AlMCM-41(Si/Al=60) with different Ni/Re ratios. GHSV = 1.4 $h^{-1}g_{cat}^{-1}$ and 10% of ethene in N_2.

Figure 6.6.2.2 illustrates the conversion of ethene and the major reaction products; propene, *1*-butene and *2*-butene (*cis*- and *trans*-butene). Clearly it can be observed that the conversion of ethene decreased with the Re content in the catalyst at all temperatures. The highest conversion of ethene was observed in the intermediate temperature reaching

a value close to 35%. The conversion of ethene was strongly influenced by the presence of Re respect to the Ni based catalysts. The selectivity of the reaction products was also strongly influenced by the presence of Re in the catalysts. The selectivity of propene reached a maximum value around 65% at 225°C on the catalyst with a Ni/Re of 2. It can be recognized that the presence of Re is modifying directly the selectivity of propene and *2*-butene. At the same temperature where the selectivity of propene increased, the selectivity of *2*-butene decreased. This is an indication that Re is acting as metathesis active site in the ETP-reaction. Thus, these results show that propene can be obtained at significant lower temperature on NiRe based catalysts than on Ni based catalysts.

In section 6.1.2 it has been shown that the acidity of the catalyst plays a crucial role in the ETP-reaction. Therefore, NiRe based catalysts were also synthesized at different Si/Al ratios. Results of the standard characterization and catalytic activity in the ETP-reaction are shown below.

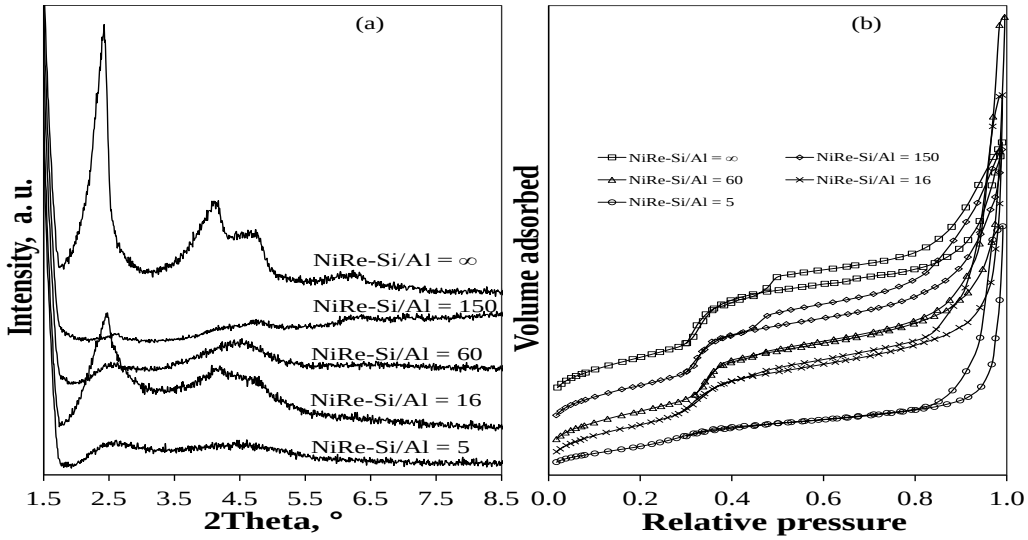

Figure 6.6.2.3. Powder XRD patterns (a) and N_2-physisorption isotherms (b) of NiRe/MCM-41 and NiRe/AlMCM-41 at different Si/Al ratio. Ni/Re=1.5.

Figure 6.6.2.3 shows the powder XRD patterns (a) and the N_2-physisorption isotherms (b) of the NiRe based catalysts prepared with different Si/Al ratio. The Ni/Re ratio was kept constant at 1.5. Powder XRD patterns revealed an irregular behavior, where the catalysts without Al and with a Si/Al ratio of 16 showed highly defined peaks corresponding to the structure of the MCM-41 materials [54]. The intensity of these peaks decreased for the catalysts with a Si/Al ratio of 150, 60 and 5. This is an indication that the hexagonal ordering degree decreased for these catalysts.

The N_2-physisorption isotherms of the catalysts with different Si/Al ratio correspond to the type IV isotherms and hysteresis of the type H3 according to IUPAC classification [44] and they are characteristics of the MCM-41 materials [54]. This hysteresis loop is observed with aggregates of plate-like particles giving rise to slit-shaped pores. Therefore, the incorporation of Al into the final catalysts is modifying the pore structure of the final catalysts.

N_2-physisorption data and metal content are shown in table 6.6.1.1 (previous section). The actual Ni/Re ratio can be also observed. The BET specific surface area decreased gradually with the increasing of the Al content. An important reduction of the BET specific surface was observed for the catalyst with the highest Al content. The pore diameter changed from 3.7 to 4.1 nm, indicating that the catalysts are mesoporous materials.

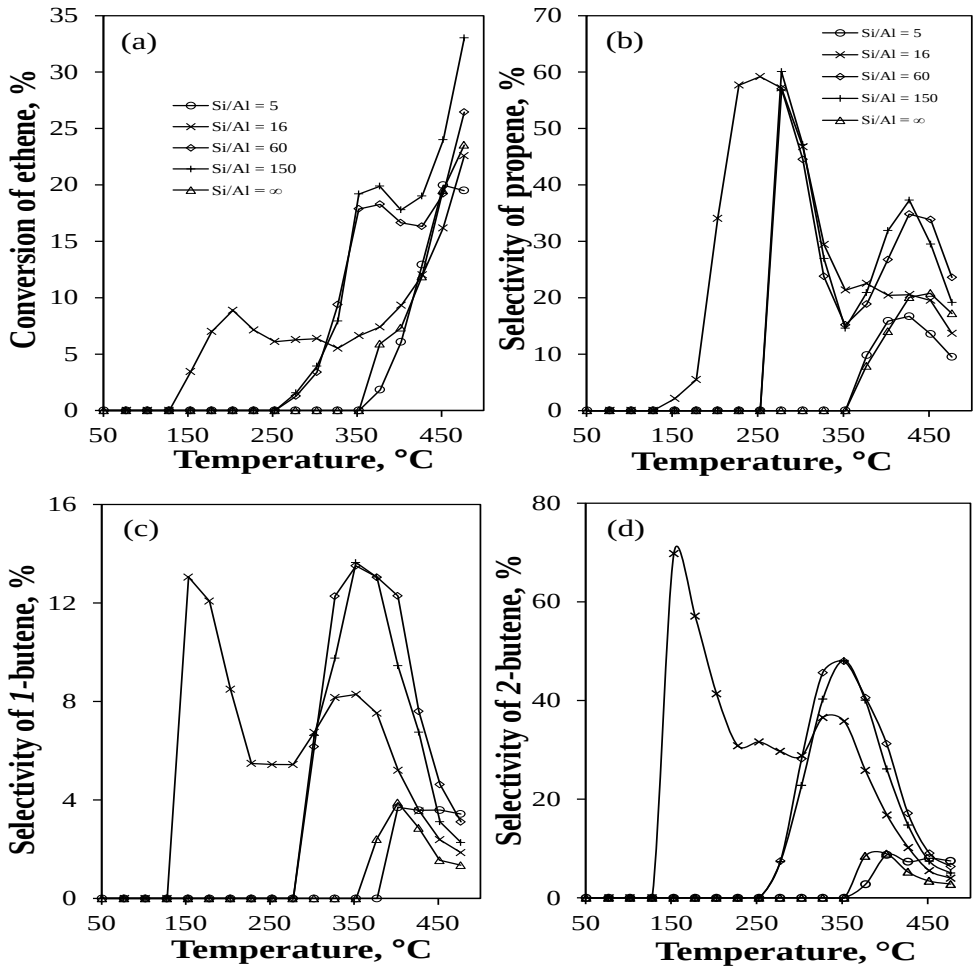

Figure 6.6.2.4. Conversion of ethene (a), selectivity of; propene (b), *1*-butene (c) and *2*-butene (d) on NiRe/MCM-41 and NiRe/AlMCM-41 with different Si/Al ratio. GHSV = 1.4 $h^{-1}g_{cat}^{-1}$ and 10% of ethene in N_2.

All NiRe based catalysts prepared with different Si/Al ratio were catalytically tested. The conversion of ethene and the selectivity of the major reaction products; propene, *1*-butene and *2*-butene (*cis*- and *trans*-butene) are depicted in Figure 6.6.2.4. The catalyst without Al and with a Si/Al ratio of 5 revealed a conversion of around 20% and a maximum selectivity of propene of 20% in the interval of high temperature The catalysts with a Si/Al ratio of 150 and 60 revealed a conversion of ethene of around 20% in the interval of intermediate temperature and around 30% in the in the interval of high temperature. The selectivity of propene reached a maximum in the interval of intermediate temperature with a value close to 60%. Ethene started to react at 150 °C on the catalyst with a Si/Al ratio of 16 and the selectivity of propene reached a selectivity close to 60% at 225 °C. On the other hand, the behavior of the selectivity of *2*-butene suggests that Re is acting as a metathesis active site, where while the selectivity of propene increases the selectivity of *2*-butene decreases.

The catalytic results revealed; the NiRe catalysts are effective to obtain propene at considerable lower temperature that the corresponding Ni based catalysts. However, deeper characterization has to be done in order to understand and to improve the catalytic behavior of the NiRe based catalysts in the ETP-reaction.

The reducibility of the NiRe based catalysts with different Si/Al ratio was studied by H_2-TPR and the results are illustrated in the Figure 6.6.2.5. The Figure (a) shows the H_2-TPR spectra of the catalysts with different Ni/Re ratios and Figure (b) with different Si/Al ratios. Two regions can be distinguished in all catalysts. A low temperature peak centered around 330 °C and a high peak centered in the interval from 635 to 650 °C can be recognized. The well-defined peaks suggest that the interaction between Re and Ni species is not strong. The peak centered at low temperature can be assigned to the reduction of Re species, where the reduction of Re^{+7} surface ions is taking place [141]. The peak in the interval of high temperature might correspond to the reduction of the different Ni species of the catalysts, as it has been discussed in section 6.1.7. A gradual and small shift of the reduction peak of this to lower temperatures could be observed with the increasing amount of Re, low Ni/Re ratio. The peak corresponding to the catalysts with a Ni/Re ratio of 1 showed a shoulder at a temperature lower than 300 °C. This peak corresponds to the reduction of NH_4ReO_4 crystallites due to the high Re content on this catalyst. The reduction of the Re and Ni species in the catalysts with different Si/Al ratios was very similar to the reduction of the catalysts with different

Ni/Re ratios. Both peaks are slightly shifted to higher temperature with the increasing amount of Al.

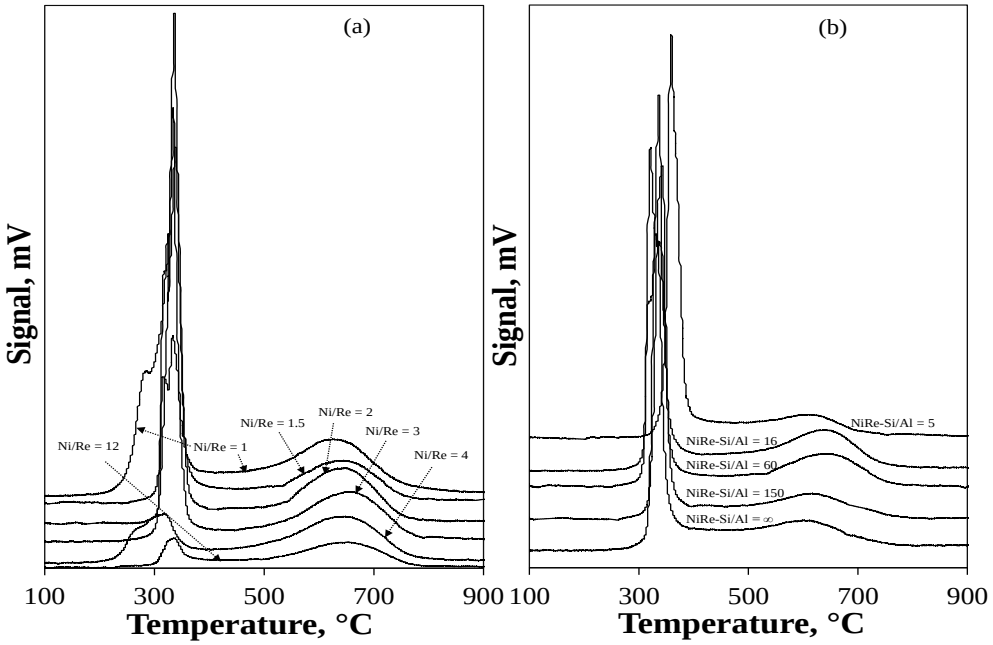

Figure 6.6.2.5. H_2-TPR of (a) NiRe/AlMCM-41(Si/Al=60) at different Ni/Re ratios, and (b) NiRe/MCM-41 and NiRe/AlMCM-41 with different Si/Al ratio prepared by TIE. Ni/Reo=1.5.

Very interesting results were observed for the NiRe based catalysts, where high selectivity of propene was observed at significant lower temperature than the corresponding Ni based catalysts. However, more characterization and a carefully analysis of the synthesis conditions are mandatory to understand the nature of the active sites of this type of catalysts. Catalytic and characterization results suggested that Re catalyze the metathesis reaction between *2*-butene and ethene. However, further optimization of this type of catalysts is very convenient because propene is produced at low temperature, where no strong deactivation of the Ni based catalysts was observed and the regeneration of these catalysts was possible (see Figures 6.4.4.1, 2 and 3). For these reasons, further optimization and characterization of the NiRe based catalyst can be considered as future research work.

6.6.3 Summary

In this part if the chapter, *bi*-metallic catalysts were synthesized and tested in the ETP-reaction. These catalysts were prepared with the goal of optimizing the Ni bases catalysts. The conversion of ethene decreased considerably in comparison to the Ni

based catalyst. However, the selectivity of propene was considerably higher at lower temperature. The characterization of these catalysts was only focus to observe changes in the structure of the catalysts and on the interaction between the active metals and the AlMCM-41 support.

6.7 Experimental error analysis

When random variability is intrinsic to a problem, uncertainty becomes inevitable. This uncertainty is also associated to results obtained from the synthesis of catalysts and catalytic experiments (conversion, selectivity and yield). In the previous sections was shown that the Si/Al ratio is a key parameter in the catalytic behavior of Ni/AlMCM-41 catalysts and it is important to distinguish differences of activity between catalysts with different Si/Al ratios. Considering these characteristics and that all experimental measurements have intrinsically associated an uncertainty, an experimental error analysis is crucial to give certainty to the measurements. Therefore, in the next section an experimental error analysis is presented. This analysis was carried out for the measurements associated to the synthesis of AlMCM-41 with a Si/Al = 60, synthesis of Ni/AlMCM-41, and for the standard ETP experiment.

a) Statistics

When random variability is genuine intrinsic to a problem, uncertainty becomes inevitable, but the problem can be solved systematically and with confidence [142]. Every measurement has some uncertainty. Conclusions can be expressed with a high or low confidence, but never with complete certainty. Experimental errors can be classified as either systematic or random [143]. Systematic error arises from a flaw in the design of an experiment or an equipment flaw. In principle, systematic error can be discovered and corrected, although this may not be easy [143]. Random error arises from the effects of uncontrolled (and maybe uncontrollable) variables in the measurement. Random error has an equal chance of being positive or negative. It is always present and cannot be corrected [143].

If an experiment is repeated many times, and if the errors are purely random, then the results tend to cluster symmetrically about the average value. The more times the experiment is repeated, the more closely the results approach to an ideal smooth curved that can be described by one of the probability density functions (pdf), e. g. normal,

Student t [142]. In general, it is not possible to carry out many measurements in a lab experiment. All experiments can be repeated from 3 to 5 times than 2000 times.

Given a random sample $x_1, x_2, \ldots, x_n$, regardless of the underlying population distribution from which the sample came, the estimators $\overline{x}$ and s^2 defined as

$$\overline{x} = \frac{1}{n}\sum_{i=1}^{n} x_i$$

$$s^2 = \frac{\sum_{i=1}^{n}(x_i - \overline{x})^2}{n-1}$$

are both unbiased for the population mean μ and variance σ^2, respectively. They are thus accurate and valid for any specific set of observations. Therefore, $\overline{x}$ represents the central value at which a set of measurements are distributed (the mean value) and s is defined as the standard deviation of the set of measurements. It measures how closely the data are clustered about the mean [143].

In statistic, a confidence interval (CI) is a type of interval estimate of a population parameter and is used to indicate the reliability of an estimate. The uncertainty of a set of measurements can be performed by doing an estimation of confidence intervals [143], for this reason in this study a calculation of the CI was performed and used as an estimation of the uncertainty of the measurements in the ETP experiments.

Student´s t is a statistical tool used most frequently to express confidence intervals from finite number of experiments by using the following equation

$$\mu = \overline{x} \pm \frac{ts}{\sqrt{n}}$$

where s is the measured standard deviation, n is the number of observations, and t is the value of the t random variable and its value depends on the required confidence level. The confidence interval is an expression stating that the population mean, μ, is likely to lie within a certain distance from the measured mean, $\overline{x}$.

b) Error analysis

In a classical synthesis of Ni/AlMCM-41 procedure and in an ETP experiment, different sources of uncontrolled uncertainty are present e. g. mass of components in the synthesis

of the catalysts, flow rates, temperature control, GC/MS analysis, etc. During the synthesis of the catalysts, it is necessary to weight different compounds that will be used in the synthesis procedure. In the standard ETP experiment are associated different parameters (temperatures, flows, GC/MS analysis, etc.) that will present an effect on the kinetic parameters that give useful information to evaluate the performance of the catalysts e. g. conversion of ethene and selectivity of the products. Therefore, the error analysis was performed to estimate the experimental error of the following measurements; preparation of the mixture for the synthesis of AlMCM-41 and Ni/AlMCM-41 with a Si/Al ratio of 60, the conversion of ethene and the selectivity of the major reaction products at different temperature (ETP experiment). A repetition of five syntheses procedures of AlMCM-41 and Ni/AlMCM-41 was performed. These catalysts were used to perform the ETP experiment and the CI was computed for the conversion of ethene and the selectivity of the reaction products. The CI was estimated with a 95% of confidence.

Table 6.7.1.
Confidence intervals in the synthesis of AlMCM-41 (Si/Al = 60).

Components									
[a]CTABr		[b]TBAOH		Silica fumed		Water		Total amount	
$\overline{x}$, g	C. I., %	$\overline{x}$, g	C. I., %	$\overline{x}$, g	C. I., %	$\overline{x}$, g	C. I., %	$\overline{x}$, g	C. I., %
3.42	0.06	5.43	0.43	1.62	0.25	9.16	1.82	3.37	4.92

[a]cetyltrimethylammonium bromide, [b]tetrabutylammonium hydroxide.

Table 6.7.1 shows the mean and the CI expressed as a percentage of the mean value for the measurements of the amount of the different substances involved in the synthesis of AlMCM-41. Last column shows the amount of AlMCM-41 that is obtained at the end of the synthesis procedure. As it can be observed the step with the highest CI is the weighted amount of water with around 2%. The amount of the AlMCM-41 at the end of the synthesis procedure has associated a CI of around 5%. With these results it can be concluded that the synthesis of AlMCM-41 has associated an experimental error of 5%. For $NaAlO_2$, $\overline{X} = 0.04\ g$ and *C. I.=0.61%*.

Table 6.7.2 provides the mean and the CI expressed as a percentage of the mean value for the measurements of the amount of the different substances involved in the synthesis of the Ni/AlMCM-41. The CI associated to the synthesis of Ni/AlMCM-41 is around 3.5%. The weight of AlMCM-41 is the step with the highest CI with around 1%.

Table 6.7.2
Confidence intervals in the synthesis of Ni/AlMCM-41 (Si/Al = 60).

Components							
AlMCM-41		Ni-nitrate		Water		Total amount	
$\overline{x}$, g	C. I., %	$\overline{x}$, g	C. I., %	$\overline{x}$, g	C. I., %	$\overline{x}$, g	C. I., %
3.02	1.03	0.26	0.08	60.24	0.43	1.31	3.52

The estimation of CI was also performed for the standard ETP experiment. The estimation of the CI intervals was performed for the conversion of ethene and the selectivity of the major reaction products. These results are shown in Table 6.7.3. This table shows the temperature that is set directly in the reactor which is the desired temperature in the catalyst. The actual temperature that is directly measured in the reactor is also shown. It can be observed that the CI in the control of temperature is low, less than 1%. The conversion of ethene is shown also in Table 6.7.2. At low conversion of ethene, the CI is high because of the low concentration of the reaction products. But in general, the CI for the conversion of ethene is less than 9% at all temperatures.

Table 6.7.3
Confidence intervals of the temperature, conversion and selectivity in the standard ETP experiment.

[a]Tset, °C	[a]T measured		[b]Conv. of ethene		[c]Sel. of propene		[c]Sel. of *1*-butene		[c]Sel. of *2*-butene	
	$\overline{x}$, °C	C. I., %	$\overline{x}$, %	C. I., %	$\overline{x}$, %	C. I., %	$\overline{x}$, %	C. I., %	$\overline{x}$, %	C. I., %
50	49.4	3.7	--	--	--	--	--	--	--	--
75	79.9	0.6	4.8	98.1	--	--	2.9	87.1	15.8	87.4
100	103.5	0.4	18.4	6.4	--	--	9.1	14.6	72.8	2.4
125	128.6	0.2	21.6	5.9	--	--	7.8	2.9	75.3	1.2
150	154.2	0.2	24.5	8.3	--	--	7.7	3.1	75.9	1.1
175	179.5	0.1	27.6	8.1	--	--	7.8	3.9	75.8	1.1
200	204.8	0.1	31.1	6.7	0.2	10.6	8.3	6.0	74.8	1.0
225	229.5	0.1	34.5	5.9	0.4	8.6	8.8	6.6	72.8	1.4
250	254.3	0.04	39.3	5.8	0.9	9.4	9.3	7.2	69.7	1.8
275	278.9	0.1	45.1	5.8	2.2	8.7	9.7	7.6	65.5	2.1
300	303.8	0.08	52.0	5.8	4.8	7.4	9.9	7.4	59.6	2.8
325	328.6	0.06	59.3	5.8	9.1	5.9	9.6	10.8	52.1	3.5
350	353.3	0.04	65.6	5.6	14.7	4.8	8.8	11.5	43.4	5.0
375	378.3	0.06	70.0	5.1	20.73	3.4	7.6	9.3	34.8	6.1
400	402.9	0.06	73.2	5.4	25.3	3.3	6.6	10.0	27.1	8.0
425	427.8	0.04	73.8	5.6	29.2	3.1	5.9	11.3	21.8	9.9
450	452.7	0.04	73.0	6.0	31.3	3.7	5.2	12.2	17.7	12.1
475	477.7	0.04	71.0	6.3	32.3	4.2	4.7	12.4	14.8	12.9

[a]Temperature; [b]Conversion; [c]Selectivity.

The selectivity of propene, *1*-butene and *2*-butene are presented in the Table 6.7.3. For the case of propene, the CI was around 10% at low temperature and decreased at higher temperature reaching a value of around 4%. The selectivity of *1*-butene presented a high

CI for low conversion of ethene (low temperature), ca. 88%, but it decreased considerably for high temperature, reaching a value of around 10%. Finally, the CI interval for the selectivity of *2*-butene was also around 10% at high temperature.

As it can be observed, at low level of conversion of ethene the CI is always high because of the difficulty to analyze low concentration of the reaction products. The CI strongly decreased for higher conversions of ethene and it is centered at around 10%. Therefore, according to this analysis it can be concluded that the ETP experiment has intrinsically associated an experimental error of around 10% with a level of confidence of 95%. Based on these results, it is also possible to assume that all catalytic experiments results reported in this project have an experimental error of 10%. The experimental error for the C-balance was also estimated. At low temperature, the mean of the C-balance was centered to 82% with a confidence interval of 4%. The mas balance started to decrease at 250° where gradually decreased until 64% at 475°C. The confidence interval was not bigger than 3.7% at all temperatures.

6.8 Summary of the chapter

This section summarizes the results that were shown in this chapter 6, where Ni mesostructured catalysts were synthesized, tested and optimized in the ETP-reaction.

MCM-41 and AlMCM-41 were synthesized using two different synthesis procedures, the so called Noreña-Franco et al. and Vinu et al. procedures. Ni/MCM-41 and Ni/AlMCM-41 catalysts were synthesized by different methods. These catalysts were characterized using a wide spectrum of characterization techniques. This characterization included structural characterization, determination of the acidity of the catalysts and the nickel state in the final catalysts. A study of the effect of the reaction conditions on the performance of the ETP-reaction was carried out for Ni/AlMCM-41 (Si/Al=60) catalyst. The study was completed by performing deactivation and regeneration experiments. Characterization of the catalyst was also performed after the ETP experiments. This characterization was focused on studying changes of the structure of the catalyst and the formation of carbonaceous species during the ETP-reaction.

The study of the reaction mechanism was carried out by studying separately the *sub*-reactions of the overall reaction mechanism, namely isomerization of butene isomers, metathesis of ethene and *2*-butene and the *retro*-metathesis of propene. Using

in-situ DRIFTS it was possible to understand the way in which ethene adsorbs and reacts on the synthesized catalysts.

To further optimize Ni/AlMCM-41 catalysts, the incorporation of metathesis active sites in the catalysts was proposed. In the first part, this optimization included the catalytic evaluation of the so called *mono*-metallic catalysts. Considered were Mo and Re based catalysts. The second part was based on the incorporation of these metals into the nickel based catalyst. Hereby, these catalysts formed so called *bi*-metallic catalysts. Characterization of *mono*-metallic and *bi*-metallic catalysts was focus on structural characterization and on studying the capacity of the reduction of the metallic species present on the surface of the catalysts.

An experimental error analysis was carried out for a series of ETP experiments.

In the next Chapter the most important results and conclusions that were obtained in the course of this work are summarized.

CHAPTER VII

Conclusions

In this work, *mono*-metallic (Ni, Mo and Re) and *bi*-metallic (NiMo and NiRe) mesostructured (MCM-41 and AlMCM-41) catalysts were synthesized, characterized and tested in the direct conversion of ethene to propene (ETP-reaction). The main conclusions are summarized as follows:

I. Ni/MCM-41 and Ni/AlMCM-41 catalysts

The main comprehensive study was done on the catalysts prepared using the Noreña-Franco et al. (2002) procedure because of their higher activity in the ETP-reaction. Therefore, in this chapter the main conclusions are focused on these catalysts

The catalysts were synthesized at different Si/Al ratio (∞, 150, 60, 16 and 5) to manipulate efficiently the acidity of the catalysts. Ni/MCM-41 revealed a very low conversion of ethene and low selectivity (or yield) of propene. The observed catalytic behavior of this catalyst, in principle, supported the reaction mechanism reported by Iwamoto et al. (2008). Ni/AlMCM-41 catalysts offered a high catalytic activity reaching a maximum on the catalyst with a Si/Al ratio of 60 (conversion of ethene close to 80% and a yield of propene of 27%). This result is similar to the results reported by Iwamoto (2008) (conversion of ethene 68% and yield of propene 32%) but it is significant higher to the reported by Lehmann et al. (2011) (conversion of ethene 35% and yield of propene 16%). Lower Si/Al ratios have a detrimental effect on the course of the ETP-reaction. Based on the characterization results, the structure of the final catalysts

was very sensitive to the presence of Al during the synthesis of AlMCM-41, where low hexagonal degree of the final catalysts was observed. Besides, highly ordered Ni/MCM-41 was synthetized but revealed low catalytic activity. Therefore, the ordering degree of the final catalysts does not have a strong influence on the ETP-reaction.

Acidity, Ni active sites and deactivation of the catalysts

Further characterization revealed that the acidity of the catalysts and the nickel state are crucial for having high catalytic activity. The presence of the Al in the catalysts increased the Brønsted acidity according to the results obtained by NH_3-TPD and pyridine-DRIFTS. According to these results modest acidity is required to synthesize catalysts with high catalytic activity in the ETP-reaction. Solid state NMR revealed the presence of $Si(OSi)_3(OAl)$ structural units in three-dimensionally connected aluminosilicate-like thermal treated structures where Al is tetrahedral coordinated (phylloaluminosilicates). This phase also corresponds to the results reported in the literature by Tanaka et al. and Lehmann et al. [24, 26]. H_2-TPR characterization revealed that Ni is present as a mixture of its cationic form and it is forming Ni composite compounds with the MCM-41 and AlMCM-41. Additionally, electron paramagnetic resonance analysis (EPR) of the catalysts was carried out, but no signal was observed. This result suggests that nickel is present in the catalysts as Ni^{+2} and in this state is active in the ETP-reaction. Characterization after the ETP experiment was carried out. The results revealed the presence of two different carbon species and partial reduction of Ni^{+2} after the ETP-reaction. These carbonaceous species correspond to monoatomic carbon and filamentous carbon. The catalysts with a Si/Al ratio of 150, 60 and 16 revealed high content of this species because of their high catalytic activity (conversion of ethene higher that 60% and selectivity of propene higher than 30%).

II More detailed study of the reaction conditions, deactivation and regeneration of Ni/AlMCM-41

Effect of the reaction conditions

A study of the reaction conditions effect during the ETP experiment was carried out. Changes in feed concentration and temperature by performing heating up and cooling down experiments were studied. The most relevant conclusions obtained by doing these changes are described as follows; a strong deactivation of the catalysts was observed

after the experiment 1, where the temperature was changed only in one direction, from 50 to 475 °C (see section 6.3.2). Gradual deactivation of the catalysts was observed for the rest of the experiments (cooling down and heating up experiments). This deactivation was not influenced by changes in the structure of the catalysts. The acidity of the catalysts decreased much stronger after the experiment 1 and a gradual decreasing was observed for the rest of the experiments. This change in the acidity of the catalysts was the responsible of the decreasing of the catalytic activity. The acidity of the catalysts decreased because of the deposition of carbonaceous species that are formed during the ETP-reaction. The reduction of nickel during the ETP-reaction also took place and might also influence the deactivation of the catalyst.

Deactivation and regeneration of Ni/AlMCM-41

Deactivation experiments were carried out at 250, 350 and 450 °C. A very strong deactivation was observed for the experiments at 450°C but the selectivity of propene was close to 45% after 10 h of experiment and did not change for the rest of the experiment. Only slight deactivation was observed at 250 and 350 °C, where the main reaction products were butene isomers. The selectivity of propene was around 15% at 350°C and it was not produced at 250 °C. No changes in the structure of the catalysts were observed during the deactivation experiments. Reduction of the acidity with the time was observed because of the formation of carbonaceous species during the course of the experiment. Based on the TPO results at 250 °C, it is possible to observe that in the initial steps only formation of the monoatomic carbon is taking place which is transformed into filamentous carbon for longer reaction times. The amount of carbonaceous species is considerable much higher at 450 °C than at 250 and 350 °C. Therefore, this fact is the reason of the strong deactivation of the catalyst at 450 °C. At this temperature, the selectivity of propene did not change significantly, indicating that the active sites that are involved in the propene production were not deactivated by carbon deposits. The regeneration of the catalysts was successfully performed after the deactivation experiments at 250 and 350 °C with a regeneration temperature of 450, 500 and 550 °C. After the deactivation experiment at 450 °C the regeneration of the catalysts was not possible even for the highest regeneration temperature. At this temperature (450 °C), the highest amount of carbonaceous species was produced. TPO results suggest that filamentous carbon is the specie that irreversibly deactivates the catalyst.

III. Study of the reaction mechanism

Isomerization of butene isomers

From the isomerization of butene isomers experiments, the following conclusions can be formulated; the Al content has a strong impact on the isomerization of butene isomers; the C-balance was close to 100% for the isomerization of *cis*- and *trans*-butene, indicating that no side reactions took place during the course of the reaction; the contrary was observed for the isomerization of *1*-butene where the C-balance was around 90% indicating that side-reactions proceeded; no catalytic cracking of butene was observed because of the modest acidity of the catalyst.

Metathesis experiments

Metathesis of ethene and *cis*- or *trans*-butene experiments revealed that propene was not the only reaction product. A high amount of *by*-products was produced which indicates that other type of reactions take place. This fact was tested by performing the *retro*-metathesis of propene where the main reaction products were hexene isomers, especially in the interval of low temperature. Therefore, under the reaction conditions applied in this work, there was no experimental evidence that nickel on AlMCM-41 revealed metathesis properties to produce propene as main reaction product. This conclusion is not in agreement with the results reported in the literature (Iwamoto et al. 2006) where the isomerization of *2*-butene to *1*-butene was not considered and is very favorable even on catalysts of light acidity, as it has been shown in this work.

Temperature effect on the reaction mechanism of the ETP-reaction

Based on the results obtained from the isomerization and metathesis experiments, it is proposed that the following phenomena are taking place in the different intervals of temperature during the ETP-reaction. In the interval of *low* and *intermediate* temperature, the main reaction product is a mixture of butene isomers produced by the dimerization of ethene and the isomerization of butene isomers. In the interval of *high* temperature, a conjunct polymerization (hydropolymerization) is taking place instead of the metathesis of ethene and *2*-butene. This hydropolymerization yields a product that is a complex mixture of saturated and unsaturated hydrocarbons. Therefore, this complex mixture produces the main reaction products in the ETP-reaction and is the precursor of the carbonaceous species responsible of the strong deactivation of the catalyst. The

formation of this carbonaceous species corresponds to the lack in the C-balance in the ETP-reaction. The previous conclusion is supported by the *in-situ* DRIFTS characterization, where evidence of the presence of oligomers could be detected. Therefore, metathesis properties of Ni/MCM-41 and Ni/AlMCM-41 catalysts could not be observed under the conditions investigated in this work.

IV. Mono-metallic(Mo and Re) and bi-metallic (NiMo and NiRe) catalysts for the ETP-reaction

Mo and Re based catalysts showed very low catalytic activity with a conversion of ethene lower than 15% on both type of catalysts. Based on the powder XRD and N_2-physisorption characterization, Mo produced an important modification of the structure of MCM-41 and AlMCM-41 materials. The highest catalytic activity was observed on the catalysts with a Si/Al ratio of 60 with a conversion of ethene of around 15%. Re based catalysts did not modify significantly the structure of the MCM-41 and AlMCM-41 materials, but its catalytic activity was lower that the Mo based catalysts, approx. 12% of conversion of ethene. This level of catalytic activity resulted significantly lower than the Ni based catalysts where the conversion of ethene reached a value close to 80%.

Under the reaction conditions selected in this work, improvement of the catalytic activity in the ETP-reaction of Ni/MCM-41 and Ni/AlMCM-41 could not be obtained with the incorporation of Mo. These catalysts showed high catalytic activity in the selective dimerization of ethene to *2*-butene (*cis*- and *trans*-butene). NiRe based catalysts revealed very interesting catalytic properties in the ETP-reaction. Very high selectivity of propene was obtained at 225 and 250 °C (approx. 70%). This result opens the possibility to produce propene at significant lower temperature which corresponds to a low deactivation rate than the corresponding Ni based catalysts. However, a much more carefully synthesis procedure should be developed and deeper characterization has to be done in order to elucidate the active sites in the ETP-reaction. The behavior of the selectivity of the major reaction products; propene and butene isomers (*cis*- and *trans*-butene), strongly suggest that Re is acting as metathesis active site.

Based on the deactivation results observed on the Ni based catalysts, NiRe based catalysts might be very attractive to obtain high selectivity of propene at low temperature where deactivation problems might not take place.

The results obtained in this PhD work represent an important contribution to the understanding of the ETP-reaction and open possibilities of producing propene from ethene at relative low temperatures.

Highlights

The results obtained in this work represent an important contribution to the understanding of the ETP-reaction. In summary, the most important contributions are:

I. A rather deep characterization of the synthesized catalysts was performed. The presence of Ni and modest acidity are crucial for having catalysts with high catalytic activity.

II. A detailed study of the deactivation and regeneration of the catalysts was done. This study revealed a strong deactivation of the catalyst at the temperature where the highest production of propene was observed. Coke deposits are responsible for this deactivation.

III. A systematic study of the reaction mechanism was performed. With this study it could be better understood how propene is produced and how the deactivation of the catalysts takes place.

IV. Finally, it was proposed an optimization of the Ni catalysts by incorporating Mo or Re as extra-active sites (*bi*-metallic catalysts). This optimization opened the possibility of producing propene at significant lower temperatures.

Future work

A proposal for further optimization of the *bi*-metallic catalysts is shortly described below.

1 The further optimization of NiMo and NiRe catalysts is considered as very promising for future research work. Due to the complexity of the conjunct polymerization mixture, a deeper study of the reaction mechanism has to be done. The estimation of kinetic parameters for each single chemical reaction of the reaction mechanism is another important aspect that has to be studied.

2 Finally, the results obtained in this work represent a contribution to the understanding of the ETP-reaction and open the possibility of producing propene at

relative low temperature. However, a more careful optimization strategy has to be developed to allow industrial applications.

References

[1] Wittcoff H. A., B. G. Reuben, J. S. Plotkin, Industrial Organic Chemicals, 2nd Edition, John Wiley & Sons, Hoboken, New Jersey, 2004.

[2] Plotkin J. S., Cat. Today, 106 (2005) 10.

[3] Weissermel K., H.-J. Arpe, Industrial Organic Chemistry, 3rd Edition, VCH Wiley Company, Printed in the Federal Republic of Germany, 1997.

[4] Dath J. P., W. Vermeiren, K. Herrebout, Patent, WO 00/78894 A1, 2000.

[5] Kogan S. B., M. Herskowitz, Catal. Commun., 2 (2001) 179.

[6] Corma A., F. V. Melo, L. Sauvanaud, F. Ortega, Catal. Today, 107–108 (2005) 699.

[7] Wang B., Q. Gao, J. Gao, D. Ji, X. Wang, J. Suo, Appl. Catal., A, 274 (2004) 167.

[8] Zhu X., S. Liu, Y. Song, L. Xu, Catal. Lett., 103 (2005) 201.

[9] Zhu X., S. Liu, Y. Song, S. Xie, L. Xu, Appl. Catal., A, 290 (2005) 191.

[10] Zhu X., S. Liu, Y. Song, L. Xu, Appl. Catal., A, 288 (2005) 134.

[11] Lu J., Z. Zhao, C. Xu, A. Duan, P. Zhang, Catal. Lett., 109 (2006) 65.

[12] Zhu X., X. Li, S. Xie, S. Liu, G. Xu, W. Xin, S. Huang, L. Xu, Catal. Surv. Asia, 13 (2009) 1.

[13] Banks R. L., G. C. Bailey, I&EC Prod. Res. Develop., 3 (1964) 170.

[14] Mol J. C., J. Mol. Catal. A: Chem, 213 (2004) 39.

[15] Chen S. L., Y. Wang, G. Yuan, D. Hua, M. Zheng, J. Zhang, Chem. Eng. Technol., 36 (2013) 795.

[16] O'Neill P. P., J. J. Rooney, J. Am. Chem. Soc., 94 (1972) 4383.

[17] Yamaguchi T., Y. Tanaka, K. Tanabe, J. Catal., 65 (1980) 442.

[18] Zhou H., Y. Wang, F. Wei, D. Wang, Z. Wang, Appl. Catal., A, 348 (2008) 135.

[19] Oikawa H., Y. Shibata, K. Inazu, Y. Iwase, K. Murai, S. Hyodo, G. Kobayashi, T. Baba, Appl. Catal., A, 312 (2006) 181.

[20] Iwamoto M., Y. Kosugi, J. Phys. Chem. C., 111 (2006) 13.

[21] Iwamoto M., Catal. Surv. Asia, 12 (2008) 28.

[22] Iwamoto M., K. Kasai, T. Haishi, ChemSusChem, 4 (2011) 1055.

[23] Ikeda K., Y. Kawamura, T. Yamamoto, M. Iwamoto, Catal. Commun., 9 (2008) 106.

[24] Tanaka M., A. Itadani, Y. Kuroda, M. Iwamoto, J. Phys. Chem. C., 116 (2012) 5664.

[25] Iwamoto M., Molecules, 16 (2011) 7844.

[26] Lehmann T., T. Wolff, V. M. Zahn, P. Veit, C. Hamel, A. Seidel-Morgenstern, Catal. Commun., 12 (2011) 368.

[27] Lehmann T., T. Wolff, C. Hamel, P. Veit, B. Garke, A. Seidel-Morgenstern, Microporous Mesoporous Mater., 151 (2012) 113.

[28] Frey A. S., O. Hinrichsen, Microporous Mesoporous Mat., 164 (2012) 164.

[29] Taoufik M., E. Le Roux, J. Thivolle-Cazat, J.-M. Basset, Angew. Chem. Int. Ed., 46 (2007) 7202.

[30] Lin B., Q. Zhang, Y. Wang, Ind. Eng. Chem. Res. , 48 (2009) 10788.

[31] Lehmann T., A. Seidel-Morgenstern, J. Phys. Chem. C., 116 (2012) 22646.

[32] Tanaka M., Y. Kuroda, M. Iwamoto, J. Phys. Chem. C., 116 (2012) 22649.

[33] Song Z., W. Liu, C. Chen, A. Takahashi, T. Fujitani, React. Kinet. Mech. Cat., 109 (2013) 221.

[34] Stöcker M., Microporous Mesoporous Mater., 29 (1999) 3.

[35] Phillips C. B., R. Datta, Ind. Eng. Chem. Res., 36 (1997) 4466.

[36] Gayubo A. G., A. Alonso, B. Valle, A. s. T. Aguayo, J. Bilbao, Ind. Eng. Chem. Res., 49 (2010) 10836.

[37] Sugiyama S., Y. Kato, T. Wada, S. Ogawa, K. Nakagawa, K.-I. Sotowa, Top. Catal., 53 (2010) 550.

[38] Hayashi F., M. Iwamoto, ACS Catal., 3 (2013) 14.

[39] Iwamoto M., S. Mizuno, M. Tanaka, Chem. Eur. J. , 19 (2013) 7214.

[40] Li L., R. Palcheva, K.-J. Jens, Top. Catal., 56 (2013) 783.

[41] Lehmann T., A. Seidel-Morgenstern, Chem. Eng. J. http://dx.doi.org/10.1016/j.cej.2013.08.071

[42] Haber J., Pure Appl. Chem., 63 (1991) 1227.

[43] Ertl G., H. Knözinger, F. Schüth, J. Weitkamp, Handbook of Heterogeneous Catalysis, 2008.

[44] Sing K. S. W., D. H. Everett, R. A. W. Haul, L. Moscou, R. A. Pierotti, J. Rouquerol, T. Siemieniewska, Pure Appl. Chem., 57 (1985) 603.

[45] Niemantsverdriet J. W., Spectroscopy in Catalysis An Introduction, Third Edition, 2007.

[46] Fuller M. P., P. R. Griffiths, Anal. Chem., 50 (1978) 1906.

[47] Armaroli T., T. Bécue, S. Gautier, Oil & Gas Scie. Tech. - Rev. IFP, 59 (2004) 215.

[48] Rosenholm J. B., H. Rahiala, J. Puputti, V. Stathopoulos, P. Pomonis, I. Beurroies, K. Backfolk, Colloids Surf., A., 250 (2004) 289.

[49] Lallemand M., A. Finiels, F. o. Fajula, V. Hulea, J. Phys. Chem. C., 113 (2009) 20360.

[50] Noreña-Franco L., I. Hernandez-Perez, J. Aguilar-Pliego, A. Maubert-Franco, Catal. Today, 75 (2002) 189.

[51] Vinu A., K. U. Nandhini, V. Murugesan, W. Böhlmann, V. Umamaheswari, A. Pöppl, M. Hartmann, Appl. Catal. A, 265 (2004) 1.

[52] Yonemitsu M., Y. Tanaka, M. Iwamoto, Chem. Mater., 9 (1997) 2679.

[53] Debecker D. P., M. Stoyanova, U. Rodemerck, P. Eloy, A. Léonard, B.-L. Su, E. M. Gaigneaux, J. Phys. Chem. C., 114 (2010) 18664.

[54] Beck J. S., J. C. Vartuli, W. J. Roth, M. E. Leonowicz, C. T. Kresge, K. D. Schmitt, C. T. W. Chu, D. H. Olson, E. W. Sheppard, J. Am. Chem. Soc., 114 (1992) 10834.

[55] Kresge C. T., M. E. Leonowicz, W. J. Roth, J. C. Vartuli, J. S. Beck, Nature, 359 (1992) 710.

[56] Neimark A. V., P. I. Ravikovitch, M. Grün, F. Schüth, K. K. Unger, J. Colloid Interface Sci., 207 (1998) 159.

[57] Groen J. C., L. A. A. Peffer, J. Pérez-Ramírez, Microporous Mesoporous Mater., 60 (2003) 1.

[58] Hulea V., F. Fajula, J. Catal., 225 (2004) 213.

[59] Hartmann M., A. Pöppl, L. Kevan, J. Phys. Chem., 100 (1996) 9906.

[60] Jacobs P. A., L. J. Declerck, L. J. Vandamme, J. B. Uytterhoeven, J. Chem. Soc., Faraday Trans. 1, 71 (1975) 1545.

[61] Kloetstra K. R., H. W. Zandbergen, H. Bekkum, Catal. Lett., 33 (1995) 157.

[62] Magi M., E. Lippmaa, A. Samoson, G. Engelhardt, A. R. Grimmer, J. Phys. Chem., 88 (1984) 1518.

[63] Engelhardt G., D. Michel, High-Resolution Solid-State NMR of Silicates and Zeolites, Page Bros., Norwich, Great Britain, 1987.

[64] Corma A., V. Fornes, M. T. Navarro, J. Perezpariente, J. Catal., 148 (1994) 569.

[65] Kolodziejski W., A. Corma, M.-T. Navarro, J. Pérez-Pariente, Solid State Nucl. Magn. Reson., 2 (1993) 253.

[66] Kosslick H., G. Lischke, G. Walther, W. Storek, A. Martin, R. Fricke, Microporous Mater., 9 (1997) 13.

[67] Kosslick H., G. Lischke, B. Parlitz, W. Storek, R. Fricke, Appl. Catal., A, 184 (1999) 49.

[68] Bolis V., J. C. Vedrine, J. P. Van de Berg, J. P. Wolthuizen, E. G. Derouane, J. Chem. Soc., Faraday Trans. 1, 76 (1980) 1606.

[69] van den Berg J. P., J. P. Wolthuizen, J. H. C. van Hooff, J. Catal., 80 (1983) 139.

[70] Beran S., J. Mol. Catal., 30 (1985) 95.

[71] Maache M., A. Janin, J. C. Lavalley, E. Benazzi, Zeolites, 15 (1995) 507.

[72] Bergström L., E. Bostedt, Colloids Surf., 49 (1990) 183.

[73] Rosenholm J. B., H. Rahiala, J. Puputti, V. Stathopoulos, P. Pomonis, I. Beurroies, K. Backfolk, Colloids and Surfaces A, 250 (2004) 289.

[74] Morterra C., A. Chiorino, G. Ghiotti, E. Garrone, J. Chem. Soc., Faraday Trans. 1, 75 (1979) 271.

[75] Wojcieszak R., S. Monteverdi, M. Mercy, I. Nowak, M. Ziolek, M. M. Bettahar, Appl. Catal., A, 268 (2004) 241.

[76] Hadjiivanov K., M. Mihaylov, D. Klissurski, P. Stefanov, N. Abadjieva, E. Vassileva, L. Mintchev, J. Catal. , 185 (1999) 314.

[77] Yang Y., S. Lim, G. Du, Y. Chen, D. Ciuparu, G. L. Haller, J. Phys. Chem. B, 109 (2005) 13237.

[78] Clause O., L. Bonneviot, M. Che, H. Dexpert, J. Catal. , 130 (1991) 21.

[79] Richardson J. T., R. Scates, M. V. Twigg, Appl. Catal., A 246 (2003) 137.

[80] Wang S., Ind. Eng. Chem. Res., 38 (1999) 2615.

[81] Takenaka S., E. Kato, Y. Tomikubo, K. Otsuka, J. Catal., 219 (2003) 176.

[82] Buchireddy P. R., R. M. Bricka, J. Rodriguez, W. Holmes, Energy Fuels, 24 (2010) 2707.

[83] Wu C., L. Wang, P. T. Williams, J. Shi, J. Huang, Appl. Catal., B, 108–109 (2011) 6.

[84] Wang S., G. Q. Lu, Appl. Catal., B, 19 (1998) 267.

[85] Tanaka M., A. Itadani, Y. Kuroda, M. Iwamoto, J. Phys. Chem. C, 116 (2012) 5664.

[86] Chen X., L. Huang, G. Ding, Q. Li, Catal. Letters, 44 (1997) 123.

[87] Moulijn J. A., A. E. van Diepen, F. Kapteijn, Appl. Catal. A, 212 (2001) 3.

[88] Bartholomew C. H., Appl. Catal. A, 212 (2001) 17.

[89] van Leeuwen P. W. N. M., Appl. Catal. A, 212 (2001) 61.

[90] Guisnet M., P. Magnoux, Appl. Catal. A, 212 (2001) 83.
[91] van Donk S., J. H. Bitter, K. P. de Jong, Appl. Catal. A, 212 (2001) 97.
[92] Froment G. F., Appl. Catal. A, 212 (2001) 117.
[93] Sie S. T., Appl. Catal. A, 212 (2001) 129.
[94] Trimm D. L., Appl. Catal. A, 212 (2001) 153.
[95] Twigg M. V., M. S. Spencer, Appl. Catal. A, 212 (2001) 161.
[96] Arends I. W. C. E., R. A. Sheldon, Appl. Catal. A, 212 (2001) 175.
[97] Thevenin P. O., A. G. Ersson, H. M. J. Kušar, P. G. Menon, S. G. Järås, Appl. Catal. A, 212 (2001) 189.
[98] Subramaniam B., Appl. Catal. A, 212 (2001) 199.
[99] Rabinowitz H. N., S. J. Tauster, R. M. Heck, Appl. Catal. A, 212 (2001) 215.
[100] Wiersma A., E. J. A. X. van de Sandt, M. Makkee, J. A. Moulijn, Appl. Catal. A, 212 (2001) 223.
[101] Meima G. R., P. G. Menon, Appl. Catal. A, 212 (2001) 239.
[102] Holmlid L., P. G. Menon, Appl. Catal. A, 212 (2001) 247.
[103] van den Berg J. P., J. P. Wolthuizen, A. D. H. Clague, G. R. Hays, R. Huis, J. H. C. van Hooff, J. Catal., 80 (1983) 130.
[104] Beran S., J. Molec. Catal., 30 (1985) 95.
[105] Ghosh A. K., L. Kevan, J. Am. Chem. Soc., 110 (1988) 8044.
[106] Hartmann M., L. Kevan, J. Phys. Chem., 100 (1996) 4606.
[107] Speiser F., P. Braunstein, L. Saussine, Acc. Chem. Res., 38 (2005) 784.
[108] Pillai S. M., M. Ravindranathan, S. Sivaram, Chem. Rev., 86 (1986) 353.
[109] Kimura K., H. A-I, A. Ozaki, J. Catal., 18 (1970) 271.
[110] de Souza M. O., L. R. Rodrigues, R. M. Gauvin, R. F. de Souza, H. O. Pastore, L. Gengembre, J. A. C. Ruiz, J. M. R. Gallo, T. S. Milanesi, M. A. Milani, Catal. Commun., 11 (2010) 597.
[111] Ghosh A. K., L. Kevan, J. Am. Chem. Soc., 94 (1990) 3117.
[112] Ng F. T. T., D. C. Creaser, Appl. Catal. A, 119 (1994) 327.
[113] Bonneviot L., D. Olivier, M. Che, J. Molec. Catal., 21 (1993) 415.
[114] Bogus W., L. Kevan, J. Phys. Chem., 93 (1989) 3223.
[115] Hubert A. J., H. Reimlinger, Synthesis, 1970 (1970) 405.
[116] Hong Y., F. R. Chen, J. J. Fripiat, Catal. Letters, 17 (1993) 187.
[117] Misono M., Y. Yoneda, J. Phys. Chem., 76 (1972) 44.
[118] Forni L., L. Zanderighi, S. Carr'a, J. Catal., 12 (1968) 298.

[119] Gerberich H. R., W. K. Hall, J. Catal., 5 (1966) 99.
[120] Nakamura K., K. Eda, S. Hasegawa, N. Sotani, Appl. Catal. A, 178 (1999) 167.
[121] Chang C. C., W. C. Conner, R. J. Kokes, J. Phys. Chem., 77 (1973) 1957.
[122] Engelhardt J., I. Zsinka, J. Molec. Catal., 28 (1985) 169.
[123] Kapteijn F., A. J. v. d. Steen, J. C. Mol, J. Chem. Thermodyn., 15 (1983) 137.
[124] Haag W. O., H. Pines, J. Am. Chem. Soc., 82 (1960) 2488.
[125] Béres A., I. Hannus, I. Kiricsi, React. Kinet. Catal. Lett., 56 (1995) 55.
[126] Hightower J. W., W. K. Hall, J. Phys. Chem., 71 (1967) 1014.
[127] Golden D. M., K. W. Egger, S. W. Benson, J. Am. Chem. Soc., 86 (1964) 5416.
[128] Egger K. W., D. M. Golden, S. W. Benson, J. Am. Chem. Soc., 86 (1964) 5420.
[129] Lucchesi P. J., D. L. Baeder, J. P. Longwell, J. Am. Chem. Soc., 81 (1959) 3235.
[130] Olah G. A., Á. Molnár, Hydrocarbon Chemistry, 2003.
[131] Dewing J., M. S. Spencer, T. V. Whittam, Catal. Rev., 27 (1985) 461.
[132] Bilhou J. L., J. M. Basset, R. Mutin, W. F. Graydon, J. Am. Chem. Soc., 99 (1977) 4083.
[133] Engelhardt J., I. Zsinka, React. Kinet. Catal. Lett., 21 (1982) 529.
[134] Kapteijn F., E. Homburg, J. C. Mol, J. Chem. Thermodyn., 15 (1983) 147.
[135] Spoto G., S. Bordiga, G. Ricchiardi, D. Scarano, A. Zecchina, E. Borello, J. Chem. Soc., Faraday Trans., 90 (1994) 2827.
[136] Wu Z., C. Li, P. Ying, Z. Wei, Q. Xin, J. Phys. Chem. B, 105 (2001) 9183.
[137] Bordiga S., S. Bertarione, A. Damin, C. Prestipino, G. Spoto, C. Lamberti, A. Zecchina, J. Mol. Catal. A, 204–205 (2003) 527.
[138] Bodoardo S., R. Chiappetta, F. Fajula, E. Garrone, Microporous Mater., 3 (1995) 613.
[139] Rajagopal S., H. J. Marini, J. A. Marzari, R. Miranda, J. Catal., 147 (1994) 417.
[140] Qu L., W. Zhang, P. J. Kooyman, R. Prins, J. Catal., 215 (2003) 7.
[141] Arnoldy P., E. M. van Oers, O. S. L. Bruinsma, V. H. J. de Beer, J. A. Moulijn, J. Catal., 93 (1985) 231.
[142] Ogunnaike B. A., Random Phenomena Fundamentals of Probability and Statistics for Engineers, CRC Press, United States of America, 2010.
[143] Harris D. C., Quantitative Chemical Analysis, Fifth Edition, W. H. Freeman and Company New York, United States of America, 1999.

Appendix

Appendix A: List of equipment and gases

Appendix B: List of hydrocarbons used

Appendix C: List of chemicals used

Appendix D: Metathesis of ethene and *cis*- and *trans*-butene on Ni/AlMCM-41 with a Si/Al ratio of 150, 16 and 5

Appendix E: *Retro*-metathesis of propene on Ni/AlMCM-41 with a Si/Al ratio of 150, 16 and 5

Appendix A

List of the equipment and gases

Table A.1: Equipment used in this work

Equipment	Company
Q Gard 01 *(System for physical water treatment)*	Millipore
Excellence XS Analysen Waage *(analytical accurate balance)*	Mettler Toledo
Navigator Waagen *(balance)*	Ohaus Corporation
MR-Hei-Standard *(magnetic stirrer with heating)*	Heidolph Instruments
pH-Meter S20 *(pH meter)*	Mettler Toledo
pH-Sonden: InLab Viscous *(measurement chain)*	Mettler Toledo
Harvard Apparatus 44 *(syringe pump)*	Krüss
Laborofen VMK-135 (*laboratory furnace*)	Limhightherm GmbH
Membranpumpe 2-köpfig Typ MPC 301 Z *(membrane pump)*	ILMVAC
Wasserstrahlpumpe *(water jet pump)*	Brand GmbH
Trockenschrank Typ LUT 6050 *(drying chamber or oven)*	Kendro Laboratory Products

Table A.2: List of gases (produced by Westfalen AG company)

IUPAC name (purity)
nitrogen (99.999 %)
nitrogen (99.98 %)
liquid nitrogen
ethene (99.95 %)
5 vol.% 1-butene (99.0 %) in nitrogen (99.998 %)
5 vol.% cis-2-butene (99.0 %) in nitrogen (99.998 %)
5 vol.% trans-2-butene (99.0 %) in nitrogen (99.998 %)
argon (99.996 %)
helium (99.9990 %)
10 vol.% hydrogen (99.9990 %) in argon (99.9990 %)
1 vol.% ammonia (99.98 %) in nitrogen (99.996 %)

Appendix B

List of hydrocarbons used

Table B.1: List of hydrocarbons. Reactants and products in the ETP-reaction

IUPAC name	condensed formula	skeletal formula	structure formula	3 D- model
ethene (ethylene)	C_2H_4		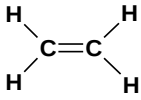	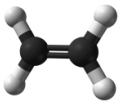
propene	C_3H_6	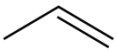	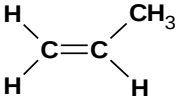	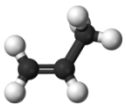
1-butene	C_4H_8	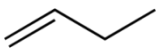	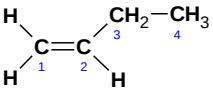	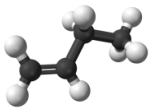
cis-2-butene	C_4H_8	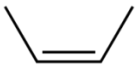	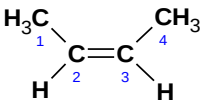	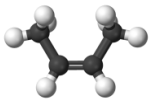
trans-2-butene	C_4H_8	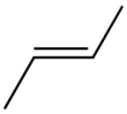	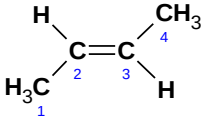	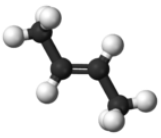
2-methylpropene (*iso*-butene)	C_4H_8	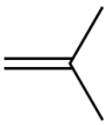	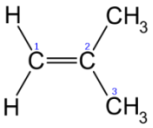	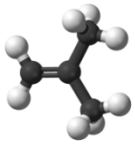
1-pentene	C_5H_{10}		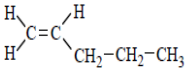	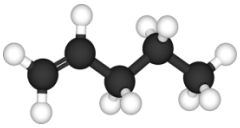
1-hexene	C_6H_{12}	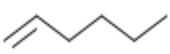	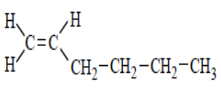	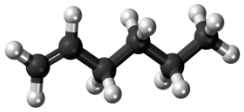

Appendix C

List of chemicals used

Table C.1: List of chemical substances used for the synthesis of the catalysts

IUPAC name	molecular formula	Company (purity)
cetyltrimetylammonium bromide (hexadecyl-trimethylammonium bromide, CTABr)	$C_{19}H_{42}BrN$	Merck (>97%) Sigma-Aldrich (99%)
myristiltrimethylammonium bromide (tetradecyltrimethyl-ammonium bromide, TDTABr)	$C_{17}H_{38}BrN$	Sigma-Aldrich (99%)
tetrabutylammonium hydroxide 40wt.% (TBAOH)	$C_{16}H_{37}NO$	Sigma-Aldrich
ammonia solution 32%	NH_3	Merck
ammonium heptamolybdate tetrahydrate	$(NH_4)_6Mo_7O_{24}.4\ H_2O$	Merck (99.3%)
ammonium metatungstate hydrate	$(NH_4)_6H_2W_{12}O_{40}.H_2O$	Sigma-Aldrich (99.99%)
ammonium perrhenate	NH_4ReO_4	Sigma-Aldrich (99+%)
molybdenum(VI) oxide (molybdenum trioxide)	MoO_3	Merck
nickel nitrate hexahydrate	$Ni(NO_3)_2{\cdot}6H_2O$	Merck
silica fumed (silicon(IV) oxide)	SiO_2	Sigma-Aldrich
sodium aluminate anhydrous	$NaAlO_2$	Sigma-Aldrich (tech.)
sodium silicate solution	Na_2SiO_3	Sigma-Aldrich
sulfuric acid	H_2SO_4	Merck (95-97%)
water	H_2O	deionized

Appendix D

Metathesis of ethene and cis-butene on Ni/AlMCM-41 with a Si/Al ratio of 150, 16 and 5

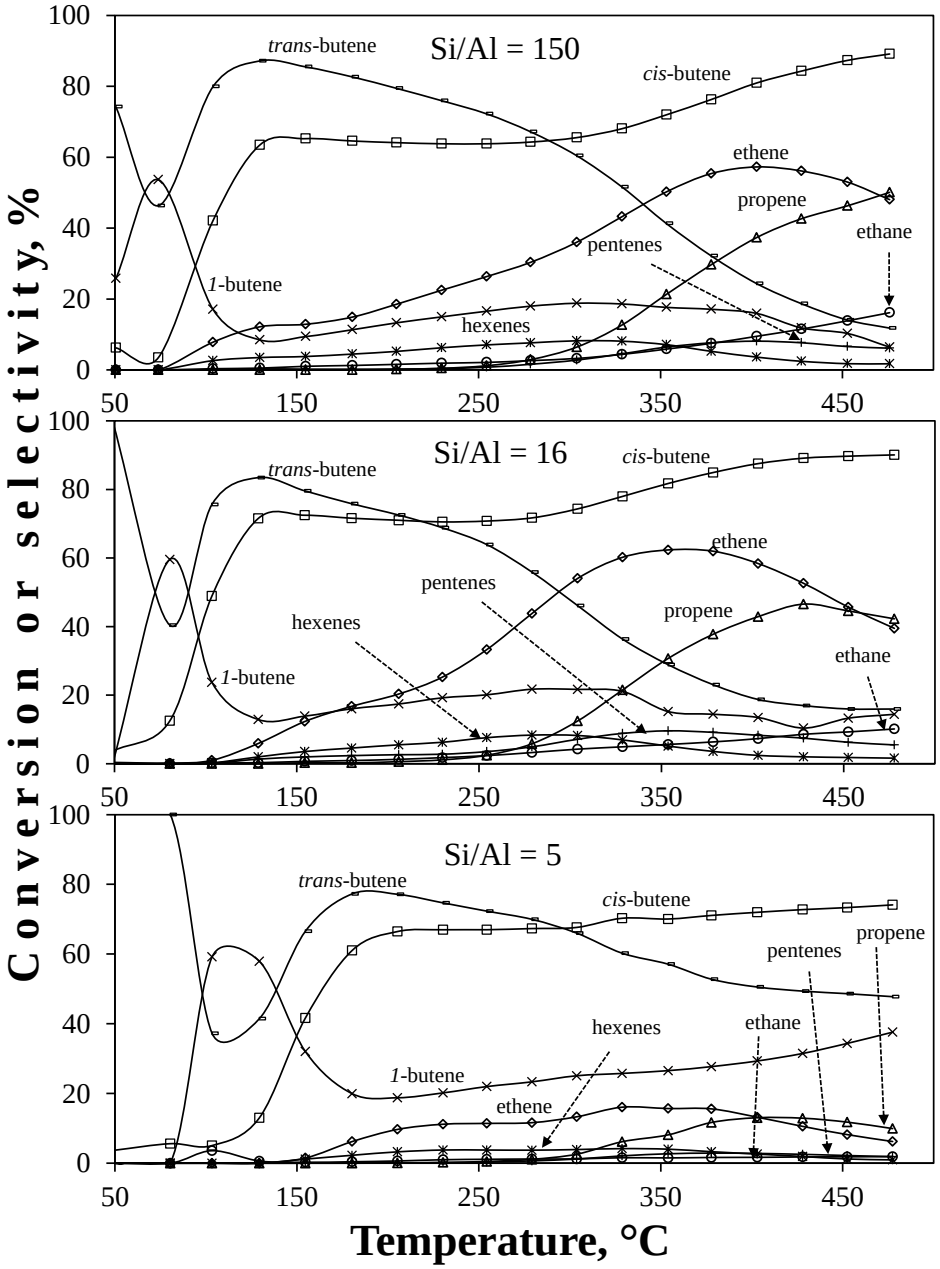

This Figure shows the metathesis of *cis*-butene and ethene on Ni/AlMCM-41 with a Si/Al ratio of 150, 16 and 5 at different temperature. This Figure is supporting the information concerning to Figure 6.4.3.1 depicted in section 6.4 where the reaction mechanism of the ETP-reaction was studied.

Metathesis of ethene and trans-butene on Ni/AlMCM-41 with a Si/Al ratio of 150, 16 and 5

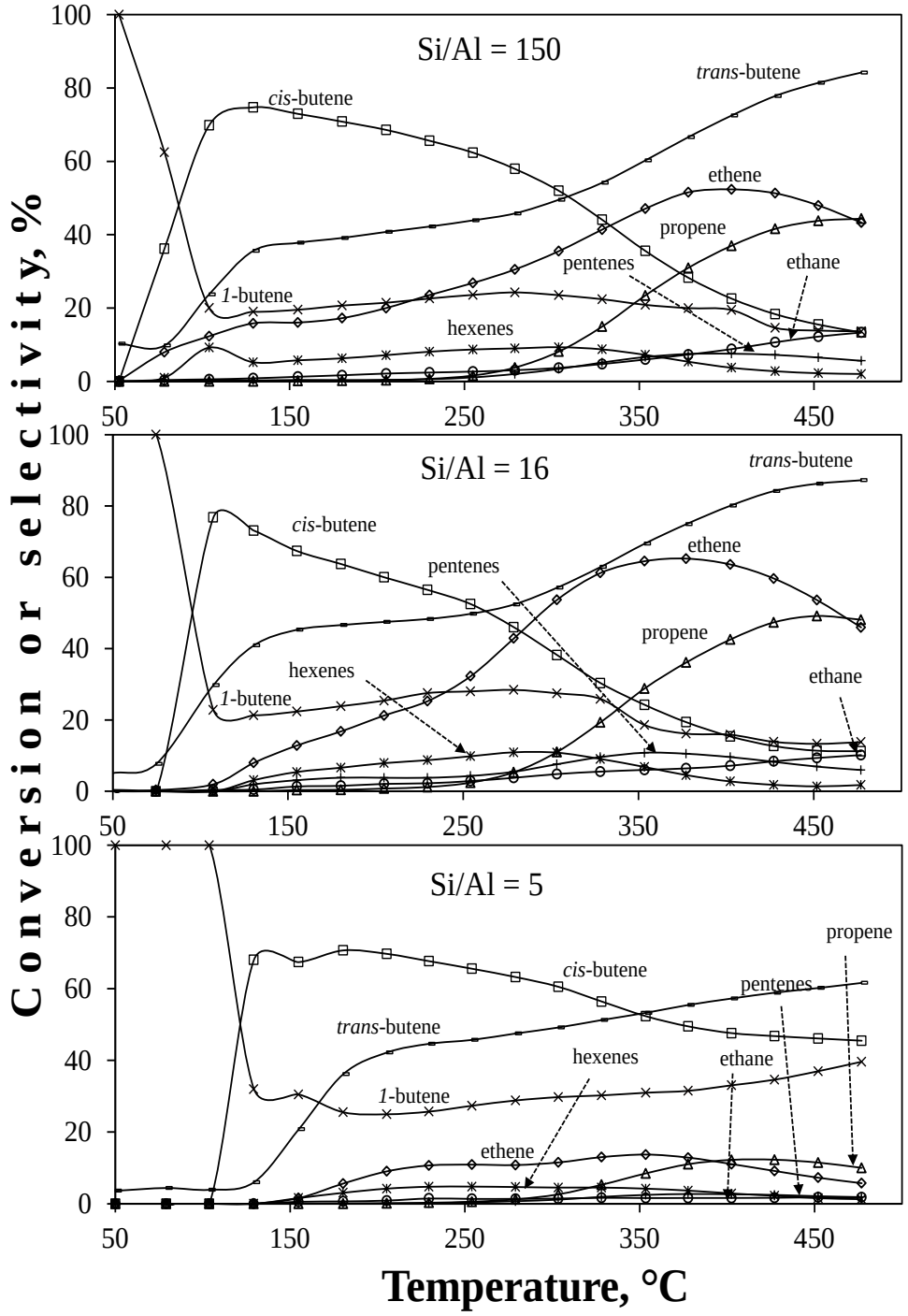

This Figure shows the metathesis of *trans*-butene and ethene on Ni/AlMCM-41 with a Si/Al ratio of 150, 16 and 5 at different temperature. This Figure is supporting the information concerning to Figure 6.4.3.2 depicted in section 6.4 where the reaction mechanism of the ETP-reaction was studied.

Appendix E

Retro-metathesis of propene on Ni/AlMCM-41 with a Si/Al ratio of 150, 16 and 5

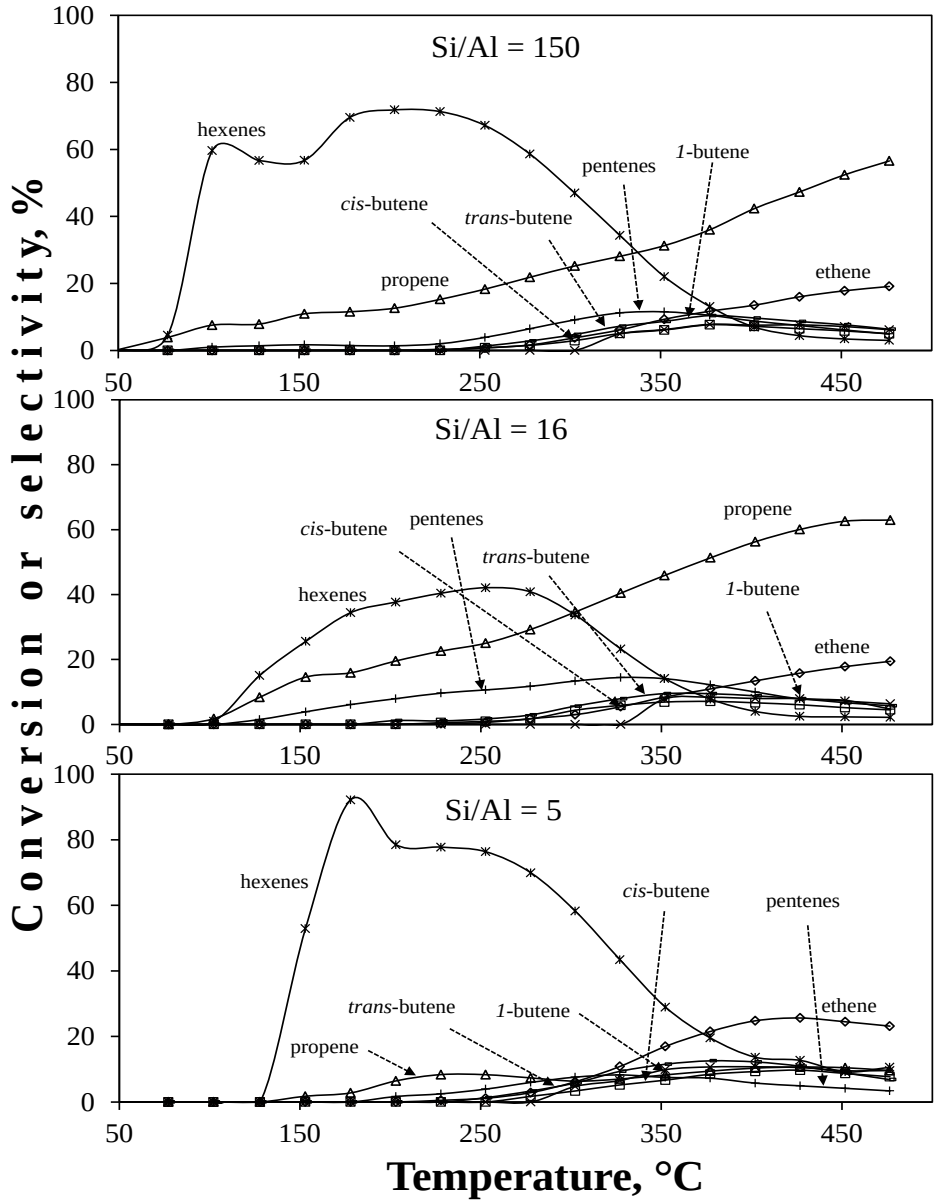

This Figure shows the *retro*-metathesis of propene on Ni/AlMCM-41 with a Si/Al ratio of 150, 16 and 5 at different temperature. This Figure is supporting the information concerning to Figure 6.4.3.3 depicted in section 6.4 where the reaction mechanism of the ETP-reaction was studied.